Contributors to Proximal Femur Fracture Force: Multiscale Considerations of Rate, Toughness, and Bone Composition

by

Daniel R. Martel

A thesis
presented to the University of Waterloo
in fulfillment of the
thesis requirement for the degree of
Doctor of Philosophy
in
Kinesiology

Waterloo, Ontario, Canada, 2022

©Daniel R. Martel 2022

Examining Committee Membership

The following served on the Examining Committee for this thesis. The decision of the Examining Committee is by majority vote.

External Examiner	Heidi Ploeg, Ph.D. Associate Professor Queen's University
Supervisor(s)	Andrew C. Laing, Ph.D. Associate Professor, Kinesiology and Health Sciences
Internal Members	Jack C. Callaghan, Ph.D. Professor, Kinesiology and Health Sciences, Mechanical and Mechatronics Engineering
	Marina Mourtzakis Associate Professor, Kinesiology and Health Sciences
Internal-external Member	Thomas Willett, Ph.D. Associate Professor, Systems Design Engineering

Author's Declaration

This thesis consists of material all of which I authored or co-authored: see Statement of Contributions included in the thesis. This is a true copy of the thesis, including any required final revisions, as accepted by my examiners.

I understand that my thesis may be made electronically available to the public.

Statement of Contributions

I would like to acknowledge the following collaborators for their contributions to the work presented in this thesis:

Study 1,

Stephanie Auer, medical imaging
Taylor Winberg and Jackie Zehr, assistance with data collection
Stephen Pretty, MATLAB code for femur geometry from DXA scans

Study 2,

Stephanie Auer, medical imaging
Taylor Winberg and Alyssa Tondat, assistance with data collection
Stephen Pretty, MATLAB code for femur geometry from DXA scans

Study 3,

Dr. Thomas Willett, assistance with data collection
Daniel Dapaah, assistance with data collection and MATLAB code for fracture toughness

Study 4,

Dr. Thomas Willett and Taylor Winberg, assistance with data collection

Abstract

Fall-related hip fractures are a major concern facing the older adult population, especially as rates of these injuries increasing worldwide. Based on the strong positive relationship between femoral areal bone mineral density (BMD) and femoral bone strength, various methods and tools have been developed to predict hip fracture risk and ultimately prevent these injuries. However, these BMD-based methods are currently limited in their sensitivity, with commonly used methods like the T-Score failing to predict approximately 70% of hip fracture case. This begs the question: What is currently limiting our ability to accurately predict hip fracture risk? One potential explanation is that currently established methods to predict bone strength may be limited as they are based on non-physiological, low loading rate experiments measuring bone strength. Additionally, current predictive methods are solely focused on the inorganic phase of bone which may limit their accuracy. Despite understanding the role of collagen in bone structure and on the mechanical properties of bone at the microscale, such as its influence on fracture toughness, the organic phase of bone has not been directly considered in the context of femoral bone strength and fall-related hip fractures.

Therefore, the overarching purpose of this thesis was to investigate the contributions of loading rate, fracture toughness, and bone composition (including both the inorganic and organic phases of bone) on the strength of the proximal femur in the context of fall-related hip fractures. The secondary purpose of this thesis was to investigate the effect of bone-affecting inflammatory disease states on these factors. These purposes were achieved through four studies which aimed to answer the following questions: 1) Does a biofidelic experimental paradigm, a vertical drop tower hip impact simulator (HIS), produce different bone strength measures than a traditional low displacement rate material testing system (MTS) approach? 2) Does a predictive bone strength model developed using a biofidelic test paradigm result in a model that is more accurate than previously developed models? 3) Does collagen network integrity and connectivity affect the fracture toughness of inferior femoral neck cortical bone under impact-like loading? 4) Are metrics of collagen quality significant predictors of proximal femur bone strength?

Matched pairs of fresh frozen cadaveric femurs were used to compare measures of femoral bone strength extracted from both inertially driven HIS experiments and constant displacement

rate MTS experiments, with the femurs of each pair being split between experiments (Study 1). Using a separate sample of matched pairs of femurs, measures of proximal femur bone strength (Study 2) were linked to measures of fracture toughness and collagen connectivity of cortical bone samples from the inferior femoral neck of the paired contralateral femur (Study 3). This allowed for direct consideration of site-specific measures of toughness and collagen in predictions of femoral bone strength (Study 4).

Although loading rate was significantly higher for specimens tested using the HIS in Study 1, there was no significant difference in the femoral bone strength measured between experimental paradigms. Within each experimental paradigm, there was a significant positive relationship between loading rate and bone strength which was likely mediated by individual specimen stiffness. In Study 2, the combination of femoral neck areal BMD, sex, and their interaction was identified as the strongest overall model for predicting femoral bone strength (adj. $R^2 = 0.688$, $p < 0.001$). Model predictions of bone strength from four published materials testing system-based models revealed that each model produced significantly lower predictions of bone strength compared to the model developed in this study. When split by sex, each of the published models predicted significantly lower bone strength for males when compared to measured values. Study 3 revealed a significant relationship between collagen network connectivity (*Max Slope*) and both elastic and elastic-plastic fracture toughness (K_{Max} and J_{Max}), of inferior femoral neck cortical bone samples when evaluated at, or up to, the point of peak load (adj. $R^2 = 0.229$, $p = 0.002$, and adj. $R^2 = 0.163$, $p = 0.021$, respectively). Collagen network thermal stability (T_d), however, was not associated with fracture toughness. Towards addressing the secondary purpose of this thesis, presence of bone affecting disease states was considered as a categorical variable, where it was found to be significantly associated to fracture toughness metrics alongside *Max Slope* and led to a marked improvement of model strength for J_{Max} (adj. $R^2 = 0.324$, $p = 0.003$). After aggregating results for matched pairs of femurs that were split between Studies 2 and 3, regression analyses in Study 4 revealed that while fracture toughness was not associated with bone strength, T_d was significantly associated with bone strength (adjusted $R^2 = 0.395$, $p = 0.017$). T_d explained an additional 3.2% of the variance in the prediction of femoral bone strength when included alongside BMD and sex. The combination of these three variables resulted in the strongest overall model predicting bone strength (adj. $R^2 = 0.942$, $p < 0.001$). Considering that the T_d is known to be associated with the connectivity of the collagen network, crosslinking content, and organization of

the collagen network, this finding suggests that these molecular level characteristics of bone collagen are important contributors to femoral bone strength.

Through multiscale investigations of whole bone strength at the macroscale and characterization of aspects of the collagen network at the micro-scale, this thesis represents the first investigations to directly measure the influence of collagen on whole bone strength, specifically in the context of fall-related hip fractures. The aspects of collagen connectivity captured by T_d were found to significantly contribute to femoral bone strength in simulated lateral hip impacts. However, the inclusion of T_d as a predictor alongside BMD and sex only resulted in an additional 3.2% of the variance being explained, which brings into question the clinical significance of these findings. The difference between the bone strength regression model generated in Study 2 compared to other published models based on materials testing systems experiments suggests that it may be important to use more biofidelic test paradigms for the development of models to predict bone strength. These findings may lead to improvements in our ability to accurately predict femoral bone strength and consequently result in better estimations of injury risk. By improving the accuracy of our estimates of injury risk, we can ultimately aid in the prevention of fall-related hip fractures. Further research into the molecular-level aspects of collagen that relate to T_d is needed to properly understand the mechanism through which collagen contributes to bone strength. This would then allow for the identification of potential biomarkers that could be used clinically to estimate bone strength.

Acknowledgements

I would like to acknowledge the support and insight provided by my supervisor, Dr. Andrew Laing, my committee members Dr. Jack Callaghan, Dr. Marina Mourtzakis, and Dr. Thomas Willett, as well as for the support from my lab mates, colleagues and collaborators. A special thanks to my colleagues Jeffery Barrett, Daniel Dapaah, Thomas Hoshizaki, Steven Pretty, Alyssa Tondat, Daniel Vigianni, Taylor Winberg, and Jackie Zehr. I would also like to acknowledge the support and assistance from Jeff Rice, Stephanie Auer, Jeremy Roth, Tamara Maciel, Jindra Tupy, and Denise Hay. This thesis could not have been completed without the help of any of these individuals, and for their help and support, I am eternally grateful. For their moral support, I would like to thank my friends and family, especially to my mom and dad for their unflinching support and belief. Lastly, I cannot thank my wife, Dr. Alex Hirniak, enough for her unending support and boundless reserves of patience and love.

Table of Contents

Examining Committee Membership ii
Author's Declaration iii
Statement of Contributions iv
Abstract v
Acknowledgements viii
List of Figures xiii
List of Tables xvi
List of Equations xviii
Chapter 1 Thesis Overview 1
1.1 Introduction 1
1.2 Overview of Proposed Studies 4
Chapter 2 General Introduction & Literature Review 9
2.1 General Introduction: 9
2.2 Fall Related Hip Fractures 9
2.2.1 Epidemiology and Statistics 9
2.2.2 Consequences and Outcomes 10
2.2.3 Risk Factors 12
2.2.4 Screening and Prevention 16
2.3 Hip Fracture Mechanics 18
2.3.1 Loading and Failure 18
2.3.2 Experimental Findings 22
2.3.3 Determinants of Bone Strength 26
2.3.4 Mechanistic Fracture Risk: 27
2.4 Bone Biology 29
2.4.1 Femoral Structure and Morphology 30
2.4.2 Bone at the Molecular Level 38
2.5 Literature Review Summary 42
Chapter 3 Study 1: Investigating the Influence of Test Paradigm on Fracture Force of the Proximal Femur During Lateral Impacts 44

3.1 Introduction 44
3.2 Methods 46
3.2.1 System Development 46
3.2.2 Sample Acquisition and Preparation 49
3.2.3 Testing Protocol 53
3.2.4 Data Analysis 55
3.2.5 Statistics and Data Interpretation 55
3.3 Results 55
3.4 Discussion 61
3.5 Conclusion 66
Chapter 4 Study 2: Development of Predictive Models to Estimate Fracture Force of the Proximal Femur 67
4.1 Introduction 67
4.2 Methods 69
4.2.1 Sample Acquisition and Preparation 69
4.2.2 Specimen Characterization 69
4.2.3 Testing Preparation and Protocol 77
4.2.4 Data Analysis 79
4.2.5 Statistics and Data Interpretation 80
4.3 Results 85
4.3.1 Statistical Model Robustness and Repeatability 91
4.3.2 Disease Analysis 95
4.4 Discussion 97
4.5 Conclusion 103
Chapter 5 Study 3: The Role of Bone Collagen Integrity on Fracture Toughness of the Inferior Femoral Neck Under Simulated Impact Loading Rates 105
5.1 Introduction 105
5.2 Methods 107
5.2.1 Sample Acquisition and Preparation 107
5.2.2 SENB Fracture Toughness Testing 109
5.2.3 Hydrothermal Isometric Tension Tests 113

5.2.4 Data Analysis 116
5.2.5 Statistics and Data Interpretation 117
5.3 Results 117
5.3.1 Disease Analysis 120
5.4 Discussion 124
5.5 Conclusion 130
Chapter 6 Study 4: Investigating the Relationship Between Femoral Collagen Connectivity, Quality, Bone Toughness, and Bone Strength 131
6.1 Introduction 131
6.2 Methods 133
6.2.1 Data Aggregation 133
6.2.2 Statistics and Data Interpretation 133
6.3 Results 135
6.4 Discussion 138
6.5 Conclusion 146
Chapter 7 Thesis Summary 148
7.1 Study 1: Investigating the influence of test paradigm on fracture force of the proximal femur during lateral impacts 148
7.2 Study 2: Development of predictive models to estimate fracture force of the proximal femur 149
7.3 Study 3: The role of bone collagen integrity on fracture toughness of the inferior femoral neck under simulated impact loading rates 149
7.4 Study 4: Investigating the relationship between femoral collagen connectivity, quality, bone toughness, and bone strength 150
7.5 Significance and Implications 150
7.5.1 Significance 150
7.5.2 Clinical Implications 151
7.6 Future Research and Next Steps 154
Bibliography 156
Appendices 185
Appendix A 185

Appendix B 188
Appendix C 192
Appendix D 193
Appendix E 194
Appendix F 195
Appendix G 197
Appendix H 200

List of Figures

Figure 1-1: Thesis Study flow diagram with current study titles included. 5

Figure 1-2: A simplified overview of the femur specimen split between studies and the general flow of data and results between studies. Specimen numbers present only reflect specimens and data that could be used for analysis. 6

Figure 2-1: Canadian hip fracture rates by age and by sex (From Jean et al., 2013) 10

Figure 2-2: Taken from Santos et al., 2017 [Figure 1]: "Bone mass density (BMD) across the lifespan. Men exhibit higher BMDs throughout life and are less susceptible to age-related bone loss than women. Adapted from Hendrickx et al. (2015)." 15

Figure 2-3: Taken from de Bakker et al. 2009 [Figure 1]: "The magnitude and nature of the stresses on the femoral neck differ depending on the applied load" 21

Figure 2-4: From Wiener 1998 – "The 7 hierarchical levels of organization of the bone family of materials". 30

Figure 2-5: Taken from Maedea 2011, used to illustrate various morphological measures. Segment B'G represents the FSNA, while segment BE represents the FNAL; the angle between these two (at F) represents the NSA. 32

Figure 2-6: Taken from Launey et al. 2010; Schematic representation of the inner structure of cortical bone. 34

Figure 2-7: Taken from Launey et al. 2010 [Figure 3]; The toughness of bone results from a mutual competition between extrinsic (crack tip shielding) toughening mechanisms, which predominate at length scales at more than 1 μm, and intrinsic (plastic deformation) toughening mechanisms, which are active at length scales at primarily less than 1 μm. 37

Figure 2-8: Taken from Shoulders and Raines 2019 [Figure 1]; Overview of the collagen triple helix" 40

Figure 2-9: Taken from Shoulders and Raines 2009 [Figure 2]; modified figure to focus on the multi-level complexity of collagen, from single strands to collagen fibers. 41

Figure 3-1: Simplified 2D graphical representation of the test paradigms employed in this study, the HIS (left) and the MTS (right). 46

Figure 3-2: Rendered model of the pelvis system. 48

Figure 3-3: Complete experimental setup. 49

Figure 3-4: Example of Hologic Discovery output for a "High Quality" hip scan of an excised femur specimen. 51

Figure 3-5: Potted specimen (left) and frontal plane X-ray (right) of the potted specimen. 53

Figure 4-1: High quality hip specific DXA scan of a femur specimen, with associated image analysis results, including the measure for femoral neck aBMD used in this study. 70

Figure 4-2: Proximal femur specimen mounted in the mounting jig. The jig was affixed to the top surface of the force plate and placed beneath the load carriage of the vertical drop tower Hip Impact Simulator (HIS)..... 78

Figure 4-3: Example force time trace of a HIS impact trial. Diamonds and square points represent possible frames aligned with visual identification for the start of impact (diamonds) and moment of fracture (squares). 80

Figure 4-4: Measured F_x over *BMD* for females (filled circles) and males (open squares); lines of best fit (dotted line = female; dashed line = male) included to help illustrate the interaction. 88

Figure 4-5: Mean(SD) Predicted F_x for the forward selection model developed in this study (GLM) and the four previously published models included in this analysis (Courtney 1994, Courtney 1995, Dall'Ara 2013, Roberts 2010). Connected bars are significantly different ($p < 0.05$). 91

Figure 4-6: Mean Z score for AICc (Blue) and MSE (Orange) for the 4 models evaluated. 93

Figure 5-1: Isolated proximal portion of the femur, with SENB specimen extraction site highlighted (A - Inferior Femoral Neck). 108

Figure 5-2: Single Edge Notch Bending (SENB) target dimensions. 109

Figure 5-3: Image captured from high-speed microscopy-enabled videography during a high displacement rate (12 mm/s) experiment at: A) Frame 1, B) The frame of max stable crack growth, C) The first frame of unstable crack growth (frame of max stable crack growth +1) ... 110

Figure 5-4: Sample load displacement data, where the raw data (light gray) was filtered (black line), from which the linear stiffness region (green line) was defined from a linear fit between 20% and 50% of peak force. By extrapolating this linear fit for the full-displacement range (blue dotted line), the 95% secant modulus (dashed yellow line) was defined. P_q (red diamond) was defined as the final crossing point of the filtered line with the 95% secant line. Smoothness criteria (dashed red line) was defined between 50% P_q and P_q. 112

Figure 5-5: A) Example of a hydrothermal isometric tension (HIT) testing system, taken from Lee et al., 1995 for reference; B) actual HIT experimental setup. 114

Figure 5-6: Example of stress-temperature curves (dark gray lines) for paired-samples of a single specimen during a HIT experiment. *Max Slope* was extracted as the slope of the 5 °C segment with the largest gradient (solid black lines) observed between 70 °C and 85 °C. T_d (black circles) was identified as the temperature at which the backward projection of the linear portion of the curves (dashed black lines) intersected with the lowest observed stress (dashed gray lines). 116

Figure 5-7: Linear relationship between Max Slope and both K_q (blue dots) and J_q (red dots). 120

Figure 5-8: Linear relationship between Max Slope and both K_{Max} (blue dots) and J_{Max} (red dots). 123

Figure 6-1: Predicted F_x regressed over measured F_x, with linear fits (dotted lines). 138

Figure 7-1: Probability density distributions of Factor of Risk (FOR) from the Martel et al., 2020 probabilistic model of hip fracture risk. Solid lines represent distributions using the model developed in Study 2 of this thesis, whereas the dashed lines represent distributions using the Roberts et al., 2010 published model. In both cases, blue represents males and red represents females. 153

List of Tables

Table 2-1: List of previously conducted experiments wherein proximal femur bone strength was related to bone mineral density. Adapted from Table 1 of Dall'Ara et al. 2013a, with the addition of Gilchrist 2014. 28

Table 3-1: Specimen information for the A) Full Sample, B) HIS Sample, C) MTS Sample. Respective sample size, sex split, and mean (SD) are presented for the independent variables age, sex, BMD, FNAL, NSA, r, and CSMI, as well as for the dependent variables Fx and LR. Impact velocity (V) is presented for the HIS sample, while actual displacement rate (m) is presented for the MTS sample. 56

Table 3-2: Inidividual specimen details for all specimens included in this study. 57

Table 3-3: Results of the paired samples t-test comparing variables between the HIS and MTS experiments. 58

Table 4-1: Specimen details, including grouping used to block-randomly select specimens for the validation sample; specimens were ordered in order of ascending F_X 81

Table 4-2: Previously published models to predict femoral neck bone strength from femoral neck aBMD (BMD). 83

Table 4-3: Specimen information for the A) Full Sample, B) Model Sample, C) Validation Sample. Respective sample size, sex split, and mean (SD) are presented for the independent variables *a*, *s*, *BMD*, *r*, and *CSMI*, as well as for the dependent variable F_x 86

Table 4-4: Results for the GLM analysis of the main effects of the independent variables (*age*, *sex*, *BMD*, *r*, and *CSMI*) on the dependent variable (*Fx*). 87

Table 4-5: Results of the paired samples t-test comparing predicted F_x of the full sample obtained from the forward selection model developed in this study against the predicted F_x from four previously published models. 89

Table 4-6: Results of the paired samples t-test comparing sex specific predicted F_x of the full sample obtained from the forward selection model developed in this study against the predicted F_x from four previously published models. 90

Table 4-7: Resulting forward selection stepwise regression models for the 10 repetitions. 92

Table 4-8: The normalized Z Scores for the four models (BMD, Main, Inter, and Fwd) over the 10 repetitions. 93

Table 4-9:Results for the GLM analysis of the main effects of the independent variables (*a*, *s*, *BMD*, *r*, *CSMI*, and *d*) on the dependent variable (F_x). 96

Table 5-1: Variable syntax for elastic fracture toughness equations. 111

Table 5-2: SENB specimen information; total sample size, sex split, and mean (SD) of the independent variables *Max Slope* and T_d, as well as for the dependent variables K_q and J_q. 117

Table 5-3: Specimen details for the entire sample, including independent and dependent variables. 118

Table 5-4: Linear models predicting fracture toughness (K_q and J_q) from *Age*, *Max Slope*, and T_d. 119

Table 5-5: Linear models predicting fracture toughness (K_q and J_q) from *Age*, *Max Slope*, T_d, and *d*..... 121

Table 5-6: Linear models predicting fracture toughness (K_{Max} and J_{Max}) from *Age*, *Max Slope*, and T_d. 122

Table 5-7: Linear models predicting fracture toughness (K_{Max} and J_{Max}) from *Age*, *Max Slope*, T_d, and *d*..... 124

Table 6-1: Mean (SD) for the independent and dependent variables for the 12 samples used in this study. Note: BMD is from the femur that underwent the HIS bone strength experiments.. 133

Table 6-2: Specimen details for the entire sample, including independent and dependent variables 134

Table 6-3: Regression analyses adding in fracture toughness metrics (K_{Max} and J_{Max}) to both benchmark models. 136

Table 6-4: Regression analyses adding in collagen connectivity and stability metrics (*Max Slope* and T_d) to both benchmark models. 137

Table 6-5: Strongest overall linear model with all significant predictors. 137

List of Equations

$F = 2ghmk$ **[Equation 1]** 19

$F = mk \cdot v$ **[Equation 2]** 19

$Fx \sim 6492.97 * BMD * sex + 1522.53 * BMD - 2900.83 * sex + 2643.21$

[Equation 3] 87

$Fx \sim 1144.8 * age * BMD * r + 808.3 * age * sex * r - 20873.9 * age * sex * BMD - 95456.1 * BMD * r - 64455.0 * sex * r + 1572699.2 * sex * BMD - 2162.8 * age * r + 3651735 * age * BMD + 6841.7 * age * sex + 174342.0 * r - 2691381.5 * BMD - 496971.3 * sex - 11280.2 * age + 789042.7$ **[Equation 4]** 88

$Fx \sim 4601.15 * sex * BMD + 51.46 * age * sex - 20.19 * age * sex - 2.52 * r * age - 2.59 * r + 1878.57$ **[Equation 5]** 89

$Fx \sim 11007.7 * BMD + 1315.7 * sex - 3273.4$ **[Equation 6]** 96

$Fx \sim 1701.5 * sex * d + 7547.6 * sex * BMD - 10926.3 * CSMI * d - 6465.7 * CSMI * BMD - 5155.8 * CSMI * sex + 9944.7 * d + 10925.6 * BMD - 746.2 * sex + 26718.7 * CSMI - 24295.8$ **[Equation 7]** 96

$Kq = PqSBW32\ faW$ **[Equation 8]** 110

$faW = 3aW1.99 - aW1 - aW2.15 - 3.93aW + 2.7aW221 + 2aW1 - aW32$ **[Equation 9]** 111

$Jq = 2 * UqB(W - a)$ **[Equation 10]** 112

Chapter 1
Thesis Overview

1.1 Introduction

Due to continually increasing life expectancy and decreasing birth rates, the proportion of the population that is constituted by older adults has consequently increased. This has inevitably led to a similar "ageing" of healthcare problems, with consistently increasing rates of health issues experienced by older adults. One of those issues which occur predominately in older adults is fall-related hip fractures, an injury whose frequency is increasing by 1-3% yearly, worldwide (Cummings, 2002). From a Canadian perspective, fall-related hip fractures are a frequent and serious affair, with the rates of these injuries increasing almost exponentially after age 60 (Jean et al., 2013). With 90-95% of hip fracture hospitalization being the result of a fall-related event (Grisso et al., 1991; Wolinsky et al., 2009), these injuries are one of the most common and most costly of all "major osteoporotic fractures" (Burge et al., 2007). In fact, Nikitovic and colleagues in 2013 reported that the estimated annual cost of these injuries in Canada was $1.1 billion, a 69% increase from the $650 million estimate provided by Wiktorowicz and colleagues 2001 estimate (Nikitovic et al., 2013; Wiktorowicz et al., 2001). Similarly, an estimated 1.7 million hip fracture cases occur every year in the United States, which have an estimated cost of $12 billion annually (Burge et al., 2007). Clearly, these numbers convey the magnitude and severity of this problem, which is further emphasized by the associated one-year mortality of these injuries, occurring in 20-40% of cases (Ioannidis et al., 2009; Jiang et al., 2005).

Briefly, these injuries tend to occur as the result of standing height falls that end with lateral contact to the hip (Greenspan et al., 1998; Hayes et al., 1993; Pinilla et al., 1996), resulting in a unique loading scenario (de Bakker et al., 2009; Lotz et al., 1995). In fact, the loading experienced during lateral hip impacts (inferior femoral neck tension with superior femoral neck compression) is almost a mirror of what is typically experienced during stance and gait (inferior femoral neck compression with superior femoral neck tension), which may help explain the mechanics of this injury. Further research into the underlying mechanics of hip fractures have used cadaveric femurs, loading them in a manner similar to the loading experienced during a lateral hip impact, and studying the behavior and resulting fracture. In their 1994 and 1995 papers, Courtney and colleagues (1994, 1995) investigated hip fracture mechanics as a function of age and loading rate,

finding that both factors significantly affect the force required to fracture the femur. Specifically, specimens from older donors fractured at much lower loads (12-21% lower), and specimens loaded at lower rates also fractured at lower loads (regardless of age). However, one of their main findings was that of a strong positive correlation between the degree of mineralization of the proximal femur, quantified as the areal bone mineral density (BMD) of the femoral neck, and fracture force ($r^2 = 0.72$). This work has inspired many other studies, further investigating the effects of BMD, while also including other factors such as loading direction (Dragomir-Daescu et al., 2018; Pinilla et al., 1996) and femoral morphology (Cheng et al., 2007; Crabtree et al., 2002; Dinçel et al., 2008; Hansen et al., 2011). Though the relative influence of these factors on fracture force varies from study to study, the relatively consistent strength of the relationship between BMD and fracture force has led to measures of BMD, via low-dosage X-ray clinical methods such as Dual Energy X-ray Absorptiometry (DXA), being used as an easily accessible metric for assessing hip fracture risk (Akdeniz et al., 2009; S L Greenspan et al., 1994; Johnell et al., 2005; Kröger et al., 1994).

This relationship between femoral BMD and fracture load, also referred to as bone strength, has formed the foundation for many different methods and tools to assess an individual's risk of suffering a hip fracture. While some of these tools assess risk purely from an epidemiological perspective, using factors such as family history and personal habits estimate likelihood of fracture (ex: FRAX without BMD), the majority of these tools include femoral BMD as one of the primary factors to estimate risk or likelihood of suffering a future hip fracture (such as FRAX with BMD, Garvan, CAROC, Qfracture) (Aspray, 2015; Dagan et al., 2017; Kanis et al., 2012, 2008b). However, the most commonly employed method in a clinical setting is the T-score, which relates an individual's BMD to that of a young, healthy cohort to produce a score (similar to a Z-score). This score, which is used to classify bone health in relation to osteoporosis (with scores below -2.5 being associated with osteoporosis), is also used to categorize hip fracture risk. Specifically, individuals in the osteoporosis category of T-score are at an elevated risk of suffering hip fractures, based on epidemiological findings (Ardawi et al., 2005; Cummings, 2002; Fatayerji et al., 1999; Yeung et al., 2006). Unfortunately, this method lacks sensitivity, as only ~20-30% of hip fracture cases occur in individuals classified as having osteoporosis (Faulkner et al., 1999; Järvinen et al., 2015; Schuit et al., 2004; Siris et al., 2004; Stone et al., 2003). Consequently, a great deal of hip fractures occur in individuals who wouldn't be flagged as "high risk". This issue is further compounded by that fact that these similar methods that combine BMD with epidemiological

factors , such as FRAX, tend to underestimate risk in males and in certain disease states, such as diabetes mellitus (Fraser et al., 2011; Giangregorio et al., 2012). While it may be unreasonable to expect perfection in our ability to predict hip fractures, it is likely that our ability to do so is currently hindered by an incomplete understanding of fall-related hip fracture mechanics and the underlying mechanisms that contribute to the femoral bone strength. Further, despite the strong relationship between bone strength and BMD observed *in vitro*, it is possible that limitations and assumptions associated with current testing methodologies are some of the sources hindering accurate hip fracture risk assessment. Most notably, the use of high-rate constant displacement experiments to extract bone strength and the omission or lack of consideration of the potential role of the organic phase of bone are likely culprits, with clear gaps in the literature associated with both. While the lack of consideration for the organic phase of bone in relation to bone strength and clinical assessment of hip fracture risk may be a result of current limitations for clinical, *in-vivo*, methods to measure this phase, there currently exists a substantial gap in literature in terms of basic science research.

Interestingly, in the realm of materials science, the organic phase of bone is seriously considered, with researchers consistently finding that collagen plays an integral role in the material and mechanical behaviour of bone. Not only does the collagen content and quality of cortical bone affect material properties of cortical bone such as Young's modulus, strength and stiffness (Luo and Wu, 2020; Saito et al., 2011; Viguet-carrin et al., 2006), but also the resistance to crack growth, known as fracture toughness (Granke et al., 2015; Poundarik et al., 2015; Uppuganti et al., 2016; Vashishth et al., 1997; Willett et al., 2019; Zioupos et al., 2020, 1999). Indeed, studies investigating the fracture resistance of cortical bone have found that integrity of the collagen network, as well as the quality or maturity of the collagen (typically quantified via the types of crosslinks present) correlate strongly with fracture toughness (Burton et al., 2014; Willett et al., 2015; Zioupos et al., 1999). This is thought to have important implications for age-related fragility fractures, as age and disease-related changes in the organic phase of bone, such as increased presence of non-enzymatic crosslinks and advanced glycation end-products (AGE) (Modaresi et al., 2015; Ravarotto et al., 2018; Saito et al., 2006; Silva et al., 2009; Tomasek et al., 1994), may lead to lower fracture toughness due to the embrittlement of cortical bone, which may ultimately result in a decrease in bone strength. However, this body of work is not without its limitations, specifically in its applicability to fall-related hip fracture mechanics, as most of these collagen-

related investigations have used samples from bone sites that are not typical hip fracture locations, as well as using a loading rate that is much lower than what is experienced during a fall-related hip impact. While this does not diminish the importance and strength of the findings, it does hinder our ability to confidently apply these findings to the context of proximal femur bone strength related to fall-related hip fractures. Furthermore, despite the strong evidence of the role of collagen on the mechanical behaviour of cortical bone, little research has bridged the gap between this body of work (relating to the organic phase of cortical bone) and bone strength at the whole bone level, and none in the specific context of fall-related hip fractures.

These gaps in the literature, as well as a keen personal interest in injury biomechanics and fracture mechanics, led to the completion of this thesis. Specifically, the completed work aimed to address some of the limitations of the current understanding of hip fracture bone strength by challenging established *in vitro* testing methodologies (at both the macro and mesoscale) and by considering the role of the organic phase of bone on the strength of the proximal femur during fall-related hip fractures. Four studies were conducted to answer the four following questions: 1) Does a biofidelic experimental paradigm, a vertical drop tower hip impact simulator (HIS), produce different bone strength measures than a traditional low displacement rate material testing system (MTS) approach? 2) Does a predictive bone strength model developed using a biofidelic test paradigm result in a model that is more accurate than previously developed models? 3) Does collagen network integrity and connectivity affect the fracture toughness of inferior femoral neck cortical bone under impact-like loading? 4) Are metrics of collagen connectivity and quality significant predictors of proximal femur bone strength?

1.2 Overview of Proposed Studies

The ultimate goal of this thesis was to synergistically couple work in the domains of femoral bone strength testing and cortical bone collagen investigations to further improve our understanding of hip fractures, as well as potentially improve our ability to assess hip fracture risk. This thesis addressed this through four studies, a flow diagram of which can be seen in Figure 1-1. Beginning with a literature review (Chapter 2), the thesis follows with the details of the four proposed studies.

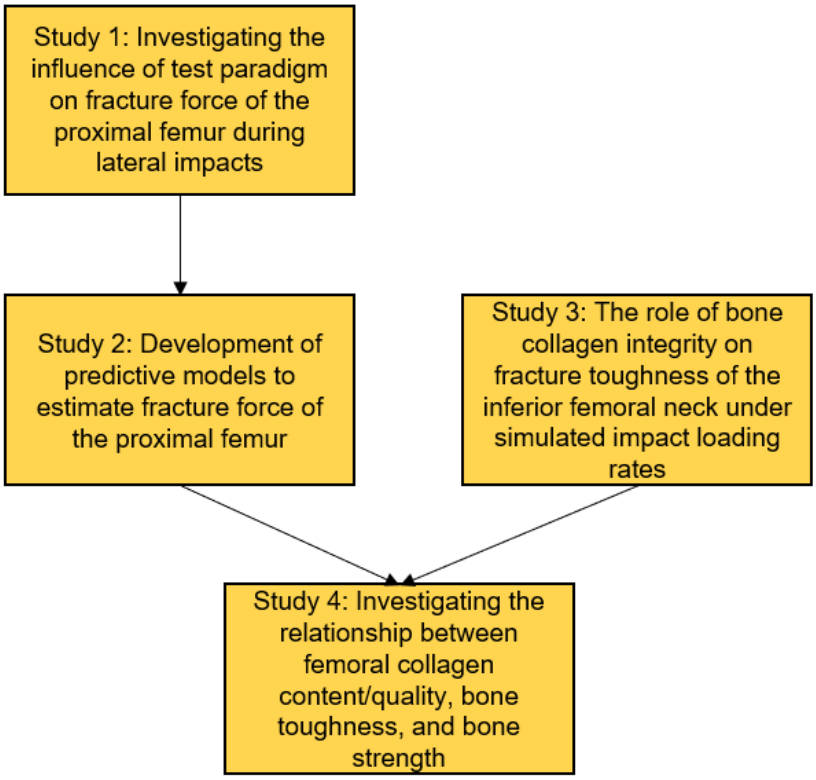

Figure 1-1: Thesis Study flow diagram with current study titles included.

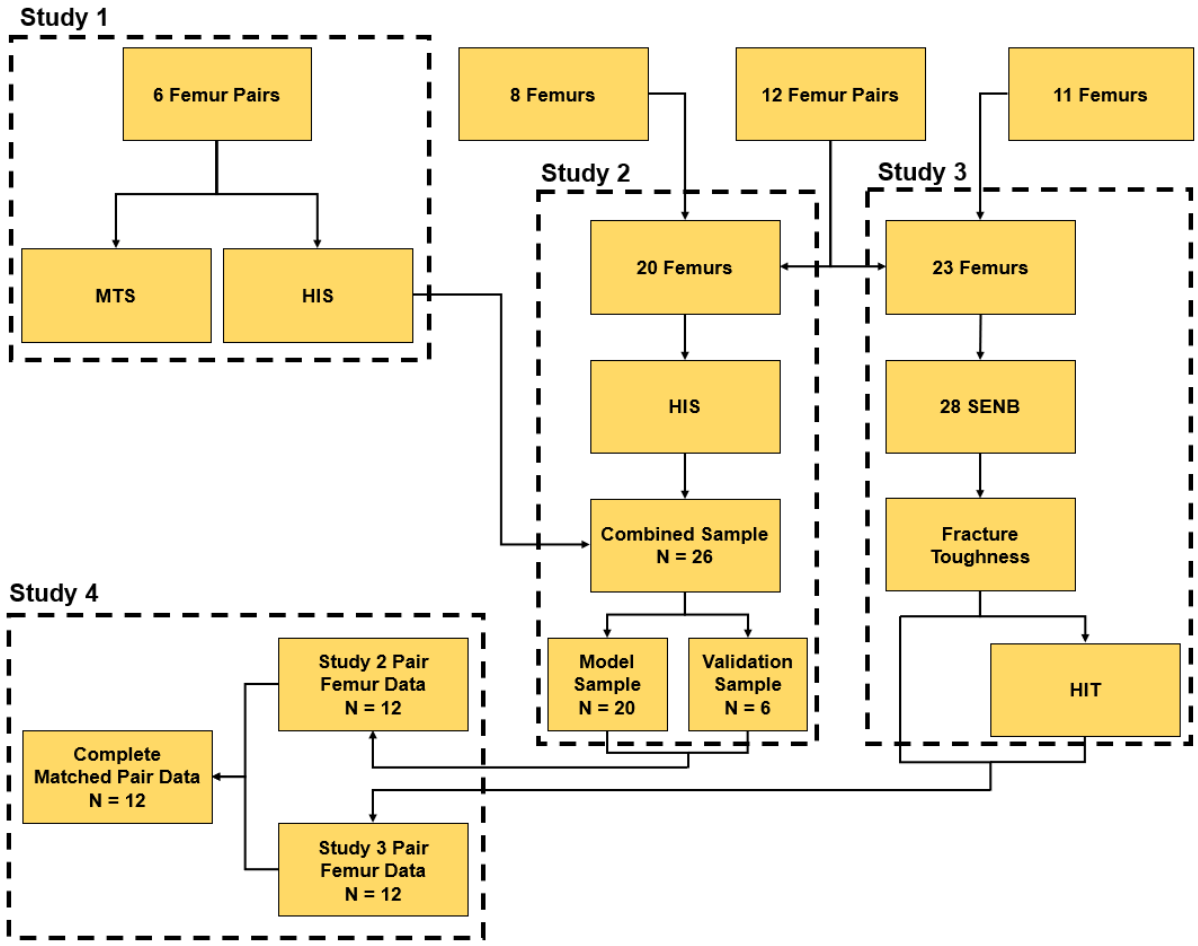

Figure 1-2: A simplified overview of the femur specimen split between studies and the general flow of data and results between studies. Specimen numbers present only reflect specimens and data that could be used for analysis.

In Study 1 (Chapter 3), a sample of matched-pairs fresh-frozen cadaveric femurs (N = 6 pairs) were used to compare the fracture force (bone strength) measured by two *in vitro* testing methodologies, where the standardized materials testing system (MTS) approach popularized by Courtney and colleagues (Courtney et al., 1995, 1994) was compared to a vertical drop tower hip impact simulator (HIS) paradigm. It was hypothesized the drop tower paradigm, which should produce more physiologically accurate hip impact dynamics, would result in significantly higher fracture force values compared to the matched-pair specimens tested in the materials testing system under high-rate constant displacement. This study aimed to fill a gap in the literature related to the effect of loading rate and impact dynamics on bone strength. While this question has been

previously investigated, the conclusions have been varied and often contradictory between studies (Askarinejad et al., 2019; Courtney et al., 1994; Dragomir-Daescu et al., 2018; Gilchrist et al., 2014). Additionally, while more recent investigations have attempted to address this question using more biofidelic experimental paradigms (Fleps et al., 2018; Jazinizadeh et al., 2020), this had yet to be investigated using a sample matched pairs of femurs tested with CSA aligned biofidelic experimental paradigm, as done in Study 1. This work also helped illuminate and contextualize the findings and conclusions of Study 2.

Study 2 (Chapter 4) built upon this concept, by introducing a novel regression model to predict bone strength, based on bone strength measured from the vertical drop tower hip impact simulator. Using a larger sample of fresh-frozen cadaveric femurs (N = 26), the relationship between measured fracture force (F_x) and factors such as age, sex, femoral morphology, and femoral neck areal BMD were investigated through multiple linear regression. This resulted in the development of identification of the strongest overall model for the prediction of femoral bone strength, based on a biofidelic experimental paradigm, the first of its kind. This model was then compared to models developed from the traditional material testing system approach. More specifically, the accuracy of the model developed in this study was compared to that of published models developed from material testing system experiments predicting bone strength from BMD; this was achieved via the use of a validation subset of the sample (N = 6) that was not used in the model development. The results of this study highlight the potential importance of using biofidelic experimental methods when investigating the underlying biomechanics of injury, and that models based on these methods may result in more physiologically accurate predictions. Furthermore, these results guided the model development strategy used in Study 4.

Focusing on the organic phase of bone, Study 3 (Chapter 5) investigated the relationship between cortical bone collagen quality (specifically network integrity and thermal stability) and fracture toughness of cortical bone samples (N = 28) from the inferior femoral neck when subjected to three point bending experiments at an impact-like loading rate. The purpose of this work was to investigate if the previously reported relationship between cortical bone fracture toughness and collagen observed during low-rate, quasi-static loading of non-clinical sites also applied to impact-like loading of a clinically relevant bone site like the inferior femoral neck. Additionally, the results of this study assisted in understanding of the role of bone collagen in the context of fall-related hip fractures as these findings were used in Study 4.

Finally, data from matched pairs split between Study 2 and Study 3 (N = 12) were aggregated in Study 4 (Chapter 6) towards investigating the role of the bone collagen on the bone strength of the proximal femur during fall-related hip fractures. More specifically, femoral fracture force (F_x) as well as femoral neck aBMD measured in Study 2 were combined with the metrics of collagen quality and fracture toughness that were measured in Study 3. Multivariate regressions were performed to investigate the relative roles of factors such as sex, femoral neck BMD, collagen network connectivity, collagen thermal stability, and fracture toughness on femoral bone strength (F_x). Forced entry approaches were used to quantify the additional variance explained by collagen related metrics when included in models predicting bone strength from a combination of femoral neck BMD and sex (significant predictors of F_x identified in Study 2). The results of this study provide direct evidence of the important contribution of collagen proximal femur bone strength in the context of fall-related hip fractures

Chapter 2
General Introduction & Literature Review

2.1 General Introduction:

Each year, approximately 1.7 million hip fracture cases are reported in the United States (Burge et al., 2007), which has an associated cost of roughly 12 billion dollars. While Canada has a smaller population, the relative rates oh hip fractures are no different than elsewhere in North America (Jean et al., 2013; Leslie, 2009; Loughlin et al., 1993; Stevens et al., 2008; Stevens and Sogolow, 2005), or worldwide (Hwang et al., 2011; Korhonen et al., 2013). Though fall-related injuries in general are a concerning issue for older adults, hip fractures are disproportionally costlier and more burdensome than other fall-related injuries, including other major osteoporotic fractures (Burge et al., 2007; Cummings, 2002; Heinrich et al., 2010) Potentially most concerning is the increased risk of death following a hip fracture, with a hazard ratio over 4 for both males and females in the first year following a hip fracture, which is higher than any other major osteoporotic fracture type (including vertebral, pelvic, forearm/wrist, rib, and other fractures) (Ioannidis et al., 2009). Considering these factors, it is no surprise that hip fractures are so widely researched and investigated. Yet, despite the vast amounts of research that has been conducted to better understand, predict, and prevent fall-related hip fractures, these injuries are still prevalent, and the intricacies of the mechanism of injury are still unclear. Therefore, the purpose of this literature review will be to review the scope of the problem that is fall-related hip fractures, the mechanics behind them, and the biology that may play a role, all within the context of the goals and hypotheses of this thesis.

2.2 Fall Related Hip Fractures

2.2.1 Epidemiology and Statistics

Fall related hip fractures, which account for 90-95% of all hip fractures (Wolinsky et al., 2009), fall under the largest categories of fall-related injuries, making up the large majority of associated hospitalizations in older adults (Billette and Janz, 2011, Canadian Community Health Survey, 2012). By reflecting on these two categories, we gain valuable insight into the epidemiology of hip fractures in older adults, namely that increased risk of falls and compromised

bone health are strongly associated with older age. While these factors will be more thoroughly explored when discussing risk factors (section 2.2.3), both will be briefly discussed here in the context of the epidemiology of fall-related hip fractures.

Beginning with increased fall risk, previous work has established that 29 to 45% of older adults report falling at least once a year, with 11.5% of individuals experiencing two or more falls a year (Blake et al., 1988; Gryfe et al., 1977; Loughlin et al., 1993). Previous estimates suggest that 30% of all fall-related hospitalizations are hip fracture cases (Canadian Community Health Survey, 2012). The increased rates of falls in older partly explains the dramatic increase in hip fracture rates after age 60 (Jean et al., 2013) (Figure 2-1). While worldwide rates of hip fractures have generally decreased over the years (Holt et al., 2009; Jean et al., 2013; Korhonen et al., 2013; Leslie, 2009), the relative aging of the population is projected to increase the annual number of hip fractures (Holt et al., 2009; Korhonen et al., 2013). Therefore, fall related hip fractures will likely become a large issue, consequently leading to an increase in the economic and healthcare burden of these injuries increases.

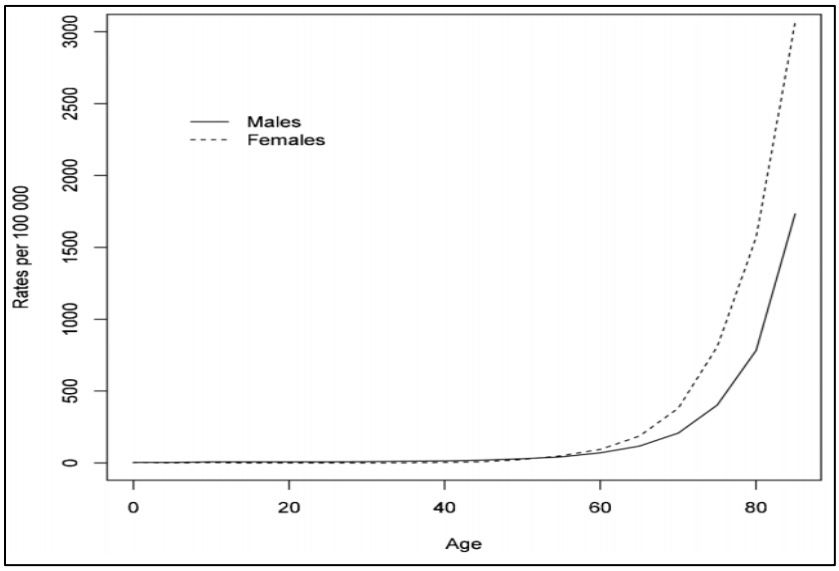

Figure 2-1: Canadian hip fracture rates by age and by sex (From Jean et al., 2013)

2.2.2 Consequences and Outcomes

As the foremost cause of fall-related hospitalizations in older adults, hip fractures are not only burdensome on healthcare services, but there are also many other negative consequences associated with these injuries. From an economic perspective, hip fractures are one of the most

costly injuries suffered by older adults, with a study by Burge and colleagues in 2007 reporting that while hip fractures made up 14% of all 2.05 million major-osteoporotic fractures (a classification of fractures related to compromised bone structure, or very low bone mineral density) in the US in 2015, they accounted for 72% of the $16.9 billion cost of this class of injury (Burge et al., 2007). With the relatively smaller population, hip fractures still pose a large economic burden, with the estimated annual cost of hip fractures ranging from 650 million to 1.1 billion dollars (Nikitovic et al., 2013; Wiktorowicz et al., 2001), with individual hip fractures costing an average $21 385 in Canada. As the overall cost of these injuries is inexorably linked to the number of hip fractures, the projected increase in hip fractures will consequently lead to an increase in cost, which is projected to reach $2.4 billion by 2041 in Canada (Wiktorowicz et al., 2001).

However, arguably more concerning than the economic burden are other direct physical consequences from these injuries. As a major traumatic injury to a critical load-bearing bone, hip fractures are debilitating at any stage of life, greatly reducing mobility and independence. In older adults, this loss of mobility can lead to long-lasting or permanent reductions in mobility, often resulting in important lifestyle changes such as transitioning from community to institutional dwellings (Wiktorowicz et al., 2001). Treatment and fixation of these injuries are also more complex in older adults and results in joint arthroplasty (rather than internal fixation) more often than younger individuals (Parker and Gurusamy, 2005). Additionally, as with other geriatric trauma, mortality is a very real issue associated with fall-related injuries, and more specifically, fall-related hip fracture (Spaniolas et al., 2010). Not only does mortality following a fall-related injury increase with age (Bhattacharya et al., 2016), mortality in these cases is significantly higher for older adults when compared to younger adults (Spaniolas 2010, 4.4% and 1.6% respectively). Furthermore, hip fractures account for most of these types of injuries in the older adult population, with a survey of 5088 older adult fall-related injury patients reporting 2346 (46.3%) hip fractures (Bhattacharya et al., 2016). More concerning is the morbidity and ultimately mortality related to these injuries (Johnell and Kanis, 2004). A study by Folbert and colleagues in 2017 reported 3.8% in-hospital mortality rate, similar to the 4.3% reported by Magaziner and colleagues in 1989, who also reported 17.4% of patients died within the first year following fracture (Folbert et al., 2017; Magaziner et al., 1989). Ioannidis and colleagues reported 23.5% of hip fracture cases resulting in death, a higher percentage than pelvic and vertebral fractures, the next two injuries with the highest

mortality (17.4% and 16%, respectively) (Ioannidis et al., 2009). Similarly, Jiang and colleagues in 2005 found one-year mortality was higher for males when compared to females (37.5% and 28.2%, respectively) (Jiang et al., 2005). However, these values do not capture the full extent of the morbidity related to these injuries.

Often overlooked due to the finality associated with mortality rates are the non-fatal complications that often occur subsequent to fall related hip fractures, where approximately 23% of older adult hip fracture patients undergo what is deemed a "Complicated Course" while in hospital. The associated complications that are most common with these injuries include delirium, anemia, UTIs and Pneumonia (Folbert et al., 2017). Not only do these complications increase the potential suffering of the individual, but can increase the length of the hospital stay (including an increase in the associated costs), and can place an additional burden on the patients physiologic reserve (Bhattacharya et al., 2016). Although none of these complications and concerns are unique to fall-related hip fractures, the substantive economic and physical burden associated with these injuries, coupled with relatively high mortality, makes hip fractures a unique sort of geriatric trauma worthy of further investigation and research.

2.2.3 Risk Factors

As previously mentioned, age seems to be one of the leading risk factors for suffering fall-related hip fractures. This is clearly demonstrated via the reported trends in hip fractures rates, with the rates increasing drastically after age 60 (Jean et al., 2013) (Figure 2-1), and by the reported number of fall-related hip fracture hospitalizations (Billette and Janz, 2011). However, the issue is indeed more complex, as it is in fact multiple age-related changes that lead to increased hip fracture risk, and therefore warrant assessment as individual risk factors. One of the primary age-related risk factors is the increased likelihood of falling. In fact, approximately 20% to 50% of older adults will experience at least one fall each year (Bergland and Wyller, 2004; Stinchcombe et al., 2014), with individuals living in long-term care institutions having higher rates of falls than community dwelling individuals (Rubenstein, 2006). This risk factor in itself is complex and has many associated factors that affect fall risk, including (but not limited to) gait impairments (or low gait speed), muscle weakness, sensory neuropathy, and visual impairments (Caillet et al., 2015; Campbell et al., 1989; Davis et al., 2019; Greenspan et al., 1998; Grisso et al., 1991; Rubenstein, 2006) While some of these factors are themselves age-related, it is important to note that others

are independent of age, yet still can greatly impact fall risk, and ultimately hip fracture risk. Despite the increased rates of falls in older adults, which increases risk of injury through a shear amplification of exposure, fall risk is not the sole contributor to the increased hip fracture rates observed in this population group. Indeed, the resilience or the strength of the bone is another key component in hip fracture risk.

Often the result of age-related physiological changes, the resilience of the bone to withstand fall-related hip impacts decreases with age, attributing partly to the increase in hip fracture risk. In studies by Courtney and colleagues in 1994 and 1995, in vitro experiments of cadaveric femurs revealed that the applied force necessary to cause fracture (fracture force or bone strength) was significantly lower in the sample of older adult femurs compared to the sample from younger adults (a mean fracture force of 3440 N compared to 7200 N) (Courtney et al., 1995, 1994). This difference has further been investigated in order to determine what specifically changes with older age leading to a decrease in bone strength, which in turn can be considered risk factors affecting hip fracture risk. One of the age-related physiological changes to have been found to be related to decreased bone strength are morphological and geometrical changes of the proximal femur, such as thinning of the cortices at both the femoral neck and trochanteric areas (Kaptoge et al., 2003), coupled with periosteal expansion (Luo, 2020). In general, morphological parameters like the ratio between femoral neck length and width seem to be important factors, such that femurs with relatively narrower femoral necks were more likely to be part of a fracture group (Dinçel et al., 2008). In fact, the geometry of the proximal femur may also determine which type of hip fracture occurs, as reported by Maeda and colleagues in 2011, where they observed that femurs with smaller neck shaft angles were more likely to have trochanteric fractures compared to a femoral neck fracture (Maeda et al., 2011). However, one of the greatest age-related changes that appear to affect bone strength is the demineralization of bone that occurs with age.

2.2.3.1 BMD and Osteoporosis

The factor often reported as the most important age-related change in bones strength is the relative decrease in bone mineral content (BMC), or more specifically bone mineral density (BMD), which has been observed with age (Hendrickx et al., 2015; Santos et al., 2017) (Figure 2-2). These changes in BMC and BMD, when coupled with the strong relationship between BMD and bone strength, may also help explain the higher rates of hip fractures experienced by females.

While the specifics of sex-dependent hip fracture risk differences will be discussed in a later section, it is important to draw the parallels between the increased number hip fractures and the more severe decrease in BMD observed in females (compared to males) (Hendrickx et al., 2015; Santos et al., 2017). Regardless of sexes, having low BMD, particularly of the femur, has often been identified as a risk factor for fall-related hip fractures (Akdeniz et al., 2009; Caillet et al., 2015; Dinçel et al., 2008; Greenspan et al., 1994; Johnell et al., 2005). As mentioned previously, studies have determined a relatively strong link between femoral bone strength and femoral BMD (R2 range = 0.64-0.92), often quantified via measures of areal BMD (aBMD) extracted from X-ray-based imaging methods such as Dual-Energy X-ray Absorptiometry (DXA) (Courtney et al., 1995, 1994; E. Dall'Ara et al., 2013; Manske et al., 2009; Roberts et al., 2010). While various studies have focused on different sites from which femoral BMD was measured (femoral neck, trochanteric area, total hip BMD, Ward's Triangle), the general findings report low femoral BMD as a risk factor (Ahn et al., 2014; Dinçel et al., 2008; Johnell et al., 2005; Rivadeneira et al., 2007), though some studies note that low BMD may be the result of other changes associated with increased risk, such as body composition, anthropometrics, age-related morphological changes, and even alcoholism (Ahn et al., 2014; Akdeniz et al., 2009; Beck et al., 2009; Berg et al., 2008; Compston et al., 1992; Edelstein and Barrett-connor, 1993). Specifically, due to the load-bearing nature of the femur, higher mass and higher BMI (specifically higher proportion of lean body mass) are associated higher BMD levels, which could partly explain the high risk of hip fractures in frail older adults who tend to have low BMI (Akdeniz et al., 2009; Beck et al., 2009), while morphological changes such as cortical thinning and increasing CSA (due to periosteal expansion) lead to less mineral distributed over a larger area, decreasing BMD (Kaptoge et al., 2003; Luo and Wu, 2020).

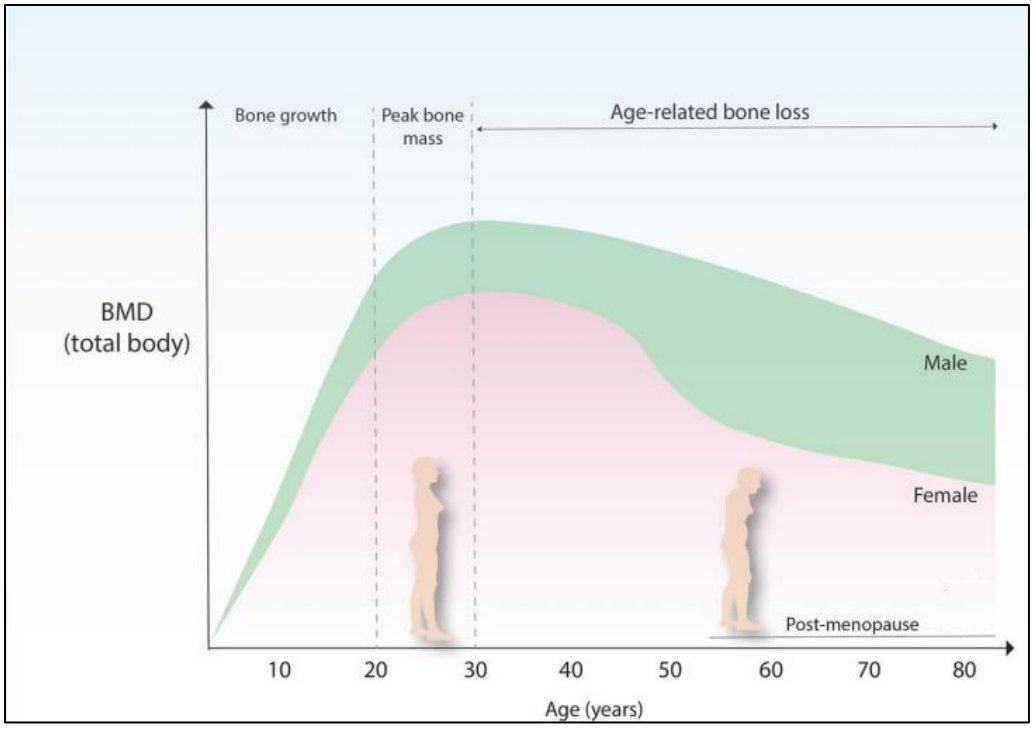

Figure 2-2: Taken from Santos et al., 2017 [Figure 1]: "Bone mass density (BMD) across the lifespan. Men exhibit higher BMDs throughout life and are less susceptible to age-related bone loss than women. Adapted from Hendrickx et al. (2015)."

Regardless, the relatively strong epidemiological evidence supporting low bone mineral density as a risk factor, coupled with the non-invasive, low radiation dose methods (DXA) used to quantify it, have driven the use of BMD based models as the primary method to distinguish hip fracture risk. In particular, DXA measures of BMD at various sites have been used as the main clinical method of identifying and diagnosing osteoporosis in individuals. Osteoporosis, the state of compromised or deficient bone structure, is itself a predominant risk factor for hip fractures, and all other fall-related fractures (often defined as major osteoporotic fractures) (Barry et al., 2012; Burge et al., 2007; Cummings, 2002). Based on site-specific measures of areal BMD, the World Health Organization (WHO) has developed a clinical criterion for identifying osteoporosis in the form of the T-Score, which relates an individual's BMD to that of a young healthy cohort. While it's typical for older adults to have lower BMD than younger individuals, resulting in a negative T-Score value, T-score between -1.5 and -2.5 are deemed as osteopenia, and scores below -2.5 being classified as osteoporosis. The osteoporosis classification is directly related to very low BMD levels, which has epidemiologic ties to fragility fractures, such as fall-related hip fractures

(Barry et al., 2012; Burge et al., 2007; Cummings-Vaughn and Gammack, 2011; Ioannidis et al., 2009). Therefore, the osteoporosis classification of T-Score for hip BMD is commonly used to identify individuals at high risk of suffering a fall-related hip fracture. However, despite the in vitro and epidemiological findings showing a strong relationship between femoral BMD (specifically trochanteric and femoral neck BMD) and bone strength or hip fractures, it is important to note that approximately 70%-80% of hip fracture cases occur in individuals who aren't classified as having low BMD (Schuit et al., 2004; Siris et al., 2004; Stone et al., 2003).

2.2.4 Screening and Prevention

Due to the many risk factors, as well as the steep consequences of these injuries, various methods for screening and preventing fall-related hip fractures have been established worldwide. With each method unique in its approach, or in the population it was designed for, the majority utilizes a combination of epidemiological trends or mechanistic relationships to estimate an individual's hip fracture risk. As previously mentioned, (in section 2.2.3), one of the most widely used screening methods is the T-Score, a metric whose purpose is to quantify an individual's bone health in order to diagnose osteoporosis. The T-Score takes into account age, sex, and BMD (typically measured via DXA) to compare an individual's bone health relative to a that of a healthy cohort and assigns a score, from which one of three classifications are assigned. These groups are directly linked to osteoporosis, and due to the epidemiological evidence of osteoporosis being a major risk factor for fall-related fractures in general, these categories are roughly related to hip fracture risk (particularly when the T-Score is based on proximal femur BMD measures). However, these general classifications do not provide sufficient specificity, resulting in many (approximately 70%) of fall-related hip fracture cases occurring in outside of the "high risk" osteoporosis classification (Schuit et al., 2004; Siris et al., 2004; Stone et al., 2003). Furthermore, T-score is highly site specific, with BMD measurements of different sites resulting in different T-Scores, with further discrepancies resulting from potential differences in BMD measurement (DXA vs. quantitative computed tomography, QCT) (Faulkner et al., 1999).

While the BMD based T-score may be an appropriate tool to diagnose osteoporosis, other methods have been developed in an attempt to provide further specificity when estimating hip fracture risk. The prime example of this is the Fracture Risk Assessment Tool (FRAX) developed by Kanis and colleagues (Kanis et al., 2008a). With 60-nationality specific tools, FRAX provides

an individual's 10-year risk of major osteoporotic fracture, as well as a risk of fall-related hip fracture. Citing the lack sensitivity from solely assessing risk based solely on BMD threshold, Kanis and colleagues developed a model that considers the presence of known risk factors (such as alcoholism, family fracture history, sex and age) when assessing probability of fracture, and can also include a measure of femoral neck BMD if available (Kanis et al., 2008a). More recent research from this group has revealed that the FRAX model without BMD provides comparable predictions to those based on BMD alone (Kanis et al., 2012), showing that FRAX can be a remarkably useful tool, especially in cases where BMD measures are not available

While FRAX is the most internationally recommended tool, other similarly structured models/screening tools include CAROC in Canada, QFracture in the UK, and GARVAN in Australia (Aspray, 2015; Dagan et al., 2017). All three of these tools incorporate both the presence of risk factors and BMD values, however, unlike FRAX, BMD is required to provide a prediction. When comparing the sensitivity of these models, AUC values of 82.7%, 81.5%, and 77.8% for hip fractures were found using QFracture, FRAX, and Garvan respectively (Dagan et al., 2017). These values were higher than the sensitivity for major osteoporotic fractures (AUC range 71.2-71.4%). However, it should be noted that previous studies comparing FRAX to Garvan reported lower AUC values for hip fractures, ranging from 0.67 to 0.70 (Bolland et al., 2011). Despite the relatively high sensitivity of these tools, the authors report that the evaluated tools still underestimate fracture risk. More specifically, FRAX has been found to underestimate risk in certain subsets of populations, such as underpredicting risk for men in Canada (Fraser et al., 2011), and individuals with diabetes (Giangregorio et al., 2012), and more generally, other investigations report that fracture risk calculators and tools such as FRAX or Garvan did not provide better fracture discrimination than models based on age and BMD (Bolland et al., 2011). In a seminal paper, Järvinen and colleagues report that currently used methods (BMD and multifactorial prediction tools) "are unable to identify a large proportion of patients who will sustain a fracture" and that these methods also generate a large number of false positives (Järvinen et al., 2015). In an attempt to address these issues, more mechanistically based methods, such as FOR, have been developed. These methods attempt to quantify hip fracture risk by predicting femoral bone strength and hip impact force (Bouxsein et al., 2007; Dufour et al., 2012; Martel et al., 2020; Roberts et al., 2010). While FOR methods, which are commonly and successfully applied in engineering settings, do significantly differentiate groups who have suffered hip fractures from those who haven't, using

currently developed models to predict bone strength from BMD result in the more than half of older adult males and almost all older adult females to fall below the predicted threshold of risk (Dufour et al., 2012). This suggests that, either the relationship is wrong (in that the model to predict bone strength from BMD are off), or there are currently undetermined mitigating or mediating factors that influence the relationship between BMD and bone strength. Therefore, our understanding of hip fractures is currently incomplete, and needs to be further studied if we want to better predict and prevent hip fractures.

2.3 Hip Fracture Mechanics

In order to properly address the issue of fall-related hip fractures, a more complete understanding of the underlying dynamics and mechanics of these injuries is needed. As previously discussed, older adults fall more frequently, and while age-related changes may explain why they are more prone to falls, it is also important to consider how they might fall. Specifically, investigations into how older adults fall compared to younger individuals revealed that, not only do older adults fall more often, but that older adults are less likely to break their falls with their hands or other limbs to slow the fall, resulting in more severe impacts (Feldman and Robinovitch, 2007). Additionally, the orientation of the body and the direction of the fall during the hip impact (Greenspan et al., 1998; Greenspan et al., 1994; Nankaku et al., 2005; Pinilla et al., 1996), as well as the impact location are important factors relating to hip fracture risk (Keaveny and Hayes, 1993). The following sections will explore the underlying mechanics of hip fractures by investigating the loading of the structures during the fall-related impact event, how this loading leads to failure, and what's been studied in terms of quantifying bone strength and ultimately fracture risk.

2.3.1 Loading and Failure

Many researchers have established that the biomechanics of any fall is an important factor to consider when studying any injury, especially traumatic ones like fractures (Blaha and Logue, 1989; Cummings and Nevitt, 1994; King, 2000). In the case of hip fractures, studies have found that the mechanics of the fall and impact are important factors (Cummings and Nevitt, 1994), and that previously mentioned BMD-based predictions of hip fracture risk depend on the loading experienced (Dall'Ara et al., 2013a), which can be influenced by the loading direction (Greenspan et al., 1994; Pinilla et al., 1996) and impact location (Keaveny and Hayes, 1993). During a fall,

which can be initiated through various means, the potential energy from the body that will be converted to kinetic energy upon impact depends on many factors. Anthropometrics, such as height and mass, any pre-existing velocity (from gait or the fall-inducing event), and even the orientation of the body (which will influence the kinematics of the fall) will all directly influence the impact energy (Greenspan et al., 1994; Pinilla et al., 1996). In a 1991 study, Robinovitch and colleagues set out to model the dynamics of lateral hip impacts, wherein they reported that the human hip-pelvis system behaves as a mass-spring-damper 2nd order system during these impacts (Robinovitch et al., 1991). More importantly, this group also found that, when predicting peak impact force, a simplified mass-spring model predicts impact force just as well as the full mass-spring-damper model, allowing for a simpler computation for predicting peak impact force of a fall-related hip impact (Robinovitch et al., 1991). Specifically, peak impact force can be estimated by computing

$$\boldsymbol{F = \sqrt{2ghmk}} \quad \textbf{[Equation 1]}$$

Where *g* is the gravitational acceleration, *h* is the height of the fall (specifically the vertical height of that the hip must travel to impact the ground), *m* is the effective mass of the hip-pelvis system (which is the portion of total body mass that contributes to the impact), and *k* which is the stiffness of the hip-pelvis system (which acts like the spring in the mass-spring model). This equation can be further simplified if using impact velocity rather than fall height, where

$$\boldsymbol{F = \sqrt{mk} \cdot v} \quad \textbf{[Equation 2]}$$

Modelling lateral hip impacts as such not only provides valuable insight into the dynamics of fall-related lateral impacts, but it also allows for an estimate of the impact force of a fall. This latter portion is of vital importance when predicting hip fracture risk from a mechanistic perspective, specifically by providing a value which can be compared to the estimated femoral bone strength. As in the case of FOR estimates, the ratio between predicted impact force and estimated bone strength should provide a quantitative assessment of risk of fracture (Bouxsein et al., 2007; Dufour et al., 2012; Roberts et al., 2010)

Further refinements of the above approaches and frameworks have yielded greater insight into the dynamics of fall-related hip fractures, even leading to more mechanistically based methods of hip fracture risk predictions. Building from Robinovtich and colleagues' 1991 work, estimates of pelvic stiffness have been refined (Laing and Robinovitch, 2008; Levine et al., 2013;

Robinovitch et al., 1997), the force-attenuating properties of the soft tissue overlying the greater trochanter have been considered (Bouxsein et al., 2007; Robinovitch et al., 1995), and effective mass have been identified such that biofidelic hip impacts can be simulated, as outline in the testing standard for simulated lateral impact tests of hip protectors has been developed (CSA Group, 2020). However, there are more unique aspects than impact energy and bone strength to fall-related hip fractures. In fact, the very modes of loading experienced at different aspects of the proximal femur are entirely unique to this lateral impact scenario. Specifically, the proximal femur undergoes loading most often when standing or load-bearing, which results in a particular combination of loading modes, particularly with the inferior femoral experiencing compression while the superior aspect is under tension. According to Wolff's Law (1892), bone tends to adapt and remodel based on the loading experienced (Wolff, 1892). Though general, the concept of bone adapting due to mechanical loading is supported by the skeletal adaptations seen in exercise and aging (Jones et al., 1977; Keaveny and Hayes, 1993; Woo et al., 1981), and may be better explained through the "Mechanostat" theory proposed by Frost, wherein mechanical induced signaling leads to skeletal adaptations (Frost, 1996). In the context of the proximal femur, typical loading experienced during stance and gait have resulted in the inferior femoral neck being relatively more resilient to compressive loading than the superior aspect (de Bakker et al., 2009). Consequently, during lateral hip impacts, the unique loading experienced is reversed, which the bone structure is not optimized for (de Bakker et al., 2009), as illustrated in Figure 2-3. This results in a unique loading scenario where the proximal femur may be more vulnerable and less resilient, which in theory would suggest that a lower force is necessary to induce fracture. This exact hypothesis was tested by Dall'Ara and colleagues in 2013, and by others (Eckstein et al., 2002; Lochmüller et al., 2003), wherein the ultimate strength of the proximal femur during stance loading was compared to that of lateral loading (such as in lateral hip impacts). The authors report that the ultimate strength of the proximal femur (bone strength) was three times less when laterally loaded (Dall'Ara et al., 2013a). Due to the unique morphology of the femur, specifically at its proximal portion, the orientation of the impact itself, which was previously defined as a risk factor, can influence the loading at the proximal femur and mechanically affecting fracture risk (Pinilla et al., 1996).

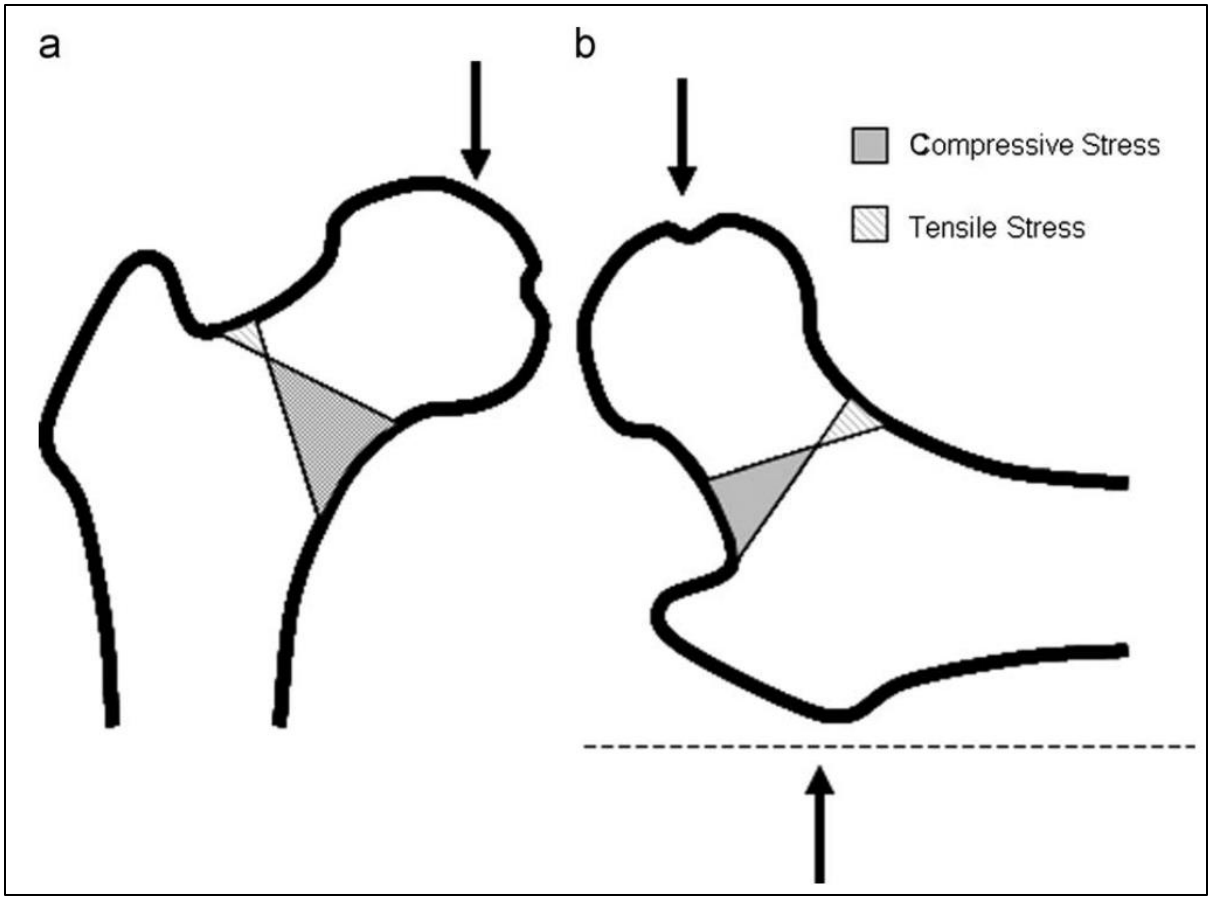

Figure 2-3: Taken from de Bakker et al. 2009 [Figure 1]: "The magnitude and nature of the stresses on the femoral neck differ depending on the applied load"

A limitation of the simplified mass-spring approach of predicting impact force is that it neglects certain characteristics of the fall; specifically, what may occur between fall initiation and impact. While it was previously mentioned that older adults are less likely to break or slow their falls by using their hands or limbs, pre-impact body adjustments can still occur, potentially reducing the severity of the impact. A study by Choi and colleagues in 2015 assessed security video recordings of older adult falls in long-term care facilities, wherein it was found that many different fall severity reducing strategies are employed, from a compensatory step following a loss of balance, to the use of hands to arrest or slow a fall (Choi et al., 2015). From these videos, vertical and horizontal impact velocities were estimated for the pelvis, hands, and head, and while limited to only forward or backwards falls, found that the impact velocity of most limbs were higher in general during forward falls. Regardless of the cause of the fall and the original orientation of the body during the fall, individuals most often attempt to reorient their bodies such that they land

posteriorly. Additionally, when the fall occurs, other bodily adjustments can occur, such as abduction of the impacting leg or bending of the knees to slow the fall. These various factors increase the variability of proximal femur loading during lateral hip impacts, ultimately increasing the variability of hip fracture risk.

As the hip contacts the impact surface, the soft tissue overlying the greater trochanter and the general hip area acts as a cushion, attenuating and deflecting some of the impact force. While the specifics are discussed in the following section, a study by Robinovitch and colleagues in 1995 quantified the force attenuation of these soft tissues, finding a 71 N reduction in peak impact force with every millimeter of soft tissue (Robinovitch et al., 1995). These findings provide a mechanistic explanation for the protective effects of the increased soft tissue which often accompanies larger mass and BMI, leading to lower hip fracture risk, up to a certain degree (after which risk increases with rising BMI) (Bouxsein et al., 2007; De Laet et al., 2005; Majumder et al., 2013). Further, these soft tissues may alter the path of force transmission of the hip impact, as well as further modulate the dynamics of the event, such as the loading rate, and ultimately affecting the stress and strains experienced at the proximal femur (Majumder et al., 2013). To further understand the specific loading experienced at the proximal femur during lateral hip impacts, researchers have use experimental simulations of these events to more accurately quantify impact loading.

2.3.2 Experimental Findings

As femoral bone strength and impact force are key mechanistic considerations when assessing hip fracture risk, much research has been devoted to experimentally investigating fall-related hip fractures. This body of work can generally be divided into two classes of experiments; those that quantify impact force and loading, and those that quantify bone strength and fracture force. Beginning with the quantification of impact force, insights can be gleaned through both observation and experimentation. Investigation into older adult falls via retrospective video analyses, such as those conducted by Choi and colleagues as well as Robinovitch and colleagues, not only provide information on the cause of the fall and pre-fall context, but can also reveal important details about the fall-impact event (Choi et al., 2015; Robinovitch et al., 2013). Choi and colleagues 2015 study reports a mean vertical impact velocity of 2.14 m/s, which was 46% lower than expected from a free-fall from standing height. While none of these falls included falls

that started in a lateral direction, these results may suggest that falls may be less severe than predicted, and yet hip fractures occur, further highlighting the current limitations and flaws in current hip fracture risk predictions.

In order to more directly quantify impact force and loading, many studies have used different experimental methods to simulate lateral hip impacts and measure the resulting impact force. While measuring falls from standing height is not entirely ethical or possible due to the fact that, even in younger adults, fall-related hip impacts are high-energy events that could lead to fracture (Kannus et al., 2006), researchers have employed methods to lessen the severity of the impacts. For example, Robinovitch and colleagues 1991 subjected human volunteers to relatively low-energy pelvis release experiments, wherein their pelvis was raised above a force plate and released to induce an impact (Robinovitch et al., 1991). This test paradigm uses sub-injurious impacts (impact velocity = 0.5 – 1.0 m/s) to quantify the associated impact dynamics, which is then used to inform simulations or estimates at clinically relevant impact velocities. Although this experimental paradigm continues to be used to further investigate hip impact mechanics (Bhan et al., 2013; Laing and Robinovitch, 2010; Levine et al., 2013; Martel et al., 2018; Pretty et al., 2017), other experimental paradigms have been developed and used, the first of which includes standing height falls onto mats or other cushioning material. This paradigm, as employed by Nankaku et al., 2005, allow for a more fulsome investigation into the kinematics of the fall and impact, while being limited in the ability to quantify the impact dynamics (Nankaku et al., 2005). However, these investigations were able to quantify impact velocity for various types of falls, specifically finding an average impact velocity of approximately 2 m/s for lateral hip impacts. These values generally align with the observational findings of Choi et al. 2015, providing values which can be used to ultimately estimate impact force (Choi et al., 2015). Another more recent paradigm developed by Fleps and colleagues simulated pendulum-like lateral hip impacts involving the use of whole cadaveric femur and pelvis skeletal structures encased in ballistics gel (Fleps et al., 2019). This paradigm not only allowed the investigators to quantify the dynamics of the fall and impact, but also allows for hip fractures to be induced and measured. Using this approach, the simulated impacts had an average velocity of 3.07 m/s, resulting in peak impact forces ranging from 2947 N to 7601 N. The range of values was mostly driven by differences in the thickness of the simulated soft tissue, ballistics gel in this case, overlying the greater trochanter, which is known to contribute to force attenuation during lateral hip impacts (Bouxsein et al., 2007; Majumder et al., 2013;

Robinovitch et al., 1995). This approach provides a novel alternative to study hip impact dynamics, as well as bone strength.

In terms of quantifying the strength of the proximal femur during lateral hip impact and subsequent fractures, the realities of the situation necessitate the use of cadaveric tissue or surrogate materials and systems. Investigations into proximal femur strength in the context of fall-related impacts performed by Courtney in 1994 and 1995 (citing Lots and Hayes 1990 for the specific methodology) revealed the age-related decline in bone strength of the proximal femur, as well as reaffirmed the relationship between bone strength and BMD (Courtney et al., 1995, 1994; Lotz and Hayes, 1990). The paradigm involves the use of a material testing system (MTS), typically a servo-hydraulic instrument such as an Instron MTS, to laterally compress a cadaveric proximal femur specimen at a constant displacement rate until failure. Specifically, in the investigations by Courtney and colleagues, the specimen was fixed such that the testing system cross head would compress the head of the femur while the greater trochanter (covered with a hemispherical polymethylmethacrylate cap) rested on an impact plate (supported by a load cell to measure compressive force). To accurately emulate the position of the femur during lateral hip impacts, the specimen was further positioned with a slight (10 degrees) adduction angle and rotated to 15 degrees internal rotation. A displacement rate of 100 mm/s was used to emulate the high-rate loading of lateral hip impacts. This same methodology has been used and replicated many times since then, and has since been unofficially been adopted as the standard for this type of work (Dall'Ara et al., 2013a; Dragomir-Daescu et al., 2018; Eckstein et al., 2002).

While elements of this method aren't necessarily biofidelic, such as the use of constant displacement and the absence of soft tissue or pelvic compliance, it has been used to reliably induce hip fractures, resulting in relatively consistent results relating to the relationship between bone strength and BMD. In fact, it is from experiments using this, or very similar, methodology that most currently used BMD based predictions of bone strength have stemmed (Courtney et al., 1995; Dall'Ara et al., 2013a; Roberts et al., 2010). However, this methodology does have its limitations, primarily in terms of boundary conditions and physiological accuracy, or biofidelity. It should be noted that certain experiments have attempted to address these limitations in the hopes of developing methodologies that result in more physiologically accurate testing and results. One notable example is the study by Gilchrist and colleagues in 2014, wherein the effect of loading rate and test paradigm on the mechanical behaviour of the proximal femur was investigated. While

the results of this experiment revealed that, when tested at sub-fracture levels, there were no differences in the mechanical behaviour of bone between constant displacement rate and fall simulation paradigms, a significant difference was observed between the paradigms during fracture trials (Gilchrist et al., 2014). Specifically, the investigators found that displacement rate is mediated by the stiffness of the specimen, and therefore, uniformly applying a constant high-displacement rate may result in non-biofidelic (or nonphysiological) loading conditions, which could result in inaccurate bone strength measurements. Though these results suggest that test paradigm may influence bone strength, and that the use of the standard high-displacement rate testing paradigm may result in higher measures of bone strength, the authors note that certain limitations of the study, such as the lack of matched-pair samples and large intergroup variance in aBMD, prevents a definitive conclusion (Gilchrist et al., 2014). Regardless, the findings of this study bring into question the use of bone strength estimates based on constant displacement rate experiments, potentially explaining some of the discordance in hip fracture risk assessment; this necessitates further investigation. Additionally, there has been a recent trend of investigators moving towards, or at the very least including, fall simulation paradigms rather than just constant displacement rate tests when studying lateral hip impact mechanics (Enns-Bray et al., 2019a; Fleps et al., 2018; Jazinizadeh et al., 2020).

Beyond extracting simple fracture force, these experiments have also been used to investigate fracture mechanics on a more fundamental level, specifically quantifying the stresses and strains experienced during this type of loading. While the material properties of bones are briefly discussed in a later section (section 2.4.1.1), studies have used these values, coupled with the current understanding of fall-related hip fracture impact dynamics, to estimate tissue level loading. Specifically, Finite Element Models (FEM) and Analyses (FEA) have further revealed the unique loading that occurs during lateral hip impacts, as compared to gait-related loading, where a complete inversion of compressive and tensile loading is observed (Lotz et al., 1995). In fact, Lotz and colleagues 1995 investigation revealed that, unlike during gait, an estimated 96% of the load is concentrated at the cortical bone of the femoral neck, potentially providing a mechanistic explanation for the clinical relevance of this site (Lotz et al., 1995). A more recent FEA investigation by Dall'Ara and colleagues in 2013 reported a high-stress area in the inferior femoral neck during lateral hip impact-like loading, even allowing for the determination of failure location (Dall'Ara et al., 2013b). Using this mechanistic approach, their FE model predicted

femoral bone strength better than typical aBMD approaches. Various FEM and FEA studies have since been conducted, further refining the model meshes while also adding other elements, such as the inclusion of the pelvis and soft tissue (Enns-Bray et al., 2019b; Majumder et al., 2007). Some of these models have even been applied to clinical populations albeit retrospectively. One such case is Enns-Bray and colleagues 2019 report, wherein subject specific biofidelic FEMs were able to classify hip fracture cases. Furthermore, when removing individuals who didn't fall (deemed non-fallers), this approach performed significantly better than BMD based methods (AUC of 0.85 vs 0.74 for model predicted maximum volumetric strain and total femur aBMD, respectively). While these FEM models continue to provide better hip fracture prediction than typical BMD based methods, their reliance on computationally heavy models, some of which must be subject specific, prevents them from being applied clinically on a wide scale. Despite this limitation, FEM and FEA provide access to a level of detail that is not typically available during standard in vitro experiments, further improving our understanding of the underlying mechanics of fall-related hip fractures.

2.3.3 Determinants of Bone Strength

As evident from the previous sections, a fair amount of research has been conducted with the goal of better understanding bone fracture mechanics, and more specifically fall-related hip fractures. These investigations have revealed much, with the most commonly cited finding being the strong positive association between bone strength and the degree of bone mineralization (often capture by areal BMD measurements (Courtney et al., 1994, 1995; Dall'Ara et al., 2013a; Roberts et al., 2010). Other factors that have been identified and found to influence bone strength include femoral geometry (Cheng et al., 2007; Crabtree et al., 2002; Dinçel et al., 2008; Gregory et al., 2004; Hansen et al., 2011), loading rate (Courtney et al., 1994; Dragomir-Daescu et al., 2018; Gilchrist et al., 2014; Jazinizadeh et al., 2020), and loading direction (Dall'Ara et al., 2013a; Eckstein et al., 2002; Lochmüller et al., 2003; Pinilla et al., 1996). Additionally, cortical bone strength is affected by its microstructure, referring to organizations of the osteons, Haversian and Volkman's canals, as well as any related defects or damage (such as pores and accumulated microdamage) (Augat and Schorlemmer, 2006; Bouxsein, 2005). However, despite these findings, there are still aspects of bone fracture mechanics that are unclear or haven't yet been directly investigated. Furthermore, despite strong relationships drawn from thorough *in-vitro*

experimentation, our ability to accurately predict those at risk of fall-related hip fractures is still limited.

2.3.4 Mechanistic Fracture Risk:

The results of *in-vitro*, *in-silico*, and *in-vivo* experiments on the dynamics of fall-related hip fractures have been synthesized into various models and methods to predict bone strength, and ultimately hip fracture risk. While some of the most commonly clinically utilized methods of hip fracture risk assessment, such as FRAX, CAROC, GARVAN, and the T-Score, are partly mechanistically based on the relationship between bone strength and femoral aBMD (Aspray, 2015; Cummins et al., 2011; Dagan et al., 2017; Fraser et al., 2011; Johansen, 2012; Kanis et al., 2018, 2012, 2008b; W. D. Leslie et al., 2012), these methods have been shown to have their limitations in terms of predicting individuals at risk fall-related hip fractures (Faulkner et al., 1999; Giangregorio et al., 2012; Siris et al., 2004; Stone et al., 2003). However, other more mechanistically based methods of predicting bone strength and hip fracture risk exist. Firstly, some of the earliest work investigating the relationship between femoral BMD and bone strength provided regression equations to estimate bone strength from measures of femoral neck BMD (Cheng et al., 1997; Courtney et al., 1995, 1994). Since then, other estimates have been developed using similar methods, resulting in some age or sex specific estimates, all with moderate to strong R^2 values, as displayed in a table from Dall'Ara et al. 2013 (Table 1, adapted from Table 1 of Dall'Ara et al. 2013a).

Table 2-1: List of previously conducted experiments wherein proximal femur bone strength was related to bone mineral density. Adapted from Table 1 of Dall'Ara et al. 2013a, with the addition of Gilchrist 2014.

Reference	Loading Rate (mm/s)	Sample Size	Best Predictor	Best R2
Bouxsein et al., 1999	100	25	Trochanteric BMD	0.92
Cheng et al., 1997	14	70	Trochanteric BMD	0.88
Courtney et al., 1994	100	20	Femoral Neck BMD	0.72
Courtney et al., 1995	2	17	Femoral Neck BMD	0.92
Dall'Ara et al., 2013a	0.082	36	Femoral Neck BMD	0.80
Dragomir-Daescu et al., 2011	100	18	Total Hip BMD	0.79
Gilchrist et al., 2014	0.5	20	Total Hip BMD	0.94
Hansen et al., 2011	0.033	31	Trochanteric BMD	0.78
Kolta et al., 2012	2	12	Trochanteric BMD	0.78
Le Corroller et al., 2012	0.167	21	Femoral Neck BMD*	0.77
Manske et al., 2009	100	35	Femoral Neck BMD	0.64
Pinilla et al., 1996	100	11	Total Hip BMD	0.68
Roberts et al., 2010	100	73	Femoral Neck BMD	0.70

Towards predicting hip fractures risk, some of these bone strength models have been combined with impact dynamics models in order to provide a more mechanistically based evaluation of hip fracture risk. One such approach is the application of the Factor of Risk principles, or FOR, which relates the potential exposure to the tolerance of the tissue in question (Bachmann et al., 2014; Dufour et al., 2012; Hayes et al., 1991; Martel et al., 2020; Roberts et al., 2010). A similar approach is often used in engineering contexts, for example, when determining the safety factor for various designs and structures, which is the ratio between the theoretical strength of the material and the applied load. In the realm of hip fracture risk estimates, the exposure comes in the form of an estimated impact force, and the tissue tolerance stems from predicted bone strength (Bouxsein et al., 2007; Cummings and Nevitt, 1994; Robinovitch et al., 1997, 1991; Sarvi and Luo, 2019). Driven by various impact dynamics models, such as the lumped-parameter model (i.e.: mass-spring model) outlined by Robinovitch 1991, or other more complex models, such as van den Kroonenber et al. 1995 and Majumder et al. 2007, the impact force resulting from a fall onto the hip can be estimated for a given individual or scenario (Majumder et

al., 2007; Robinovitch et al., 1991; van den Kroonenberg et al., 1995). This, when coupled with a predicted bone strength (from one of the above discussed models) allows for a Factor of Risk to be computed, which, theoretically, gives a mechanistic insight into an individual's relative fracture risk (Bachmann et al., 2014; Dufour et al., 2012; Roberts et al., 2010).

One great example of the clinical applicability of Factor of Risk (FOR) as a method to quantify hip fracture risk is Dufour et al.'s 2012 retrospective analysis of the Framingham data set (Dufour et al., 2012). Specifically, the authors computed FOR a sample of 1100 older adult who were followed over a two-year period. Individuals were divided first by sex, and then into groups who either experienced a hip fracture, or did not, where they found that FOR was significantly higher for both the fracture groups for both sexes (Dufour et al., 2012). While promising, one major flaw of this approach was also revealed in the results reported by this group, which was that, using current knowledge, fractures often occurred when estimated FOR was well below the value of 1 (which is when the applied load would be equal to the tolerance). This was apparent in the female groups, where the fracture group had a mean FOR of 0.49, meaning that fractures occurred even though the estimated applied load (impact force) only reached half the magnitude of the estimated tolerance (bone strength). While this limitation is partly due to the simplification associated with this approach, the majority of the blame lies with how the applied force and the tissue tolerance are estimated. While further details on the limitations are provided in the Dufour 2012 article, as well as Martel et al. 2020, the main factors that contribute to this mismatch is the likely overestimation of the force attenuation provided by the soft tissues overlying the hip (greater trochanter) (Robinovitch et al., 1995), and the potential inaccuracy in the predictions of the bone strength (Dufour et al., 2012; Martel et al., 2020). Part of the aim of this thesis is to investigate this potential inaccuracy in bone strength predictions, which may be due to the non-physiologic loading used in standard proximal femur bone strength testing.

2.4 Bone Biology

Bones are complex biological structures that provide various functions for the human body. The complexity of this material stretches across multiple scales (Figure 2-4), from the overall structure and morphology of the individual bones (each bone fulfilling unique roles, from protection to anchor points for tissue and musculature), all the way down to the molecular level, where hydroxyapatite crystals, constituting the majority of the inorganic phase, are embedded in a

matrix of type I collagen (Stock, 2015; Weiner and Wagner, 1998). This section of the literature review will explore bone from various perspectives towards providing a holistic overview of this class of tissue, specifically focusing on the femur, its structure and composition. Additionally, further emphasis will be provided on the organic phase of bone, its role in bone structure and function, and how it may contribute to bone strength, ultimately affecting fracture risk.

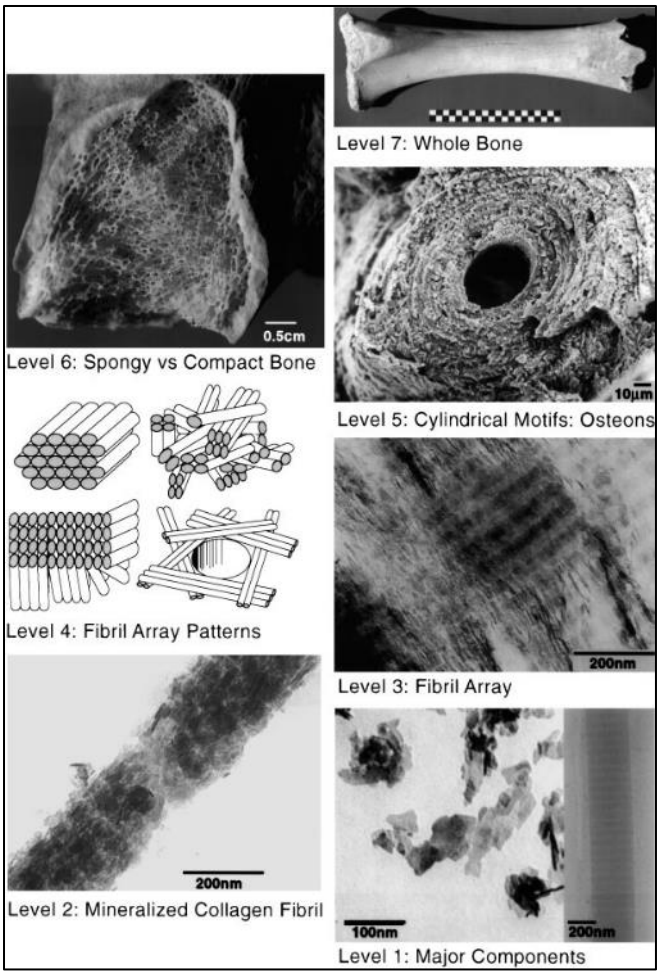

Figure 2-4: From Wiener 1998 – "The 7 hierarchical levels of organization of the bone family of materials".

2.4.1 Femoral Structure and Morphology

At the largest scale, the whole bone (Level 7 on Figure 2-4) is a complex structure, with each bone of the body having a unique shape, as well as a purpose uniquely related to its shape and form. The femur is no exception, with a particularly unique shape and function well suited to the typical loading experienced through human stance and gait. Of interest in the context of fall-

related hip fractures is the proximal portion of the femur (Figure 2-3) which is where these fractures typically occur (Tal et al., 2015). During the lateral hip impacts, the effective mass of the pelvis and upper body are transferred and driven downward (toward the impacting surface) through the interface of the femoral head and pelvic acetabulum. All the while, the lateral aspect of the femur, particularly the greater trochanter, make indirect contact with the impacting surface (through overlying soft tissue), directed upwards, creating a bending load scenario in the proximal femur. This results in the inferior aspect of the femoral neck to be subjected to tensile loading, compared to the typical compressive loading experienced during stance and gait. Due to the unique loading experienced during lateral hip impacts (de Bakker et al., 2009) (Figure 2-3 from section 2.3.1), hip fractures often occur in the cervical (femoral neck) or trochanteric regions of the proximal femur (Tal et al., 2015).

The loading, or more specifically the stresses and strains, resulting from these impacts are directly affected by the shape and geometry on the femur itself, especially since bone is not simply a uniform block of isotropic material. Rather, with the dense cortical shell and the more diffuse trabecular (or cancellous) bone on the interior, bone more closely resembles an orthotropic material, and the resulting stresses will not be uniform throughout the structure. It is for these reasons that, when studying bone strength and bone fracture mechanics, morphology and geometry are often quantified and considered (Cheng et al., 2007; Crabtree et al., 2002; Dinçel et al., 2008; Gregory et al., 2004; Hansen et al., 2011). While previous research does not necessarily reach consensus, it does provide insight into features of femoral geometry and morphology that seem to influence the stresses and strains experienced during lateral hip impacts. Aspects such as the length of the femoral neck axis (Femoral Neck Axis Length, FNAL), its intersection with the long axis of the diaphysis (from Femoral Shaft Neutral Axis, FSNA), and the angle between the two (Neck-Shaft Angle, NSA) directly influences the relative moment arm through which bending moments act during lateral hip impacts (Chappard et al., 2010; Elbuken et al., 2012; Maeda et al., 2011; Partanen et al., 2001). If the shape of the femoral neck is simplified to a narrow pipe or cylinder, its width or cross-sectional area (CSA) of the femoral neck, along with the relative thickness of the cortical shell (Cortical Thickness), will directly affect the area moment of inertia (influenced primarily by the difference between the outer and inner diameter of the cross-section) (Cheng et al., 2007; Gong et al., 2016; LaCroix et al., 2010) (Figure 2-5). Add to this the influence of the relative density of the bone across this cross-section, and the cross-sectional moment of inertia

(CSMI) directly relates to the structures bending resistance (Gong et al., 2016; Szulc et al., 2006). These morphological features and measures have all been found to, in one way or another, affect the stresses, strains, or more general loads experienced in the proximal femur during lateral hip impacts.

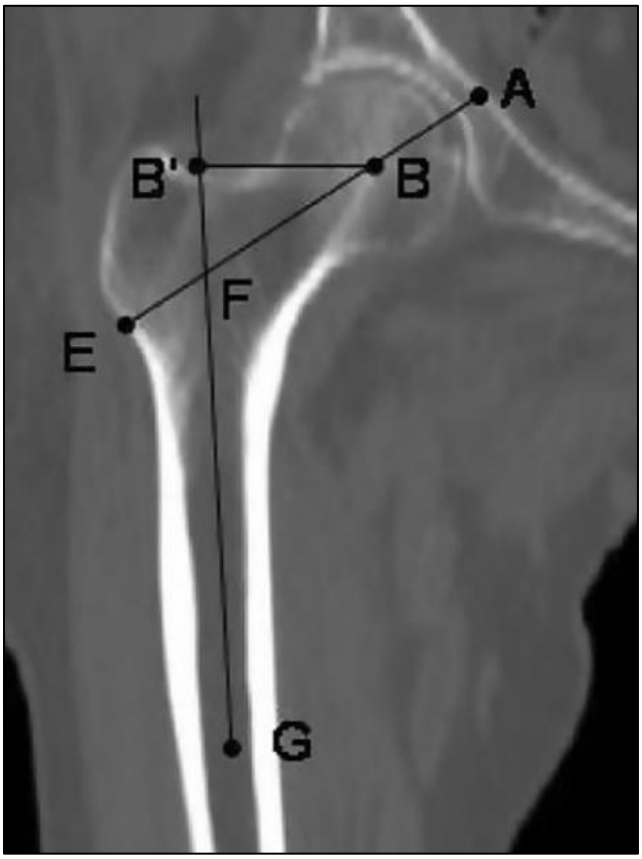

Figure 2-5: Taken from Maedea 2011, used to illustrate various morphological measures. Segment B'G represents the FSNA, while segment BE represents the FNAL; the angle between these two (at F) represents the NSA.

While briefly introduced in the previous paragraph, both the cortical and cancellous bone can affect loading at the proximal femur during lateral hip impacts, affecting not only shape and geometry, but also influencing the relative density at any point within the structure. However, for the purposes of this thesis, the focus will be placed primarily on the cortical bone of the proximal femur. The reasoning for this emphasis is not only a result of logistic considerations (as will be detailed in the methods of the proposed studies), but also because cortical bone provides an excellent source for extracting mineralized type I collagen, the investigation of which (in the context of proximal femur bone strength) is one of the key purposes of this thesis. Beyond these

points, there is also a mechanical basis for this emphasis, as previous Finite Element Analyses (FEA) have estimated that approximately 96% of the load experienced at the femoral neck during lateral hip impacts occurs in cortical bone (Lotz et al., 1995). The following section will explore cortical bone in further detail, specifically detailing it as a structured tissue and as a material.

2.4.1.1 Cortical Bone

Cortical bone consists of tightly packed structures known as osteons (Level 5 of Figure 2-4), which are formed from concentric layers of bone, or lamellae. Osteons are centered about openings known as the Haversian canals, with inter-osteonal canals known as Volkmann's canals; these canals are where blood vessels can be found in bone (Figure 2-6). Further organization can be found on a smaller level, within and between lamellae, wherein lacunae, which are small oval cavities containing osteocytes, are housed between lamellae, and canaliculi, which are small canals that span across the lamella. This collection of structures and features, across various scales, constitute the "microstructure" of cortical bone, which helps explain the inherent complexity of bone as a material. In fact, as imaging capabilities have developed to allow for quantification of these features with ever-increasing resolution, research has shown that these microstructures influence bone fracture, potentially through various toughening mechanisms (Nalla et al., 2003). In fact, the lamellar structure of the osteon may contribute to fracture toughness via crack deflection, similar to that seen in fiber-reinforced composites (Carter and Hayes, 1977; Guo et al., 1998). However, other features of cortical bone microstructure, such as porosity, low relative mineral density, and the presence of microcracks (or the accumulation of microdamage) may contribute to bone fragility and increased fracture risk seen in older age (Augat and Schorlemmer, 2006; Bell et al., 1999; Bouxsein, 2005; Chevalley et al., 2012; Frost, 1960; Hazenberg et al., 2007; Schaffler et al., 1995). While not a focus for this thesis, microstructure may indeed play a role in bone strength related to fragility fractures, major osteoporotic fractures, and even fall related hip fractures.

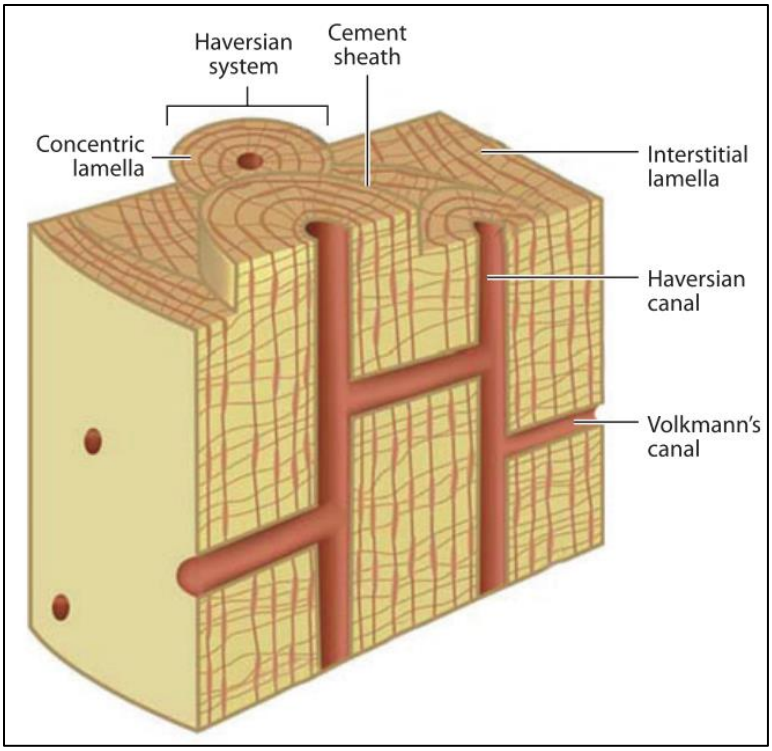

Figure 2-6: Taken from Launey et al. 2010; Schematic representation of the inner structure of cortical bone.

As previous investigations have revealed that almost all stress experienced at the femoral neck during lateral hip impacts is at the cortical shell (Lotz et al., 1995), the cortical bone has been the focus of much research. Beyond quantifying bone strength at the whole bone level, cortical bone has been isolated in order to quantify material properties such as Young's modulus (E) Poisson's ratio (ν) and Fracture Toughness (K or J). In general, the elastic modulus of human cortical bone (under longitudinal, tensile loading) is approximately in the range of 15-20 GPa (Vashishth et al., 2001; Woodside, 2015; Zioupos and Currey, 1998; Zysset et al., 1999); however, the modulus seems to vary with the site which is tests. In the femur, Zysset and colleagues reported that the elastic modulus of diaphyseal femoral bone was approximately 3-4 GPa higher than that of bone from the femoral neck (Zysset et al., 1999). While much research has been conducted on the material properties of the bone, fracture toughness, a property referring to a material's resistance to crack growth or propagation, is of particular interest in the context of this thesis, as it relates to an important gap in the literature.

2.4.1.1.1 Fracture Toughness

The fracture toughness of a material is an intrinsic property relating to the stress intensity (stress intensity factor, *K*) necessary for a crack to grow, also known as critical fracture toughness, *Kc*. Specifically, the stress intensity factor (*K*) is important in fracture mechanics, as it: "describes completely the severity of the stress in the singularity region near a crack tip" (Pruitt and Chakravartula, 2011). Due to the stress singularity that occurs at the crack tip (first described by Inglis in 1913), defects in materials harbor a concentration in stress, or a higher stress intensity. Linear elastic fracture mechanics, first theorized by Griffith in 1921, build from this concept. Specifically, Griffith showed that the fracture strength of a brittle material is related not only on the material properties, but also by the size of the crack, where a larger crack size results in lower fracture strength. Ritchie, Knott and Rice applied these concepts in 1973, wherein the critical linear elastic fracture toughness of mild steel was quantified and related to its critical tensile stress (fracture strength) (Ritchie et al., 1973). Similarly, elastic-plastic fracture toughness (*J*) has also been defined, which was first detailed by Rice in 1968, which allows for the same concepts to be applied to the investigation of elastic-plastic material (Rice, 1968).

While commonly used in the field of metallurgy, these metrics have been applied to investigations of cortical bone (which can be viewed as a brittle material) as a metric used to quantify the resilience of the bone, specifically with its ability to prevent a crack in cortical bone from growing and ultimately result in fractures (Gauthier et al., 2019, 2017; Poundarik et al., 2015; Vashishth et al., 1997; Thomas L Willett et al., 2019). In fact, fracture toughness has often been quantified in the context of ageing bone and bone fragility, as a means to better understand the mechanistic underpinnings of age-related bone fragility and increased fracture risk (Gauthier et al., 2019, 2017; Granke et al., 2015; Uppuganti et al., 2016; Zioupos et al., 2020, 1999). These investigations have even focused on common sites of major osteoporotic fractures, such as the radius and the femur. Particularly relevant to this thesis are investigations into the underlying toughening mechanisms present in cortical bone, influencing the material's resistance to crack growth. A review by Launey and colleagues in 2010 provides a great overview of the multi-scale toughening mechanisms that are engaged during bone crack growth and fracture (Launey et al., 2010a). As illustrated in Figure 2-7 (which is Figure 3 from Launey et al. 2010), the mechanisms that contribute to the toughness of cortical bone and prevent crack growth are often tied to unique structure and composition of cortical bone, such as crack deflection driven by the organization of

osteons (Nalla et al., 2003). Other toughening mechanisms present relate to collagen, such as collagen fiber bridging (which provide resistance to crack mouth widening) (Nalla et al., 2003), the breaking of inter-fibrillar crosslinks (Buehler, 2007), and even hydrogen bond breaking within tropocollagen molecules (Gautieri et al., 2009). Indeed, more recent investigations into the fracture toughness of cortical bone have found that there is a significant relationship between fracture toughness and collagen-related metrics, such as the relative integrity or connectivity of the collagen network (Burton et al., 2014; Willett et al., 2019; Willett et al., 2015; Woodside and Willett, 2016), and the type of crosslinks present (enzymatic vs. non-enzymatic) (Granke et al., 2015; Poundarik et al., 2015; Vashishth et al., 2001; Viguet-carrin et al., 2006). Most recently, Willett and colleagues observed a significant relationship between collagen network integrity and elastic-plastic fracture toughness, specifically evaluating both critical toughness (*Jc*, K_{init} in the article; $R^2 = 0.244$, $p < 0.001$) and the total energy dissipated during crack growth (*Jint*; $R^2 = 0.351$, $p < 0.001$). These results quantified for bone specimens from a heterogeneous sample of the population (with an age range of 21-98 years, some with comorbidities and disease states), echo the results from Zioupos et al., 1999, wherein strong correlations were observed (Zioupos et al., 1999).

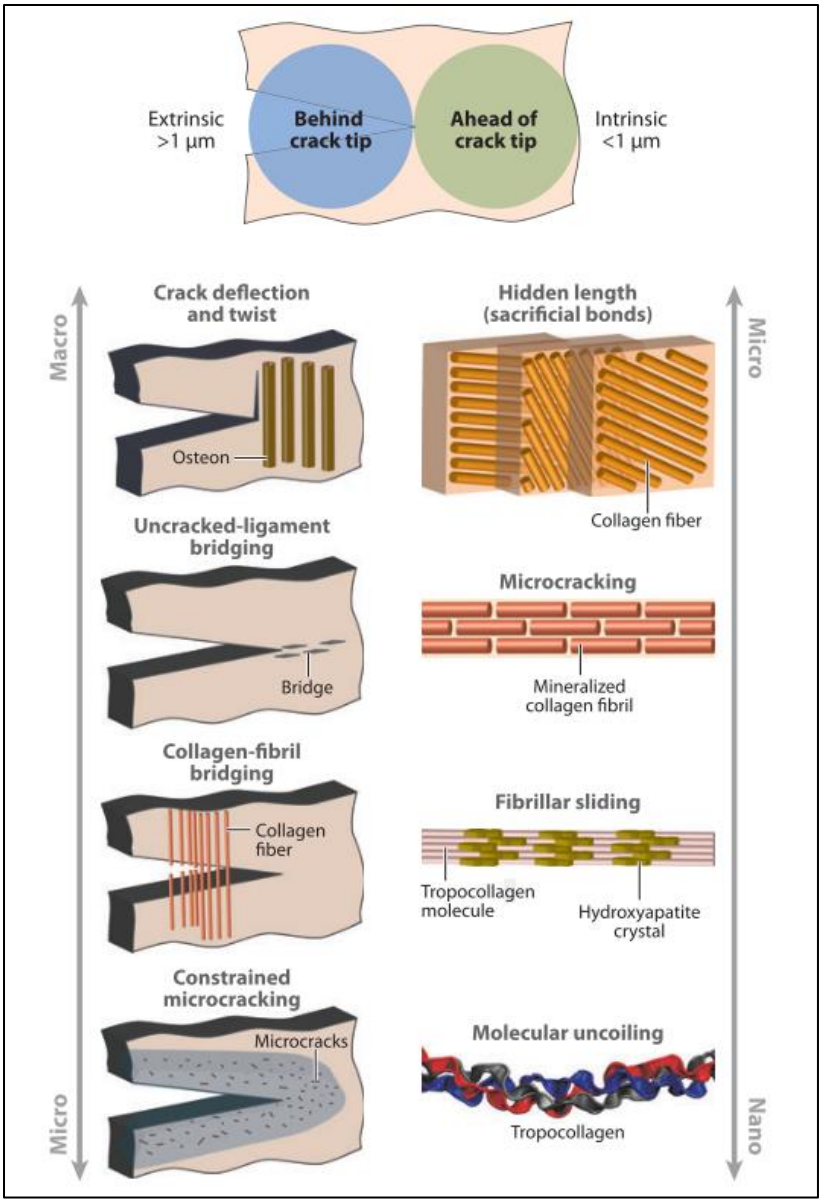

Figure 2-7: Taken from Launey et al. 2010 [Figure 3]; The toughness of bone results from a mutual competition between extrinsic (crack tip shielding) toughening mechanisms, which predominate at length scales at more than 1 μm, and intrinsic (plastic deformation) toughening mechanisms, which are active at length scales at primarily less than 1 μm.

These studies clearly demonstrate the role of the organic phase on fracture toughness of cortical bone, and how fracture toughness of bone is affected by the state of the organic phase (Poundarik et al., 2015; Vashishth et al., 2001; Viguet-carrin et al., 2006). While fracture toughness and strength are often considered alongside each other in metallurgical research (Ritchie et al.,

1973), the two are not regularly considered together in the context of bone. In fact, neither fracture toughness nor the underlying state of the collagen have been investigated in the context of bone strength at the macro-scale. Specifically, there is currently a gap in the literature existing between investigating bone as a material and quantifying whole bone strength in the context of injuries and fractures.

2.4.2 Bone at the Molecular Level

2.4.2.1 Organic Phase: Collagen

Type I collagen is the predominant type of collagen present in human bone (Shoulders and Raines, 2009). Collagen, as a molecule, is tri-helical in nature, consisting of three polypeptide chains held together by hydrogen bonds. Shoulders and Raines 2008 provides an excellent review of the history of our understanding of the collagen molecule, and detail the composition of collagen, from a single strand of collagen, to the tropocollagen triple helix molecule, and on the microfibrillar and fiber structure of collagen (Shoulders and Raines, 2009). This section will provide a brief summary of collagen at each of these levels, with the specific goal of providing insight into its structure and function, as some of the measures and techniques to be employed in this thesis aim to quantify and probe collagen at the molecular level.

Beginning at the level of a single polypeptide strand that makes of one of the three strands found in the tropocollagen molecule, a collagen strand consists primarily of the amino acids proline, hydroxyproline, and glycine (Lodish et al., 2000). Three of these strands coil together to form a triple helix structure known as tropocollagen, with hydrogen bonds (between amines and carbonyls) between strands (Figures 2-8). Breaking of these hydrogen bonds is thought to be one of the collagen-mediated toughening mechanisms seen in bone fracture (Gautieri et al., 2009). Collagen fibrils are made up of a collection of tropocollagen molecules, specifically made up of staggered parallel collections of in-series tropocollagen (Figure 2-9). Holding this collection of tropocollagen together are crosslinks between adjacent molecules (Figure 2-8), with many molecules together creating a collagen fiber. As bone forms, or more specifically, as new collagen is produced and arranged during osteogenesis, enzymatically mediated crosslinks are formed between adjacent tropocollagen (via the lysyl-oxidase enzyme) (Figure 2-9). However, this is not the only type of crosslinks that have been observed in collagen fibrils. In fact, other crosslinks, also referred to as advanced glycation end-products (AGEs), occur as a result of glycation of sugars

and oxidative stress leading to non-enzymatic crosslinks between molecules (Burr, 2002; Fessel et al., 2014; Vashishth et al., 2001). These non-enzymatic crosslinks are thought to occur during aging and in diseases, or facilitated by the carbonylation that results from oxidative stress (Burton et al., 2014). In addition to AGE crosslinks, various non-crosslinking AGE ligands, such as carboxy methyl lysine (CML), can form as a result of glycation and oxidative stress (McCarthy et al., 2001; Saito and Marumo, 2015). A recent publication by Arakawa and colleagues suggests that, due to the finite number of intermolecular crosslinking sites, both crosslinking and non-crosslinking AGEs prevent or block the formation of enzymatic crosslinks (Arakawa et al., 2020). Previous studies investigating the type and number of crosslinks in collagen fibrils found that they directly affect stiffness and fracture toughness of collagen, and ultimately bone (Knott et al., 1995; Massé et al., 1996; Nyman et al., 2007; Vashishth et al., 2001). The amount and types of crosslinks can therefore affect the connectivity of the collagen network and alter the lattice structure of the collagen molecules. Changes to both collagen network connectivity and organization have been found to alter the material properties of demineralized segments of cortical bone, altering the fracture toughness and even strength of the tissue (Burton et al., 2014; Oxlund et al., 1995; Saito et al., 2011; Willett et al., 2015). These findings provide evidence for the link between the state of the collagen network and bone strength. Additionally, this link may help explain the increased risk of fracture experienced by individuals with bone affecting or inflammatory disease states such as Diabetes Miletus and Chronic Kidney disease (Janghorbani et al., 2007; Kazama et al., 2013; Miller, 2014). Either through the presence increased blood sugar content or reactive oxygen species, increased presence of these AGEs have been observed in individuals with these diseases (Modaresi et al., 2015; Ravarotto et al., 2018; Saito et al., 2006; Silva et al., 2009; Tomasek et al., 1994).

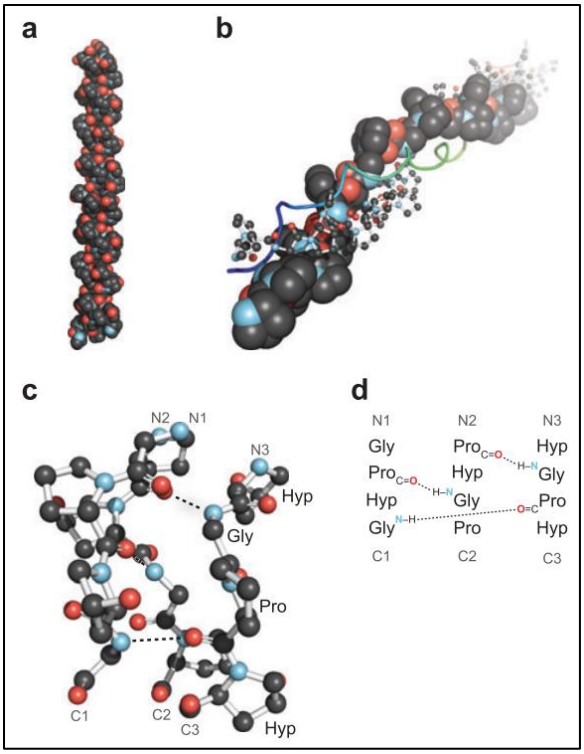

Figure 2-8: Taken from Shoulders and Raines 2019 [Figure 1]; Overview of the collagen triple helix"

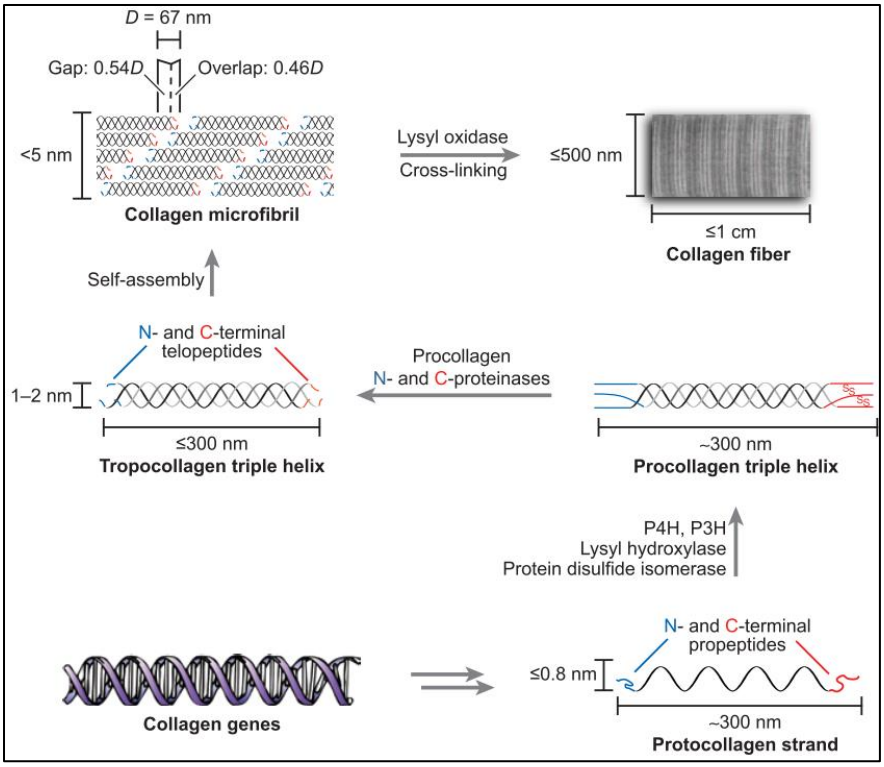

Figure 2-9: Taken from Shoulders and Raines 2009 [Figure 2]; modified figure to focus on the multi-level complexity of collagen, from single strands to collagen fibers.

2.4.2.2 Inorganic Phase: Hydroxyapetite

However, bone is not solely made of collagen fibers, but is rather made up of mineralized collagen, wherein calcium phosphate is bound to collagen. Specifically, carbonated hydroxyapatite (cAp) makes up the bulk of the non-organic phase of bone, and it is this component that gets measured when concerning bone mineral content (BMC) or density (BMD). While The review by Stock in 2015 titled "The Mineral-Collagen Interface in Bone" provides an in-depth look outline, this section will provide a brief overview. Firstly, groups of cAp molecules form together into "nanoplatelets" (or crystals), with these being found within the matrix that is the collagen molecules. More precisely, cAp crystals of varying sizes are found in the gaps between sequential tropocollagen (known as intrafibrillar), as well as between collagen fibrils (extra fibrillar). The degree which bone (including both collagen and mineral components) is mineralized will directly affect its mechanical properties (Currey, 2012; Stock, 2015). Specifically, hydroxyapatite crystals have a much higher Young's modulus than unmineralized collagen strands (E = 116 GPa and 4.8 GPa, respectively) (Dubey et al., 2012; Lorenzo and Caffarena, 2005).This may explain the

changes in material properties and strength of bone on a macro, such as stiffness, that is observed with changes in BMC, and more generally BMD (as explored in section 2.2.3.1). Thus, the relationship and interplay between the organic and non-organic phase of bone is important to consider, across all scales. While some research has considered this interplay across scales, such as relating collagen content to the mechanical properties of bone at the meso (cm) scale, a gap remains in the literature when in comes to relating molecular level understanding of bone to the overall strength of bone, and specifically in the context of fall-related hip fractures.

2.5 Literature Review Summary

In summary, fall related hip fractures are a major issue, particularly for the older adult population. Though methods currently exist to predict an individual's risk of suffering of hip fractures, clear limitations exist, resulting in many hip fractures occurring in individuals who wouldn't typically be considered at high risk. This literature review has established some clear gaps in the literature that may pertain to this discrepancy. Specifically:

- The use of high-displacement rate MTS experiments of cadaveric bone may result in inaccurate, or unphysiological, measures and subsequent estimates of bone strength. However, a gap in the literature exists in terms of biofidelic experiments of proximal femur bone strength in the context of fall-related hip fractures.
    - Though a difference between testing modality (MTS vs. biofidelic simulated impacts) has been suggested by the results of Gilchrist et al., 2014, the lack of matched pair specimens prevents establishment of a clear conclusion.
    - There are currently no predictive models of proximal femur bone strength based on biofidelic simulated hip impact experiments. Additionally, differences in measured bone strength between test paradigms are unknown.
- Previous research into the strength of the proximal femur in fall-related hip fractures has focused primarily on the inorganic phase of bone. While likely being the result of currently available clinical imaging modalities (such as X-ray-based methods like DXA and QCT), the organic phase of bone has not been considered in this context.
- While research focusing on the organic phase of cortical bone (from the femur) has revealed that the organic phase, specifically the connectivity and integrity of the collagen

network, relates directly to fracture toughness, the link to ultimate fracture force or bone strength and hip fracture risk has yet to be established.

- Additionally, while fracture toughness is known to relate to ultimate strength of certain materials (such as metals), the relation between fracture toughness and femoral bone strength in the context of fall-related hip fractures has not been directly investigated.
- To our knowledge, no study has investigated the link between the organic phase of bone, specifically collagen, and the ultimate strength of the proximal femur during fall-related hip fractures.

The following studies conducted as part of this thesis aimed to collectively address these gaps in the literature. The research presented in this thesis provided the first steps in filling these gaps and ultimately aided in the understanding of hip fracture mechanics. Additionally, this multidisciplinary work provided a unique opportunity to link research into bone fracture mechanics in the context of fall-related hip fractures, across multiple scales, as the studies conducted span from the macro scale of whole bones, to the mesoscale of small rectangular bone samples, and ultimately down to the molecular (or nano) scale during the experiments into collagen network connectivity.

Chapter 3
Study 1: Investigating the Influence of Test Paradigm on Fracture Force of the Proximal Femur During Lateral Impacts

3.1 Introduction

Fall related injuries are the common type of injury experienced by older adults, accounting for approximately 30% of all fall-related hospitalizations in Canada (Billette and Janz, 2011; Canadian Community Health Survey, 2012). Of these, hip fractures are one of the most severe injuries, as they lead to a severe loss of mobility and independence, and over 20% of cases result in death within the first year of injury (George Ioannidis et al., 2009; Jiang et al., 2005). Additionally, these injuries have a high societal cost, with an estimated annual cost ranging between $650 million to $1.1 billion in Canada alone (Nikitovic et al., 2013; Wiktorowicz et al., 2001). Thus, the severity and the associated costs of these injuries have driven a serious focus into fall-related hip fracture prediction and prevention.

Injury prevention often relies primarily on methods to identify and quantify individuals at risk or their associated level of risk of experiencing the injury. Identifying "at risk" individuals allows for earlier and more efficient intervention to prevent injurious outcomes. Clinical screening tools such as the Fracture Risk Assessment Tool (FRAX), Garvan Fracture Risk Calculator, QFracture, or the CAROC 10 year Fracture Risk Assessment tool are commonly used to assess the risk of bone fracture (Aspray, 2015; Cummins et al., 2011; Dagan et al., 2017; Fraser et al., 2011; Johansen, 2012; Kanis et al., 2018, 2012, 2008b; Leslie et al., 2012). While each of these screening tools includes unique elements, such as history of falls, family history, and other demographic information, most of these include some metric of bone quality, typically through the use of a measure of femoral bone mineral density (BMD), or associated metrics (such as the T-score of femoral BMD). The prevalence of BMD metrics use in fracture risk assessment stems from the established relationship between lower bone mineral density and higher rates of fracture (Akdeniz et al., 2009; Caillet et al., 2015; Dinçel et al., 2008; Greenspan et al., 1994; Johnell et al., 2005) , and further the strong relationship between BMD and excised cadaveric femurs (Cheng et al., 1997; Courtney et al., 1994, 1995; Dall'Ara et al., 2013a; Davis et al., 2010).

Estimating the impact force required to result in a hip fracture allows for a mechanistic and physically based estimate of fracture risk. While some risk assessment methods, such as the T-

score, are closely linked to relationship between bone strength and fracture vulnerability, other methods such as hip fracture factor of risk use estimates of femoral bone strength directly to quantify risk of fracture outcomes in the event of a fall-related impact (Bachmann et al., 2014; Bouxsein et al., 2007; Davis et al., 2010; Dufour et al., 2012). These more direct risk assessment methods use models (typically regression based) to estimate bone strength from variables such as BMD, age and sex. These models were developed in previous studies where excised femurs were loaded till failure to extract bone strength. However, the method typically used in these experiments (a material testing system uniaxially loading the femur at 100 mm/s constant displacement) may not accurately replicate the impact dynamics of a fall-related lateral hip impact, particularly in relation to the loading rate. While the loading rate experienced by the femur during a lateral hip impact is unknown, recent experiments using a biofidelic hip impact simulator (HIS) have revealed that the loading rate may be in the range of 10^6 – 10^7 N/s (Fleps et al., 2019; Jazinizadeh et al., 2020). Compared to the roughly ~200 kN/s induced load of traditional MTS experiments (extrapolated from Roberts et al. 2010), these recent experiments suggest that femoral loading rate during lateral hip impacts may be much higher in reality. Due to the viscoelastic nature of bone, higher loading rates should yield higher fracture forces, and so it is possible that previous femoral bone strength estimates provide an artificially lowered fracture force, which could negatively affect the predictive accuracy of fracture risk assessment. In fact, Gilchrist and colleagues (2014) first suggested this in their 2014 study, where fracture force of the proximal femur tested in slow and fast deflection MTS experiments were compared to fall simulation experiments. However, this study could not directly compare and quantify the effects of testing paradigm due to the experimental design, as matched pairs were not used.

The goal of the current study was to investigate the influence of test paradigm associated differences on bone strength, also referred to as fracture force (F_x). This was achieved by using a sample of matched pairs of femurs, with one specimen of each pair tested in a material testing system (MTS), and the other tested in a vertical drop tower hip impact simulator (HIS). A primary difference between these testing paradigms relates to the loading profile, with MTS utilizing constant displacement rate, and the HIS uses an impulse driven exposure with non-uniform loading rates. This difference is influenced by the essential boundary condition differences between these paradigms. While both paradigms use the same mounting and fixture (Figure 3-1), there are inherent differences in system stiffness, as the MTS is a closed system with a high-stiffness stroke

arm, whereas the HIS's free-fall impactor results in an open system, with the stiffness driven primarily by the coil springs as well as the foam soft tissue simulant. Therefore, it was hypothesized that specimens tested in the HIS will yield significantly higher fracture force values than those in the MTS. It was also hypothesized that specimens tested in the HIS testing paradigm would experience higher overall loading rates.

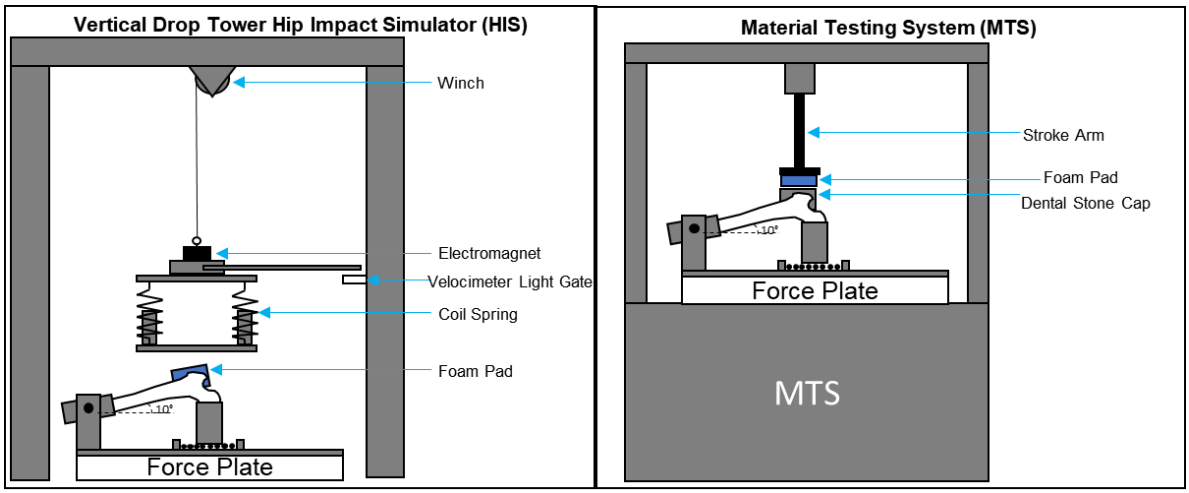

Figure 3-1: Simplified 2D graphical representation of the test paradigms employed in this study, the HIS (left) and the MTS (right).

3.2 Methods

3.2.1 System Development

Lateral impact simulations were conducted in a custom-built, CSA standards aligned vertical drop tower impact simulator (CSA Group, 2020), as seen in the left pane of Figure 3-1. A steel support frame (2.55 m height x 1.2 m width x 0.15 m depth) housed two stainless steel guide bars (2.5 m height x 0.04 m diameter, 0.75 m spacing between) used to guide a central load carriage (0.8 m width, 0.15 m depth, 0.05 m height). The carriage was mounted to the guide bars via 4 pillow block bearings, allowing for near frictionless vertical (single degree of freedom) movement, and a simulated pelvis system was fixed to the inferior side of the load carriage. A custom specimen mounting jig was affixed onto a force plate placed at the base of the drop tower.

The mounting jig was comprised of two main mechanisms including the mounting mechanism and the simulated pelvis system. The mounting mechanism was designed in order to

mount and adjust the orientation and position of the proximal half of cadaveric femur specimens. Specimens (a cadaveric femur cut transversely at the mid diaphysis) were set with dental stone (gypsum) within a cylindrical pipe/bracket. The specimen receptacle was then fitted to a mounting bracket, which was connected to the rest of the mechanism by an axle. The axle was connected to the mounting jig base plate through 2 support pillars, each with height adjustable bearings; this mechanism allowed for specimen positional adjustment akin to abduction/adduction of the thigh (note the 10° specimen angle in Figure 3-1). While the femoral head was not directly attached to the mechanism, it was supported by a pillar consisting of a cylindrical 2" (5.08 cm) ABS pipe (10 cm length) filled with dental stone; the superior aspect of the dental stone filled pipe was press-molded to the femoral head to allow for a more natural interface (mimicking the acetabulum-femoral head interface). The inferior aspect of the support pillar was capped with a ¼ inch-thick steel plate, acting as an end cap. Rather than be directly attached to the mounting jig base plate, the support pillar complex was placed on a layer of ball bearings housed in a rectangular collar mounted to the base plate; this allowed for 2 degrees of freedom translation of the support pillar-specimen complex (aligned with the x-y plane of the force plate). The previously mentioned mechanisms, including the base plate, made up the mounting mechanism. This mounting mechanism, also referred to as mounting jig, was affixed to the top of an AMTI OR3-6-2000 force plate (AMTI, Watertown, MA, USA).

The simulated pelvis system (Figure 3-2), attached to the underside of the load carriage, consisted of four coil springs mounted between two aluminum plates. In order to limit system movement to the vertical axis, two guide bars were attached to the bottom plate (via screws). These bars passed through the center space of the springs and protruded through the top plate, passing through a set of bearings, and held in place with ring clamps. The entire system was compressed to press-fit the springs into position, and the ring clamps were used to set the systems unloaded configuration. Total system stiffness was measured at 44973.5 N/m.

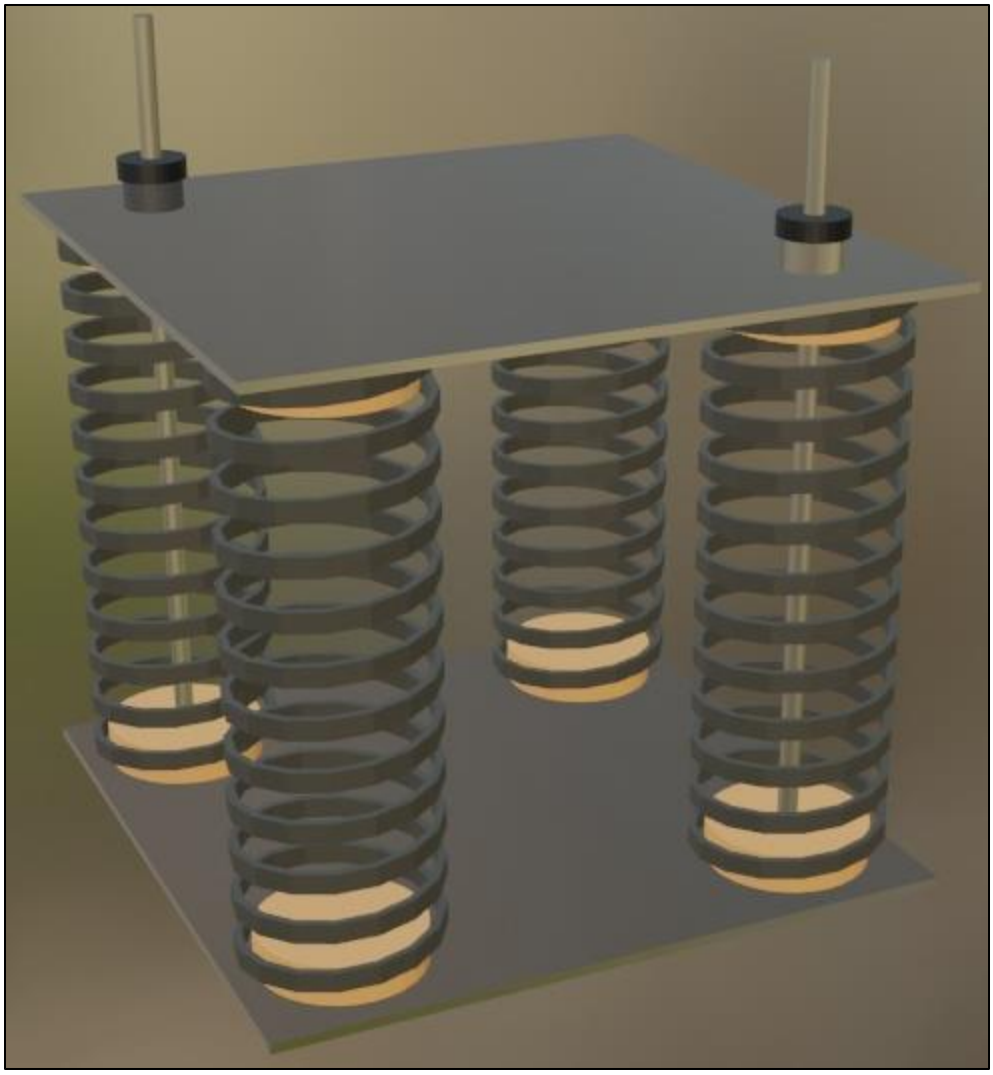

Figure 3-2: Rendered model of the pelvis system.

The load carriage was adjusted via an electric winch attached to the top of the drop tower's steel frame, using an electromagnet as the coupling/release mechanism for the load carriage. A light-gate velocimeter (VS300, GHI systems Inc., California, USA) was fixed to the exterior of the steel frame of the drop tower system, and a thin aluminum sheet was affixed to the anterior face of the load carriage, such that the aluminum sheet extended out beyond the load carriage towards the steel frame. This allowed for the aluminum sheet to interrupt the velocimeter's light gate during an impact simulation, extracting load carriage impact velocity (via light gate interference time). Figure 3-3 shows a complete example of the experimental setup.

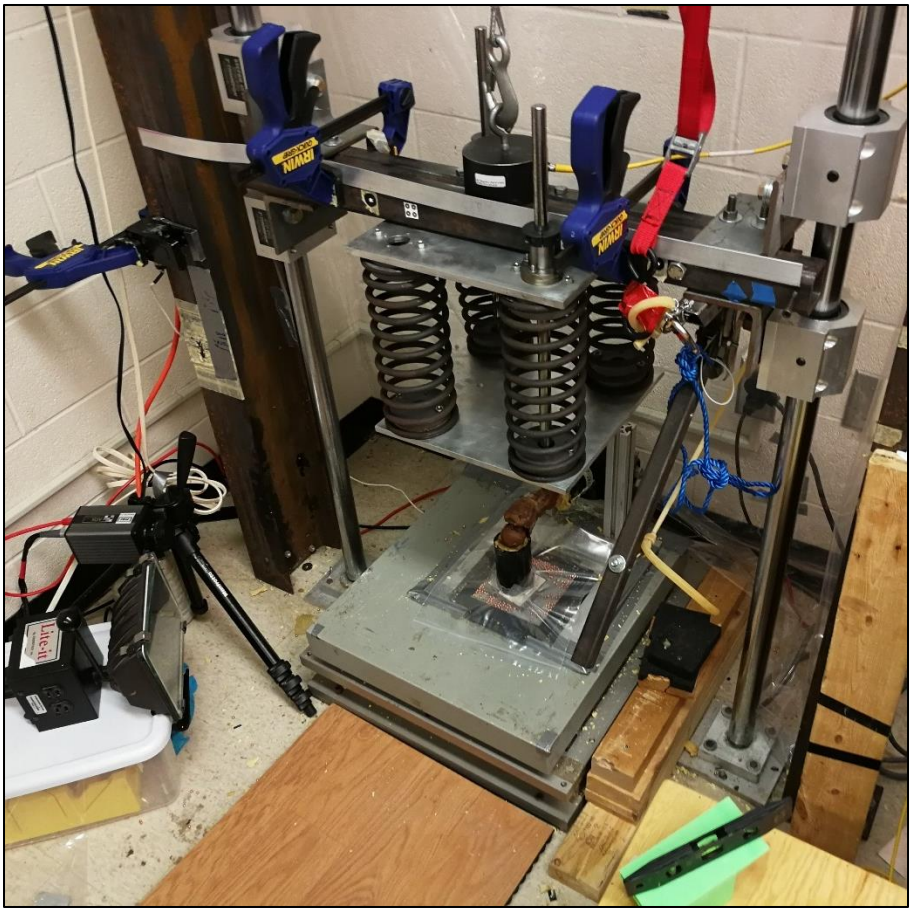

Figure 3-3: Complete experimental setup.

3.2.2 Sample Acquisition and Preparation

A total of 6 matched pairs of femurs (12 specimens total) extracted from fresh frozen postmortem human subjects (PMHS) were obtained through the University of Waterloo School of Anatomy's Human Body Bequeathal program. While frozen, PMHS were transected at the mid-torso, and above the knee at each leg, resulting in a pelvis-thigh section. These sections were thawed until the point that tissue could be dissected, and the femurs extracted and stripped of all surrounding soft tissue. Specimens were then sealed in a plastic bag and stored in a tissue specimen freezer (freezer temperature ranging from -20 °C to -30 °C).

3.2.2.1 Specimen Characterization

While frozen, individual femur specimens were removed from the tissue specimen freezer to undergo both clinical and morphological characterization (via DXA scan analysis). First, specimens were housed in a clear plastic container and held in position via a clamp mounted to the

interior of the container. The clamp interfaced with the distal aspect of the femur, and the femur was placed in a position matching that of the femur during a typical DXA hip specific scan. The container was placed on the patient table of the DXA scanner (Hologic Discovery W fan-beam bone densitometer, Hologic, Inc. Bedford, MA, USA) and positioned to align with the hip specific scan position. A high-quality hip specific scan was conducted with the assistance from a qualified Medical Radiation Technician, and scan analyses were performed in the Hologic Discovery W software to extract femoral neck aBMD (sample output seen in Figure 3-4). Following the DXA procedures, the specimen was returned to the specimen freezer until test day. The acquired DXA scans then underwent additional analyses to extract the neutral femoral shaft axis (*NFSA*), femoral neck axis length (*FNAL*) and neck shaft angle (*NSA*), as defined by Levine et al. 2018 (Levine et al., 2018). From these, the moment arm (*r*) between the axis of rotation of the femoral head and the intersection of the *NFSA* and *FNAL*. Furthermore, the cross-sectional moment of inertia (*CSMI*) was computed, using the methods outlined in Steven Pretty's 2018 Master's Thesis (Pretty, 2018). Briefly, the narrow neck was defined in the DXA scan image, from which the thickness (or depth) was estimated at each pixel along that cross section (as described in the Pretty 2018 thesis, referencing Mourtada et al., 1996; Yang et al., 2009). Following this, the pixel representing the centroid location was identified, allowing for the calculation of *CSMI*, where the thickness of a given pixel was multiplied by the distance from the centroid pixel squared, and this was summed across all pixels in the cross section. A scaling factor was applied to account for the distance between pixels. While fully explained in the Pretty 2018 thesis document, these same methods were applied in this study to compute *CSMI*, which was used as an independent variable representing bending resistance.

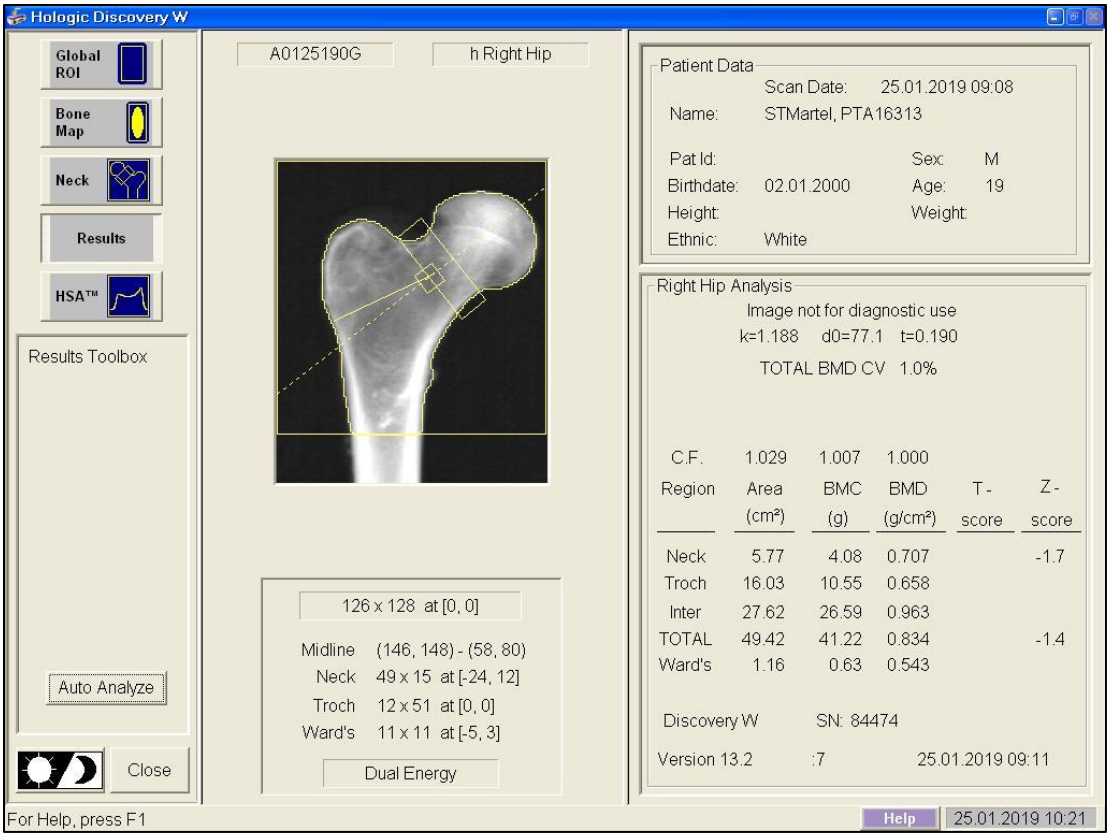

Figure 3-4: Example of Hologic Discovery output for a "High Quality" hip scan of an excissed femur specimen.

The rationale for selecting these geometric/morphological factors, specifically cross-sectional moment of inertia (*CSMI*), femoral neck axis length (*FNAL*) and femoral neck angle (also referred to as neck shaft angle, *NSA*), was that each of these factors directly affects the bending stress experienced in the femoral neck. The intersection of *NFSA* and *FNAL*, along with *NSA*, directly determine the moment arm (*r*) (see Figure 2-5), while the *CSMI*, which takes into account the distribution of bone mineral content, affects the bending resistance. The experimental configuration for both the HIS and MTS paradigms result in a form of three-point bending. These morphological factors, along with femoral neck aBMD (*BMD*) were compared between the experimental paradigm samples; if any of these factors were significantly different between paradigms, the dependent variables would be normalized to these factors. However, no significant differences were observed, and none of the dependent variables needed to be normalized.

3.2.2.2 Specimen Testing Preparation

All specimens were housed in a freezer (-20 to -30 °C range) for at least 24 hours prior to testing. Due to the nature of PMHS tissue work and the irregular intervals between the acquisition of new specimens, specimens were kept frozen anywhere from weeks up to 2 years, with the long time spent frozen being due to the restrictions related to the COVID-19 pandemic. Specimens were removed from the freezer and brought to the lab on the day of testing. Prior to mechanical testing, specimens were transected at the mid diaphysis; to ensure uniformity during mechanical testing, all specimens were transected 15 cm distal to the greatest lateral protuberance of the greater trochanter. The distal 5 cm of the diaphysis was encased in dental stone (gypsum) within a 10 cm length of 2" (5.08 cm) diameter ABS pipe (Figure 3-5). To minimize dehydration and drying of specimens, potting of the specimens began within 30 minutes of arrival in the lab. The potting process took approximately 1 hour, which included placement of specimens in the ABS pipe segment container, filling of dental stone, and setting of the dental stone. Following this, frontal plane X-ray images were captured using an M3001125 Mercury Module (Faxitron, Tuscon, AZ, USA) (Figure 3-5); the X-ray images were used as a secondary assessment of bone quality as well as a method to identify any gross mechanical defects or pre-existing damage in the bone that may not be visible on the surface of the tissue, in addition to identifying of voids or defects in the dental stone potting. The specimen was then be placed in the universal mounting jig and oriented in the standard femur fracture testing orientation (Courtney et al., 1995, 1994), wherein a 10-degree abduction angle and 15 degrees internal rotation were emulated. To prevent rotation of the specimen about the femoral shaft axis, two screws were drilled into the specimen mounting jig ABS pipe interface. Time between X-ray imaging and beginning of testing was approximately 30 minutes. Altogether, specimens underwent thawing for approximately 2 hours prior to testing. Though specimen temperature was not measured, inspection of the fractured specimens revealed no sign of frozen or dehydrated material. All specimens were handled in a way to minimize the number of freeze-thaw cycles, with a maximum of three cycles occurring.

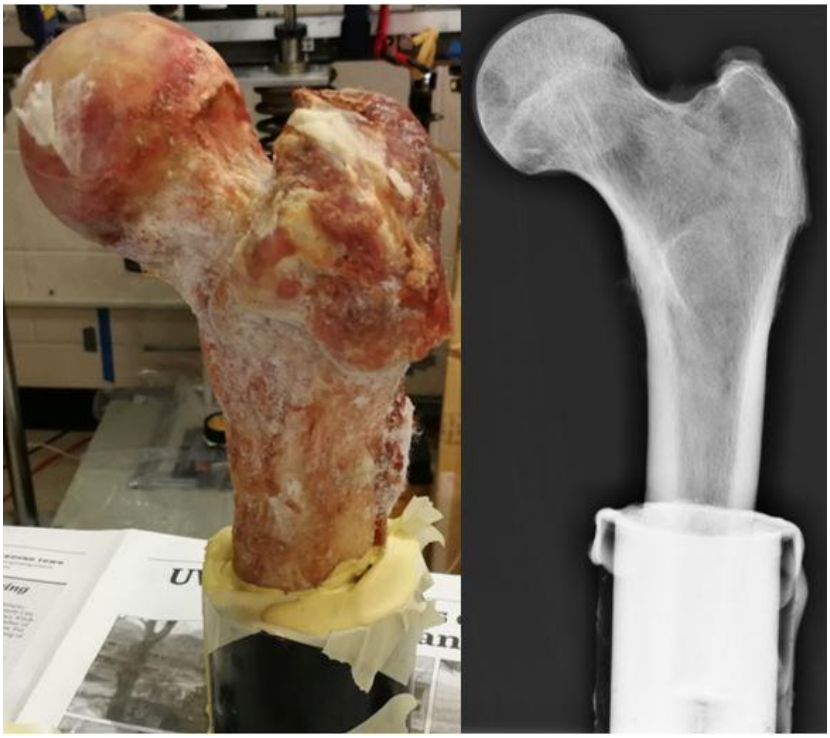

Figure 3-5: Potted specimen (left) and frontal plane X-ray (right) of the potted specimen.

3.2.3 Testing Protocol

As the goal of this experiment was to investigate influence of test paradigm differences in bone strength (F_x), matched-pair specimens were split into two conditions; one femur undergoing the MTS constant-displacement protocol, and the other femur from the pair undergoing a fracture inducing impact condition in the vertical drop tower HIS. Block randomization was used to assign an equal number of right an left femurs to either experimental paradigm. As a supplementary data source, high-speed videography was used to record the fracture events in both test paradigms to assist in characterizing fracture location and timing. To accomplish this, a high-speed camera (HSV, AOS Technologies, Cheshire, CT) was placed near the base of the drop tower, capturing video of the inferior-anterior aspect of the specimens at a sampling rate of 2000 Hz.

3.2.3.1 HIS Protocol

For the simulated hip impact experiments, the vertical drop tower HIS described in Section 3.2.1 was used. To induce fracture during simulated lateral hip impacts, an impact velocity of 4 m/s was targeted. While slightly higher than the typical vertical impact velocity observed for fall-related hip impacts (Choi et al., 2015; Robinovitch et al., 2013), this impact velocity was

used to elicit fractures. As mentioned previously, the pelvis system had a total system of ~45 kN/m, while the whole load carriage and pelvis system had a combined mass of 40 kg. Affixed to the bottom side of the impact plate was a rectangular piece of foam soft tissue simulant (a foam pad of soft tissue simulant 5x5x5 cm in dimension; 3cm width over the greater trochanter) (CSA Group, 2020). It should be noted that the 40 kg mass used in this study was 12 kg greater than the recommended 28 +/- 1 kg mass outlined in the CSA standard for hip protector testing. The decision to increase the mass was to effectively increase the impact energy (beyond simply increasing the impact velocity, which was physically limited to a max velocity of 4 m/s); additionally, the CSA standard is not designed to induce fractures during testing, nor does the standard use cadaveric tissue. The specification of the CSA standard is instead used as a guideline to simulate biofidelic lateral hip impact simulations, while modifying certain parameters to achieve hip fractures. Loading rate was extracted from the force time data in order to compare loading rates with the MTS experiments. Force data from the force plate was sampled at 20 000 Hz using the NIAD 3.0 software. Prior to impact tests, specimens were preloaded with a static load of 400 N for 30 seconds in order to normalize specimen stress state history, as well as allow for the specimen to settle into the mounting jig.

3.2.3.2 MTS Protocol

A servo-hydraulic material testing system (MTS) was used for this experiment. The mounting jig used for the HIS protocol was used for the MTS experiments as well. To achieve this, the mounting jig's baseplate was affixed to the top of a force plate set beneath the system's stroke arm. A five-centimeter rectangular piece of steel plate was attached to the system's stroke arm, through which load was applied to the specimen via the combination of molded dental stone cap and a 3cm thick piece of soft tissue simulant foam, ensuring that the load was distributed over the greater trochanter in an attempt to avoid crush fractures of the trochanter. A constant displacement rate of 60 mm/s (system maximum displacement rate) was used to load the specimen until failure. Similar to the HIS protocol, the specimens were preloaded with a static load of 400 N for 30 seconds in order to normalize specimen stress state history, as well as allow for the specimen to settle into the mounting jig. Force data from the force plate was sampled at 20 000 Hz using NIAD 3.0 software.

3.2.4 Data Analysis

The force measured by force plate represented the total load, or force, applied through the system. This overall force represented the externally applied load during the experiments and has traditionally been used to determine specimen fracture force (femoral bone strength in this case) (Cheng et al., 1997; Courtney et al., 1995, 1994; Dragomir-Daescu et al., 2018; Gilchrist et al., 2014). Specifically, the peak force (prior to specimen fracture) recorded during the trial, was identified as the fracture force (F_x), the primary dependent variable for this study. Loading rate (LR) was defined as the slope between two identified points of the linear portion of the load-time trace prior to fracture. All force data was processed with a custom-developed MATLAB (MATLAB R2020a, Mathworks, Natick, Massachusetts, USA) script.

The dependent variables for this study were fracture force (F_x) and loading rate (*LR*). The independent variables were femoral neck aBMD (*BMD*), and the four previously described geometric parameters extracted from DXA scans (*FNAL*, *NSA*, *r*, *CSMI*).

3.2.5 Statistics and Data Interpretation

To assess the differences in dependent variables between test paradigm specimen groups, matched-paired t-tests (one-sided for F_x and *LR*; two-sided for other variables) were conducted with an alpha of 0.05. It was hypothesized that fracture force and loading rate measured in HIS experiments would be significantly higher than in MTS experiments. It was also hypothesized that there would be no significant difference between groups for any of the other dependent variables.

3.3 Results

Characteristics of the specimens included in the analysis, and descriptive statistics of dependent measures, are presented in Table 3-1 below. A table including individual details for each specimen is presented in Table 3-2. Shapiro-Wilk's tests of normality for *age*, *BMD*, *FNAL*, *NSA*, *r*, and *CSMI*, as well as for the dependent variables F_x and *LR*, were completed for each paradigm specific sample, and revealed no violations to the assumption of normality.

Table 3-1: Specimen information for the A) Full Sample, B) HIS Sample, C) MTS Sample. Respective sample size, sex split, and mean (SD) are presented for the independent variables age, sex, BMD, FNAL, NSA, r, and CSMI, as well as for the dependent variables Fx and LR. Impact velocity (V) is presented for the HIS sample, while actual displacement rate (m) is presented for the MTS sample.

A)	**Full Sample: Mean (SD)**								
N (pairs)	*sex* (F/M)	*age* (years)	*BMD* (g/cm^2)	*FNAL* (cm)	*NSA* (cm)	*r* (cm)	*CSMI* (cm^4)	*LR* (N/s)	F_x (N)
12 (6)	2/4	85.8 (15.0)	0.550 (0.051)	10.72 (0.87)	129.2 (7.3)	5.14 (0.72)	1.06 (0.46)	1250106 (1379351)	3868.9 (1245.6)

B)	**HIS Sample: Mean (SD)**							
N	*V* (m/s)	*BMD* (g/cm^2)	*FNAL* (cm)	*NSA* (cm)	*r* (cm)	*CSMI* (cm^4)	*LR* (kN/s)	F_x (N)
6	4.119 (0.063)	0.542 (0.052)	10.67 (0.92)	130.3 (8.5)	5.21 (0.59)	1.01 (0.37)	2463.49 (807.38)	4096.4 (1272.6)

C)	**MTS Sample: Mean (SD)**							
N	*m* (mm/s)	*BMD* (g/cm^2)	*FNAL* (cm)	*NSA* (cm)	*r* (cm)	*CSMI* (cm^4)	*LR* (kN/s)	F_x (N)
6	58.22 (0.28)	0.558 (0.053)	10.78 (0.91)	128.1 (6.5)	5.06 (0.88)	1.10 (0.58)	27.78 (10.03)	3641.3 (1285.8)

Table 3-2: Individual specimen details for all specimens included in this study.

Specimen Pair	*Age (years)*	*Sex*	*Paradigm*	*BMD* (g/cm^2)	F_x (N)	LR (kN/s)	Side
1	57	M	HIS	0.490	5678.5	3661249	L
			MTS	0.470	4225.9	31532	R
2	90	M	HIS	0.545	3290.0	2139286	R
			MTS	0.538	3190.8	22397	L
3	90	M	HIS	0.638	5389.8	3087854	R
			MTS	0.603	5599.4	43544	L
4	100	F	HIS	0.539	2320.2	1582640	R
			MTS	0.617	2219.7	16851	L
5	85	F	HIS	0.535	3758.5	1728665	L
			MTS	0.573	4212.3	32733	R
6	93	M	HIS	0.505	4141.7	2581258	L
			MTS	0.547	2400.2	19595	R

Two-sided paired t-tests revealed no significant differences between the paradigms for any of the independent variables (p = 0.194—659) (Table 3-3). For the dependent variables, there was no difference in F_x between paradigms (mean difference = 455.1 N, p = 0.132). However, a significant difference was observed for *LR* (mean difference = 2435.7 kN/s, p = 0.0003) (Figure 3-6, Figure 3-7). The coefficient of variability for *LR* in the HIS sample was 0.328, whereas the coefficient of variability in the MTS sample was 0.361. Post-hoc linear-regression analyses were performed to investigate the relationship between *LR* and F_x within each paradigm. Significant relationships were observed for both the HIS sample (adjusted R^2 = 0.833, p = 0.007) and the MTS sample (adjusted R^2 = 0.983, $p < 0.0001$) (Figure 3-8).

Table 3-3: Results of the paired samples t-test comparing variables between the HIS and MTS experiments.

	BMD	*FNAL*	*NSA*	*r*	*CSMI*	*LR*	F_x
95% CI	-0.062 0.030	-0.302 0.079	-1.60 6.05	-0.666 0.963	-0.427 0.245	1775.8 ∞	-296 ∞
t	-0.902	-1.500	1.496	0.468	-0.697	7.44	1.22
p	0.408	0.194	0.195	0.659	0.517	<0.001*	0.132

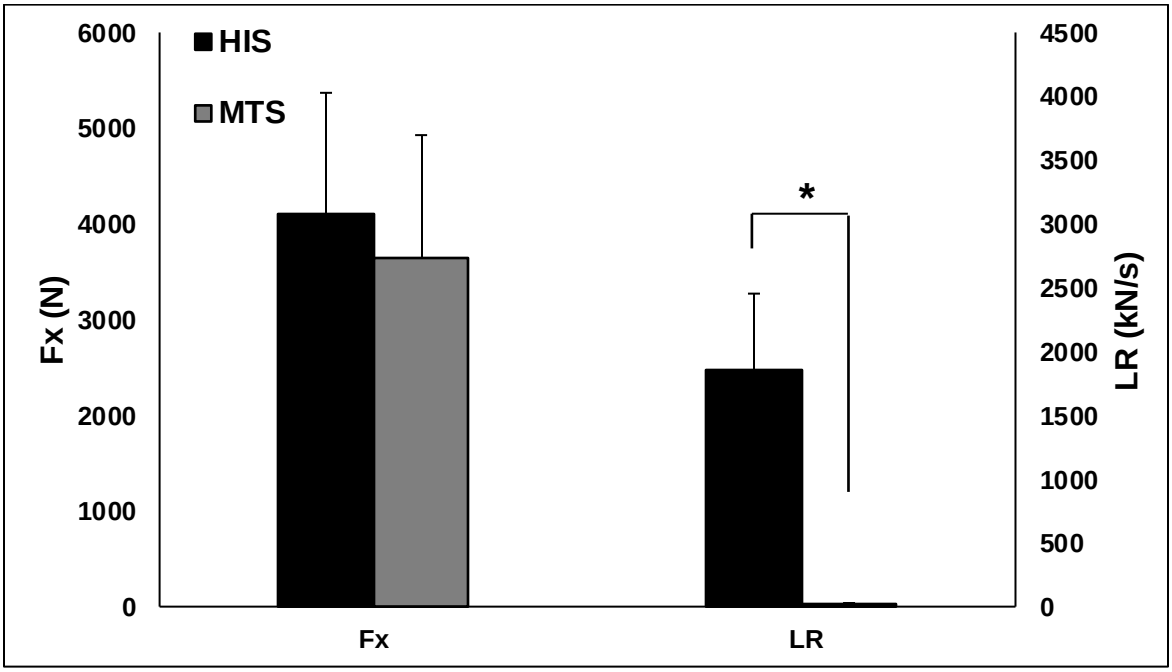

Figure 3-6: Mean and standard deviation presented for Fx and LR (HIS paradigm = black bar; MTS paradigm = gray bar). * Denotes a significant difference p < 0.001.

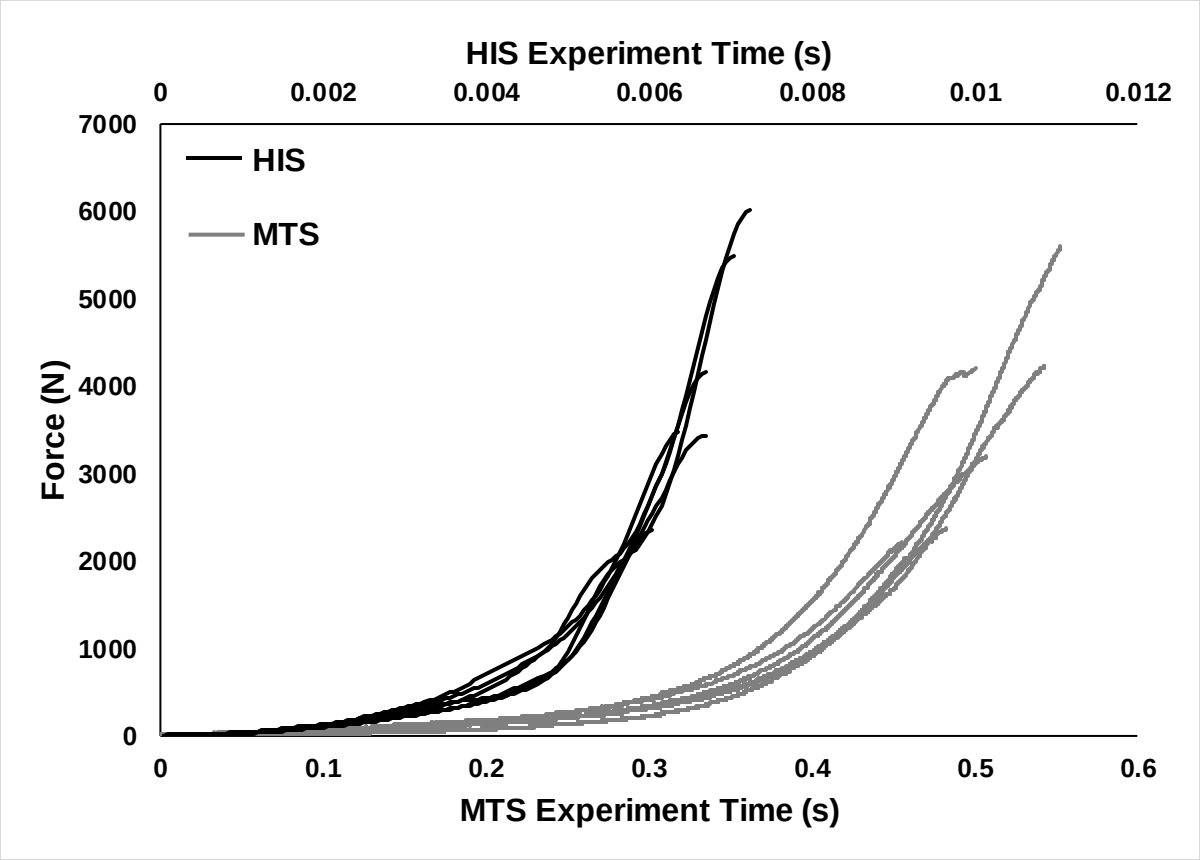

Figure 3-7: Force-Time traces for HIS (black) and MTS (gray) experiments. Due to the difference in loading profile, the time axis for the HIS experiments (top axis) has been magnified 50x to aid in the comparison of loading profile shapes between experiments.

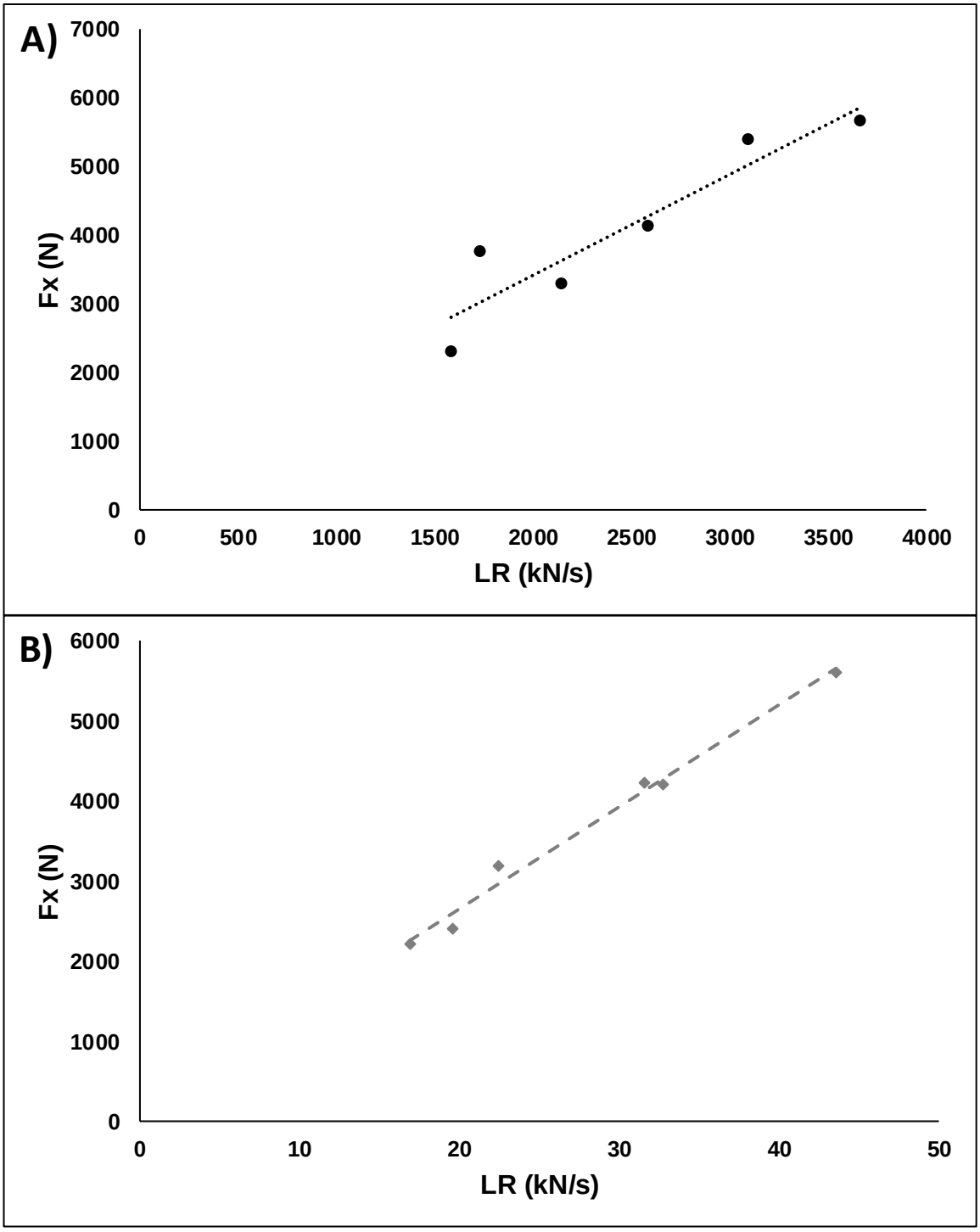

Figure 3-8: Relationship between F_x and LR for A) HIS experiments (adjusted $R^2 = 0.833$, $p = 0.007$), and B) MTS experiments (adjusted $R^2 = 0.983$, $p < 0.001$).

3.4 Discussion

The primary goal of this study was to investigate influence of test paradigm associated differences on bone strength. Despite observing a significant difference in *LR* ($p < 0.001$), there was no significant difference in measured F_x between HIS and MTS experiments ($p = 0.132$). Post-hoc analyses revealed that, while no overall relationship between F_x and *LR* was observed for the full sample, significant relationships between F_x and *LR* existed within each paradigm, separately. As the loading impulse, or input energy, were maintained relatively stable within each paradigm, this observation was likely driven by differences in material, or more broadly, structural stiffness of the specimens. While measures of strain at the inferior femoral neck, which were initially planned, would have provided some relative insight, a combination of technical issues and signal dropout resulted in unreliable strain data for certain specimens, and missing data for others. Stiffness was computed from the load-displacement data of the MTS experiments (stiffness range: 312.9 – 744.2 kN/m), and a post-hoc analysis revealed that the rank order generally aligned with the rank order of the *LR* for these experiments (4/5, $R^2 = 0.893$). However, the rank order of specimens was not the same between paradigms for either F_x or *LR*, separately, suggesting stiffness also differed within pairs. Regardless, when the results are compared to previously published studies, certain similarities arise, despite differences in statistical significance.

Previous studies have investigated the effect of loading rate on femoral bone strength, albeit within the same experimental paradigm (MTS). Some specific examples include Courtney et al., 1994 and Dragomir-Daescu et al., 2018, were both studies found a significant effect of loading rate. However, upon review of their analyses, the report effects appear to be modest. In the case of the study by Courtney and colleagues, they report significantly higher fracture loads in their high-displacement rate (100 mm/s) MTS experiments for both their younger and older groups when compared to the low rate (2 mm/s) experiments. While the authors do not report any statistics related to the full sample (combining both groups), nor do they report the mean differences within groups (between loading rates), digitization of the published figures reveal a mean difference of ~ 690 N for the younger group and ~ 730 N for the older group. When compared to the results observed in this investigation, the mean difference between the HIS and MTS experiments was 455 N. While this mean difference is lower than the estimated mean difference of either group in the Courtney et al., 1994 study, it does not differ in orders of magnitude. Further, it is possible that effect of loading rate on femoral bone strength is larger or more apparent at the lower spectrum of

loading rates. Similarly, Dragomir-Dascue and Colleagues 2018 study investigated the effect of loading rate, or more specifically displacement rate, by using three displacement rates for MTS experiments (5, 100, and 700 mm/s). Once again, reported findings are limited, however, displacement rate significantly related to femoral bone strength. However, the authors state that the addition of this factor (as well as NSA, another significant factor) to a regression model that already included femoral neck aBMD, sex, and age, R^2 was only improved by 0.008. While it isn't possible to make any direct comparisons with this study, the fact that so little additional variance was explained by the addition of displacement rate may suggest that it had a relatively small effect on bone strength. It should also be noted that in both studies, a much larger sample size was achieved (Courtney et al., 1994 N = 20 pairs; Dragomir-Daescu et al., 2018 N = 197 femurs); a post-hoc power analysis revealed that a sample size of 38 pairs would have resulted in a significant effect of loading rate on F_x (assuming the mean and standard deviation of the differences remained the same). However, significant relationships between F_x and *LR* were observed when assessed within paradigms. It is likely that, due to the relatively consistent loading input, this relationship is driven by the stiffness of the individual specimens.

As previously mentioned, specimen stiffness of the MTS specimens generally aligned with *LR* ($R^2 = 0.893$), as well as with F_x ($R^2 = 0.879$). While stiffness couldn't be directly measured in the HIS experiments, it is likely that HIS specimen stiffness was also positively correlated with both F_x and *LR*. Though the impact velocities of the HIS experiments were slightly more variable (CV = 0.015) than the displacement rate of the MTS experiments (CV = 0.005), the level of variability in *LR* within paradigms was similar (HIS CV = 0.328, MTS CV = 0.361). Coupled with the very strong positive relationship between *LR* and F_x that was observed in both paradigms, these results suggest that individual specimen stiffness contributes more to the ultimate strength of the bone when compared to either impact velocity or displacement rate. More specifically, the results of this study suggest that the elastic stiffness (Young's modulus, *E*) of the specimens largely dictates the mechanical response to load, and that any viscoelastic stiffness component not significantly contributing to the response, at least not at the impact velocities nor the displacement rates used in this study. While previous studies have observed rate dependent mechanical behaviour of cortical bone specimens and of whole femurs (Carter and Hayes, 1977; Courtney et al., 1994; Currey, 1988; Dragomir-Daescu et al., 2018; McElhaney, 1966) it is possible that the

impact velocity and displacement rate used in the currents experiments were either too high, or too close to each other, for this study to have observed a similar effect.

A more recent study by Jazinizadeh et al., 2020 seems to suggest this. The authors performed a similar experiment to investigate a similar question related to loading rate and femoral bone strength in the context of fall-related hip fractures. In Jazinizadeh and colleagues' 2020 study, bone strength was evaluated using a cohort (N = 8) of matched pairs of cadaveric femurs, subjecting the femurs of a given pair to two different experimental paradigms. These included a "high rate" loading experimental paradigm, involving a pneumatic projectile system to emulate a fall-related hip impact, and a "low rate" loading paradigm that used mechanical test system to emulate quasi-static loading. The mean (SD) loading rate achieved by the impact "high rate" experiments, 4634 (1774) kN/s, was slightly higher but near to the range of loading rates observed during this study's HIS experiments (range = 1582.64 – 3661.25 kN/s), despite using an impact velocity of 3 m/s compared to the 4 m/s impact velocity targeted in this study. While the impact dynamics of "high rate" loading scenarios are similar between this study and the study by Jazinizadeh and colleagues', the loading scenario of the respective "low rate" group is drastically different. While the MTS experiments conducted in the present study achieved a mean (SD) loading rate of 27.78 (10.03) kN/s (range = 16.85 – 43.54 kN/s), a quasi-static loading scenario with a loading rate of 0.017 mm/s was used in Jazinizadeh et al.'s 2020 study, with a mean (SD) loading rate of 2(1) N/s. As Jazinizadeh and colleagues used a similar sample size and similar "high rate" experimental paradigm yet observed a significant difference where the present study did not, it is possible that the reason for the difference lies in the "low rate" experimental paradigm used, or more specifically, the relative rate disparity between the "high" and "low" rate conditions (that is, the HIS or IM experiments compared to the MTS experiments) used in the studies. These findings further suggest that the effect of loading rate is likely more apparent at the lower end of the loading rate spectrum, as posited above. However, as there are other important differences between the studies, it is not possible to draw any clear conclusions. Further limiting the ability to arrive to specific conclusions are the several limitations of this study.

As previously mentioned, the included sample size (N = 6 pairs) is the first limitation of this study. Based on findings from previous research identifying a significant effect of loading rate on femoral bone strength in the context of fall-related hip fractures (Courtney et al., 1994; Dragomir-Daescu et al., 2018; Gilchrist et al., 2014; Jazinizadeh et al., 2020), it was thought that

the proposed sample size of 10 pairs would be sufficient to identify a significant difference in F_x between experimental paradigms. As the statistical implications of the limited sample size were discussed in the previous paragraphs, it is important to highlight the source of this limitation. Despite continued efforts, trends in body donation through the University of Waterloo's School of Anatomy Body Bequeathal Program changed over the course of the COVID-19 pandemic. As this study, and the larger thesis, was planned previous to the emergence of the COVID-19 virus, observed trends in the frequency of body donations (both for research and teaching purposes) suggested that there would be no issue achieving the desired number of femur pairs acquired through the program within the proposed timeline of the thesis. However, COVID-19-related barriers and limitations caused a halt in the acceptance of donors during the early period of the pandemic, and donations did not return to their normal frequency in the mid-to late-COVID-19 period. Since time of the proposal, only 1 additional donor was received; this includes a substantial period beyond the initial proposed timelines of the thesis. Regardless, as previously mentioned, it is possible that the results of this study would not have changed even with the inclusion of additional specimens. Indeed, the findings of previous investigations, when compared to the findings of this study, suggest that the effect of loading rate on F_x may be less pronounced at the range of loading rates used in this study, explaining why no significant difference in F_x was observed between experimental paradigms.

A second limitation of this study relates to the experimental paradigms used, and more specifically, their design and associated parameters. While the HIS paradigm, specifically the simulated pelvis system, was designed to be more biofidelic compared to the MTS paradigm, the HIS consequently has many more degrees of freedom. This could have led to greater variance or random error introduced trial to trial. Indeed, the guide rods failed to prevent the springs from deforming differently, resulting in the impact plate assuming an orientation that was not parallel to the top of the force plate. This change in the orientation of the impact plate during the impact and loading of the specimens may have changed the direction of loading slightly. However, it is unlikely that this affected the measured F_x, as the standard deviation in F_x is similar between experimental paradigms. In fact, the variance is actually lower in the HIS paradigm experiments (1272.6 N) when compared to that of the MTS paradigm experiments (1285.8 N). This latter point may suggest that, despite the greater degrees of freedom, there wasn't any more variance introduced into the experiments due to this effect. Appendix A (Chapter 8.1) provides further detail

on the potential limitations associated with the current HIS. The parameters used in both experimental paradigms, specifically the impact velocity of the HIS experiments (4 mm/s), does potentially limit the clinical relevance of the results. While the HIS experiments were designed to be overall more biofidelic of fall-related hip impacts and fractures, this impact velocity is higher than what is typically observed during fall-related hip impacts (1.29 – 3.51 m/s) (Choi et al., 2015). The reason for this, as explained in section 3.2.3.1, was to help ensure (or increase the odds) of a fracture being induced during the experiments. While loading rate would likely have been lower if a lower impact velocity was used, it would have likely been still significantly higher than the loading rate of the MTS experiments. An additional investigation comparing loading rate of the current HIS experiments and lateral pelvis release experiments with live volunteers does suggest that the impact dynamics of HIS experiments are much more closely aligned with those of actual hip impacts compared to MTS experiments) (see Appendix B, Chapter 8.2). Indeed, based on the proposed definition of biofidelity, which is "the degree to which the simulated lateral impact produces loading of a cadaveric proximal femur specimen that matches that measured from human volunteers during a fall-related lateral hip impact" (Appendix B, Chapter 8.2), the HIS experiments are more biofidelic than MTS when compared to the impact dynamics of lateral pelvis release experiments conducted in a previous investigation (Martel et al., 2018).

While it is speculated that sufficient specimen thawing time was employed in this study, the lack of explicit surface and internal temperature measurements, in addition to the lack of quantification of specimen hydration or moisture levels, is a third limitation. Beyond implications related to changes in the mechanical behaviour of frozen tissue compared to fully thawed and hydrated tissue, a recent study by Ma and colleagues revealed that the strain behavior and compressive strength of cortical bone samples differed when tested at 38.5 degrees Celsius compared to room temperature, observing a general decrease in strength at this elevated temperature (Ma et al., 2020). Future work should include measures of specimen hydration, surface temperature, and if possible, internal temperature to confirm common test conditions for specimens. Additional considerations related to testing specimens in thermostatic conditions replicating the internal environment of the body should be investigated.

A final, yet similar, limitation relates to the displacement rate used for the MTS experiments (~60 mm/s), as using displacement rate of 100 mm/s would have allowed for more direct comparisons with previous studies (Courtney et al., 1994; Dragomir-Daescu et al., 2018;

Roberts et al., 2010). Unfortunately, mechanical limitations with the Instron MTS system limited displacement rate to 60 mm/s. However, the loading rate associated with the 100 mm/s displacement rate would likely still have been significantly lower than the HIS experiments, based on an estimated 200 kN/s loading rate presented in Roberts et al., 2010 (extrapolated from a digitized version of a load-displacement figure presented in the manuscript). While being able to achieve a displacement rate of 100 mm/s would have been ideal, doing so would not have significantly changed the findings of this study, and is thus not a true limitation.

3.5 Conclusion

In order to determine the importance of using a biofidelic experimental paradigm to quantify femoral bone strength in the context of simulated lateral hip impacts, this study used matched pairs of fresh frozen cadaveric femurs to compare the bone strength obtained through the use two different experimental paradigms. The first of these paradigms was a vertical drop tower HIS experimental paradigm, which is proposed to be more biofidelic in emulating the impact dynamics of fall-related lateral hip impacts, and the second paradigm being an MTS experimental paradigm using a constant displacement rate, which is the most commonly used method to quantify femoral bone strength. While a significant difference in the loading rate was observed, with HIS experiments inducing significantly higher loading rates, there was no observed difference in the measured bone strength between the two paradigms. When compared to results reported from previous investigations, it is possible that previously observed relationship between loading rate and bone strength was not observed in this study as the effect of loading rate may be more apparent at lower rates. Though the loading rate induced by the HIS was much higher than both previously observed loading rates, the loading rate induced by the MTS was also higher than the loading rates observed in the "low rate" conditions of previous studies that have found an effect of loading rate. Regardless, the results of this study suggest that, while there seems to be no difference in measured bone strength when using either the HIS or MTS paradigms, HIS experiments are a valid method to measure femoral bone strength in the context of fall-related hip fractures. Furthermore, these results also suggest that the results of HIS experiments can be directly compared to previous investigations that use the MTS paradigm.

Chapter 4
Study 2: Development of Predictive Models to Estimate Fracture Force of the Proximal Femur

4.1 Introduction

The frequency and severity of fall-related hip fractures in older adults necessitate methods to predict risk of hip fractures. With an estimated annual cost ranging from $650 million to $1.1 billion in Canada alone, older adults suffer the greatest number of hip fractures of any age group (~30 000 annually), with rates of hip fracture rising dramatically after age 60 (Jean et al., 2013; Nikitovic et al., 2013; Wiktorowicz et al., 2001). While the rates and cost of these injuries are concerning on their own, the reality that approximately 20% to 40% of these cases result in death within the first year of injury is alarming (Ioannidis et al., 2009; Jiang et al., 2005). As a clear public health concern for this population group, there is a concerted effort to prevent these injuries. One of the primary strategies employed to address this issue has been through the prediction or estimation of individual risk of hip fracture.

While determining an individual's risk can be difficult, due to the plurality of variables that may affect risk (many of which are age-related) (Caillet et al., 2015; Campbell et al., 1989; Davis et al., 2019; Greenspan et al., 1998; Grisso et al., 1991; Rubenstein, 2006 Kaptoge et al., 2003 Dinçel et al., 2008 Courtney et al., 1995), risk assessment is a crucial step for injury prediction and ultimately prevention. Traditionally, hip fracture risk has primarily been assessed through measures of femoral areal Bone Mineral Density (aBMD), which has been repeatedly shown to strongly correlate with femoral bone strength under lateral loading thought to be experienced during fall-related hip fractures (Cheng et al., 1997; Courtney et al., 1995, 1994; Dall'Ara et al., 2013a; see Table 2-1). The relationship between bone strength and aBMD, supported by the fact that aBMD tends to decrease in older age (Hendrickx et al., 2015; Santos et al., 2017), has largely driven our current efforts of hip fracture risk prediction (Aspray, 2015; Cummins et al., 2011; Dagan et al., 2017; Fraser et al., 2011; Johansen, 2012; Kanis et al., 2018, 2012, 2008b; Leslie et al., 2012). Furthermore, the relationship between femoral aBMD and hip fracture risk is also supported by epidemiologic evidence wherein individuals identified as being osteoporotic, a state of low bone mineral density, have been observed to have elevated risk and rates of fall-related fractures, including hip fractures (Barry et al., 2012; Burge et al., 2007). Therefore, hip fracture risk can be inferred from an epidemiologic perspective, comparing measured aBMD to a value

representative of healthy levels (as done in the T-score, which categorizes individuals as normal, low bone mass/osteopenia, osteoporosis, each having higher risk of fracture than the last), or by using a mechanistic approach, predicting bone strength from the measured aBMD to estimate tissue tolerance and ultimately fracture risk. Regardless of which approach is used, however, accurate prediction of hip fracture risk remains difficult as many hip fractures go unpredicted (Schuit et al., 2004; Siris et al., 2004; Stone et al., 2003).

Previous studies have developed predictive models of femoral bones strength for the purpose of fracture risk prediction (Dall'Ara et al., 2013a; Table 2-1), yet many fall related hip fractures occur in individuals whose predicted bone strength was associated with a low risk of fracture (Schuit et al., 2004; Siris et al., 2004; Stone et al., 2003) . As suggested by Gilchrist et al. 2014, and further investigated in Chapter 3, it is likely that the standard method of measuring femoral fracture force using constant displacement rate materials testing system tests lead to significantly lower measures of fracture force compared to those experienced in fall like loading (Gilchrist et al., 2014). Consequently, predicting femoral bone strength using models developed from these experiments may produce results that underestimate the actual tolerance of the femur, leading to inaccurate predictions of fracture risk. Additionally, we must consider if the difference in measured fracture force between test paradigms is simply a systematic difference driven entirely by loading profile and rate, or due to further interactions involved in testing the femur in different paradigms.

Therefore, the goal of this study was to measure the fracture force of the proximal femur in simulated lateral impacts using a biofidelic test paradigm and ultimately develop a model for the prediction of bone strength. In general, it was hypothesized that bone strength (F_x) would increase with increasing femoral neck aBMD (*BMD*) and cross-sectional moment of inertia (*CSMI*) (as higher values of both are associated with increased stiffness and bending resistance), and a decrease in F_x with increasing age (*a*) and moment arm (r). Additionally, it was hypothesized that F_x would be lower for specimens from female donors when compared to those from male donors. In addition, it was hypothesized that the developed model would result in significantly higher predicted bone strength values when compared to predictions from previously developed models that utilized relatively low (and constant) displacement rate paradigms.

A secondary goal of this experiment was to investigate the potential influence of bone quality affecting disease states, such as Diabetes Mellitus and Chronic Kidney Disease, on bone

strength. It was hypothesized that the presence of these disease states would be negatively associated with F_x, and that accounting for the presence these disease states would improve the ability to accurately predict bone strength.

4.2 Methods

4.2.1 Sample Acquisition and Preparation

All femurs used in this study were acquired from fresh frozen cadavers either received through the University of Waterloo School of Anatomy's Human Body Bequeathal program (N = 6 femurs collected in Study 1), or acquired through licensed organ and tissue banks, specifically: Innoved Institute L.L.C., RegenMed, and National Disease Research Interchange (N = 26 femurs). After testing, six specimens failed to fracture after two impacts, and were excluded from the study (see Section 4.2.3.1), resulting in a final sample size of N = 26 femurs. Similar to the preparation methods used in Study 1 (Chapter 3), the femurs were transected at the mid-diaphysis, 15 cm distally to the greatest lateral protuberance of the greater trochanter, resulting in a proximal femur specimen. Following transection, each proximal femur specimen was sealed in a plastic bag and stored in one of two tissue specimen freezers (freezer temperature ranging from -20 to -80 degrees Celsius); all specimens were handled in a way to minimize the number of freeze-thaw cycles, with a maximum of three cycles occurring.

4.2.2 Specimen Characterization

The proximal femur specimens underwent characterization using the methods described for Study 1 (Chapter 3.2.2.1). Briefly, the specimens underwent clinical characterization via high-resolution hip specific DXA scans to extract femoral neck areal bone mineral density (*BMD*) (Figure 4-1). Additional geometric parameters (*r* and *CSMI*), were extracted from the DXA scans using custom MATLAB code (Pretty, 2018). A table including specimen images and details is presented below (Table 4-1).

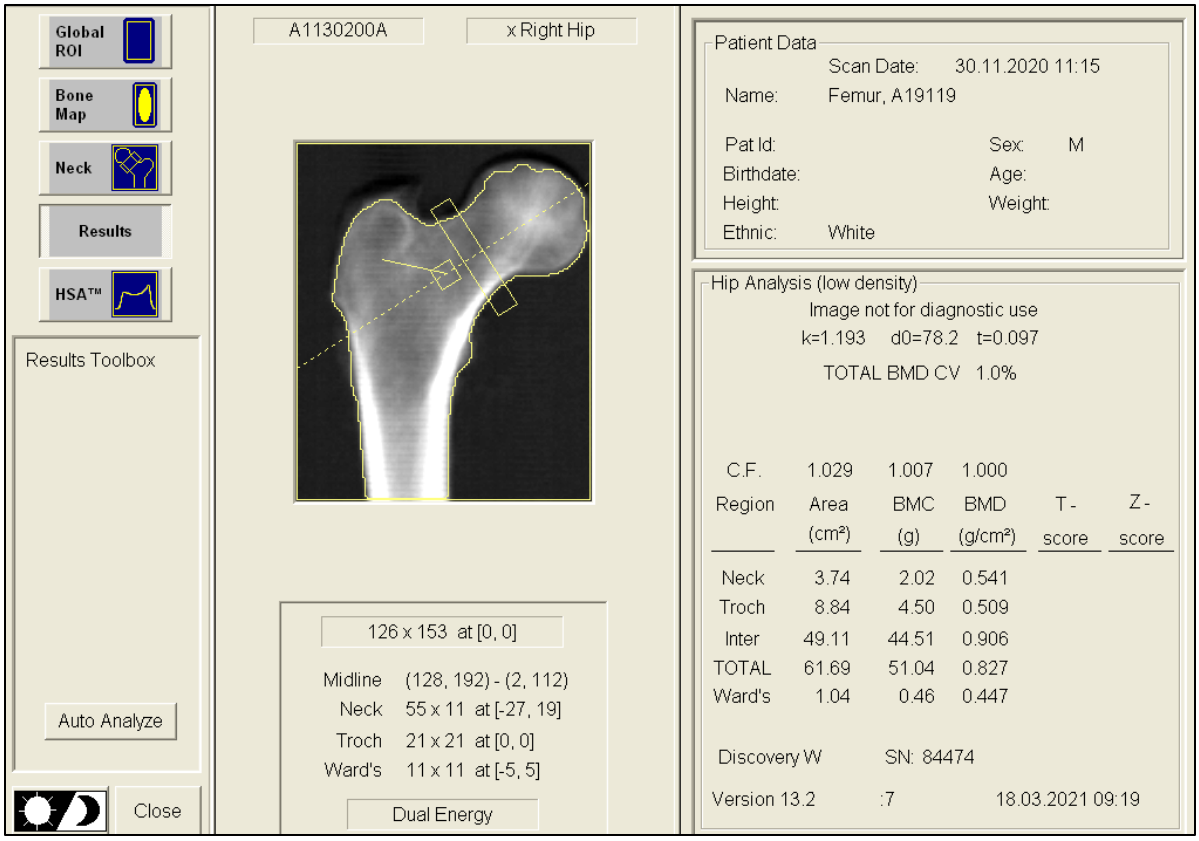

Figure 4-1: High quality hip specific DXA scan of a femur specimen, with associated image analysis results, including the measure for femoral neck aBMD used in this study.

Table 4-1: Specimen ID Table consisting of DXA images, X-ray images, Experimental images, and specimen ID.

Specimen ID	DXA Image	X-ray Image	Experimental Image
1	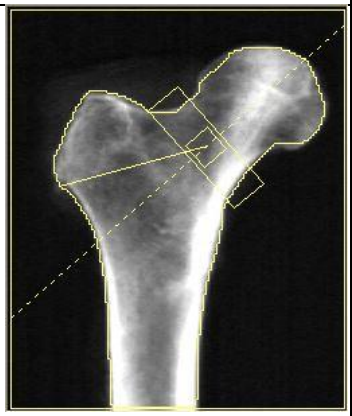		
2	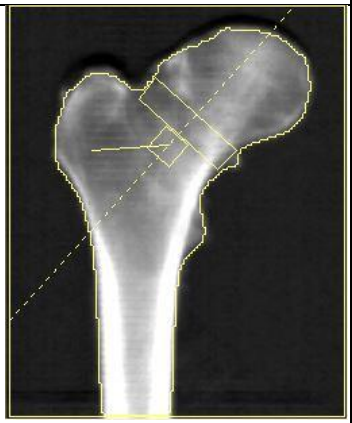	X-ray Unavailable	
3	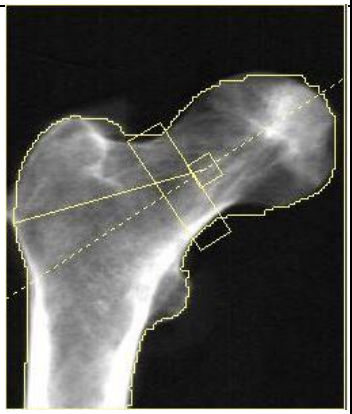		

4	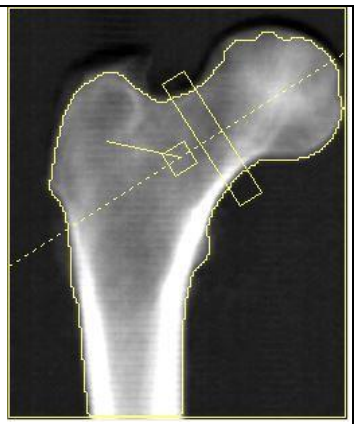	X-ray Unavailable	
5	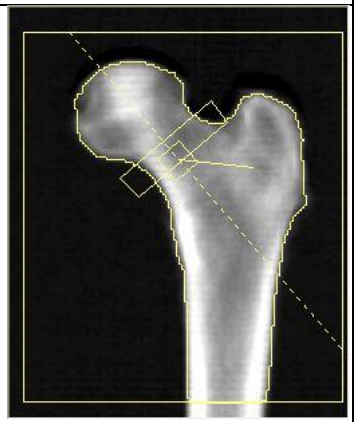	X-ray Unavailable	
6	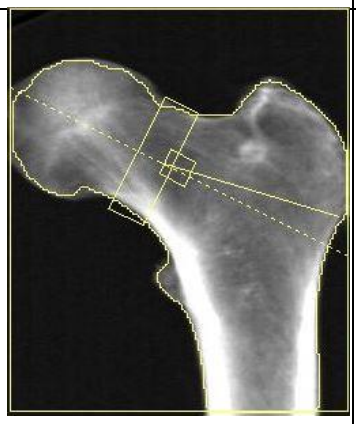	X-ray Unavailable	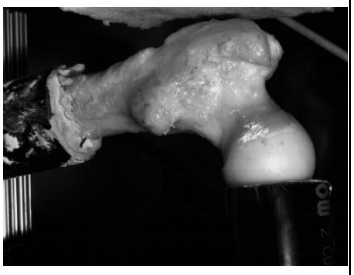
7	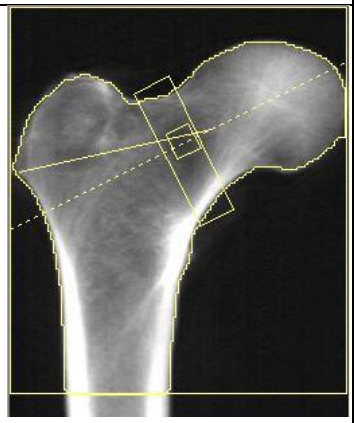		

8	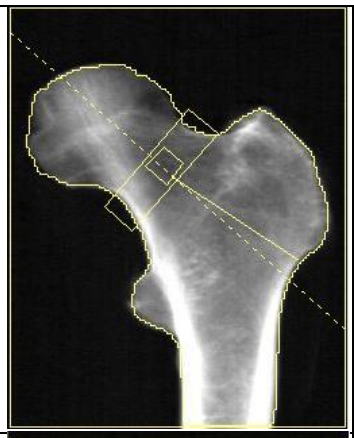	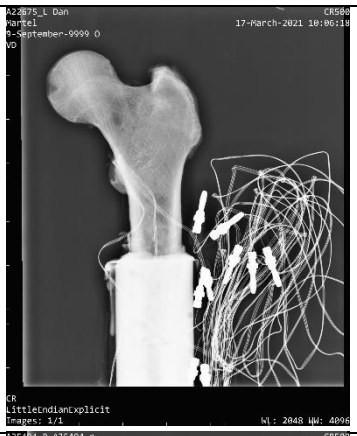	
9	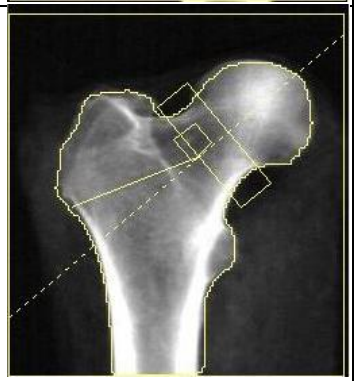		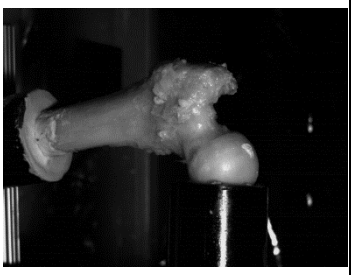
10	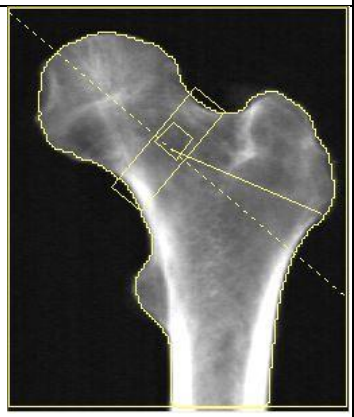		
11	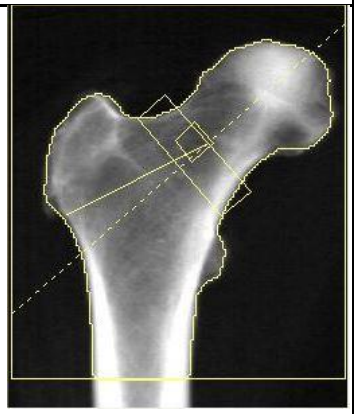	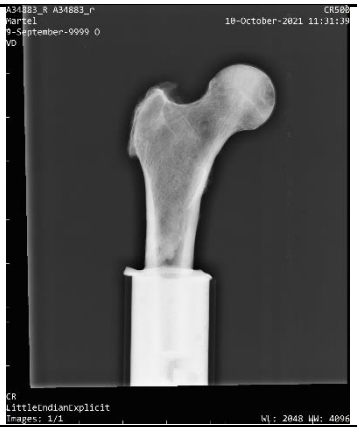	

12	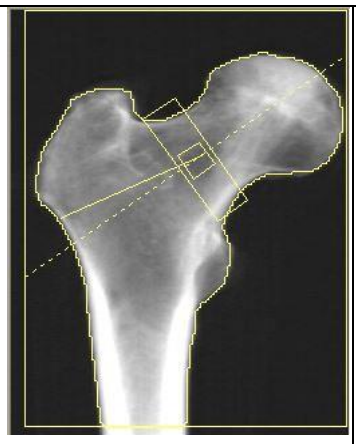		
13	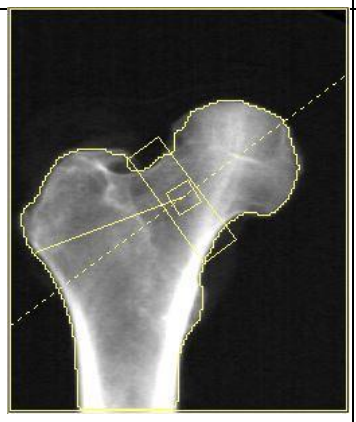		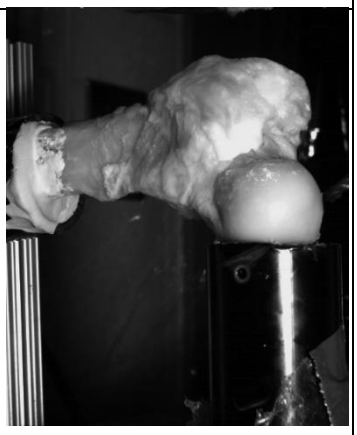
14	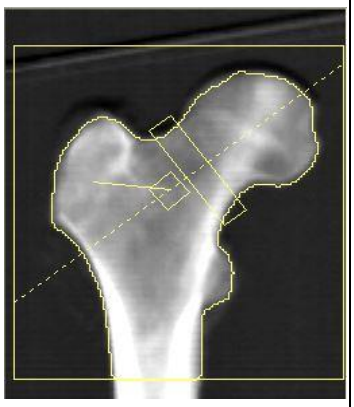	X-ray Unavailable	
15	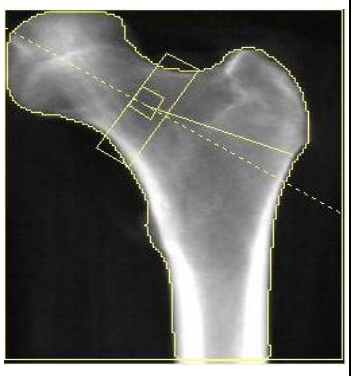		

16	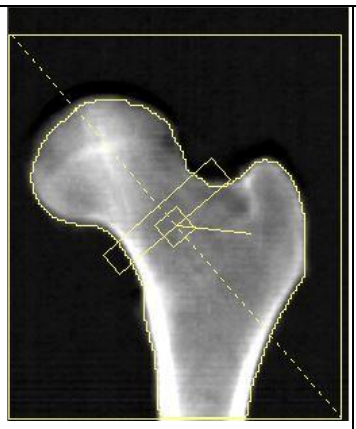	X-ray Unavailable	
17	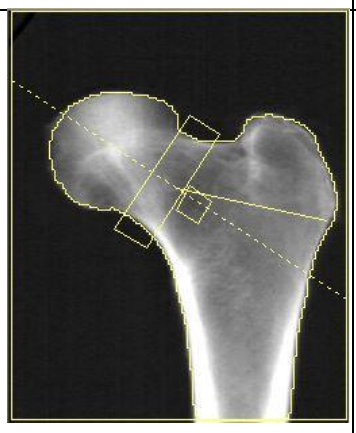		
18	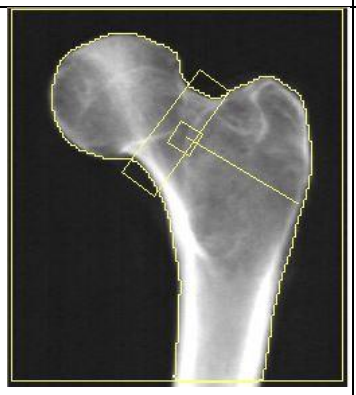		
19	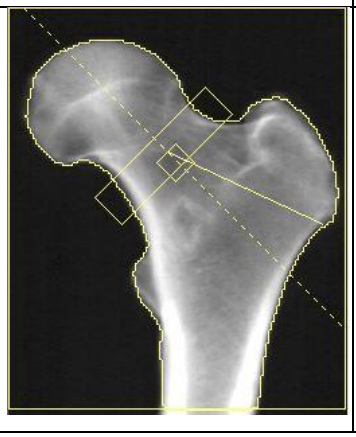		

20	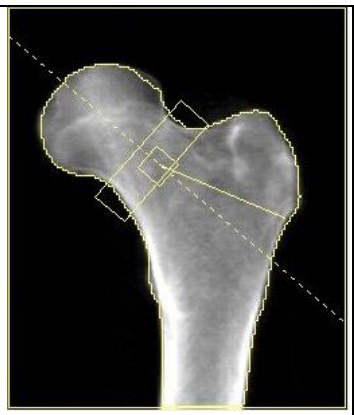		
21	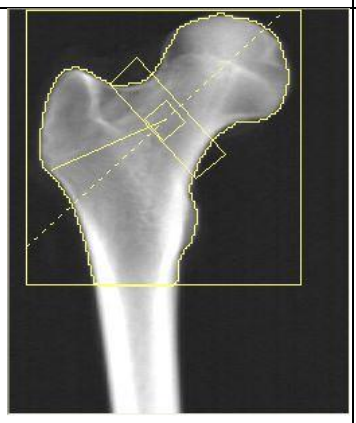		
22	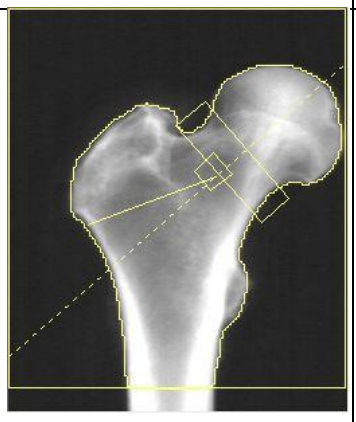		
23	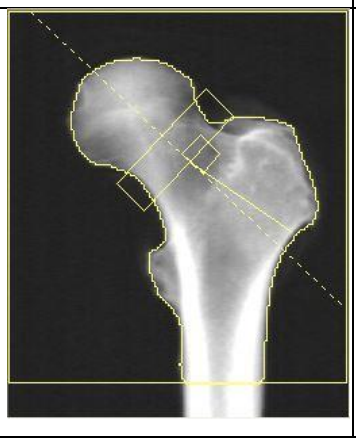		

24	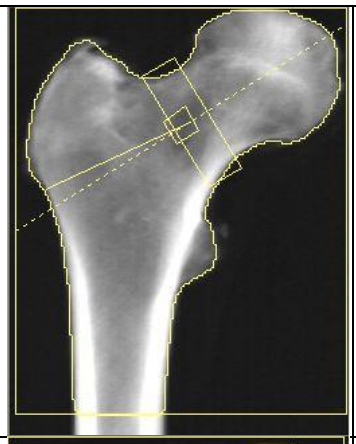		
25	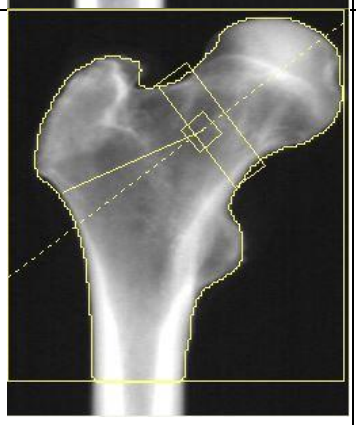		
26	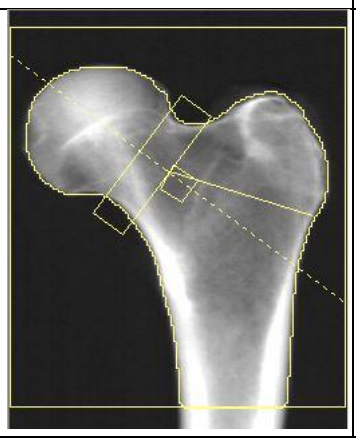	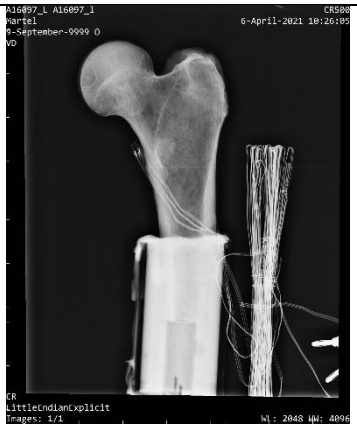	

4.2.3 Testing Preparation and Protocol

Specimens were prepared to undergo testing in the drop tower HIS, as detailed in Study 1 (Chapter 3.2.2.2). Briefly, the distal 5 cm of the specimen was encased in dental stone within a 10 cm long, 2" (5.08 cm) diameter ABS pipe, and then set in the mounting jig with a 10-degree abduction and 15 degrees internal rotation angle (Courtney et al., 1995, 1994). Similar to the methods used in Study 1, a frontal plane X-ray image of the potted specimen was captured using an M3001125 Mercury Module (Faxitron, Tuscon, AZ, USA) as a secondary assessment of bone

quality, as well as a method to identify any potential defects or pre-existing damage of the specimen. Similar to Study 1, axial rotation was limited by fixing the potted specimen to the mounting jig via screws (Figure 4-2), and a foam pad (5x5x5 cm cube, 3 cm thickness at greater trochanter) was placed over the greater trochanter, emulating the soft tissue overlying the hip. Using the same parameters as those used in the HIS tests of study 1 (40 kg mass, 4 m/s impact velocity, 45 000 N/m system stiffness), specimens were subjected to a single, high-energy impact to induce a fracture of the specimen. Time-varying load applied to the proximal femur was measured by a force plate (AMTI OR3-6-2000, AMIT, Watertown, MA, USA).

Figure 4-2: Proximal femur specimen mounted in the mounting jig. The jig was affixed to the top surface of the force plate and placed beneath the load carriage of the vertical drop tower Hip Impact Simulator (HIS).

4.2.3.1 Failed Trial Contingency Protocol

In the event that the impact did not result in a fracture, the specimen was removed from the mounting jig and a second X-ray image was acquired to assess any potential structural changes, or the presence of mechanical defects. In the event that the specimen did not fracture in the first impact trial, yet noticeable changes were observed on the second (post-impact trial) X-ray image, the situation was noted, and the specimen was excluded for the purposes of this study. If no defects are present, or more specifically if no noticeable changes are present when compared to the pre-trial X-ray image, the specimen was noted as such, and the specimen was subjected to a second impact. Finally, if a fracture was not produced after a second impact trial, the specimen was excluded. Additional details can be found in Appendix C (Chapter 8.3).

4.2.4 Data Analysis

Similar to study 1 (Chapter 3), the dependent variables for this study were fracture force (F_x) which is measured by the HIS force plate. Specifically, the peak force (prior to specimen fracture) recorded during the trial, was identified as the fracture force (F_x), the primary dependent variable for this study. To help identify the start of the impact, as well as the point of fracture, time-varying force data was down sampled to match synchronized high-speed video of the experiments. The frames of first visual contact and of visual fracture were identified, and these frames (as well the two preceding and proceeding frames) were plotted on a time-varying force curve to help identify F_x (Figure 4-3).

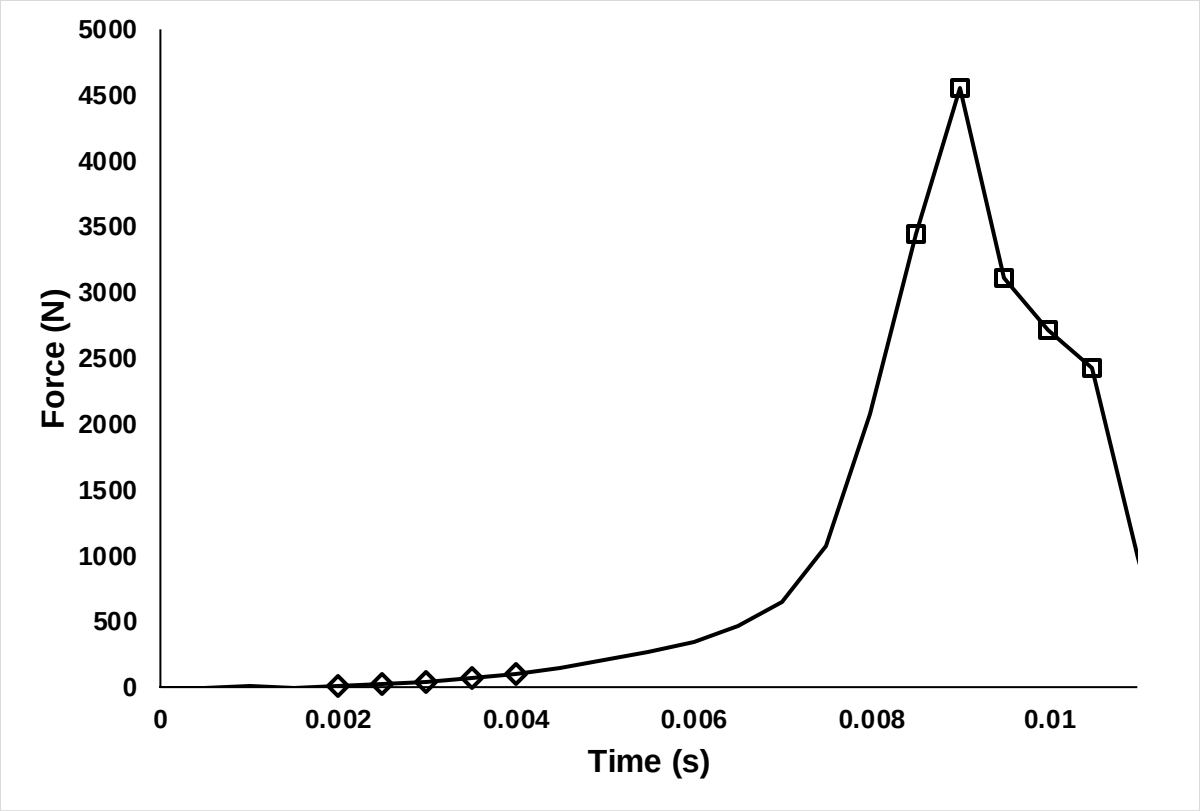

Figure 4-3: Example force time trace of a HIS impact trial. Diamonds and square points represent possible frames aligned with visual identification for the start of impact (diamonds) and moment of fracture (squares).

4.2.5 Statistics and Data Interpretation

All statistical analyses were conducted using the R programing language within the RStudio integrated development environment (IDE). Multiple linear regression (generalized-linear models, GLM) was used to investigate the effects of the independent variables (*age*, *sex*, *BMD*, *r*, *CSMI*) on F_x. Based on the estimated power of the analyses (using the effect size derived from previous femoral bone strength studies), there was sufficient power to allow for linear regression analyses with up to four predictors. Thus, the four strongest independent variables (based on the level of significance) were retained for multiple linear regression analyses. As the main goal of this study was to develop a robust predictive model for proximal femur bone strength (fracture force), a subset of the sample (~25%, N = 6) was reserved as a validation (or test) set, with the remaining portion of the sample (~75%, N = 20) being used as the model (or training) data set. To ensure the validation sample covered the full range of measured Fx values, the full sample was

ordered by increasing F_x, with the ordered list being split into 6 groups (four groups of 4, two groups of 5, Table 4-2); one specimen was randomly selected from each group and assigned to the validation sample (N = 6). The remaining specimens (N = 20) were assigned to the model sample.

Table 4-1: Specimen details, including grouping used to block-randomly select specimens for the validation sample; specimens were ordered in order of ascending F_X.

Group	Specimen Identifier	*r* (cm)	*CSMI* (cm^4)	*age* (years)	*Sex*	*BMD* (g/cm^2)	F_x (N)	Validation selections
1	1	5.01	0.83	63	F	0.533	2230.8	
	2	5.65	1.23	100	F	0.617	2320.1	V
	3	6.51	1.04	103	M	0.504	3201.5	
	4	4.76	0.94	90	M	0.545	3288.5	
2	5	5.63	0.39	85	F	0.535	3763.7	
	6	5.09	1.54	93	M	0.505	4141.7	
	7	3.97	1.73	74	M	0.469	4395.2	
	8	5.52	0.68	92	M	0.333	4471.1	V
	9	3.27	0.79	87	F	0.487	4500.1	
3	10	5.17	1.50	88	M	0.583	4557.6	
	11	5.68	1.14	80	F	0.532	4642.6	
	12	4.57	1.26	96	M	0.607	5157.1	
	13	4.48	1.00	55	F	0.646	5168.7	V
	14	4.32	1.09	90	M	0.638	5391.2	
4	15	5.01	1.22	91	M	0.621	5418.0	V
	16	5.82	1.02	57	M	0.490	5678.6	
	17	4.30	1.02	76	M	0.550	5787.1	
	18	2.87	1.06	76	F	0.680	5952.5	
5	19	5.27	1.64	70	M	0.709	6106.6	
	20	4.61	1.30	75	F	0.891	6685.3	
	21	4.34	1.05	48	F	0.808	7498.0	V
	22	5.06	1.30	68	M	0.766	7761.3	
6	23	4.44	1.05	84	M	0.727	8019.0	
	24	5.09	1.98	83	M	0.757	8442.8	
	25	5.34	2.04	83	M	0.762	8800.3	
	26	5.00	1.73	65	M	0.749	9104.8	V

With the goal to develop the most accurate predictive model, both forward selection and backward elimination stepwise regression were conducted, with the strongest of the two models being retained. These stepwise regression analyses used the four strongest predictors identified in

the previous GLM, considering main effects and interactions. Evaluation of model strength at this phase was based on a combination of the Akaike Information Criterion values corrected for small sample sizes (AICc), the adjusted R^2 values, and *p* values. Additionally, due to the potentially large number of predictors that could be retained, particularly through the backward elimination process, a parallel stream of model development was also explored, wherein regularization of the linear models was completed via the least absolute shrinkage and selection operator (LASSO) method (Li et al., 2019; Tibshirani, 2011, 1994). This regularization method removes predictors from the regression model (as with backward elimination stepwise regression) while including an additional term in the minimizing function that penalizes for large numbers of included factors. The purpose for this parallel stream of analysis was to strike a balance between developing the most robust model with relatively few predictors, which is an important model characteristic which facilitates implementation and adoption in clinical fracture risk prediction (particularly for potential clinical purposes). Thus, this process was used to develop a model that sits somewhere between the forward selection and backward elimination stepwise regression models in terms of model complexity. Additional detail about the LASSO process can be found in Appendix D (Chapter 8.4). Following the identification and development of these models (GLM and LASSO-GLM), F_x was predicted for the validation set for both models. The predictions were compared to their actual measured F_x values, and the mean squared error (MSE) was computed; the model with the lowest overall MSE in this step was determined to be the stronger overall model, to be used in the final analysis of this study.

Finally, towards comparing this study's model predictions to the predicted F_x obtained from four previously published models (Table 4-3), one paired-samples t-tests comparing F_x each of the published models to this study's model were conducted.

Table 4-2: Previously published models to predict femoral neck bone strength from femoral neck aBMD (BMD).

Model (Source)	Equation	Testing Rate (Constant Displacement)	R^2
Courtney et al., 1994	10 500 * BMD -1810	High – 100 mm/s	0.72
Courtney et al., 1995*	12524.54 * BMD - 4035.3	Low – 2 mm/s	0.92
Dall'Ara et al., 2013a	6365 * BMD – 688	Low – 0.083 mm/s	0.80
Roberts et al., 2010	8207 * BMD – 568.62	High – 100 mm/s	unreported

4.2.5.1 Statistical Model Robustness and Repeatability

In addition to developing the best overall and most accurate predictive model of femoral bone strength, there is value in evaluating the robustness of the proposed model. Though not typically performed in the published literature, conducting repetitions of statistical analyses, particularly in the case of stepwise regressions, can provide valuable insight on the robustness of the resulting model in terms of the retained model predictors. It also allows investigators to determine whether the model resulting from a stepwise regression will be repeatedly found if a different subset of the sample is used as the model or training set. Towards these ends, a robustness and repeatability analysis was conducted, wherein new model and validation samples were defined from the data collected in this study. The previously described regression analyses were then conducted on these new model samples and the predictions of the resulting models were compared against the measured values of the validation samples to assess model accuracy. This allowed the identification of the most commonly retained factors following the stepwise regression analyses, as well as evaluation of the relative accuracy of these models.

Using the same methods described in section 4.2.5, 10 new paired model and validation samples were defined, and the stepwise regression analyses were performed, considering both forward selection and backward elimination models (labeled "Fwd" and "Bwd", respectively); each analysis was identified as a repetition, with 10 repetitions total. To facilitate comparison to models published in the literature, two additional models were evaluated for each newly generated model and validation sample. These models were

- $F_X \sim BMD$, labeled "BMD"
- $F_X \sim BMD + Sex$, labeled "Main"

Lastly, the model identified as the best overall model prior to the robustness and repeatability analysis was also evaluated (labeled "Inter", for the interaction effect between BMD and Sex, in addition to the main effects of BMD and Sex). Relative performance of each of the evaluated models was based firstly on the MSE for the predictions of Fx for the validation sample, followed by the model's AICc. From this set of analyses, the following were identified:

- The models most commonly emerging from the stepwise regression analyses
- The most commonly retained main and interaction effects
- The models with the lowest normalized MSE. Normalized MSE was computed by:
    - Computing Z score for each model for each repetition
    - Calculating mean Z score for each model
    - Identifying the model with the lowest mean Z score is best, as negative values indicate improvements in model performance
- The models with the lowest mean AICc. Normalized AICc was computed by:
    - Computing Z score for each model for each repetition
    - Calculating mean Z score for each model
    - Identifying the model with the lowest mean Z score is best, as negative values indicate improvements in model performance

A Z score was computed for each of MSE and AICc for the four models in all of the 10 repetitions, and the mean Z score of each model (across the 10 repetitions) was calculated in order to compare between models. Based on these four summary observations, it was determined whether the model identified as the best overall model prior to the robustness and repeatability analysis ("Inter") was indeed the most appropriate model (based on relative model performance),

and identified which factors should always be considered and included in the predictive model (based on the frequency of factor emergence).

4.2.5.2 Disease Analysis

Towards investigating the effect of disease state on bone strength, a secondary analysis was performed wherein presence of an inflammatory disease state was added to the dataset. As this information was not available for all specimens, this analysis was conducted on a subset of the study sample (N = 20). Following a similar protocol to the previous analyses, a multiple linear regression analysis was conducted in order to investigate the main effects of the independent variables (*age*, *sex*, *BMD*, *r*, *CSMI*) as well as an additional variable (*d*) representing disease state (with a 1 representing the presence of an inflammatory disease state, and a 2 representing no such disease state), on F_x. Due to the limited power afforded from the sample size, only the three strongest predictors (based on the level of significance) were retained, in addition to disease state, which was forcibly retained for the purpose of addressing the goal of this analysis. The four retained predictors were then used in a stepwise regression analysis to identify the strongest overall model. If resulting models retained disease state, the strength (R^2), the significance (p), and the AICc scores of the models would be compared to the models without disease state to determine whether this variable added predictive value.

4.3 Results

Characteristics of the specimens included in the analysis, and descriptive statistics of dependent measures, are presented in Table 4-4 below. Shapiro-Wilk's tests of normality for *age*, *BMD*, *r*, and *CSMI*, as well as for the dependent variable F_x, revealed that none of the variables violated the assumption or normality.

Table 4-3: Specimen information for the A) Full Sample, B) Model Sample, C) Validation Sample. Respective sample size, sex split, and mean (SD) are presented for the independent variables *a*, *s*, *BMD*, *r*, and *CSMI*, as well as for the dependent variable F_x.

A)	**Full Sample: Mean (SD)**					
N	*sex* (F/M)	*age* (years)	*BMD* (g/cm^2)	*r* (cm)	*CSMI* (cm^4)	F_x (N)
26	9/17	79.7 (14.2)	0.617 (0.128)	4.88 (0.78)	1.21 (0.39)	5480.2 (1908.5)

B)	**Model Sample: Mean (SD)**					
N	*sex* (F/M)	*age* (years)	*BMD* (g/cm^2)	*r* (cm)	*CSMI* (cm^4)	F_x (N)
20	6/14	81.0 (11.4)	0.614 (0.120)	4.84 (0.85)	1.23 (0.41)	5425.2 (1816.4)

C)	**Validation Sample: Mean (SD)**					
N	*sex* (F/M)	*age* (years)	*BMD* (g/cm^2)	*r* (cm)	*CSMI* (cm^4)	F_x (N)
6	3/3	75.2 (21.9)	0.629 (0.164)	5.00 (0.53)	1.15 (0.35)	5663.5 (2371.2)

A GLM analysis of the main effects of *age*, *sex*, *BMD*, *r*, and *CSMI* on the measured fracture force (F_x) of the full study sample (N = 26) revealed significant effects for of *BMD* (p = 0.0005) and *s* (p = 0.0079); following these two predictors, in order of significance, were *age* (p = 0.0558), *r* (p = 0.3476), and *CSMI* (p = 0.7546) (Table 4-5). As the following stepwise regression analysis was anticipated to have sufficient power to perform linear regression analyses with up to four predictors (based on the Cohen's f^2 effect size estimation from previous bone strength studies), *age*, *sex*, *r*, and *BMD* were retained, and *CSMI* was removed. The following stepwise regression analyses were conducted on the model sample (N =20).

Table 4-4: Results for the GLM analysis of the main effects of the independent variables (*age*, *sex*, *BMD*, *r*, and *CSMI*) on the dependent variable (*Fx*).

Predictor		*B*	*t*	*p*
Intercept		790.80	0.317	0.755
age		-35.50	-2.030	0.056
sex (1F, 2M)		1710.67	2.951	0.008
BMD		9391.86	4.193	<0.001
r		-288.19	-0.962	0.348
CSMI		246.46	0.317	0.755
		F (df)	Adj. R^2	*p*
		10.74 (5,20)	0.661	<0.001

Forward selection and backward elimination regression analyses predicting *Fx* from *age*, *sex*, *BMD*, and *r* were conducted to identify the strongest overall model, based on AIC (log-likelihood) value corrected for the small sample size (AICc). The model resulting from the forward selection process,

$$F_x \sim 6492.97 * BMD * sex + 1522.53 * BMD - 2900.83 * sex + 2643.21$$

[Equation 3]

(where *sex* is represented as a 1 for females and a 2 for males) had an adjusted R^2 value of 0.688 ($p < 0.001$) and an AICc value of 279.95. In general, this model predicts higher F_x with higher levels of *BMD* and for males (*sex* = 2), with increasing *BMD* resulting in larger increases in F_x for males compared to females (Figure 4-4). Post-hoc power analysis using Cohen's f^2 (2.21) revealed an achieved power of 0.999.

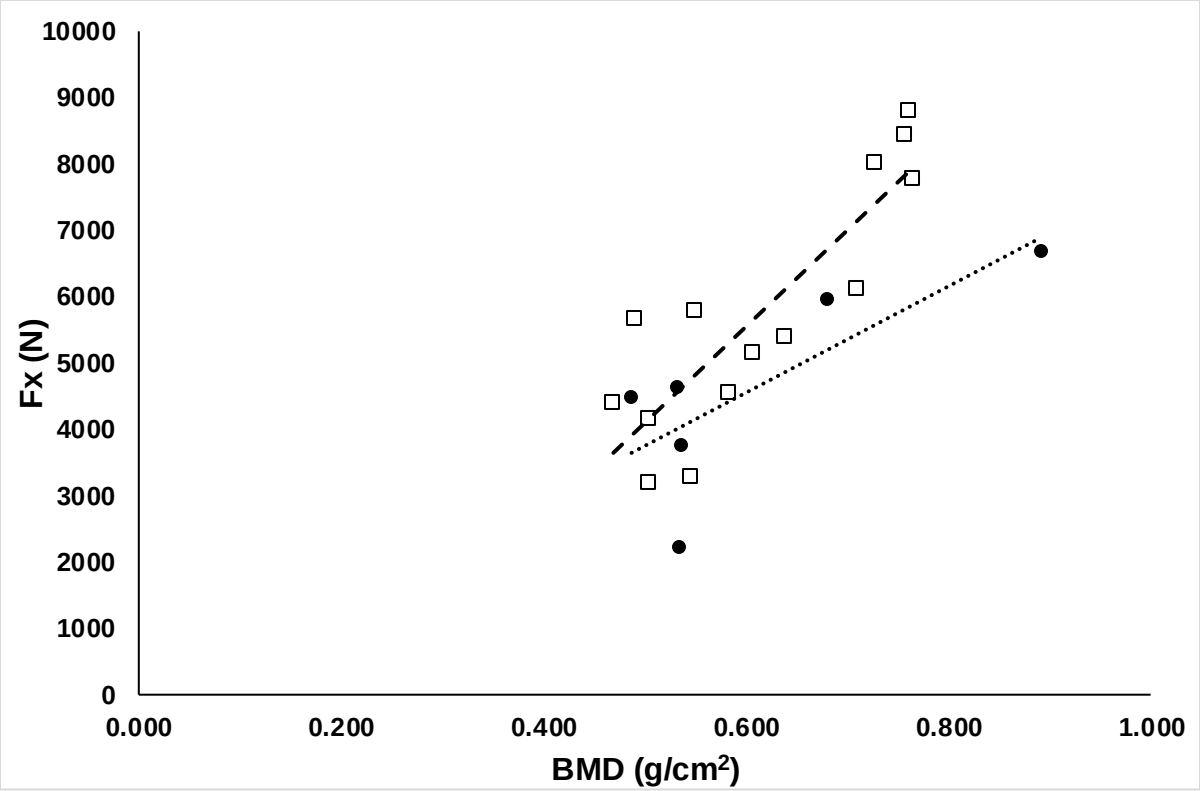

Figure 4-4: Measured F_x over *BMD* for females (filled circles) and males (open squares) for the model sample; lines of best fit (dotted line = female; dashed line = male) included to help illustrate the interaction.

The model resulting from the backward elimination process,

$$\boldsymbol{Fx \sim 1144.8 * age * BMD * r + 808.3 * age * sex * r - 20873.9 * age * sex * BMD - 95456.1 * BMD * r - 64455.0 * sex * r + 1572699.2 * sex * BMD - 2162.8 * age * r + 3651735 * age * BMD + 6841.7 * age * sex + 174342.0 * r - 2691381.5 * BMD - 496971.3 * sex - 11280.2 * age + 789042.7}$$ **[Equation 4]**

had a larger adjusted R^2 value of 0.867 (p = 0.004), and a larger AICc value of 332.42. Therefore, the forward selection model was identified as the stronger of the two models, as it's AICc value that was over 2 points lower than the AICc of the backward elimination model, which indicates a significant difference in the models.

The 10 repetitions of the 10-fold cross-validation of the possible LASSO-GLM models resulted in a mean λ_{min} value of 33.25. When using this λ_{min} value, the resulting LASSO-GLM model,

$$Fx \sim 4601.15 * sex * BMD + 51.46 * age * sex - 20.19 * age * sex - 2.52 * r * age - 2.59 * r + 1878.57$$ **[Equation 5]**

had an adjusted R^2 value of 0.731 ($p < 0.001$) and an AICc value of 281.21. Using both the forward selection GLM and LASSO-GLM models to predict F_x for the validation sample, the MSE for the models were 2863993.4 and 3458434.3, respectively. In addition to having the lower overall MSE, the forward selection model also had a similar AICc value to the LASSO-GLM model (279.95 vs 281.21, respectively). Accordingly, for the purposes of this study, the forward selection model was identified as the strongest overall model.

Paired t-tests demonstrated that the predicted F_x from the forward selection regression were significantly higher than the previously published models in the literature (Table 4-6, Figure 4-5). Post-hoc analyses investigating sex specific differences in model predictions revealed that the Courtney et al., 1995, Dall'Ara et al., 2013, and the Roberts et al., 2010 models all significantly overpredict F_x for females, while the Courtney et al., 1994 did not produce significantly different predictions of F_x for females. For males, each model significantly underpredicted F_x (Table 4-6). When these model predictions were compared to the measured F_x, only the Dall'Ara et al., 2013 model predictions produced significantly lower F_x for females ($p = 0.013$), while each model produced significantly lower predictions of F_x for males ($p < 0.001$). When comparing predictions of the validation sample alone, the model developed in this study had the lowest overall MSE (2863993) when compared to the MSE of the predictions from the four previously published models (3458434-8713346).

Table 4-5: Results of the paired samples t-test comparing predicted F_x of the full sample obtained from the forward selection model developed in this study against the predicted F_x from four previously published models.

	Courtney et al., 1994	**Courtney et al., 1995**	**Roberts et al., 2010**	**Dall'Ara et al., 2013**
95% CI	-969.8 -425.5	-1953.1 -1411.0	-1177.9 -545.6	-2484.4 -1735.8
t	-5.269	-12.756	-5.603	-11.589
p	<0.001*	<0.001*	<0.001*	<0.001*

** denotes significance at an α level of 0.05*

Table 4-6: Results of the paired samples t-test comparing sex specific predicted F_x of the full sample obtained from the forward selection model developed in this study against the predicted F_x from four previously published models.

		Courtney et al., 1994	Courtney et al., 1995	Roberts et al., 2010	Dall'Ara et al., 2013
Females	**95% CI**	-233.1 291.4	-1383.3 -431.5	-209.3 -168.9	-1655.2 -1306.8
	t	0.256	-4.397	-21.575	-37.3
	p	0.804	0.002*	<0.001*	<0.001*
Males	**95% CI**	-1309.6 -812.6	-2192.4 -1946.4	-1588.7 -807.4	-2929.5 -1919.8
	t	-9.009	-35.499	-6.470	-9.761
	p	<0.001*	<0.001*	<0.001*	<0.001*

** denotes significance at an α level of 0.05*

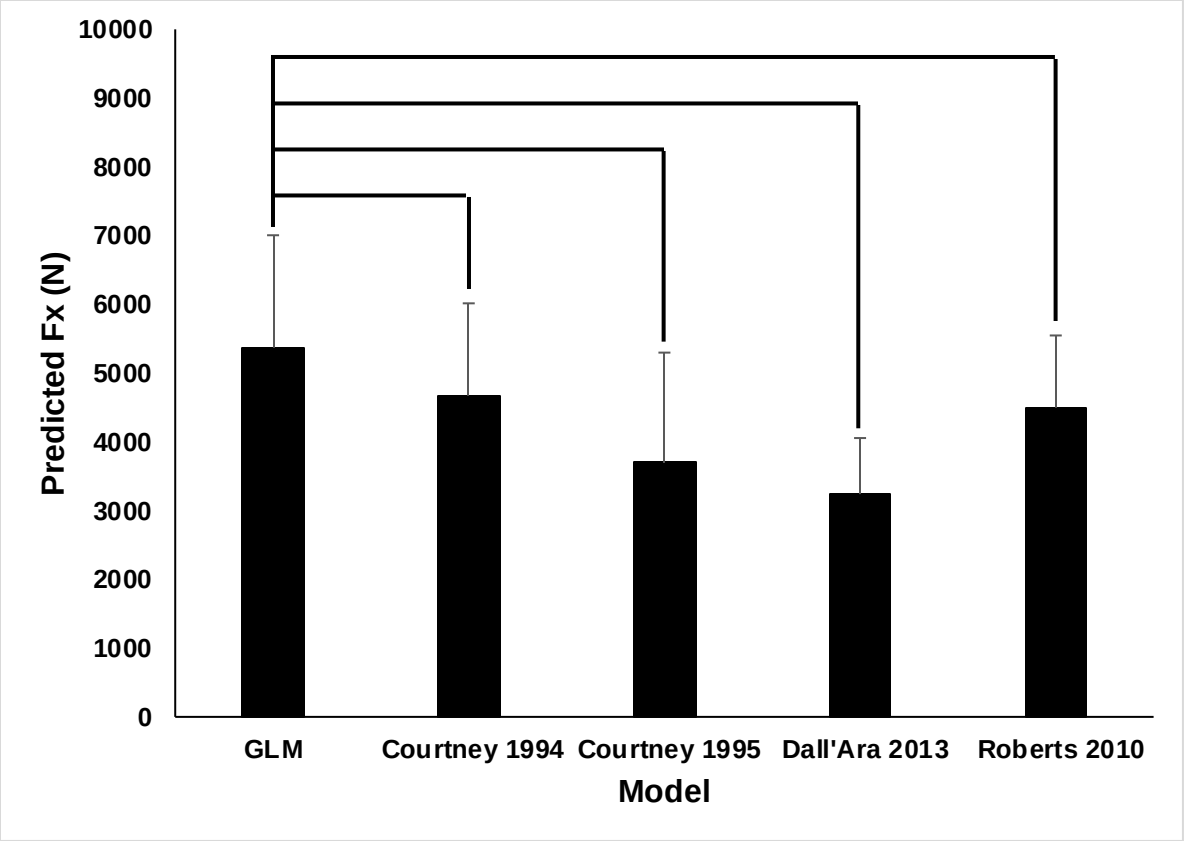

Figure 4-5: Mean(SD) Predicted F_x for the forward selection model developed in this study (GLM) and the four previously published models included in this analysis (Courtney 1994, Courtney 1995, Dall'Ara 2013, Roberts 2010). Connected bars are significantly different ($p < 0.05$).

4.3.1 Statistical Model Robustness and Repeatability

Following the 10 repetitions of the statistical robustness and repetition analysis, it was found that the backwards elimination model always resulted in the highest AICc and MSE error, and was therefore excluded from further analyses. In all 10 repetitions, the forward selection model always results in a model that retained BMD and Sex as main effects along with other elements, with the exception of 2 cases, where only BMD and Sex main effects were retained. The most commonly emerging model was BMD + Sex + Age (3/10), followed by BMD + Sex (2/10), with the remaining 5 models including BMD, Sex, Age, and other predictors. The resulting models for the 10 repetitions are presented in Table 4-7 below.

Table 4-7: Resulting forward selection stepwise regression models for the 10 repetitions.

Repetition	Resulting Forward Selection Stepwise Regression Model
1	*BMD + Sex + age*
2	*BMD + Sex + age*
3	*BMD + Sex + age + BMD*Sex + Sex*age*
4	*BMD + Sex*
5	*BMD + Sex + age + r + BMD*Sex + BMD*age + Sex*r*
6	*BMD + Sex + age + BMD*Sex*
7	*BMD + Sex + age*
8	*BMD + Sex + age + r + BMD*Sex + Sex*r + Sex*age*
9	*BMD + Sex + age + Sex*age + BMD*Sex*
10	*BMD + Sex*

The mean and repetition specific Z scores for MSE and AICc for each of the four models (BMD, Main, Inter, and Fwd) for all 10 repetitions are presented in Table 4-8 below; Figure 4-6 represents the mean overall Z scores for MSE and AICc for each of the four models. The model including the main effects of BMD and Sex ("Main"), had the lowest mean Z score for AICc (-0.404), followed by the forward selection models ('Fwd") (-0.244), the previously defined model of BMD + Sex + BMD*Sex ("Inter") (0.138), and lastly BMD alone ("BMD") (0.509). In terms of mean MSE Z scores, the "Main" model had the lowest Z score (-0.353), followed by the "Inter" model (-0.067), "BMD" (-0.036), and lastly the "Fwd" model (0.456).

From these findings, it is evident that the main effects of BMD and Sex are the most robust effects for predicting femoral bone strength, or F_X, for this sample of data. Model robustness confirms that BMD and Sex are significant and robust predictors that should be retained, but these results provide less support for the inclusion of the interaction between BMD and Sex.

Table 4-8: The normalized Z Scores for the four models (BMD, Main, Inter, and Fwd) over the 10 repetitions.

	AICc				MSE			
Repetition	BMD	Main	Inter	Fwd	BMD	Main	Inter	Fwd
1	1.752	0.136	1.058	-0.370	-0.895	-0.620	-0.640	-0.632
2	1.304	0.402	1.315	0.363	-0.580	-0.851	-0.872	-0.965
3	-0.854	-1.554	-1.405	-1.031	0.710	0.116	0.561	0.926
4	0.388	-0.041	0.679	-0.041	-0.003	-0.578	-0.501	-0.578
5	-0.564	-0.926	-1.371	-0.691	0.649	-0.016	1.041	5.045
6	0.814	0.084	0.814	-0.909	-0.172	-0.654	-0.567	0.151
7	1.669	-0.030	0.914	-0.594	-0.786	-0.495	-0.299	-0.376
8	1.323	-0.456	-0.104	2.582	-0.494	-0.256	0.195	0.341
9	-0.575	-1.277	-1.142	-1.369	0.666	0.113	0.681	0.939
10	-0.168	-0.375	0.626	-0.375	0.543	-0.289	-0.270	-0.289
Mean	0.509	-0.404	0.138	-0.244	-0.036	-0.353	-0.067	0.456
Rank Order	4	1	3	2	3	1	2	4

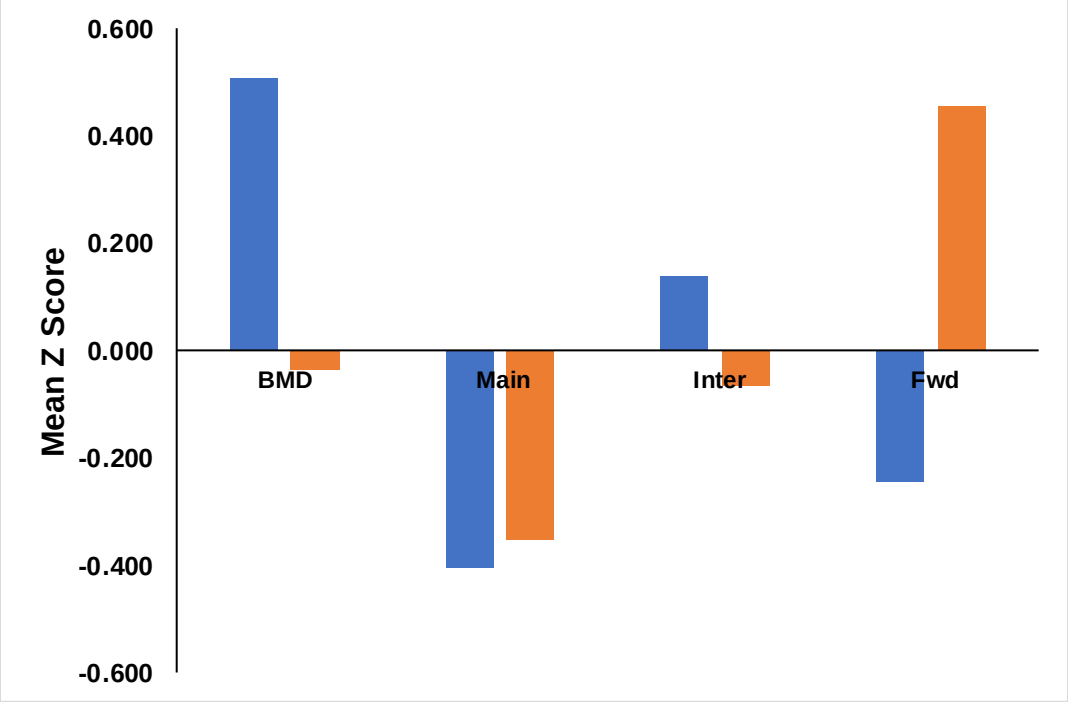

Figure 4-6: Mean Z score for AICc (Blue) and MSE (Orange) for the 4 models evaluated.

Due to further concerns that the interaction between sex and BMD was due to a potential outlier in the original model sample, additional analyses were conducted. The data point in question was a female specimen (Specimen ID 20) with a BMD of 0.891 g/cm^2 and a measured F_x of 6685.3 N. When compared to the rest of the female specimens of the full sample, this represented a BMD that was 1.853 SD greater than the mean and an F_x that was 1.068 SD greater than the mean. Neither the BMD or F_x of this specimen resulted in a Grub's test value that achieved or surpassed the critical t value, which demonstrated that this point was not a statistically significant outlier. Regardless, due to concerns that this point was still driving the interaction between BMD and Sex, this data point was removed from all 10 model samples from the Robustness and Repeatability analysis (when present), and sex specific regressions between BMD and F_x were plotted to visualize these relationships without this point (Figure 4-7). While there were differences in the relationships depending on the model sample used, in general, a clear main effect of Sex exists, while an interaction was observed in some model samples. These results echo the findings of the Robustness and Repeatability analysis and add further evidence for the importance of considering sex effects, while there is less evidence for a clear interaction between BMD and Sex.

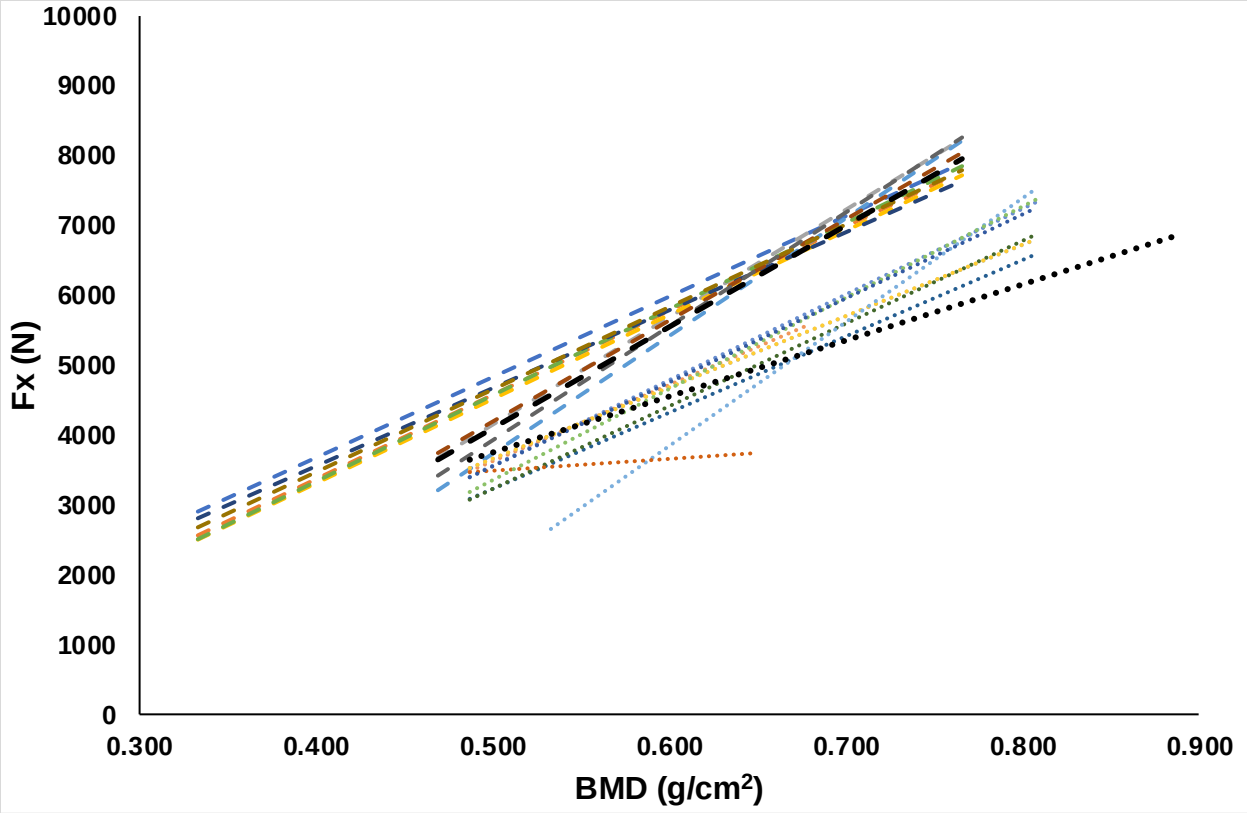

Figure 4-7: Sex specific regression lines (Males = dashed lines; Females = dotted lines) for the 10 model samples of the robustness and repeatability analysis after having removed (specimen ID 20). The bolded black lines represent the regression lines of the original model sample (wherein an interaction between BMD and Sex was observed).

4.3.2 Disease Analysis

As the secondary goal of this study was to investigate the influence of disease on F_x, and more specifically, if accounting for the presence of inflammatory disease states improves the ability to predict F_x. Towards addressing this goal, similar regression analysis methods were conducted, beginning with a main effects GLM to quantify the relative strength of each predictor. This analysis revealed that the four strongest predictors were, in order of significance, *BMD*, *sex*, *CSMI*, and *r*, with *d* and *age* being the least significant (Table 4-9).

Table 4-9:Results for the GLM analysis of the main effects of the independent variables (*a*, *s*, *BMD*, *r*, *CSMI*, and *d*) on the dependent variable (F_x).

Predictor	*B*	*t*	*p*
Intercept	-1467.8	-0.478	0.640
age	-20.7	-0.873	0.399
sex (1F, 2M)	1823.2	2.759	0.016*
BMD	10409.3	5.102	0.001*
r	-96.7	-0.253	0.804
CSMI	-459.4	-0.873	0.294
d	389.3	0.576	0.574
	F (df)	R^2	*P*
	7.88 (6,13)	0.685	0.001

For the stepwise regression, *BMD*, *s*, and *CSMI* were retained alongside *d*. Forward selection and backward elimination regression analyses predicting *Fx* from *BMD*, *s*, *r*, and *d* (including up to second order interactions) were conducted to identify the strongest overall model, based on AIC (log-likelihood) value corrected for the small sample size (AICc). The model resulting from the forward selection process,

$$F_x \sim 11007.7 * BMD + 1315.7 * sex - 3273.4 \quad \textbf{[Equation 6]}$$

had an adjusted R^2 value of 0.673 ($p < 0.001$) and an AICc value of 343.67 yet did not retain *d* as a predictor. The model resulting from the backward selection process,

$$F_x \sim 1701.5 * sex * d + 7547.6 * sex * BMD - 10926.3 * CSMI * d - 6465.7 * CSMI * BMD - 5155.8 * CSMI * sex + 9944.7 * d + 10925.6 * BMD - 746.2 * sex + 26718.7 * CSMI - 24295.8 \quad \textbf{[Equation 7]}$$

(where *d* is represented as a 1 for the presence of a relevant disease state and a 2 for the lack of disease) had an adjusted R^2 value of 0.873 ($p < 0.001$) and AICc value of 358.50. In this case, while the backward elimination model had a larger adjusted R^2 value, the results suggest that the backward elimination model much less likely to fit new data based on AICc values, and the forward selection model is the overall stronger model.

4.4 Discussion

The main objective of this study was to develop a model for the prediction of proximal femur bone strength based on hip impact experiments using a biofidelic test paradigm. Comparing models by a combination of adjusted R^2 values, Akaike Information Criterion values adjusted for small sample sizes (AICc) and mean squared error for F_x predictions of the validation sample, the model resulting from the forward selection process was identified as the strongest overall model. This model included *BMD* and *s* as predictors, as well as their interaction, showing a significantly greater rate (or slope) at which F_x increases with increasing *BMD* for males compared to females. These findings align with the initial hypotheses related to both BMD and *sex*, however, our findings related to the other investigated factors (*a*, *r*, and *CSMI*) did not result in the rejection of our null hypothesis, as these factors did not significantly relate to F_x. Predictions of F_x based on four previously published models (Table 4-2) were all significantly lower than the predictions of this study's model predictions (Table 4-6). A post-hoc analysis revealed these models all significantly underpredict male F_x, while predictions of female F_x had a less consistent trend (Table 4-7). However, only one of the models (Courtney et al., 1994) did not have significantly different predictions of F_x for females. Towards achieving the secondary objective of this study, a separate analysis of the effect of inflammatory disease state was conducted. Using a categorical variable (*d*) which encompassed such diseases as Type I and II Diabetes, Chronic Kidney Disease, and Chronic Obstructive Pulmonary Disorder, revealed that accounting for the presence of such a disease state or its absence was not significantly related to F_x (Table 4-8). However, when including *d* with the three most significant predictors (*BMD*, *s*, and *CSMI* in this case) into a stepwise regression analysis, *d* was only retained in the backward elimination process. While the resulting model had a total of nine predictors, compared to the two predictors in the model resulting from the forward selection model, it was a significant model with a relatively large R^2 value (0.893). However, it's AICc value (358.50) was significantly larger than that of the forward selection model (343.67). Additionally, the high dimensionality of this model does hinder clear interpretation of the results, and further investigation into the effect of disease on bone strength is needed. Regardless, the findings related to the primary and secondary objectives of this study each have important implications.

The regression model developed in this study exhibited the greatest accuracy in predictions of proximal femur bone strength (for both the whole model and for the validation sample alone)

when compared to the predictions obtained from four previously published models. This finding alone has many important implications, particularly related to clinical research and injury risk prediction in the context of fall-related hip fractures. Firstly, the results suggest that sex-based characteristics (beyond sex-related differences in femoral neck aBMD) significantly affect proximal femur bone strength. Though not retained in the regression analyses, post-hoc analysis revealed that *CSMI* was significantly higher for males than females ($p = 0.021$) and predicting F_x from *CSMI* resulted in a significant model with and adjusted R^2 value of 0.257 ($p = 0.0049$); this may help explain the effect of sex that was observed. While a relatively broad grouping variables, significant differences were observed for measured F_x between sexes. When comparing this study's model predictions of F_x to BMD based predictions of previously published models, it was observed that all four models produced significantly lower predicted F_x for males, while three models produced significantly lower predicted F_x for females. Additionally, it is important to note that, while each of the four published models investigated included femoral specimens from male and female donors, none of the resulting models included sex as a factor, despite observing significant differences in bone strength and femoral neck aBMD in some cases. While it is unclear exactly why sex was not considered as a factor in these models, other published models developed from predicting proximal femur bone strength in the context of fall-related hip fractures, such as Dragomir-Daescu et al., 2018, do include sex (and age) as factors. However, the model presented in Dragomir-Daescu et al., 2018 also significantly under predicted F_x ($p < 0.001$) for both males and females, despite having sex specific models, as well as including data from a range of different MTS displacement rate experiments (5, 100, and 700 mm/s). Regardless, the fact that each of these four previously published models predict significantly lower F_x for males when compared to the measured F_x suggests the possibility that current BMD based estimates of male hip fracture risk may be inaccurate, meaning that these BMD based methods currently overpredict male hip fracture risk (by under predicting bone strength). While this may help explain some of the lack specificity in hip fracture prediction, this experiment does not allow us to answer these questions, and further research is required. Nevertheless, if the experimental design of this study does indeed provide more physiologically accurate measures of proximal femur bone strength (F_x), this study has identified the importance of considering sex when predicting F_x, and that some currently used BMD based estimates of bone strength (derived from MTS based experiments of bone strength) tend to significantly under predict F_x for males compared to females.

The results of the statistical model robustness and repeatability analysis revealed that the main effects of BMD and Sex were retained in each of the forward selection models for all 10 repetitions. Beyond this, when the model containing BMD and Sex (Main) was evaluated against the other three models, it performed the best overall, leading to the overall lowest MSE and AICc values. These results suggest that that BMD and Sex are significant and robust predictors that should be retained when developing a predictive model of femoral bone strength resulting from the vertical drop tower HIS experiments conducted in this study. Beyond this, the robustness and repeatability analysis conducted in this study present a viable framework that can be applied to future studies wherein stepwise regression approaches are applied on a training or model sample with the goal of predicting a validation or test sample. Though a single iteration of stepwise regression analyses, if properly performed, should satisfy all associated assumptions of normality and variance, performing a similar or equivalent robustness and repeatability analysis can provide additional evidence and insight into the representativeness of any proposed model.

A model developed through experimental methods that more accurately simulate the hip impact dynamics of lateral hip impacts, as done in this study, may produce more physiologically accurate bone strength predictions. However, before being able to make this conclusion, there was a need to demonstrate that the experimental methods used in this study, and the resulting model, produce significantly different results (in terms of measured and predicted *Fx*) than findings from past studies that used low or high displacement rate material testing system experiments; this was achieved in this study. Our ability to determine accuracy of the F_x measured from this biofidelic experimental method is limited, and the claim of accuracy rests on the assumption that more physiologically accurate experiments will result in more physiologically accurate measures, and ultimately more accurate predictions. As discussed in the previous Chapter, the definition for biofidelity in this context is "the degree to which the simulated lateral impacts produces loading of a cadaveric proximal femur specimen that matches that measured from human volunteers during a fall-related lateral hip impact" (Appendix B, Chapter 8.2). Currently, other groups, such as Fleps et al. 2019, are using novel and biofidelic experimental designs to investigate the underlying mechanics of lateral hip impacts, such as the loading profile of impacts and their subsequent hip fractures (Fleps et al., 2019). Indeed, the loading rates of the femur resulting from their lateral hip impact simulations (which align with the loading rates observed in this study's HIS experiments) are orders of magnitude larger than the loading rates experienced using traditional high

displacement rate MTS experiments, which may suggest that these later experiments may not be subjecting femurs to physiologically relevant or accurate loading scenarios. Findings such as this provide additional support to the notion that the HIS experiments used in this study are biofidelic and simulate physiological loading resulting in proximal femur bone strength measures that are particularly relevant for fall-related hip fractures. In general, these results suggest that bone strength estimated from previously published BMD based methods are lower than in reality, thus, previous estimates of hip fracture risk may be artificially elevated.

An argument can be made that overpredicting hip fracture risk is the better option (compared to underpredicting risk), as it will ideally capture more true positives (individuals who will suffer a hip fracture) at the expense of more false positives (individuals who will not suffer a hip fracture). However, a similar argument can be made for the opposite, and in a resource-limited ecosystem or in high-cost scenarios (for example, in overly burdened healthcare systems, or in cases of high-cost prevention methods, such as the installation of safety flooring) a higher degree of accuracy brings a higher level of efficiency that may ultimately result in more hip fractures prevented (compared to a system that casts a wider net yet does not have the ability or resources to intervene in each case). However, this study only provides the first step towards improved hip fracture risk prediction, and further research is needed, specifically related to comparing model predictions to clinical outcomes. Though this would be most appropriately achieved through a longitudinal study or retrospective data analysis, an alternative option would be the use of a probabilistic model, such as the one presented in Martel et al., 2020, to compare distributions of hip fracture risk when using different models predicting bone strength (Martel et al., 2020). For context, the probabilistic model developed by Martel and colleagues uses factor of risk (FOR) principles to assess risk of hip fracture as the ratio between predicted impact force of a lateral hip impact over the strength of the proximal femur. The probabilistic model simulates a representative sample of Canadian older adults to characterize the distribution of risk for this population. Encouragingly, when the predictive bone strength model developed in this study is used as to method to determine bone strength, and thus, set the denominator for calculating factor of risk (FOR) of a fall-related hip fracture, resulted in sex-specific distributions of risk to more closely match the relative incidence of risk observed in this population (when compared to distributions where the Roberts et al., 2010 predictive model of bone strength was used). More specifically, the use of the Roberts et al., 2010 bone strength model resulted in significantly higher risk for males

compared to females, which does not align with epidemiological evidence (Cummings, 2002; Jean et al., 2013; Leslie, 2009). The use of the predictive bone strength model developed in this study resulted in distributions that align much more closely with epidemiological evidence. However, this preliminary investigation is limited, and is only presented here as supporting evidence demonstrating the need for continued research in this area. Nevertheless, the addition of sex to BMD based estimates of bone strength appears to increase the accuracy of femoral bone strength predictions, at least in the context of simulated fall-related hip impacts via the HIS paradigm used in this study. While the addition of this factor may help allay some of the sensitivity issues of currently used BMD based estimates, there is still a portion of variance that remains unexplained. As this, and previous, investigations of femoral bone strength have been limited to metrics extracted from X-ray-based methods, and hence evaluating the gross morphological aspects of the bone as well as quantifying the inorganic phase of bone, this unexplained variance may be related to previously under-investigated aspects, such as the organic phase of bone and the state of the bone collagen, and further research in this area is needed.

Beyond the lack of consideration of the organic phase of bone, there are several additional limitations associated with this study. A first limitation relates to the sample size (total N = 26; Model N = 20, Validation N = 6). In general, a larger sample size allowing for a better balance between sexes and a more even distribution of ages would have been beneficial. Unforeseen limitations and delays associated with the COVID-19 pandemic greatly influenced the ability to obtain donors and specimens for this study, and there was a different outlook at the time of the proposal. However, the sample size used was still sufficient to identify the differences observed in this study, due to the robustness of the effects. Additionally, the sample size achieved in this study does align with previous investigations, and in a survey of 13 published studies, the sample size of 26 surpasses the median sample size of these studies (N = 21), and the number of procured femurs, prior to technical exclusion (N = 30) matches the mean sample size of this same set of previously published studies (N = 29.9). A table representing the findings of this survey can be found in Appendix E (Chapter 8.5). As mentioned in the previous Chapter, an additional limitation relates to the lack of explicit temperature and hydration measurements of the specimens prior to testing. Future work should include measures of surface temperature, and if possible, internal temperature to ensure a common testing condition for specimens. Despite using X-ray and DXA scans and visual inspection of the specimens to identify any defects or macro-scale damage,

another limitation in this study is the lack of consideration of pre-existing micro-scale damage or microcracks in the specimens. Alongside load and fracture toughness, defect size is the third key factor in the fracture mechanics triad, and the size of these defects (be it pores, microcracks or other damage) can greatly influence how and when cortical will fracture (Augat and Schorlemmer, 2006; Launey et al., 2010; Zioupos and Currey, 1998). Future work should incorporate further characterization of the bone structure at the micro-scale, such as obtained through using 3D volumetric micro computed tomography, to quantify the degree of porosity and microdamage in the regions of interest of the specimens prior to testing.

A final limitation of this study that needs to be addressed is the definition of some of the factors used in the analysis, specifically sex and disease as broad categorial variables. In relation to sex as a categorical variable, there are important discussions occurring at the intersection of science and society around the notion of sex, and the appropriateness of using sex as a categorical variable, and I believe it is important to mention here. While the effects of sex (typically as a categorical variable of declared sex by participants, sometimes simplified to gender, often limited to male or female) are often robust in the field of human sciences, specifically biomechanics, it is a relatively broad categorical variable that encompasses many difference characteristics and aspects. Indeed, in this study, sex was a significant factor, particularly the interaction between sex and femoral neck aBMD (which seems to go beyond the typical sex-based differences in BMD). However, there are likely many "sex" specific or related factors that weren't directly investigated or quantified in this study. It is therefore possible that these specific or related factors have a more mechanistically based association with femoral bone strength. It is therefore important to state that these likely myriad factors that fall under the umbrella of the categorical variable of sex seem to play an effect on bone strength. Further research into these currently unaccounted factors could ultimately improve our understanding of the underlying mechanics of bone fracture and could ultimately improve the accuracy of future predictive models of F_x. Similarly, the categorical variable of disease used in the secondary analysis of this study (specifically, the presence or lack of presence of an inflammatory disease state) was likely much too broad and may have been the reason why an effect of disease on bone strength was not identified (despite reported evidence of disease-specific differences in bone strength and fracture rates). This was likely due to the broad category of "inflammatory disease" used in this study to encompass the following diseases: Type I and 2 Diabetes, Chronic Kidney Disease, and Chronic Obstructive Pulmonary Disorder. While

the general understanding is that these diseases have a similar biological basis for the damage or deterioration of the body (specifically through oxidative stress related to inflammatory processes) (Abdollahi et al., 2005; Hamada et al., 2009; McNerny and Nickolas, 2017), these disease states have many unique aspects and it may not be appropriate to group them all together. One clear example of this is type I and type II Diabetes. While both are considered to be inflammatory diseases, the pathways and biological processes associated with each are quite different, and while the risk of hip fracture increases for both Type I and Type II diabetes (Janghorbani et al., 2007; Vestergaard, 2007), aBMD measures at the hip differ significantly, with it decreasing in Type I Diabetes and increasing in Type II diabetes (Vestergaard, 2007). It would likely have been more appropriate or accurate to differentiate the types of disease states further. However, due to a combination of factors (namely limited sample size and presence of comorbidities), this was not possible in this investigation. Additionally, relevant information for certain specimens was not available, or was limited to reported conditions disclosed by third parties. Regardless, epidemiological evidence (in the form of differences in hip fracture risk and observed rates between diseases), as well as the retention of disease in the backward elimination model in this study, support the notion that further research in this domain is warranted.

4.5 Conclusion

Through the use of a biofidelic experimental paradigm, this study successfully quantified the relationship between sex and femoral neck aBMD on the strength of the proximal femur in simulated lateral hip impacts leading to fracture. From this, a model to predict proximal femur bone strength was developed; the predictions from this model were found to be significantly higher than the predictions of previously published BMD-based models of femoral bone strength prediction. The findings of this study have important implications in both the areas of basic science and clinical research. While the results of Study 1 do not demonstrate any difference between the traditional MTS experimental paradigm and the biofidelic HIS experimental paradigm, the results of the current study suggest that a difference may exist between these experimental paradigms. Specifically, the significant differences between published MTS based model predictions and HIS based model predictions observed in this study do suggest that fracture force may be dependent on experimental paradigm. There is merit in future work to further explore this. If this interaction does exist, it would demonstrate the importance of experimental design related to the biofidelic

loading of specimens, which may produce more physiologically accurate measures of bone strength. As to the latter, this study was able to develop a relatively simple, yet robust, model for the prediction of femoral bone strength that can be used clinically to potential produce more accurate estimates of femoral bone strength, ultimately improving the ability to predict fall-related hip fracture risk. However, as elaborated in the previous sections, further research on this problem is needed in order to determine whether this experimental paradigm produces physiologically accurate estimates of bone strength, and if the use of the developed model does indeed improve our ability to predict and prevent fall-related injuries. Finally, this study represents an important first step into the evaluation of the multiscale contributions of both the inorganic and organic phase of bone on its ultimate strength, as will be more fully investigated in Study 4 (Chapter 6).

Chapter 5
Study 3: The Role of Bone Collagen Integrity on Fracture Toughness of the Inferior Femoral Neck Under Simulated Impact Loading Rates

5.1 Introduction

Human bone is a complex composite material, consisting mainly of non-organic hydroxyapatite and organic type I collagen (Shoulders and Raines, 2009; Stock, 2015). Both the organic and inorganic phases of bone are known to play contribute to the material properties and mechanical behavior of bone (Keaveny and Hayes, 1993; Luo and Wu, 2020; Zioupos and Currey, 1998; Zysset et al., 1999). However, the organic phase of bone goes largely unconsidered when investigating bone fractures, particularly in context in estimating bone strength and predicting fracture risk. Currently, the inorganic phase of bone is the focus of attention in terms of quantifying bone strength and fracture risk. This is primarily due to the strong positive correlation between the non-organic phase of bone, typically measured as amount of bone mineral per unit area or volume, and bone strength which has been used as a strong foundation towards the development of methods to predict fracture risk (Cheng et al., 1997; Courtney et al., 1995, 1994; Dall'Ara et al., 2013a; Table 2-2). In fact, previous experiments have found that areal bone mineral density (aBMD) alone explains a great deal of the variance of bone strength, and it is these relationships on which many models and predictive algorithms are based, such as the T-score and Factor of Risk (FOR) based methods for predicting hip fracture risk. However, despite the strong relationship between bone strength and aBMD, many fall related hip fractures occur in individuals who don't have low BMD and would not be deemed at risk based on these methods (Schuit et al., 2004; Siris et al., 2004; Stone et al., 2003).

One potential explanation for these failed predictions is that these methods focus almost entirely on the inorganic phase of bone despite emerging evidence that the organic materials within bone influence bone integrity. As an integral component of bone, collagen has been found to contribute to bone's resistance to crack growth (Launey et al., 2010; Willett et al., 2019; Zioupos et al., 1999), quantified via fracture toughness metrics such as elastic plastic fracture toughness (J), and even relate to bone strength in animal models (Saito et al., 2011; Uppuganti et al., 2016). More specifically, higher levels of collagen network integrity or connectivity, measured through Hydrothermal Isometric Tensions (HIT) test, are positively associated with higher fracture

toughness (Burton et al., 2014; Wang et al., 2002; Willett et al., 2019; Woodside and Willett, 2016; Zioupos et al., 1999), while higher concentrations of non-enzymatic collagen crosslinks, measured with High Performance Liquid Chromatography assays revealing concentrations of collagen crosslink type, are associated with lower fracture toughness (Knott et al., 1995; Massé et al., 1996; Nyman et al., 2007; Vashishth et al., 2001), and also affects the thermal stability of the collagen network (Bailey and Lister, 1968; Unal et al., 2016). Despite the evidence of the role of the organic phase, or it's state, on fracture toughness, the organic phase of bone is not currently included in human bone strength or fracture risk predictions. While this may be due in part to the fact that traditional methods used to assess the non-organic phase of bone, namely dual energy X-ray absorptiometry and other X-ray-based methods, do not detect the organic phase of bone, it is likely due to the fact that the relationship between bone collagen and bone strength has yet to be fully investigated in the case of human bone fracture. Despite the strong relationship between bone strength and bone mineral density, approximately 70% of hip fractures go unpredicted when solely-BMD based risk prediction is employed (Schuit et al., 2004; Siris et al., 2004; Stone et al., 2003). Considering the potential role of collagen on bone strength could have clinical importance, explaining additional variance and improving hip fracture risk prediction. However, much has yet to be investigated before this can occur, as current investigations related to collagen and fracture mechanics have not directly focused on the femur in the context of fall-related hip fractures. Specifically, the role of collagen on cortical bone fracture toughness has yet to be investigated in the context of high, impact-like, loading of a clinically relevant site.

In previous investigations of the role of collagen on bone fracture mechanics, typical fracture toughness testing of bone focuses on quasi-static loading of diaphyseal cortical bone in order to probe the underlying mechanisms contributing to crack-growth resistance and post-yield energy dissipation (Burton et al., 2014; Nyman et al., 2007; Willett et al., 2019). While use of this test paradigm has provided valuable insight into the underlying mechanics of collagen-mediated fracture toughness, specifically in the context of age-related bone fragility, it has not been directly applied to investigations of specific injury mechanisms, such as fall-related hip fractures. Specifically, the low rate of loading used, as well as the site from which bone samples are extracted (primarily the diaphysis, when the femur is used) make it difficult to infer implications in terms of fall-related hip fractures. The viscoelastic properties of bone mean that, as a material, its response to loading will be affected by the rate (McElhaney, 1966). Current understanding of bone links its

viscoelastic properties to its collagen, or more generally the organic phase of bone, and the movement of water within and around its helical structure (Fois et al., 2001; Launey et al., 2010a; Shoulders and Raines, 2009; Yamashita et al., 2001). Therefore, it is possible that fracture toughness, a property thought to be influenced by collagen (Launey et al., 2010; Nyman et al., 2007; Willett et al., 2019; Zioupos et al., 1999), may depend on loading rate (Gauthier et al., 2017). Hence, fracture toughness extracted from impact like loading rate tests may better mimic the tissue behaviour during fall-related impacts, which could relate more strongly to ultimate bone strength.

Accordingly, the primary goal of this study was to investigate the relationship between cortical bone collagen and cortical bone fracture toughness of the inferior femoral neck under high-rate, impact like loading. Specifically, metrics of collagen network integrity (or connectivity, via the maximum slope of isometric tension over temperature, *Max Slope*) and stability (the denaturation temperature, T_d), achieved through Hydrothermal Isometric Tension (HIT) tests were compared to critical elastic and critical elastic-plastic fracture toughness (K_q and J_q, respectively) metrics extracted from high-rate constant displacement three-point bending experiments. It was hypothesized that fracture toughness would be significantly and positively associated with higher collagen quality (specifically pertaining to higher collagen network connectivity and stability).

Finally, a secondary analysis of fracture toughness and collagen quality as a function of disease state was conducted, wherein it was hypothesized that fracture toughness would be lower in diseased samples, which would be mediated by overall lower collagen quality.

5.2 Methods

5.2.1 Sample Acquisition and Preparation

Femurs used in this study were acquired through licensed organ and tissue banks, specifically: Innoved Institue L.L.C., RegenMed, and National Disease Research Interchange. A total of 23 femurs were acquired and included in this study (N = 23 femurs). As in Studies 1 and 2 (Chapters 3 and 4), femurs underwent hip specific DXA scans to extract morphological and aBMD measures (to be used in Study 4, Chapter 6). Afterwards, beams were extracted from the inferior femoral neck (Figure 5-1), with the target dimensions of 35 mm length x 4 mm width x 2 mm thickness (Figure 5-2). In four of the specimens, there was sufficient material to extract an additional beam, resulting in a total sample size of N = 28. Following extraction, a 1.8 mm length by 0.3 mm width notch was cut into the side of the beam, perpendicular to the long edge of the

beam. The crack tip was sharpened to a micro-crack (0.01 mm width, 0.2 mm length) with the use of a Computerized Numerical Control system driven razor blade. Specimens were then frozen until approximately 24h prior to testing, at which point specimens were placed in a PBS solution to thaw and hydrate in advance of testing. In total, specimens underwent a maximum of 5 freeze thaw cycles (assuming that specimens remained frozen throughout the initial transport and reception of the specimens); this is a rather liberal estimate and assumes a thaw cycle occurred during the DXA scanning process. It should be noted that the protocol used to scan femurs minimized the time that each specimen was out of a freezer, in an attempt to keep specimens frozen throughout the scanning process. However, since neither surface nor internal temperature were measured during this process, this cannot be confirmed. Regardless, the general specimen preparation protocol aligned with ASTM E1820-20 specifications for the standard test method for measurement of fracture toughness and follows the methods previously established (Gauthier et al., 2017; Granke et al., 2015; Willett et al., 2019).

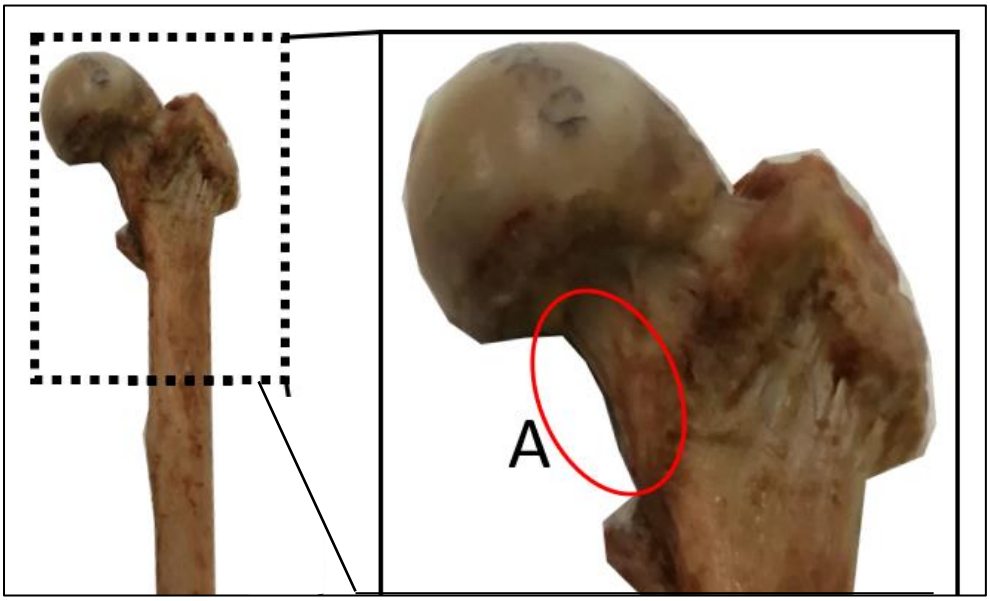

Figure 5-1: Isolated proximal portion of the femur, with SENB specimen extraction site highlighted (A - Inferior Femoral Neck).

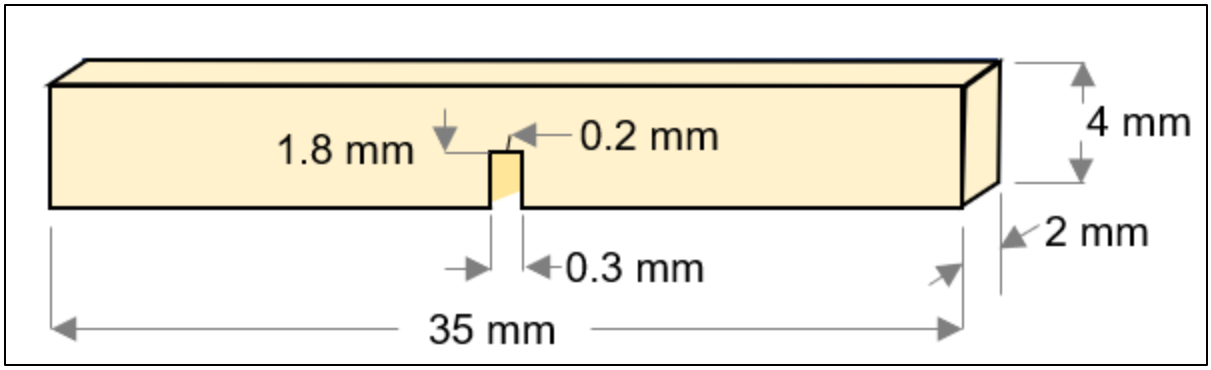

Figure 5-2: Single Edge Notch Bending (SENB) target dimensions.

5.2.2 SENB Fracture Toughness Testing

5.2.2.1 Fracture Toughness Tests

As with SENB specimen preparation, fracture toughness tests were conducted in accordance with ASTM E1820-20, following the methods previously established (Gauthier et al., 2017; Granke et al., 2015; Willett et al., 2019). Experiments were conducted with a micro material testing system (MMTS) (μTS, Psylotech Inc, Evanston, IL, USA) and a high-speed video-enabled microscope system (HSV, AOS Technologies, Cheshire, CT); both test systems were mounted on a vibration-dampening test bench. Fracture toughness tests were conducted under constant displacement three-point bending in the MMTS system, with a target displacement rate of 12 mm/s and a span length of 30 mm. A previous study by Gauthier and colleagues in 2017 applied a displacement rate of 10 mm/s to replicate impact-like loading, which was based on strain measures taken from the radius in impacts during forward falls onto outstretched hands (Földhazy et al., 2005; Gauthier et al., 2017). A recent study by Zioupos and colleagues in 2020 demonstrated that, especially for bone samples from older adult donors, this displacement rate should almost always result in completely brittle (unstable) crack growth (which should mimic what is experienced during fall-related hip fractures) (Zioupos et al., 2020). Pilot work found that the simulated impacts induced by a drop tower hip impact simulator (HIS) induces a strain at rates that would correspond with a displacement rate of 12 mm/s. Additional details supporting the rationale for using a 12 mm/s displacement rate are provided in Appendix F (Chapter 8.6). Load, measured through an in-line load cell within the MMTS system, and displacement data were a sampling frequency of 3000 Hz. High-speed video-enabled microscopy of the experiment was recorded at a resolution of 400

by 400 pixels with a sampling frequency of 1000 Hz (Figure 5-3). An external trigger, linked to both the camera and MMTS, was used to simultaneously trigger the start of data collection.

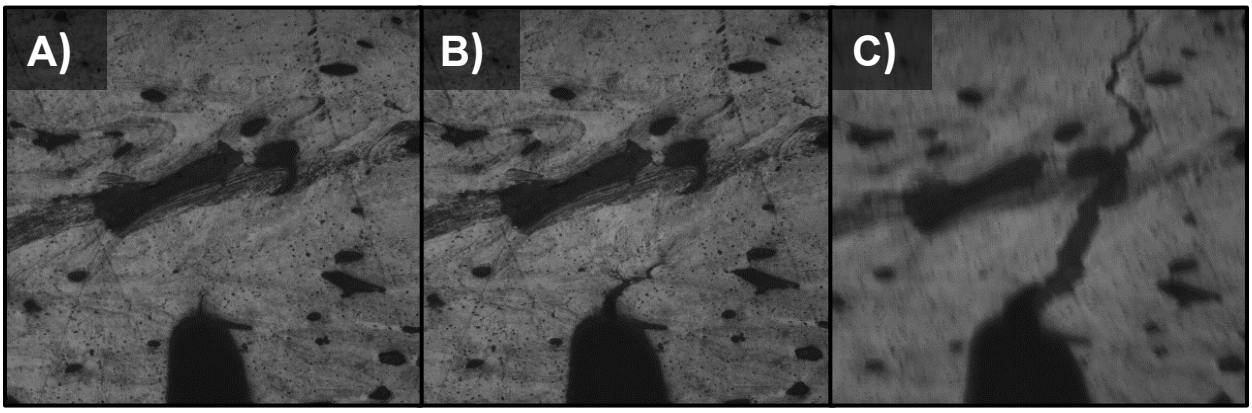

Figure 5-3: Image captured from high-speed microscopy-enabled videography during a high displacement rate (12 mm/s) experiment at: A) Frame 1, B) The frame of max stable crack growth, C) The first frame of unstable crack growth (frame of max stable crack growth +1)

5.2.2.2 Calculating Fracture Toughness

Both critical elastic fracture toughness (K_q) and critical elastic plastic fracture toughness (J_q) were computed from load displacement data that was first dual pass filtered with a 2nd order low-pass Butterworth filter (4th order equivalent) with an effective cutoff frequency of 150 Hz. This filter was used to minimize the number data smoothness criteria violations (as outlined in ASTM E1820-20 (ASTM E1820-20a, 2020).

5.2.2.2.1 Critical Elastic Fracture Toughness (K_q)

To compute critical elastic fracture toughness (K_q), also known as plane-strain fracture toughness (E399-20, 2020) the stress intensity factor (K) was computed at the point of which a 5% secant modulus loss was observed in the load displacement data according to the methods and calculations outlined in ASTM E1820-20 (ASTM E1820-20a, 2020). Specifically,

$$K_q = \left[\frac{P_q S}{B W^{\frac{3}{2}}}\right] f\left(\frac{a}{W}\right) \textbf{ [Equation 8]}$$

which follows the syntax in Table 5-1 below. Accordingly, the function $f(\frac{a_i}{W})$ represents the equation:

$$f\left(\frac{a}{W}\right) = 3\sqrt{\frac{a}{W}}\left(\frac{\left[1.99-\left(\frac{a}{W}\right)\left(1-\frac{a}{W}\right)\left(2.15-3.93\left(\frac{a}{W}\right)+2.7\left(\frac{a}{W}\right)^2\right)\right]}{2\left(1+2\frac{a}{W}\right)\left(1-\frac{a}{W}\right)^{\frac{3}{2}}}\right) \textbf{[Equation 9]}$$

Table 5-1: Variable syntax for elastic fracture toughness equations.

Variable	Name/Description
P_q	Load or Force (in N) at the point of 5% secant modulus loss
S	Span Length of the bending supports (in m)
B	Specimen Thickness (in m)
W	Specimen Width (in m)
a	Starting Crack Length (in m)

P_q was taken directly from the load displacement data (Figure 5-4), and *a* was extracted from the high-speed microscopy-enabled video collected during the experiments. This was done by importing the video into ImageJ (National Institutes of Health, Bethesda, MD, USA), where digital calipers were used to measure straight-line crack length (*a*) at the start of the trial (prior to any loading).

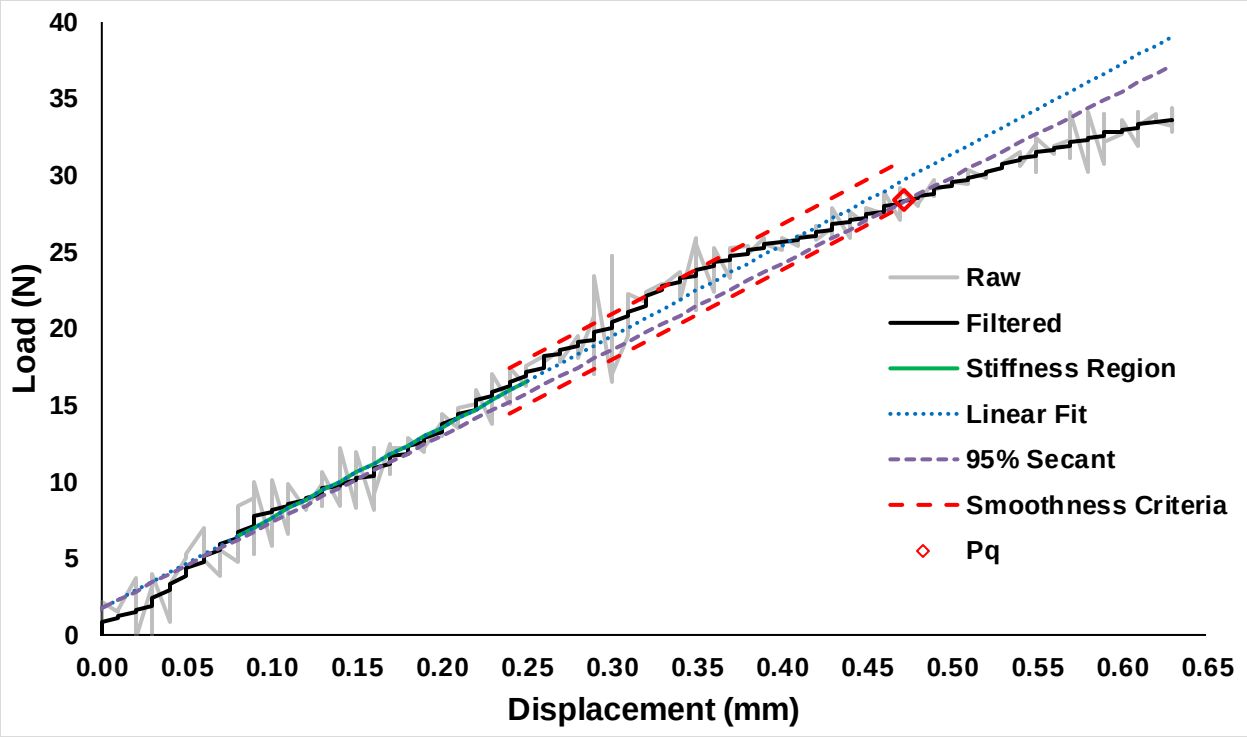

Figure 5-4: Sample load displacement data, where the raw data (light gray) was filtered (black line), from which the linear stiffness region (green line) was defined from a linear fit between 20% and 50% of peak force. By extrapolating this linear fit for the full-displacement range (blue dotted line), the 95% secant modulus (dashed yellow line) was defined. P_q (red diamond) was defined as the final crossing point of the filtered line with the 95% secant line. Smoothness criteria (dashed red line) was defined between 50% P_q and P_q.

5.2.2.2.2 Critical Elastic-Plastic Fracture Toughness (J_q)

To capture potential non-elastic behavior of the SENB specimens, critical elastic-plastic fracture toughness was determined by computing J, which describes work to fracture (Rice, 1968), relating to the energy required to grow a fracture, from the start of the trial up to the point of P_q, which will give J_q. More specifically, J_q was computed by first calculating the area underneath the load displacement curve from the start of the trial to the point P_q (U_q). From this J_q was calculated by

$$J_q = \frac{2 * U_q}{B(W-a)} \quad \textbf{[Equation 10]}$$

5.2.2.2.3 Peak Fracture toughness (K_{Max}, J_{Max})

After having characterized load-displacement curves and identifying P_q for each experiment, it was apparent that there was noticeable plastic deformation still occurring after point P_q. This revelation suggested that the method for which this study attempted to characterize J at point P_q may not have been appropriately quantifying the elastic-plastic fracture toughness of the specimens. Therefore, an additional set of analyses were conducted to compute J fracture toughness at the point of peak force (J_{Max}) allowing for more of the plastic deformation to be considered. A similar analysis was conducted with K fracture toughness (K_{Max}) in order to both maintain parity of variables as well as quantify elastic fracture toughness immediately prior to ultimate failure.

5.2.3 Hydrothermal Isometric Tension Tests

Hydrothermal isometric tension (HIT) tests were performed to quantify collagen network integrity, and connectivity, of cortical bone. Following previously established methods, a small section of cortical bone was extracted from SENB specimens following fracture toughness testing in order to perform HIT tests (Willett et al., 2019; Woodside and Willett, 2016). As outlined by Woodside and Willett in their 2016 study, the subsample was stored in a room-temperature solution of ethylenediaminetetraacetic acid (EDTA, 0.5 M, pH = 7.4) for a minimum of three weeks in order to decalcify the subsample. To ensure complete decalcification, the EDTA solution was constantly agitated using a magnetic stir rod, and the solution itself was changed after the first 7 days of agitation. Following decalcification, the subsample, was further reduced to a ~1.5 x 1.8 x 16 mm (~43.2 mm^3) beam using a razor blade. The beam was then fitted with tissue grips on both ends, with one of the tissue grips being rigidly fixed to a mounting plate, and the other attached to an in-line load cell (InterfaceMB-5, Scottsdale, Arizona, USA)) that was attached to the mounting plate (Figure 5-5). Following the methods previously established, a ~2 N preload was applied to the specimen (Willett et al., 2019). The apparatus was placed onto a large glass beaker filled with 4 liters of distilled water, such that the mounting plate above the beaker, and the specimens and clamps were submerged in the distilled water (not contacting the bottom of the beaker) (Figure 5-5). A resistance thermometer was placed in the bath to monitor temperature, as the bath's temperature was raised from 30 degrees Celsius to 90 degrees Celsius at a rate of ~1.5 degrees per minute.

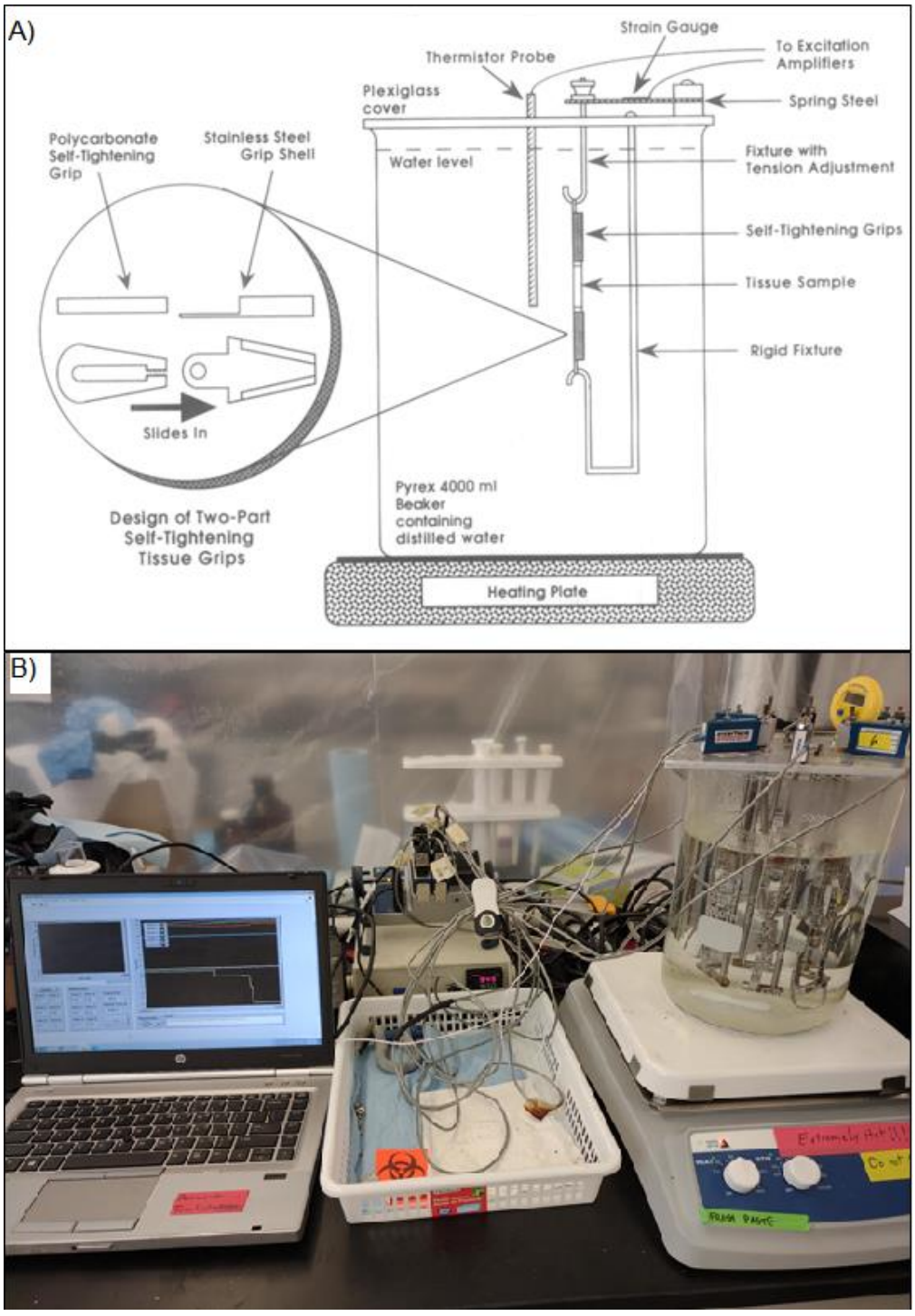

Figure 5-5: A) Example of a hydrothermal isometric tension (HIT) testing system, taken from Lee et al., 1995 for reference; B) actual HIT experimental setup.

This process caused the collagen to denature, resulting structural changes in the collagen. Specifically, the tropocollagen molecule, which is semi-crystalline in nature, uncoils and its

structure developed into an amorphous coil (Flory and Garrett, 1958; Moore et al., 1996; Willett et al., 2019; Woodside, 2015). This structural change caused the specimen to begin shrinking; as this specimen was held isometrically, the contractile force was measured by the load cell. Load and temperature data were recorded using LabVIEW (National Instruments, Austin, TX, USA) at a sampling frequency of 2 Hz, with data collections starting once the water temperature reached 30 degrees Celsius. Load data were transformed to stress by dividing the load by the cross-sectional area of the specimens. The slope of load over temperature was computed per 5 degree increase in temperature between 70 and 85 degrees Celsius, and the maximum slope (*Max Slope*) was determined as the highest observed slope. Additionally, the denaturation temperature (T_d) was extracted by projecting *Max Slope* downward and finding the temperature when this projection intercepted with the starting load (Figure 5-6).

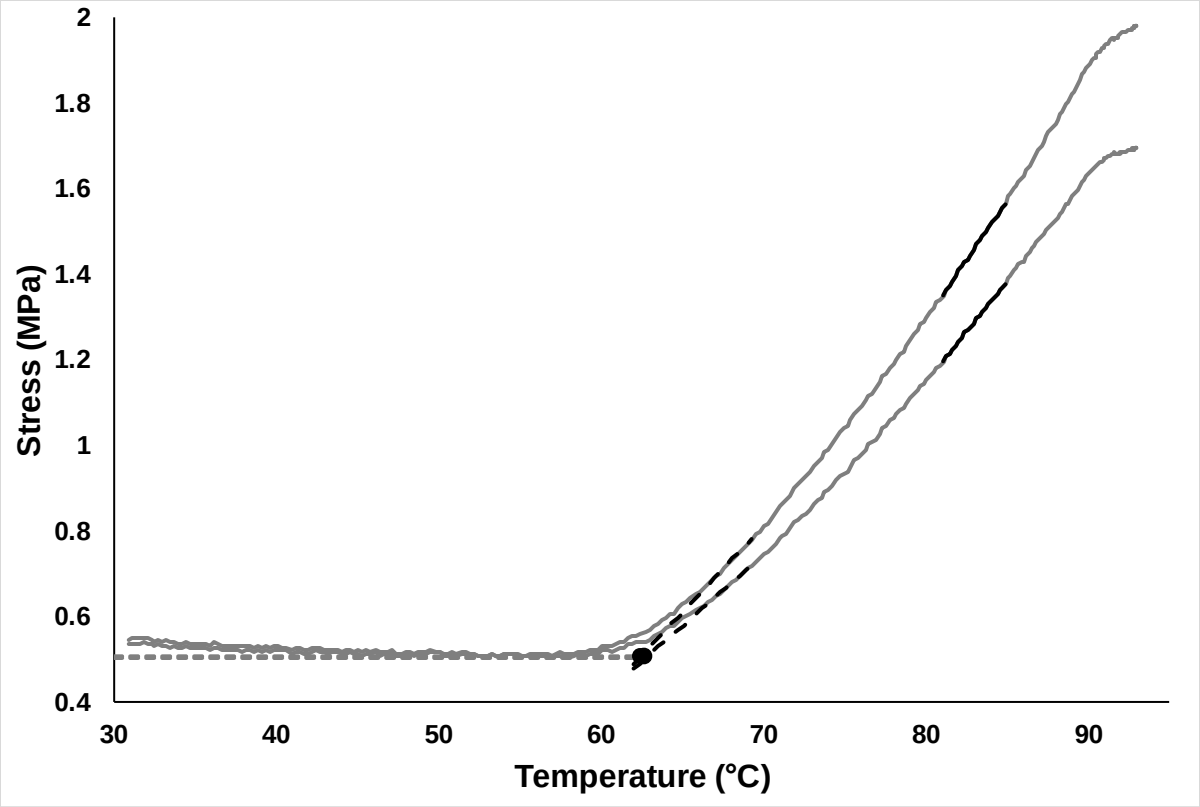

Figure 5-6: Example of stress-temperature curves (dark gray lines) for paired-samples of a single specimen during a HIT experiment. *Max Slope* was extracted as the slope of the 5 °C segment with the largest gradient (solid black lines) observed between 70 °C and 85 °C. T_d (black circles) was identified as the temperature at which the backward projection of the linear portion of the curves (dashed black lines) intersected with the lowest observed stress (dashed gray lines).

5.2.4 Data Analysis

All data were processed using custom developed MATLAB (MATLAB R2020a, Mathworks, Natick, Massachusetts, USA) scripts. Specifically, raw load and displacement data (from the fracture toughness tests), along with crack length data were imported into the MATLAB environment to perform fracture toughness calculations. Similarly, data from HIT tests were imported into the software in order to extract specific variables of interest. Following this, resulting data were processed using the R statistical software to perform statistical analyses.

5.2.5 Statistics and Data Interpretation

To investigate the relationship between fracture toughness of the inferior femoral neck SENB specimens and the integrity and connectivity of cortical bone collagen, multiple regression analyses were performed. Separate analyses were performed for each dependent variable (K_q, K_{Max}, J_q, and J_{Max}), using collagen network connectivity and stability metrics (*Max Slope* and T_d) and age as the independent variables. More specifically, regressions included all independent variables and interactions, from which backward elimination stepwise regression methods were used. In the case that this process did not produce a significant model, predictors were sequentially removed (by order of significance, starting with interactions) until a significant model emerged. In order to achieve the secondary goal of this study, the same process was conducted with an additional factor (*d*), representing either the presence or lack of presence of an inflammatory disease state) being considered. All statistical analyses were evaluated at an alpha level of 0.05 and were computed in the R statistics programming language using the R Studio IDE.

5.3 Results

Characteristics of the SENB specimens included in the analysis, and descriptive statistics of dependent measures, are presented in Table 5-2 below. Full specimen details are presented in Table 5-3. Shapiro-Wilk's tests of normality for *Max Slope* and T_d, as well as for the dependent variables K_q, K_{Max}, J_q, and J_{Max}, revealed that none of the variables violated the assumption or normality. It should be noted that, in 3 cases, a rising slope was observed in the load displacement data of the three-point bending tests of some specimens, meaning that a secant modulus loss was not observed. Therefore, K_q and J_q values are missing for 3 specimens, bringing the final sample size to 24. Of these 24 specimens, 11 came from donors with at least one reported inflammatory disease state.

Table 5-2: SENB specimen information; total sample size, sex split, and mean (SD) of the independent variables *Max Slope* and T_d, as well as for the dependent variables K_q and J_q.

N	*a (years)*	K_q *(MPa√mm)*	J_q *(kJ/m²)*	*Max slope (MPa/°C)*	T_d *(°C)*
24	73.4 (20.1)	94.66 (25.25)	1.87 (0.73)	47.17 (7.02)	63.04 (0.87)

Table 5-3: Specimen details for the entire sample, including independent and dependent variables.

Specimen ID	*Sex*	*Age (years)*	*Max Slope (MPa/°C)*	T_d *(°C)*	K_{Max} *(MPa√mm)*	J_{Max} *(kJ/m²)*	K_q *(MPa√mm)*	J_q *(kJ/m²)*
1	F	75	19.28	65.49	43.52	1.81	N/A	N/A
2	M	83	38.27	62.96	88.80	2.98	85.97	2.11
3	F	56	52.03	62.32	137.64	5.08	116.74	2.32
4	F	93	45.08	62.66	130.41	5.81	110.01	3.41
5	F	83	63.77	63.82	108.98	2.86	87.98	1.50
6	F	59	44.87	64.30	124.90	3.42	103.96	2.04
7	M	83	36.53	63.33	68.55	2.26	45.15	0.49
8	F	34	44.90	62.68	95.93	4.51	64.88	1.01
9	M	83	47.96	64.17	110.43	3.31	80.45	1.46
10	M	68	56.08	63.55	139.88	4.46	99.84	1.60
11	F	48	52.50	62.95	133.94	5.39	112.61	2.62
12	F	59	47.40	64.56	84.33	2.67	73.90	1.77
13	M	93	41.21	62.36	92.31	3.59	77.44	1.71
14	M	65	52.89	64.12	132.22	4.48	111.62	2.09
15	M	93	41.36	62.09	105.17	3.29	71.05	1.15
16	M	84	53.30	62.51	134.04	3.60	101.80	1.64
17	M	83	40.98	62.81	79.87	2.00	63.57	0.97
18	F	55	53.28	63.93	104.34	3.80	70.19	0.96
19	M	70	46.88	63.22	99.22	3.38	78.44	1.43
20	F	63	42.27	61.39	56.49	1.18	N/A	N/A
21	M	76	34.44	63.53	117.54	3.63	89.80	1.62
22	M	91	51.13	62.60	158.65	6.02	129.63	2.32
23	M	91	43.43	62.93	162.52	5.23	136.94	2.56
24	F	85	52.71	62.61	152.92	7.64	118.38	2.07
25	M	23	51.73	62.34	149.88	4.40	147.56	3.35
26	M	103	39.30	60.67	121.61	4.41	94.01	2.63
27	F	59	42.60	63.25	149.40	2.81	N/A	N/A

Using K_q as the dependent variable of interest, a full-factorial GLM revealed that none of the factors (main or interaction effects) reached significance, and the overall model did not reach significance (adjusted $R^2 = 0.326$, $p = 0.0547$). This process resulted in none of the interactions remaining. While *Max Slope* emerged as a significant factor ($p = 0.044$) in the model limited to main effects, neither of the other variables were significant, and the model itself did not reach

significance (adjusted R^2 = 0.147, p = 0.106) (Table 5-4). Removing *age* (the least significant factor) resulted in a significant model (adjusted R^2 = 0.177, p = 0.05), where *Max Slope* remained a significant factor (p = 0.025), while T_d was not significant (p = 0.114). Removing T_d did not improve the model (adjusted R^2 = 0.113, p = 0.06), and *Max Slope* did not remain a significant factor (Table 5-4, Figure 5.7). Following the same statistical process using J_q as the dependent variable of interest also resulted in none of the interactions remaining. None of the subsequent main effect models reached significance, nor did any of the factors reach significance in any model (Table 5-4); Figure 5.7 also depicts the relationship between J_q and *Max Slope* for comparison to K_q.

Table 5-4: Linear models predicting fracture toughness (K_q and J_q) from *Age*, *Max Slope*, and T_d.

Fracture Property	Linear Model			Adj-R^2 (p)
K_q	*Age*	***Max Slope***	*Td*	0.147
	(β = -0.11,	***(β = 0.44,***	*(β = -0.35,*	(p = 0.106)
	p =0.618)	***p = 0.044)***	*p = 0.106)*	
		Max Slope	*Td*	0.177
		(β = 0.47,	*(β = -0.32,*	(p = 0.050)
		p = 0.025)	*p = 0.114)*	
		Max Slope		0.113
		(β = 0.39,		(p = 0.060)
		p = 0.060)		
J_q	*Age*	*Max Slope*	*Td*	0.053
	(β = 0.12,	*(β = 0.22,*	*(β = -0.42,*	(p = 0.264)
	p =0.593)	*p = 0.332)*	*p = 0.067)*	
		Max Slope	*Td*	0.085
		(β = 0.25,	*(β = -0.39,*	(p = 0.152)
		p = 0.244)	*p = 0.072)*	
			Td	0.067
			(β = -0.33,	(p = 0.118)
			p = 0.118	

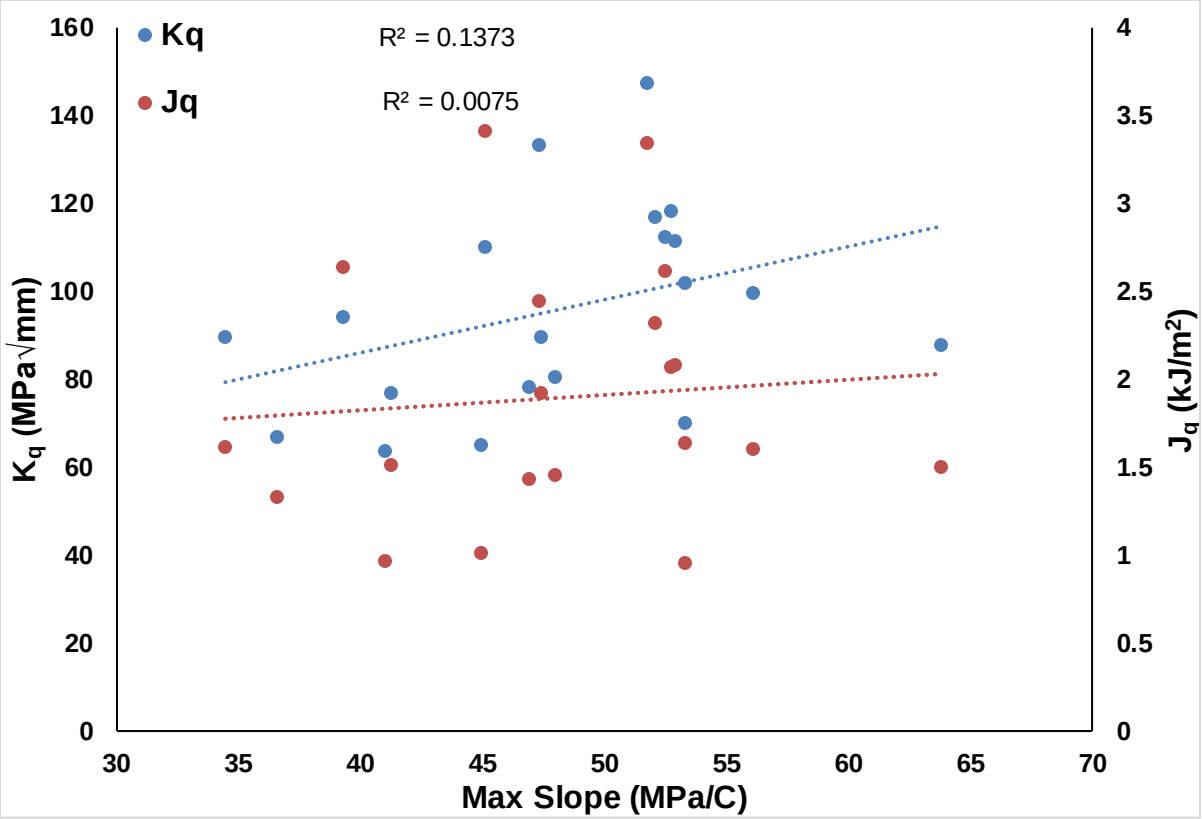

Figure 5-7: Linear relationship between Max Slope and both K_q (blue dots) and J_q (red dots).

5.3.1 Disease Analysis

This process was repeated with the addition of *d* as an independent variable, resulting in overall model improvements. Beginning with K_q, none of the interactions were retained, yet the model that included all main effects (age, *Max Slope*, T_d, and *d*) reached significance (adjusted R^2 = 0.275, p = 0.037), and both *Max Slope* and *d* emerged as significant factors (p values of 0.009 and 0.046, respectively) (Table 5-5). Sequential removal of non-significant factors (in order of least significance) resulted in overall model improvements, and ultimately resulted in a significant model that retained both *Max Slope* and *d* as significant predictors (adjusted R^2 = 0.306, p = 0.008) (Table 5-5). Similarly, no interactions were retained when J_q was used as the dependent variable of interest, and the model that included all main effects reached significance (adjusted R^2 = 0.261, p = 0.043); however, only *d* emerged as a significant factor (p = 0.003) (Table 5-5). While sequential removal of non-significant predictors resulted in improvements in overall model significance, the strongest overall model retained *Max Slope*, T_d, and *d* (adjusted R^2 = 0.325, p = 0.008), while only the latter predictor reached significance (p = 0.019). In fact, continuation of this

process resulted in a model that only retained *d* as a significant predictor (adjusted R^2 = 0.211, *p* = 0.014) (Table 5-5). One-sided independent samples t-tests revealed J_q was significantly lower for specimens in the disease group (95% CI [-1.262 kJ/m2 to -1.592 kJ/m^2], *p* = 0.007) while this was not observed for K_q (95% CI [-37.131 MPa√mm to 4.267 MPa√mm], *p* = 0.057).

Table 5-5: Linear models predicting fracture toughness (K_q and J_q) from *Age*, *Max Slope*, T_d, and *d*.

Fracture Property	Linear Model				*Adj-R^2 (p)*
K_q	*Age*	***Max Slope***	*Td*	***Disease***	0.275
	(β = 0.05,	***(β = 0.58,***	*(β = -0.18,*	***(β = 0.44,***	(*p* = 0.037)
	p =0.809)	***p = 0.009)***	*p = 0.389)*	***p = 0.046)***	
		Max Slope	*Td*	***Disease***	0.309
		(β = 0.56,	*(β = -0.20,*	***(β = 0.43,***	(*p* = 0.015)
		p = 0.006)	*p = 0.309)*	***p = 0.037)***	
		Max Slope		***Disease***	0.306
		(β = 0.53,		***(β = 0.48,***	(*p* = 0.008)
		p = 0.008)		***p = 0.014)***	
J_q	*Age*	*Max Slope*	*Td*	***Disease***	0.261
	(β = 0.07,	*(β = 0.38,*	*(β = -0.21,*	***(β = 0.54,***	(*p* = 0.043)
	p =0.736)	*p = 0.075)*	*p = 0.301)*	***p = 0.019)***	
		Max Slope	*Td*	***Disease***	0.293
		(β = 0.36,	*(β = -0.24,*	***(β = 0.51,***	(*p* = 0.019)
		p = 0.069)	*p = 0.225)*	***p = 0.014)***	
		Max Slope		***Disease***	0.274
		(β = 0.32,		***(β = 0.59,***	(*p* = 0.013)
		p = 0.102)		***p = 0.005)***	
				Disease	0.211
				(β = 0.50,	(*p* = 0.014)
				p = 0.014)	

In order to more appropriately consider the potential role of plastic deformation, these statistical methods were repeated with K_{Max} (mean[SD] = 114.20 [31.30] MPa√mm) and J_{Max} (mean[SD] = 3.85 [1.43] kJ/m^2). No interactions were retained for K_{Max}, and while the main effects model reached significance (adjusted R^2 = 0.271, *p* = 0.001), only *Max Slope* remained a significant factor throughout, and the strongest overall model was with *Max Slope* as the sole

predictor (adjusted $R^2 = 0.299$, $p < 0.001$) (Table 5-6). Similar results were observed for J_{Max}, with no interactions being retained, and *Max Slope* remaining as the sole significant predictor; however, the relationship wasn't as strong as it was for K_{Max} (adjusted $R^2 = 0.163$, $p = 0.021$) (Table 5-6) (Figure 5-8).

Table 5-6: Linear models predicting fracture toughness (K_{Max} and J_{Max}) from *Age*, *Max Slope*, and T_d.

Fracture Property	Linear Model			Adj-R^2 (p)
K_{Max}	*Age*	***Max Slope***	*Td*	0.271
	(β = 0.06,	***(β = 0.57,***	*(β = -0.15,*	(*p* = 0.016)
	p =0.735)	***p = 0.003)***	*p = 0.397)*	
		Max Slope	*Td*	0.298
		(β = 0.55,	*(β = -0.16,*	(*p* = 0.006)
		p = 0.003)	*p = 0.336)*	
		Max Slope		0.299
		(β = 0.57,		(*p* = 0.002)
		p = 0.002)		
J_{Max}	*Age*	***Max Slope***	*Td*	0.150
	(*β = 0.11,*	***(β = 0.45,***	*(β = -0.18,*	(*p* = 0.083)
	p =0.575)	***p = 0.026)***	*p = 0.340)*	
		Max Slope	*Td*	0.174
		(β = 0.42,	*(β = -0.21,*	(*p* = 0.039)
		p = 0.028)	*p = 0.263)*	
		Max Slope		0.163
		(β = 0.44,		(*p* = 0.021)
		p = 0.021)		

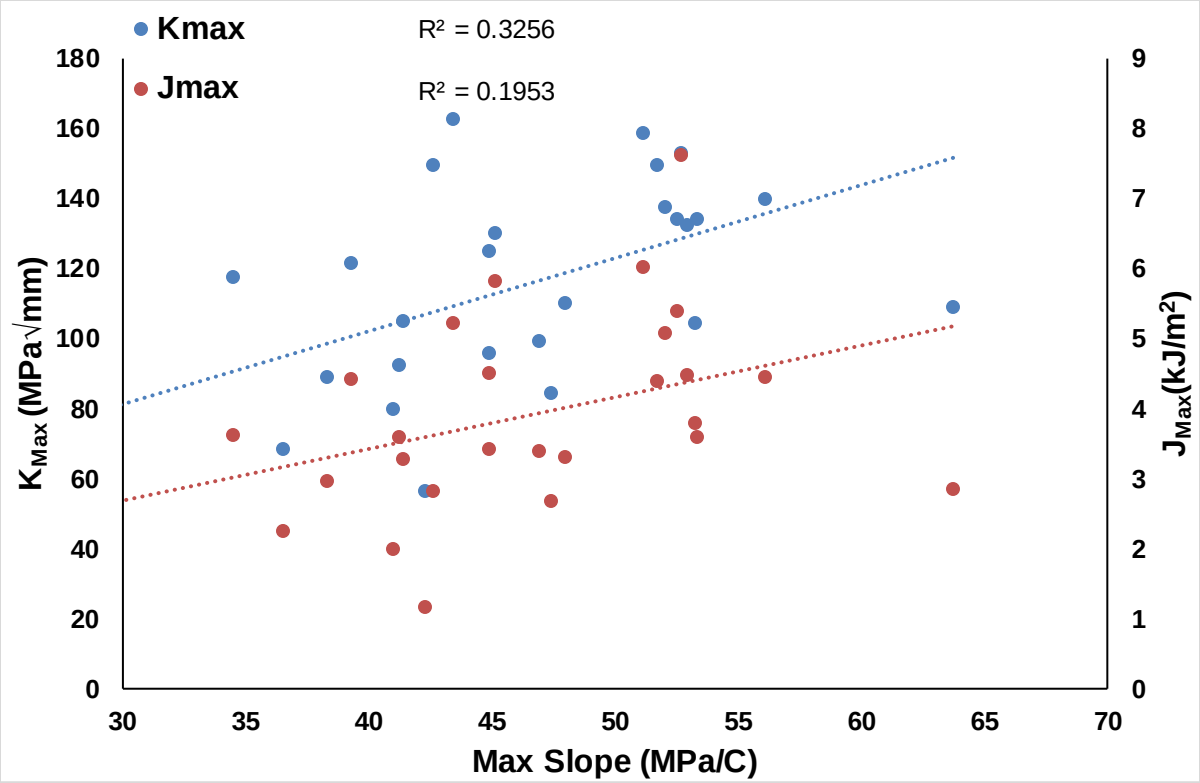

Figure 5-8: Linear relationship between Max Slope and both K_{Max} (blue dots) and J_{Max} (red dots).

Lastly, repeating the analyses of K_{Max} with the addition of disease revealed that its addition generally improved the predictive ability of models for K_{Max}. Both *Max slope* and disease remained as significant variables (adjusted $R^2 = 0.380$, $p = 0.001$) (Table 5-7). Similarly, disease remained as a significant factor for J_{Max}, and *Max Slope* and disease remained as the only remaining significant factors, with disease explaining 16.1% additional variance when compared to *Max Slope* alone (adjusted $R^2 = 0.324$, $p = 0.003$) (Table 5-7). There was no significant difference in either K_{Max} or J_{Max} between disease groups ($p > 0.05$).

Table 5-7: Linear models predicting fracture toughness (K_{Max} and J_{Max}) from *Age*, *Max Slope*, T_d, and *d*.

Fracture Property	Linear Model				*Adj-R^2 (p)*
K_{Max}	*Age*	***Max Slope***	*Td*	*Disease*	0.355
	(β = 0.13,	***(β = 0.69,***	*(β = -0.08,*	*(β = 0.34,*	(*p* = 0.008)
	p =0.452)	***p < 0.001)***	*p = 0.631)*	*p = 0.057)*	
	Age	***Max Slope***		***Disease***	0.377
	(β = 0.15,	***(β = 0.71,***		***(β = 0.36,***	(*p* = 0.003)
	p =0.359)	***p < 0.001)***		***p = 0.039)***	
		Max Slope		***Disease***	0.380
		(β = 0.67,		***(β = 0.33,***	(*p* = 0.001)
		p < 0.001)		***p = 0.049)***	
J_{Max}	*Age*	***Max Slope***	*Td*	***Disease***	0.327
	(β = 0.20,	***(β = 0.61,***	*(β = -0.09,*	***(β = 0.46,***	(*p* = 0.012)
	p =0.256)	***p = 0.002)***	*p = 0.604)*	***p = 0.014)***	
	Age	***Max Slope***		***Disease***	0.348
	(β = 0.23,	***(β = 0.63,***		***(β = 0.48,***	(*p* = 0.005)
	p =0.184)	***p = 0.001)***		***p = 0.009)***	
		Max Slope		***Disease***	0.324
		(β = 0.57,		***(β = 0.44,***	(*p* = 0.003)
		p = 0.002)		***p = 0.014)***	

5.4 Discussion

The overall goal of the study was to investigate the relationship between cortical bone collagen and cortical bone fracture toughness of the inferior femoral neck under high-rate, impact like loading. In line with the first hypothesis, neither K_q nor J_q fracture toughness was positively associated with either *Max Slope* or T_d. However, fracture toughness assessed at, and up to the point of peak load (K_{Max} and J_{Max}) was positively associated with *Max Slope*. Pertaining to the second hypothesis, only J_q fracture toughness was significantly lower in the disease group, while the addition of disease as a factor alongside *Max Slope* and T_d led to additional explained variance in almost all cases.

A potential explanation for the stronger relationships observed between *Max Slope* and the peak K_{Max} and J_{Max} fracture toughness when compared to K_q and J_q fracture toughness relates to

the methods used to quantify those metrics. By design, the methods used to quantify K_q and J_q only consider a limited amount of any potential plastic deformation, since these metrics are evaluated at, or up to, the point that the load line intersects the 95% secant modulus. In addition to providing a systematic way to evaluate fracture toughness at a common point, this method was originally chosen since very little plastic deformation was expected based on results from pilot work (Appendix G, Chapter 8.7). However, there was substantially more stable tearing and plastic deformation observed in this study. Consequently, many of the collagen related toughening mechanisms are known to be associated with plastic deformation of the material, and include collagen fiber bridging, microcracking of mineralized fibrils, breaking of interfibrillar crosslinks fibrillar sliding, and molecular uncoiling (Akkus and Rimnac, 2001; Barth et al., 2011, 2010; Buehler, 2007; Burton et al., 2014; Launey et al., 2010a; Nalla et al., 2003; Willett et al., 2015). The state of collagen network connectivity, as captured by *Max Slope*, is hypothesized to be related to some of these toughening mechanisms, thus fracture toughness metrics that capture or consider plastic deformation, such as K_{Max} and J_{Max}, are indeed expected to relate more strongly to the state of the collagen network. This study adds further support the notion that toughness of cortical bone is dependent on the integrity and connectivity of the collagen network (as captured by *Max Slope*) even under impact-like loading rates. However, its influence, or importance may be less than in quasi-static loading scenarios, as certain toughening mechanisms may be rate dependent.

A study by Gauthier and colleagues originally published in 2017 found significantly lower metrics of fracture toughness for SENB experiments for specimens tested under high-rate loading compared to those subjected to quasi-static loading (Gauthier et al., 2017), and in a follow-up experiment being published in 2019, observed a significantly lower volume fraction of microcracks in SENB specimens tested under high rate loading compared to those subjected to quasi-static loading (Gauthier et al., 2019). Similarly, Dapaah and colleagues (In Review) quantified the area of micro-damage, specifically micron-level cracks in the material, ahead of the crack tip (termed the micro-damage process zone, MDPZ) during both quasi-static and high-rate three-point bending experiments of femoral SENB (related to pilot work described in Appendix G, Chapter 8.7). The authors observed significantly smaller MDPZ, and significantly lower elastic plastic fracture toughness (J_{Max}) in the high-rate experiments compared to the quasistatic experiments. Though there are multiple fracture toughening mechanisms found in bone (Launey et al., 2010), microcracking is one of many collagen-related intrinsic toughening mechanisms.

Briefly, energy is dissipated as mineralized collagen fibrils break, creating microcracks ahead of, and in the vicinity of the crack tip. This expenditure of energy helps prevent or slow growth of the crack and consequently increases fracture toughness (Vashishth et al., 1997). Therefore, it is likely that certain toughening mechanisms, such as micro-cracking, are not able to engage to the same degree in high-rate scenarios. While collagen-related fracture toughness is an important aspect of the material behaviour of cortical bone, it is possible that it's relative importance or influence on the overall strength of bone is lessened in high-rate loading scenarios, such as fall-related hip fractures. However, the link between collagen-related fracture toughness, or more generally the connectivity of the collagen network, and femoral bone strength has yet to be investigated.

Even though disease was categorized as broad categorical variable (either the presence of an inflammatory disease or the lack thereof), it was still a significant predictor of fracture toughness, and its addition to models with *Max Slope* resulted in overall improvements in model strength. In fact, by accounting for their presence, we observed noticeable improvements in model strength, as this broad categorical variable helped explain additional variance (8.1% for K_{Max}, 16.1% for J_{Max}). Though only significant for J_{Max}, fracture toughness metrics were lower in SENB specimens from donors with inflammatory or bone-affecting diseases, such as Diabetes, Chronic Kidney Disease, and COPD. These diseases are thought to damage bone and more specifically alter the collagen network through elevated levels of oxidative stress (Modaresi et al., 2015; Ravarotto et al., 2018; Saito et al., 2006; Silva et al., 2009; Tomasek et al., 1994). The resulting oxidative damage has been hypothesized for the cause of the accumulation of advanced glycation end-products (AGEs) in the collagen networks of individuals with these diseases (Saito and Marumo, 2015; Tomasek et al., 1994). Previous studies have found the amount of AGEs changes the material properties of collagen (Poundarik et al., 2015; Saito et al., 2006; Silva et al., 2009), and higher concentrations of non-enzymatic collagen crosslinks are associated with lower fracture toughness (Knott et al., 1995; Massé et al., 1996; Nyman et al., 2007; Vashishth et al., 2001). A more recent investigation Arakawa and colleagues postulates that the presence of non-crosslinking AGEs (ligands such as carboxy-methyl-lysine, CML) may inhibit or block the formation of enzymatic crosslinks, further deteriorating the mechanical properties of the collagen network (Arakawa et al., 2020). Thus, the current understanding is that the accumulation of AGEs and the increase in NEG crosslinks observed in diseased tissue, and the resultant effect on material properties, may explain the increased rates of fractures seen in old age and in diseased states, which

provides a direct pathway of the role of collagen on bone strength and fracture risk. The findings of this study align with this general idea, and further amplify the need for additional research into the effect of changes in the connectivity or general organization of the collagen network and the material behaviour of bone, towards ultimately linking this to the overall strength of whole bone. The importance of the current work lies in the investigation of the relationship between collagen network connectivity and the behaviour of cortical bone (as quantified through fracture toughness in this study) under impact like loading towards encouraging translational research into the role of collagen on the strength of bone in the context of fall-related fractures.

There are, however, certain clear limitations that may both affect the strength of the reported findings, as well as limit their broader applicability. Firstly, despite characterizing four different metrics of fracture toughness, it is still unclear which most appropriately captures the mechanical behaviour of SENB samples of cortical bone under high-rate loading. While the peak-load based metrics (K_{Max}, J_{Max}), which captured more of the non-linear plastic deformation of the experiments, were more strongly associated with the metric of collagen network connectivity (*Max Slope*) than the more linear-elastic based metrics K_q and J_q, it is surprising to find that K_{Max}, the elastic fracture toughness measure, was more strongly associated than the elastic-plastic measure J_{Max}. Due to the viscoelastic properties of bone, it was anticipated that the response to three-point bending would be more linear elastic when loaded at a high displacement rate, at least when compared to quasi-static loading. Thus, K_q and J_q were thought to be the most appropriate metrics to quantify fracture toughness. However, it wasn't until after the load-displacement data of the experiments was analyzed that noticeable plastic deformation was observed. Though this observation led to the use of peak-load based metrics K_{Max} and J_{Max}, it was not until after the data was processed that these metrics were considered. Additionally, a post-hoc analysis was conducted wherein the plain strain fracture toughness (K) equivalent of elastic-plastic (J) fracture toughness (K_J) was computed as an alternative metric of fracture toughness (Appendix H, Chapter 8.8). This metric of fracture toughness is distinct from the other metrics of toughness used in this study in that it considers the measured elastic modulus of each specimen when computing toughness. The use of K_J fracture toughness led to improvements in the relationship between fracture toughness and *Max Slope*. This course of action highlights a need for more research into the impact-like behaviour of cortical bone at both the meso- and micro-scale and suggests the need to reconsider

the methods that are used in order to appropriately quantify the variables of interest (fracture toughness in this case).

A second limitation is related to the drawbacks of using such a heterogeneous sample of specimens in terms of the presence of multiple disease states. While this study was able to demonstrate that accounting for these diseases did help explain the relationship between fracture toughness and the connectivity of the collagen network, it likely hindered the ability to properly address the primary goal of this study. Though a minor limitation, since the heterogenous nature of the sample was specifically sought out for this study, it is nonetheless important to mention, as it may have weakened the strength of the relationships observed, as suggested in a previous study (Willett et al., 2019). Regardless, it was surprising how such a broad categorical variable as the presence or absence of certain disease states managed to explain a great deal of the variance, and it is possible that a more refined and targeted variable that more accurately or individually accounted for the different disease states could have resulted in even stronger models. Further research into the specific effect of these disease states on both the collagen network and on overall bone strength is needed. Another limitation relates to a physical limitation in the extraction of adequately sized SENB from the inferior femoral neck. While previous investigations of this nature have used SENB from the diaphysis of long bones, areas with thick and well-defined sections of cortical bone, this investigation aimed to extract SENB of cortical bone from a clinically relevant area in the context of fall-related hip fractures. As fall-related hip fractures often occur at the intertrochanteric or femoral neck areas, the goal was to extract SENB from that area. However, the cortical shell is much thinner in these sections (when compared to the diaphysis), meaning there was less cortical bone to begin with, and there is much trabecular bone present in the proximal femur. Add to this the complexities of attempting to extract a straight beam from a curved section, and the difficulties of extracting uniform cortical bone SENB become apparent. While appropriately sized SENB were extracted from all specimens, certain specimens had clear trabecular elements visible on at certain ends of the SENB. Furthermore, the specific area from which the SENB were extracted varied based on specimen morphology, with specimens with either shorter femoral neck axis lengths or more acute neck shaft angles having SENB extracted from a more distal portion of the neck and trochanteric area. Nevertheless, the use of CNC milling, and micro-level polishing allowed for a fine level of control when shaping the SENB down to the final

dimensions, and careful planning and selection of where the SENB would be extracted from ensured that the majority of the inner portion of the beams were cortical bone.

Other potential limitations include the influence of pore size or volume on crack growth and fracture toughness measures, or errors in the micro-level measurements of crack length. However post-hoc analyses revealed that the ratio of pore area to total area was not significantly related to any of the fracture toughness metrics (r^2 = 0.02-0.09, $p > 0.05$), and a sensitivity analysis revealed that a random error of +/- 0.03 mm in crack length did not significantly affect fracture toughness nor changed model or predictor significance. However, pre-existing microcracks and micro-damage were not able to be characterized, and the associated effects on the behaviour and toughness of the specimens could not be quantified. Previous work has demonstrated the presence of microdamage and the accumulation of microdamage affects cortical strength and is thought to contribute to bone fragility and increased fracture risk seen in older age (Augat and Schorlemmer, 2006; Bell et al., 1999; Bouxsein, 2005; Chevalley et al., 2012; Frost, 1960; Hazenberg et al., 2007; Schaffler et al., 1995). As part of the fracture mechanics triad alongside load (or stress) and fracture toughness, future work should identify the degree of microdamage and microcracking prior to testing, which could be achieved through the use of 3D volumetric micro computed tomography, in order to comprehensively consider multiple factors that might influence cortical bone fracture mechanics. Lastly, though T_d, a metric of collagen thermal stability that is thought to be related to the crosslinking content and connectivity of the collagen network and the presence of AGEs, was not related to fracture toughness. While not entirely surprising, as a similar study also found no correlation between T_d and measures of fracture toughness during quasi-static loading (Willett et al., 2019), it was hypothesized that metric may capture important information unique from *Max Slope*. Additional biochemical analyses to assess the crosslink content of the collagen network, such as HPLC and CML assays would have allowed for further level of detail in the analyses; however, there were cost and time-related limitations that prevented this from occurring. Regardless, while T_d did not relate to fracture toughness, it is still unknown if it will relate to bone strength, and continued consideration of this variable, as well as the underlying properties that his variable captures, is warranted.

5.5 Conclusion

Using impact-like loading of SENB from a clinically relevant site, the relationship between collagen network connectivity (as captured by *Max Slope* and T_d) and multiple metrics of fracture toughness were quantified. Significant relationships between peak-load based fracture toughness metrics K_{Max} and J_{Max} and *Max Slope* were observed, and the strength of these relationships increased considerably (~ 8 - 30%) when accounting for the presence of certain inflammatory disease states. These findings not only reiterates that collagen connectivity is an important factor in fracture toughness and crack growth at the meso-scale, but also confirms that this holds true for high-rate, impact like loading. While previous studies have investigated the influence of rate on fracture toughness of cortical bone at the inferior femoral neck (Gauthier et al., 2019, 2017), this is the first study to relate measures of fracture toughness measured under impact-like loading to metrics of collagen network connectivity and stability. Furthermore, this study was also able to demonstrate that the presence of inflammatory disease states, even when captured by a broad categorical variable, also influences fracture toughness, and its consideration greatly improves the strength of the relationship between fracture toughness and *Max Slope*, explaining up to 30% additional variance. These findings have important implications for the understanding of the role of collagen on the mechanical behaviour of cortical bone at the meso-scale under impact-like loading. More importantly, these results will allow both fracture toughness and collagen-related metrics of connectivity and stability to be compared alongside contributions of the inorganic phase on femoral bone strength in the context of fall-related hip fractures in Study 4 (Chapter 6).

Chapter 6
Study 4: Investigating the Relationship Between Femoral Collagen Connectivity, Quality, Bone Toughness, and Bone Strength

6.1 Introduction

Fall related hip fractures are a serious problem concerning older adults (Billette and Janz, 2011; George Ioannidis et al., 2009; Jean et al., 2013; Jiang et al., 2005). Due to the large-scale deleterious consequences of these injuries, including cost and related mortality, efforts have been made to identify individuals at risk in order to implement appropriate prevention strategies. While currently used X-ray-based methods can successfully identify high-risk individuals due to severe bone loss, in the form of very low measures of bone mineral density (BMD), the sensitivity of these methods suffers for individuals with BMD above these very low measures (Schuit et al., 2004; Siris et al., 2004; Stone et al., 2003). To combat this and ultimately improve the sensitivity of fracture risk prediction, most avenues of research have included other factors related to bone strength, such as morphology, or turned to more complex imaging modalities to further investigated the non-organic phase of bone (Chappard et al., 2010; Cheng et al., 2007; Enns-Bray et al., 2016; Luo, 2017; Maeda et al., 2011; Museyko et al., 2016; Partanen et al., 2001; Yeung et al., 2006). Yet, little research has been devoted to investigating the contributions of the organic phase of bone, something that isn't captured in typically used X-ray-based methods, despite the fact that it is as integral to bone as the inorganic phase.

Previous research has shown the importance of the organic phase of bone, or more simply bone collagen (type I collagen) in the behaviour of bone as a material (Luo and Wu, 2020; Vashishth et al., 2001; Zioupos et al., 1999), yet the role of collagen on bone strength is not fully understood. While many have suggested that collagen plays a critical role in bone strength (Boskey et al., 1999; Viguet-carrin et al., 2006) based on understanding of the chemical, genetic, and material properties of bone collagen, and most notably its relation to fracture toughness, the direct link between bone strength and collagen has not been studied. More specifically, this relationship has not been established in the case of fall-related hip fractures, although it has often been inferred or implied. While the link between bone collagen and fracture toughness has been established and continues to be a focus of research, the link between fracture toughness and bone strength has been inferred through the related link between fracture toughness and strength observed in brittle materials. The fact that bone is more than just a complex anisotropic/orthotropic nano-composite

material, and is in fact an organ that grows, adapts, and degrades along with the human body, brings into question this relationship, which requires further investigation.

Therefore, the overall purpose of this study was to conduct a novel investigation of the role of bone collagen on bone strength of the proximal femur in fall-related hip fractures. To achieve this, the data gathered in Studies 2, and 3 (Chapters 4 and 5) was aggregated for all matched pairs of specimens that were divided between the various studies (N = 12). As well as probing the relationship between bone strength and collagen quality, the primary goal of this study was to develop a model for predicting fracture force of the proximal femur (bone strength), similar to the model created in Study 2 (Chapter 4), which also included metrics of collagen mediated fracture toughness measured during study 3. Specifically, collagen-related metrics of toughness (K_{Max} and J_{Max} fracture toughness) were included into generalized-linear models to predict bone strength, determining whether these toughness metrics were significantly related to bone strength, and how much additional variance they explained compared to currently used clinical factors, such as bone mineral density and age. It was hypothesized that fracture toughness would be significantly associated with bone strength, with increases in either K_{Max} or J_{Max} leading to greater bone strength.

The secondary goal of this study was to investigate the relationship between collagen stability and connectivity metrics and bone strength. The reasoning for this goal was that, these metrics may be more easily assessed, or estimated from related biomarkers or other factors such as age or the presence of certain diseases, resulting in their potential use in clinical assessments of fracture risk (Eastell and Hannon, 2008; Garnero et al., 1996; Granke et al., 2015; Kuo and Chen, 2017). It was hypothesized that collagen stability metrics, specifically *Max slope* and T_d, would have significant positive associations with bone strength. Finally, it was hypothesized that the addition of these factors would improve the strength of the model predicting bone strength when compared to model without these metrics that was developed in study 2 of this thesis.

Towards investigating any potential interactions with the presence of an inflammatory disease state (as investigated in Studies 2 and 3), a secondary data analysis was performed wherein disease state presence (including Diabetes, Chronic Kidney Disease, and Chronic Obstructive Pulmonary Disorder) was included into the above-mentioned models. Towards exploring the potential mechanism underlying the increased hip fracture risk seen in these disease states (De Liefde et al., 2005; Forsén et al., 1999; Giangregorio et al., 2012), this analysis allowed for the investigation of potential disease-related differences, and if they were captured through collagen-

related metrics. Accordingly, it was hypothesized that the presence of a disease state would be significantly associated with lower bone strength, and its inclusion in the predictive model would improve the strength of the model. Additionally, it was hypothesized that collagen-related metrics would be significantly different between disease groups.

6.2 Methods

6.2.1 Data Aggregation

Data was aggregated from Studies 2 and 3 (Chapters 4 and 5) for all matched pair specimens that were acquired during the thesis and separated between the various studies. This resulted in a total sample size of 12 pairs of femurs. Demographic data, bone strength (F_x), femoral neck aBMD (*BMD*), fracture toughness (K_{Max} and J_{Max}) and collagen stability and connectivity metrics (*Max slope* and T_d) were aggregated (Table 6-1).

Table 6-1: Mean (SD) for the independent and dependent variables for the 12 samples used in this study. Note: BMD is from the femur that underwent the HIS bone strength experiments.

N	*Age* (years)	*Sex* (f/m)	*Disease* (N present)	F_x (N)	*BMD* (g/cm^2)	K_{Max} (MPa$\sqrt{}$mm)	J_{Maxc} (kJ/m^2)	*Max slope (MPa/°C)*	T_d (°C)
12	76.2 (16.8)	3/9	9	6382.5 (2234.86)	0.669 (0.105)	113.16 (30.27)	3.72 (1.31)	45.92 (7.46)	62.80 (1.01)

6.2.2 Statistics and Data Interpretation

A table including individual details for each specimen is presented in Table 6-2. In order to investigate the role of collagen and fracture toughness on fracture force, multiple linear regression was used to quantify the effect of *BMD, sex,* the two fracture toughness metrics (K_{Max} and J_{Max}), and collagen stability and connectivity metrics (*Max Slope* and T_d) on F_x. As was done in study 2 (Chapter 4), multiple linear regression via generalized-linear models was used to first re-investigate the relationship between fracture force and the variables that were retained in the strongest overall model developed in study 2 (namely *sex*, *BMD*, and their interaction). This was done to limit model comparisons to the sample available in this study. The model was then used

as the benchmark (Study 2 Benchmark Model) from which the models evaluated in this study would be compared. Additional backward elimination stepwise regression analyses were performed to determine the strongest overall model for this sample, to be used as a second, more internally valid, benchmark (Study 4 Benchmark Model).

Table 6-2: Specimen details for the entire sample, including independent and dependent variables

Specimen ID	***Age (years)***	***Sex***	***BMD*** (g/cm^2)	***Fx (N)***	***Max Slope (MPa/°C)***	T_d ***(°C)***	K_{Max} ***(MPa√mm)***	J_{Max} ***(kJ/m²)***
1	48	F	0.808	7498.0	52.50	62.95	133.94	5.39
2	76	M	0.55	5787.1	34.44	63.53	117.54	3.63
3	65	M	0.749	9104.8	52.89	64.12	132.22	4.48
4	96	M	0.607	5157.1	41.29	62.22	98.74	3.44
5	83	M	0.757	8442.8	37.40	63.15	78.68	2.62
6	91	M	0.621	5418.0	47.28	62.77	160.58	5.62
7	103	M	0.504	3201.5	39.30	60.67	121.61	4.41
8	63	F	0.533	2230.8	42.27	61.39	56.49	1.18
9	83	M	0.762	8800.3	40.98	62.81	79.87	2.00
10	68	M	0.766	7761.3	56.08	63.55	139.88	4.46
11	55	F	0.646	5168.7	53.28	63.93	104.34	3.80
12	84	M	0.727	8019.0	53.30	62.51	134.04	3.60

Following this, regression analyses were conducted to assess relationship between fracture toughness and bone strength, as well as identify if the addition fracture toughness metrics to the previously defined benchmark models resulted in additional explained variance. This was achieved by first investigating the individual relationships between fracture toughness and F_x (separately for both K_{Max} and J_{Max}), followed by regression analyses that added a fracture toughness metric into either of the benchmark models. Similar analyses were performed with the inclusion of *Max Slope* and T_d instead of fracture toughness. Individual relationships between collagen stability and connectivity metrics (*Max Slope* and T_d) and F_x were first assessed, followed by the addition of these metrics into the benchmark models. Model strength will be compared in terms of adjusted R^2, AICc, and significance. All statistical models will be developed and tested using the R programing language within the RStudio integrated development environment (IDE). Lastly, a final analysis will be performed, wherein a categorical variable representing either the presence or

absence of an inflammatory disease state (*d*) was added, and the above-mentioned analyses were repeated with the addition of this variable.

6.3 Results

Shapiro-Wilk's tests of normality for all variables (F_x, *BMD*, K_{Max}, J_{Max}, *Max Slope* and T_d) revealed that none of the variables violated the assumption or normality ($p > 0.05$). The linear regression model using *BMD*, *sex*, and their interaction to predict F_x was significant (adjusted $R^2 = 0.898$, $p < 0.001$). The model including only the main effect of *BMD* and sex was stronger, with an adjusted R^2 values of 0.910 ($p = < 0.001$). Neither K_{Max} nor J_{Max} were significantly related to F_x (adjusted $R^2 = -0.033$ and 0.072, p = 0.441 and 0.618, respectively). Including either factor into the benchmark models led to decreases in adjusted R^2 value, suggesting that the factors did not explain any additional variance (Table 6-3). While there was no effect of *Max Slope* on F_x (adjusted $R^2 = 0.023$, $p = 0.287$), there was a significant moderate relationship between T_d and F_x (adjusted $R^2 = 0.395$, $p = 0.017$). Adding both factors to either benchmark model resulted in improvements to both the Study 2 Benchmark Model (adjusted $R^2 = 0.938$, $p < 0.001$) and the Study 4 Benchmark Model (adjusted $R^2 = 0.947$, $p < 0.001$) (Table 6-4). While the latter model had the highest overall adjusted R^2 value, the model's AICc value (219.40) was significantly higher than the Study 4 Benchmark Model (200.56), Adding T_d to the Study 4 Benchmark Model did improve the adjusted R^2 to 0.942, and it's AICc value (200.07) was smaller than that of the Study 4 Benchmark model; however, this difference was not significant ($\Delta AICc > 2$). Regression analyses revealed that the model including *sex*, *BMD*, and T_d was the strongest overall model, explaining 94.2% of the variance, a 3.2% improvement compared to the strongest overall model that did not include any toughness or collagen-related metrics (Study 4 Benchmark Model) (Table 6-5). Post-hoc analyses comparing the strongest model from this study (main effects of *BMD*, *sex*, and T_d, adjusted $R^2 = 0.942$) against that of the Study 2 Benchmark Model revealed that the model including the metric of collagen thermal stability (T_d) was 12.4% more accurate based on the projection of predicted over measured F_x (Figure 6-1).

Table 6-3: Regression analyses adding in fracture toughness metrics (K_{Max} and J_{Max}) to both benchmark models.

Study 4 Benchmark	Predictor	*B*	*t*	*p*
F_x	***Intercept***	-9103.58	-5.640	<0.001
	Sex	1760.77	3.558	0.007
	BMD	18913.96	9.127	<0.001
	K_{Max}	-2.23	-0.296	0.775
		F (df)	Adj. R^2	*p*
		33.795 (3,8)	0.899	<0.0001
F_x	***Intercept***	-9085.92	-5.692	<0.001
	Sex	1740.53	3.674	0.006
	BMD	18945.39	9.214	<0.001
	J_{Max}	-68.62	-0.412	0.691
		F (df)	Adj. R^2	*p*
		34.166 (3,8)	0.900	<0.0001
Study 2 Benchmark	**Predictor**	***B***	***t***	***p***
F_x	***Intercept***	-10293.73	-1.633	0.146
	Sex	2517.14	0.647	0.538
	BMD	20832.63	2.079	0.076
	K_{Max}	-3.29	-0.340	0.744
	BMD:Sex	-1106.04	-0.196	0.850
		F (df)	Adj. R^2	*p*
		22.310 (4,7)	0.886	0.0004
F_x	***Intercept***	-11961.54	-1.651	0.143
	Sex	3548.58	0.796	0.452
	BMD	32619.48	2.026	0.082
	J_{Max}	-141.68	-0.564	0.590
	BMD:Sex	-2681.33	-0.408	0.695
		F (df)	Adj. R^2	*p*
		22.996 (4,7)	0.889	0.0004

Table 6-4: Regression analyses adding in collagen connectivity and stability metrics (*Max Slope* and T_d) to both benchmark models.

Main Effects	**Predictor**	***B***	***t***	***p***
F_x	***Intercept***	-39319.34	-3.482	0.010
	Sex	1539.19	4.184	0.004
	BMD	17231.63	8.509	<0.001
	Max Slope	-35.27	-1.316	0.230
	T_d	527.02	2.747	0.029
		F (df)	Adj. R^2	*p*
		50.16 (4,7)	0.947	<0.0001
Study 2 Factors	**Predictor**	***B***	***t***	***p***
F_x	***Intercept***	-39770.07	-3.056	0.022
	Sex	1765.93	0.757	0.478
	BMD	17791.83	2.924	0.026
	BMD:Sex	-339.76	-0.099	0.925
	Max Slope	-35.12	-1.212	0.271
	T_d	528.14	2.547	0.044
		F (df)	Adj. R^2	*p*
		34.460 (5,6)	0.938	0.0002

Table 6-5: Strongest overall linear model with all significant predictors.

Linear Model				***Adj-R^2 (p)***
F_x	***Sex***	***BMD***	T_d	0.942
	(β = 0.35,	***(β = 0.76,***	***(β = 0.22,***	($p < 0.0001$)
	p =0.001)	***p < 0.001)***	***p = 0.039)***	

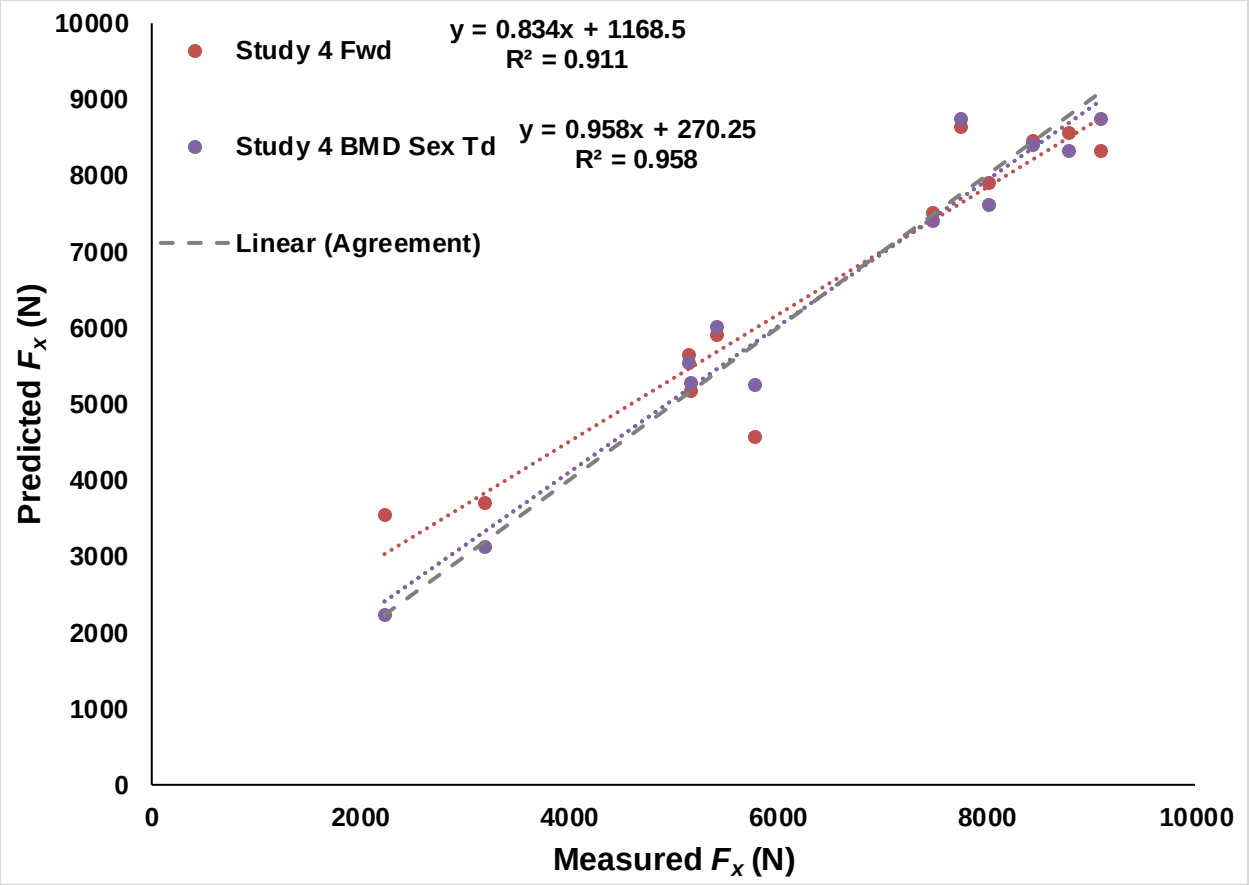

Figure 6-1: Predicted F_x regressed over measured F_x, with linear fits (dotted lines).

The addition of disease (*d*) as a factor into the regression analyses did not improve any of the models, and the presence of inflammatory disease states was not associated with F_x (adjusted R^2 = -0.096, p = 0.845). While the mean F_x for the disease group (6460.8 N) was higher than that of the non-disease group (6147.389), this difference was not significant (p > 0.05).

6.4 Discussion

The goal of this study was to quantify the role of fracture toughness and bone collagen connectivity and quality on bone strength of the proximal femur in fall-related hip fractures, as well as investigate if consideration of collagen-related factors would improve model predictions of bone strength. Though it was originally hypothesized that collagen-mediated fracture toughness was an important contributor of bone strength, fracture toughness metrics were not associated with F_x (K_{Max} adj. R^2 = -0.033, p = 0.441; J_{Max} adj. R^2 = 0.072, p = 0.618) nor did their addition improve the strength of models with BMD and sex as predictors. However, in partial support of the second

hypothesis, T_d, but not *Max Slope*, was significantly associated with F_x (adj. $R^2 = 0.395$, $p = 0.017$). In fact, T_d was a significant predictor of F_x alongside *BMD* and *sex*, and the model including these three factors had the lowest overall AICc of models considered in this study. While the combination of BMD and sex constituted a very strong positive relationship with F_x (adj. $R^2 = 0.910$), the addition of T_d led to an additional 3.2% of the variance being explained. Towards addressing the secondary goal of this study, the influence of disease was also considered, yet it was not a significant predictor of F_x and did not explain additional variance. While the mean difference between disease groups failed to reach statistical significance, it did not align with the associated hypothesis.

In Study 2 (Chapter 4), HIS experiments of a larger sample of femurs revealed a significant positive relationship between F_x and BMD, as well as with sex (higher F_x for males compared to females) was observed. Though it was demonstrated, through the use of a validation subset that *BMD*, *sex*, and their interaction resulted in the strongest overall model, the adjusted R^2 value was only 0.688, compared to the adjusted R^2 value of 0.898 for the Study 2 Benchmark model in this study, which used the same predictors. As this study only used a subset of the samples used in study 2, the results of this study may be misleading and do not properly capture the possible variance that a more representative (and larger) sample of the population contains. One of the potential consequences of the findings of this study is that some of the influence or role of collagen may have been obscured since almost all of the variance in this sample of specimens was explained by *BMD* and *sex* alone. While T_d was significantly associated with F_x (adj. $R^2 = 0.395$), adding it as a predictor alongside *BMD* and *sex* only led to an additional 3.2% of explained variance. It is entirely possible that, had T_d been able to be quantified for the entire sample of Study 2, a more sizeable portion of additional variance could have been explained by the addition of T_d. It may, however, still be possible to do so, as using bone from an alternate site (ex: diaphysis) within the same femur would allow for T_d (as well as *Max Slope*) to be quantified. While previous research by Gauthier and colleagues suggests that fracture toughness (which is known to be related to the condition of the collagen network) does not differ significantly between sites (femoral neck, femoral diaphysis, radial diaphysis, tibial diaphysis) under high-rate loading, further research is needed to determine if measures of collagen network connectivity and stability are equally site- or bone independent (Gauthier et al., 2017). Regardless, any improvement in model strength is generally encouraging. However, the question as to whether a 3.2% improvement is clinically

significant must be asked. Though its contributions are statistically significant, an argument can be made that the extra effort to quantify T_d may not be worth the slight improvement in model accuracy. Furthermore, T_d, as characterized in this study, is not currently a clinically quantifiable variable, unlike *BMD* or *sex*. While it may be possible to assess or estimate T_d via parallel regressions (for example, predicting T_d by *age* and *sex*, adj. $R^2 = 0.641$, $p = 0.004$), or via more direct measures by using other collagen rich tissue (such as skin), a major limitation of using T_d as a variable lies in the fact that the mechanistic link between T_d and material behaviour remains to be identified.

The results observed in this study do not support the hypothesis that collagen mediated fracture toughness, or the aspects of collagen connectivity captured by *Max Slope*, are significantly related to F_x. Or, more precisely, these variables do not explain any variance that is not already captured by *BMD* or *sex*. However, a post-hoc analysis of multi-collinearity (via quantification of variance inflation factors, VIF) and tolerance suggests otherwise, as >90% of the variance explained by BMD and sex are unique to those predictors, independently, while 87 and 96% of the variance explained by either K_{Max} or $\underline{J_{Max}}$ is unique to those predictors. Post-hoc analyses also revealed that neither K_q nor J_q (other fracture toughness metrics quantified in Study 3) were significantly associated with F_x (adj. $R^2 = -0.100$, 0.018, respectively, $p > 0.05$). Though different measures of collagen content were used (weight fracture of the mineral and organic phase of bone samples), a previous study by Wang and colleagues in 2000 suggested that collagen plays a role in fracture toughness but not in strength. However, the significant relationship between T_d and F_x observed in the current study contradicts this conclusion, even though fracture toughness and *Max Slope* were not associated. Therefore, the information about the collagen network that is captured by T_d seems to be unique from fracture toughness and *Max Slope*, at least as how it pertains to F_x of the proximal femur in simulated lateral hip impacts and fractures.

While T_d has been found to decrease alongside fracture toughness when comparing γ-irradiated bone to normal bone (Willett et al., 2015; Woodside and Willett, 2016), a recent study by Willett and colleagues in 2019 did not observe any correlation between T_d and *Max Slope*, despite observing significant relationships between fracture toughness metrics and *Max Slope* (Willett et al., 2019). As *Max Slope* has been described as "a function of collagen scission density and crosslink density", and is also a function of peptide chain length (Willett et al., 2015; Woodside and Willett, 2016), T_d, a measure of the thermal stability of collagen, may capture other unique

information about the state of the collagen network. Previous work has suggested that the thermal stability of the collagen network is related to the level of intramolecular bonds stabilizing the triple helix from within (Berg and Prockop, 1973; Miles and Bailey, 2001; Willett et al., 2008), the amount of connectivity and fragmentation of the collagen network (Burton et al., 2014; Gaar et al., 2020; Monnier et al., 1996; Sun and Leung, 2008; Wang et al., 2002; Willett et al., 2015, 2013; Zioupos et al., 1999), and changes in the structure or spacing of the collagen lattice (Miles and Avery, 2011; Miles and Bailey, 2001; Willett et al., 2008). Consequently, the thermal stability of collagen can be affected by the number and types of crosslinks in the collagen network (Bailey and Lister, 1968; Unal et al., 2016), which may themselves affect or relate to the fragmentation or organization of the collagen network (Arakawa et al., 2020; Woodside and Willett, 2016). Using γ-irradiation as a method to damage the collagen network, or more specifically create scissions in the peptide chain, Sun and colleagues demonstrate a dose response on the level of fragmentation, and observed a decrease in T_d as the dose, and ultimately damage, increased (Sun and Leung, 2008). Other groups have successfully used this method to demonstrate both a decrease in T_d as well as fracture toughness with γ-irradiation (Burton et al., 2014; Willett et al., 2015; Woodside and Willett, 2016). By inducing non-enzymatic crosslinks through a ribose pre-treatment, resulting in an increase in the overall connectivity of the collagen network, the γ-irradiation based damage and changes to toughness and T_d were significantly mitigated (Woodside and Willett, 2016). As for the relationship between the thermal stability of collagen and the structure and spacing of the collagen lattice, a study by Miles and Avery in 2011 demonstrated that thermal stability increased when the spacing between molecules in the collagen lattice was reduced through dehydration (Miles and Avery, 2011). A 2008 study by Willett and colleagues adds credence to this notion, as mechanical disruption of the lattice structure led to decreases in the thermal stability of collagen, with the authors suggesting that this decrease in stability was a result of increased molecular freedom within the collagen network (Willett et al., 2008). Unfortunately, while these studies help illuminate the underlying molecular level aspects that T_d may be capturing, the relationship between collagen-level connectivity or organization (pertaining to the structure and spacing of the collagen lattice) and macro scale bone strength is still unclear, and additional research is necessary. There is, however, some research related to collagen crosslink content that may help bridge the gap between collagen connectivity or organization and bone strength.

Alterations to collagen crosslink content and the presence of advanced glycation end-products (AGEs) have been hypothesized as a cause for the fragility fracture seen in older age (Brennan, 1989; Oxlund et al., 1996; Saito and Marumo, 2015; Zioupos et al., 1999), with some studies even making the link between crosslinking and the strength of bone in animal models (Oxlund et al., 1995; Saito et al., 2011). In an exhaustive review of the effect of collagen crosslinks on the material properties of bone, Saito and Marumo cover not only the pathway of typical enzymatic crosslinking (lysyl oxidase), but also discuss the formation of AGE crosslinks via non-enzymatic glycation (Saito and Marumo, 2015). As implied by the name, AGE crosslinks (as well as non-crosslinking AGE ligands such as carboxy methyl lysine, CML) are formed through glycation in the presence of free-reducing sugars (ex: glucose, pentose), or through oxidative stress (McCarthy et al., 2001; Saito and Marumo, 2015). Herein lies the link with bone affecting or inflammatory diseases, as either increased blood-sugar content, as observed in Diabetes Miletus (Saito et al., 2006; Silva et al., 2009; Tomasek et al., 1994) or oxidative stress and reactive oxygen species (Nose, 2000) resulting from inflammatory pathologies (as observed in Chronic Kidney disease) (Modaresi et al., 2015; Ravarotto et al., 2018) leads to increase presence of AGEs. Interestingly, these disease states are also associated with increase fracture risk (Janghorbani et al., 2007; Kazama et al., 2013; Miller, 2014), and in some cases increased risk is observed elevated BMD in the case of type II Diabetes (Leslie et al., 2012; Vestergaard, 2007). In addition to affecting or even disrupting crosslinking, the presence of AGEs has also been hypothesized to affect osteoblastic cellular function, affecting bone turnover, which provides another potential pathway for the influence of AGEs on bone strength (Fernandes et al., 2009; McCarthy et al., 2001; Turecek et al., 2008).

While not fully explored in human bone, and never on the macro-level of whole bone, previous studies have found that the number of enzymatic crosslinks is positively associated with ultimate strength of lumbar vertebra cancellous bone of cynomolgus monkeys (Saito et al., 2011), and conversely, Oxlund and colleagues found that a decreased concentration of enzymatic crosslinks (due to Beta-amino-proprionitrile , BAPN, binding to potential enzymatic crosslinking sites) was associated with a reduction in maximum bending stress and elastic stiffness of rat femurs (Oxlund et al., 1995). More recently, an investigation by Arakawa and colleagues helps provide a framework that connects many of these concepts, wherein the authors suggest that the presence of both crosslinking and non-crosslinking AGEs blocks the formation of immature crosslinks due to

the limited number of potential enzymatic crosslinking sites on the peptide chains (Arakawa et al., 2020). This finding may hint at a potential interaction between non-crosslinking AGEs and T_d, such that increased concentration of non-crosslinking AGEs at these potential enzymatic crosslinking sites of the carboxy and amino terminals of the collagen molecule could lead to reduced T_d. In their 2001 article, Miles and Bailey have already indirectly speculated on this possibility, as they noted that thermally labile domains of collagen are found in these terminals, which also happen to be where the enzymatic crosslinking sites are found (Miles and Bailey, 2001). These thermally labile domains are described as such due to the lack of hydroxyproline found in these regions, where it is hydroxyproline related hydrogen bonded water-bridges that provide intramolecular stability to the triple helix (Berg and Prockop, 1973; Miles and Bailey, 2001). However, these domains are typically stabilized intermolecularly through lysyl-oxidase mediated enzymatic crosslinks. Therefore, if non-crosslinking AGEs form at these sites (as suggested by Arakawa et al., 2020), resulting in a lack of intermolecular stabilization, it would follow that these regions would begin to unravel and coil at a lower temperature, or a lower T_d. However, further research into this specific link is needed, and the effect of this potential interaction on bone strength is still unknown. Arakawa and colleagues conclude that the role of non-crosslinking AGEs on bone strength needs to be investigated, and the present study may represent the first step towards addressing this gap in the literature. While limited by monetary and logistical barriers, future research into the collagen crosslink content of this sample is already planned, with high performance liquid chromatography (HPLC) and Raman spectroscopy to be used to identify relative concentrations of different crosslinks, and carboxy methyl lysine assays planned to assess the concentration of CML ligands. In general, if these planned experiments reveal that T_d is related to the concentration of crosslinking and non-crosslinking AGEs, a molecular based mechanism of bone strength may be identified.

While T_d is a relatively broad variable that appears to encompass many aspects related to the crosslinking content and overall organization of the collagen network, this study was nonetheless able to provide some of the first **potential** evidence of the role of collagen on whole bone strength, specifically in the context of fall-related hip fractures. Though the addition of T_d as predictors only led to a small improvement in an already strong model using BMD and sex as predictors, the effect was significant, and the improvement may be more substantial in a larger, more representative sample. Though further research is required to better understand the exact

mechanism through which collagen quality (as captured by its thermal stability, quantified here as T_d), our current understanding of the factors affecting thermal stability (described above) may already allow us to consider the role of collagen on bone strength in a clinical setting. While T_d may not be quantifiable without a tissue sample, recent developments in imaging techniques such as Raman spectroscopy may allow for the quantification of relative concentrations of crosslinks in the collagen network of bone (Unal, 2021; Unal et al., 2016). While this method is currently limited to direct spectroscopy of bone samples, continued improvements in the technique (such as the development of novel probes) may allow for in-situ measurements, or conversely, skin level external measures may provide a surrogate site for quantifying collagen quality at the whole-body level. Currently available methods that may provide insight into collagen crosslink content include the use of biomarkers, such as skin and urine pentosidine, which has previously been found to be positively correlated with bone pentosidine (a well-studied AGE crosslink) (Kida et al., 2019). However, further research into this avenue is necessary, as results linking pentosidine to bone strength are inconsistent (Saito et al., 2011; Saito and Marumo, 2010), despite previously being identified as a surrogate marker of the total concentration of AGEs in the collagen network (Saito and Marumo, 2015). Regardless, the findings of this study encourage further investigation into these areas, as clinically quantifiable metrics of bone collagen may allow for more accurate predictions of femoral bone strength, ultimately improving the ability to predict injury risk.

Indeed, further research into the relationship between collagen network connectivity and bone strength may reveal new clinical pathways through collagen network targeting pharmaceutical or nutritional interventions, or reveal the importance of reducing oxidative stress and the underlying causes. Lastly, simply the improvement in the accuracy of bone strength predictions, as suggested by this study and the thesis at large, could lead to improved predictive ability to identify at risk individuals. This alone could lead to improvements in the efficiency of targeted physical interventions, such as the installation of safety flooring (Lachance et al., 2017; Laing et al., 2006) or the prescription of hip protectors (Korall et al., 2015; Laing et al., 2011), with the former having larger monetary barriers, and the latter having significant limitations related to compliance. Despite the fact that much research is yet needed to fully address the problem of fall-related hip fractures, this study, and more generally this thesis, has bridged an important gap in the related literature. The work herein highlights the importance of multiscale research, and how an understanding of the problem at the macroscale is complimentary to knowledge of the micro-

scale, and this body of work demonstrates that combining the two allows for fulsome and in-depth basic research with immediate clinical applicability.

As previously suggested, there are, however, clear limitations associated with this study. Firstly, despite a concerted effort to procure matched pairs of cadaveric femurs, substantial barriers persisted, and only 12 femoral pairs were ultimately acquired. Further research using a larger sample size is clearly necessary. A possible solution, previously mentioned earlier in this discussion, relates to using samples from a surrogate site within femurs (rather than pairs) to access collagen network connectivity and quality (such as quantifying T_d). However, further validation is necessary in order to determine whether measures from surrogate sites are equivalent to that of samples from the inferior femoral neck. Secondly, by using such a representative variable as T_d, caution must be taken when interpreting the results. Though T_d is a direct measure of collagen thermal stability, this study postulates that T_d captures many aspects related to collagen network connectivity and organization, and it is in those aspects that the mechanistic link to bone strength resides. However, since the underlying aspects of collagen connectivity and organization were not directly investigated in this study, the veracity of the conclusions are limited. Additionally, the argument of correlation vs. causation must be mentioned, as T_d (and its related factors) may simply be correlated with the F_x of this sample, with the possibility of no causal link. This is unlikely, due to the body of research described earlier in this discussion, yet it is nonetheless important to mention. This is partly a limitation of the statistical methods used in this study, and further research into the determinants of T_d that are unique from *Max Slope* and fracture toughness is needed.

A third limitation relates to the methods used to collect this data, namely those used in Studies 1, 2 and 3 and are discussed in greater depth in their respective chapters (Chapters 3, 4 and 5). Briefly, the 4 m/s impact velocity used in studies 1 and 2 (4 m/s) is higher than typically observed during fall-related hip impacts (1.29 – 3.51 m/s) (Choi et al., 2015). However, as discussed in the discussions of Chapters 3 and 4, the 4 m/s impact velocity helped ensure sufficient energy to fracture the specimens. Other related limitations pertain to design flaws in the surrogate pelvis spring system that only revealed themselves during the data processing and analysis steps of Studies 1 and 2 (see Appendix A, Chapter 8.1 for more details). As for study 3, there were limitations with the availability of cortical bone in the inferior femoral neck of specimens, such that some specimens had some evident trabecular regions on the outer edges of the SENB specimens. However, the impact of this was minimal due to careful planning of cuts and a high

degree of control during the milling and polishing process. Other limitations in Study 3 related to the initial choice of computing elastic and elastic-plastic fracture toughness at the intersection of the load-displacement curve with the 95% secant modulus line (K_q and J_q). After processing of the data, clear regions of plastic deformation were observed after this point, such that a second computation of fracture toughness at the point of peak load (K_{Max} and J_{Max}) was deemed appropriate. While a case can be made for the use of either pair of fracture toughness values, the fact that anticipated load-displacement behaviour of the specimens were not accurate suggests a poor understanding of the material behaviour of cortical bone under those loading conditions, suggesting the further need for research. As discussed in previous Chapters, the lack of quantification and consideration of micro-cracking and microdamage in the SENB specimens and the larger femur specimens is a clear limitation of this work. While load and toughness are critical factors in the fracture mechanics of a material, defect size is the third point in the fracture mechanics triad. The presence of microdamage, often in the form of micro-cracks, or voids and pores in cortical bone will greatly influence its mechanical behaviour. Indeed, the accumulation of microdamage observed in aging is thought to be linked with age-related bone fragility and increased fracture risk (Augat and Schorlemmer, 2006; Bell et al., 1999; Bouxsein, 2005; Chevalley et al., 2012; Frost, 1960; Hazenberg et al., 2007; Schaffler et al., 1995). Though pore size was considered in the SENB specimens, this was limited to a 2D, planar characterization, and was further limited by the resolution of the images. In order to more fully characterize the fracture mechanics of inferior femoral neck cortical bone, all aspects of the fracture mechanics triad need to be considered, and defect size should be more precisely quantified through the use of 3D volumetric micro computed tomography. Despite these limitations, the results of the current study clearly suggest that aspects of collagen that are captured by T_d are significantly related to bone strength, and its consideration in predictive equations of femoral bone strength could improve the accuracy of those predictions.

6.5 Conclusion

Through multiscale investigations of whole bone strength at the macroscale and characterization of aspects of the collagen network at the micro-scale, this study represents the first investigation to relate the influence of measures of collagen on whole bone strength, specifically in the context of fall-related hip fractures. T_d, a measure of collagen thermal stability

that is related to the molecular crosslinking and intermolecular spacing, was a significant predictor of F_x, and its inclusion alongside the commonly used predictive variables of sex and BMD resulted in a predictive model that explained 94.2% of the variance in the small sample. Though the additional variance explained by T_d was small (3.2%), these findings suggest that the crosslinking content of the collagen network, and the resulting organization of the collagen lattice structure of cortical bone from the inferior femoral neck, plays a significant role in the not only the material behaviour of cortical bone, but also the whole-bone response to impact-like loading and ultimately fracture in the proximal femur. While limited by the relatively small sample size, the results are nonetheless encouraging, and these findings warrant continued investigation on the multiscale contributions of bone composition, specifically pertaining to the collagen phase. Further research into the underlying molecular mechanisms and post-translational modification of collagen responsible for T_d may allow for relevant biomarkers to be identified and used to measure or predict T_d, allowing for clinical application of these findings. As a whole, this thesis presented mixed results relating to the potential importance of biofidelic experimental methods towards achieving physiologically accurate measures of bone strength, but demonstrated evidence for the contribution of collagen on the strength of the proximal femur in the context of fall-related hip fractures. This work builds on a foundation of mechanistically minded basic research towards further illuminating the underlying mechanics of fall-related hip fractures in order to generate predictive models of bone strength that have clear clinical applicability.

Chapter 7
Thesis Summary

The overall purpose of this thesis work was to investigate the multiscale contributions of loading rate, fracture toughness, and bone composition (including the mineral and collagen phases of bone) on the strength of the proximal femur in the context of fall-related hip fractures. The specific goals included:

1) Investigating the relationship between loading rate and bone strength by comparing measured F_x between MTS and HIS experiments.
2) Developing a predictive model of femoral bone strength based on a biofidelic test paradigm.
3) Comparing the predictions of the developed model to the predictions of published models that were based on MTS experiments.
4) Evaluating the collagen mediated fracture toughness of cortical bone of a clinically relevant site under impact-like loading.
5) Quantifying the relative role of fracture toughness and collagen-related metrics on bone strength.
6) Developing a predictive model of F_x that considers collagen-related metrics alongside BMD and sex.

In addition to these goals, many of the studies had a secondary goal of investigating the influence of disease on fracture toughness and bone strength. These goals were achieved through four studies; a summary of the findings of these studies follows.

7.1 Study 1: Investigating the influence of test paradigm on fracture force of the proximal femur during lateral impacts

In this study, the bone strength (F_x) of 6 matched pairs of femurs was quantified through using one of two experimental paradigms: a constant-displacement rate (60 mm/s) driven deformation using a material testing system (MTS), and a vertical drop tower lateral impact (4 m/s) using a biofidelic hip impact simulator (HIS). Though the loading rate induced in the HIS experiments was significantly higher than that of the MTS ($p < 0.001$), there was no significant

difference in F_x due to this loading rate difference. These results suggest that, at least at the difference in loading rates observed in this study, loading rate does not have an effect on F_x.

7.2 Study 2: Development of predictive models to estimate fracture force of the proximal femur

Using a sample of 26 femurs, HIS experiments were used to quantify F_x. The relationship between F_x and factors such as *age*, *sex*, femoral neck areal bone mineral density (*BMD*), and morphological aspects like femoral neck moment arm (*r*) and cross-sectional moment of inertia (*CSMI*) were investigated using multiple linear regression. GLM analyses revealed that *BMD* and *sex* were significant predictors of F_x, and forward regression analyses resulted in a model that included *BMD*, *sex*, and their interaction, which had an adjusted R^2 value of 0.688 ($p < 0.001$). When comparing predictions of femoral bone strength from this model to those of four published models that were based on MTS constant displacement experiments, predictions from the published models were significantly lower ($p < 0.005$). A secondary analysis wherein the presence of an inflammatory disease state was included as a categorical variable did not reveal any relationship with F_x, nor did the inclusion of this variable improve model strength. Additionally, when the predictions of the published models were compared to the measured values, all four models significantly underpredicted F_x for male specimens, and three of the models underpredicted female F_x. The findings **related to model prediction differences** suggest not only that a biofidelic experimental paradigm **may** produces significantly different measures of bone strength, but also that considering sex in bone strength predictions may result in more accurate estimates of bone strength and ultimately hip fracture risk.

7.3 Study 3: The role of bone collagen integrity on fracture toughness of the inferior femoral neck under simulated impact loading rates

From a sample of 23 femur specimens, 28 SENB were extracted from the inferior femoral neck and subjected to high-rate (12 mm/s) three-point bending experiments to quantify two elastic and two elastic-plastic fracture toughness metrics (K_q, K_{Max}, J_q, J_{Max}). These fracture toughness metrics were compared to the measures of collagen network connectivity and stability (*Max Slope* and T_d) as measured during hydrothermal isometric tension (HIT) experiments. Regression analyses revealed that significant relationships between *Max slope* and K_{Max} and J_{Max}. In addition, accounting for the presence of certain inflammatory disease states considerably increased the

strength of the relationships. However, T_d was not significantly related to any toughness metric. These findings reveal that the previously reported relationship between cortical bone fracture toughness and collagen network connectivity (as captured by *Max Slope*) is still observed under impact-like loading of a clinically relevant site. Additionally, considering the presence of inflammatory disease states helped explain additional variance, which adds support for the hypothesis that oxidative stress resulting from inflammatory disease states negatively affects collagen network connectivity, likely through increased AGE crosslinks, resulting in the embrittlement of collagen and a decrease in fracture toughness.

7.4 Study 4: Investigating the relationship between femoral collagen connectivity, quality, bone toughness, and bone strength

In the final study of this thesis, data from 12 matched pairs of femurs that were split between studies 2 and 3 were aggregated, resulting bone strength (F_x) and collagen-related metric (K_{Max}, J_{Max}, *Max Slope*, T_d) data being quantified for each pair. This allowed for the quantification of the relative role fracture toughness and metrics of collagen connectivity and stability on F_x. While there was no observed relationship between fracture toughness and F_x, T_d was significantly and positively related to F_x (ajd. $R^2 = 0.395$, $p = 0.017$). Though *BMD* and *sex* alone explained 91% of the variance in F_x for this sample of femurs (N = 12), the addition of T_d resulted in an additional 3.2% explained variance (adj. $R^2 = 0.932$, $p < 0.0001$). While these findings do not support the hypothesis that collagen mediated fracture toughness affects bone strength, these findings do support the hypothesis that the collagen-related aspects (as captured by T_d) are significantly **related to** bone strength, and that considering collagen results in an improvement in our ability to predict bone strength. A secondary analysis considering the presence of inflammatory disease states did not reveal any relationship between F_x and disease, nor did the inclusion of disease state improve model strength.

7.5 Significance and Implications

7.5.1 Significance

This thesis work represents the first investigations to directly measure the influence of collagen on whole bone strength, specifically in the context of fall-related hip fractures. Though study 1 did not demonstrate a statistically significant difference in measured fracture force between the traditional MTS paradigm and the HIS paradigm, the model prediction differences observed in

study 2 allude to a potential difference driven by experimental paradigms that warrants further research. Beyond this, this thesis provides evidence that collagen does indeed affect femoral bone strength in the context of fall-related hip fractures. While collagen network connectivity aspects that are captured by *Max Slope* are significantly related to fracture toughness, it is the collagen network connectivity and stability aspects captured by T_d that are significantly associated with bone strength. Though the specific mechanism through which T_d captured collagen connectivity influence bone strength is still unknown, this thesis speculates that it is the concentration and type of enzymatic crosslinks, as well as the presence of crosslinking and non-crosslinking AGEs, that affects bone strength. In general, greater crosslinking is known to be positively associated with T_d, and this thesis work demonstrates that higher T_d is positively associated with bone strength. Therefore, it is possible that greater crosslinking leads to increased stiffness and strength of the collagen fibers, which has previously been reported, which contribute to bone strength alongside the mineral phase of bone. While it appears that the mineral phase of bone accounts for the majority of bone strength, the contribution of collagen is still significant and should not be ignored.

7.5.2 Clinical Implications

Beyond the significance of this work from a basic science perspective, these findings also have important clinical implications. As demonstrated in Study 2, the model developed therein produced significantly different predictions of bone strength than previously published models based on less biofidelic test paradigms. While the physiological accuracy of the model developed in study is assumed based on our current understanding of hip impact dynamics, it does provide a potential explanation for some of the inaccuracy of current hip fracture prediction methods. Indeed, the findings of this study may help explain the large number of false-positive hip fracture risk predictions. Additionally, these findings also provide evidence for the importance of sex-based effects on bone strength and considering sex may further help improve hip fracture risk prediction, particularly for males.

7.5.2.1 Fracture Risk Estimates

This model may have immediate clinical applicability, and its use may help identify true at-risk cases and prevent false-positives. Indeed, as demonstrated in Study 2 (Chapter 4), the published models produced femoral bone strength, or fracture force, estimates that were on average 1413 N lower than the measured fracture force. When split by sex, published model predictions were on average 1938 N lower for males, and 544 N lower for females. As the mean fracture

strength of the ranges from 3000 N to 7000 N (Courtney et al., 1994; Courtney et al., 1995; Dall'Ara et al., 2013; Roberts et al., 2010), these represent clinically meaningful differences. As presented in the discussion of Study 2 (Chapter 4), it is possible to estimate the effect of the predicted models developed in this thesis (versus previously published models) on hip fracture risk through the use of a probabilistic model (Martel et al., 2020). This allows for comparisons of population level distributions of hip fracture risk (using Factor of Risk (FOR) methods) when using different predictive models of femoral bone strength. When the predictive bone strength model developed in Study 2 was used to determine bone strength, and thus, set the denominator for calculating FOR of a fall-related hip fracture, it resulted in sex-specific distributions of risk that more closely matched the relative incidence of risk observed in this simulated population (when compared to distributions where the Roberts et al., 2010 predictive model of bone strength was used) (Figure 7.1). More specifically, the use of the Roberts et al., 2010 bone strength model (dashed lines) resulted in significantly higher risk for males (blue) compared to females (red), which does not align with epidemiological evidence (Cummings, 2002; Jean et al., 2013; Leslie, 2009). The use of the predictive bone strength model developed in Study 2 (solid lines) resulted in distributions that align much more closely with epidemiological evidence. Using a FOR value of 1 as a threshold for fracture risk, since this represents an impact force that is equal to or greater than the predicted bone strength, it is possible to compare the percentage of the population that would be identified at risk of hip fracture with either model. Using the Roberts et al. 2010 femur strength algorithm results in approximately 40.5% of the male population, and 10.4% of the female population, of older adults being identified at risk of sustaining a hip fracture. This increased risk for males does not align with the epidemiological evidence (Cummings, 2002; Jean et al., 2013; Leslie, 2009). When using the model developed in Study 2, this number is reduced to only 9.3% for males and down to 8.1% for females. While the change in percentage is smaller for the female population (from 10.4% to 8.1%), the important aspect is that male and female risk distributions are much more closely matched and the trends much more closely match epidemiological observations (Cummings, 2002; Jean et al., 2013; Leslie, 2009). Though this probabilistic modelling approach is dependant on many assumptions, it does provide interesting insight into population level risk and may be used to help guide clinical decisions and even help support or direct policy level changes. This alone has important research implications, urging further research into this domain.

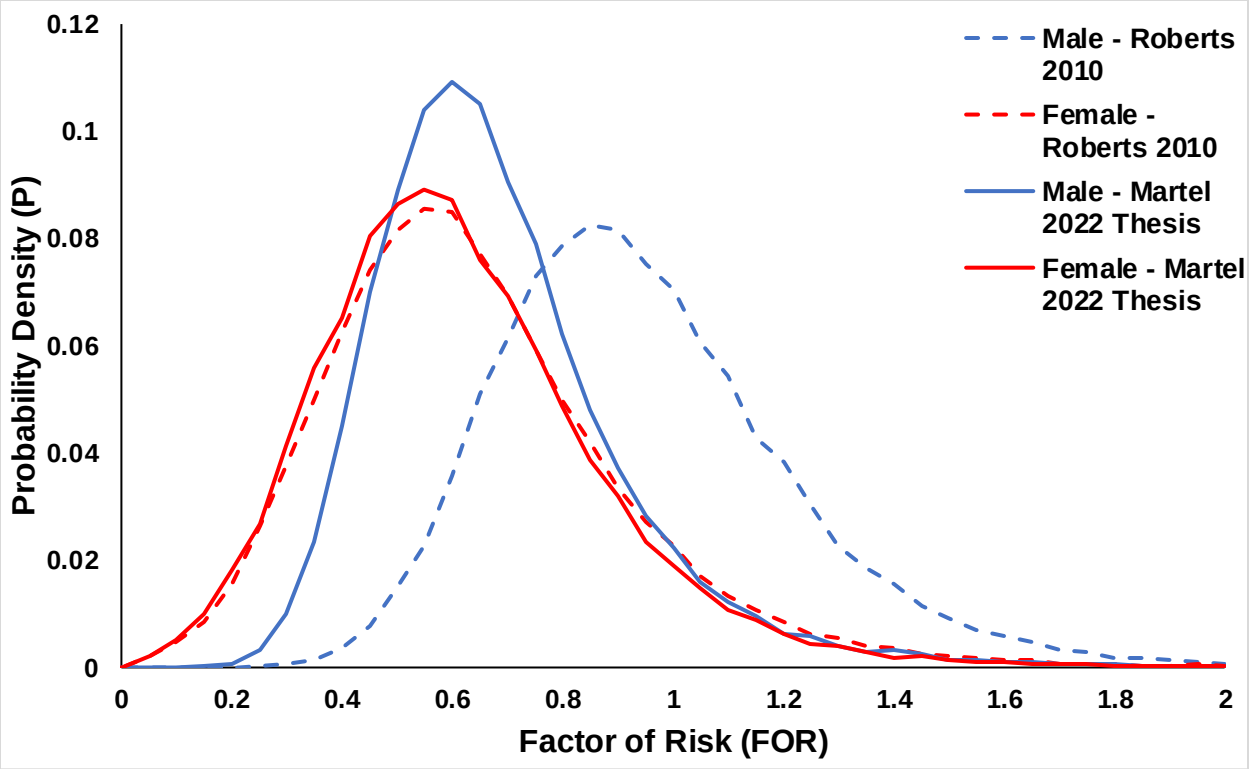

Figure 7-1: Probability density distributions of Factor of Risk (FOR) from the Martel et al., 2020 probabilistic model of hip fracture risk. Solid lines represent distributions using the model developed in Study 2 of this thesis, whereas the dashed lines represent distributions using the Roberts et al., 2010 published model. In both cases, blue represents males and red represents females.

7.5.2.2 Clinical Screening and Biomarkers

Clinically, these findings currently have limited applicability, due to the fact that T_d is both an indirect metric of the state of bone collagen, and is also currently not possible to quantify clinically, at least, not without the use of a cortical bone sample. However, as discussed previously (Study 4), recent developments in imaging techniques may allow for the quantification of relative concentrations of crosslinks in the collagen network. More specifically, the use of clinical biomarkers may provide a method of characterizing, or at the very least estimating, the state of the collagen network in terms of connectivity and quality. Previous work has used skin and urine measures of pentosidine as a method of estimating bone collagen AGE crosslink concentrations (Saito and Marumo, 2015), however, further research into this avenue is necessary, as results linking pentosidine to bone strength are inconsistent (Saito et al., 2011; Saito and Marumo, 2010), and other biomarkers should be investigated. One promising biomarker relates to the measure of

the relative amount of beta isomerization of the C telopeptide of type I bone collagen in urine samples, which specifically relates to the degradation of bone collagen (Byrjalsen et al., 2008). Beyond biomarkers extracted from blood and urine samples, another potential method of estimating the state of the bone collagen network is through Raman spectroscopy. In both a 2016 and 2021 paper, Unal and colleagues demonstrated the use of Raman spectroscopy of bone samples to quantify the relative concentrations of crosslinks in the collagen network (Unal, 2021; Unal et al., 2016). While currently limited to direct spectroscopy of bone, continued research may allow for in-situ measurements or measurements at surrogate sites, like the skin. While further research is necessary to find a viable clinical method of assessing bone collagen, the findings of these studies will lead to further investigation into these areas, as clinically quantifiable metrics of bone collagen may allow for more accurate predictions of femoral bone strength, ultimately improving the ability to predict injury risk.

7.6 Future Research and Next Steps

Beyond future research related to fracture risk estimates and clinical biomarkers mentioned in the previous two sections, there are clear next steps for research related to each of the four studies conducted in this thesis. The first clear aspect of future research applies to all four studies and more specifically relates to the need or benefit that would come from repeating or continuing these studies with a larger sample size. While the sample size achieved in studies 2 and 3 mimic common sample sizes for similar experiments, there is a lack of statistical power for some of the more advanced or in-depth analyses in these studies, and a lack of power for even simple analyses exists in studies 1 and 4. While the results of most of the studies allow for certain hypotheses to be addressed, further research with a larger sample is needed to more clearly identify or characterize relationships (e.g. the relationship between T_d and femoral bone strength). As the sample sizes of each of the studies was negatively affected by the emergence and presence of the COVID-19 global pandemic, there is hope that the availability of research specimens will eventually reach pre-pandemic levels and allow for continued research of this nature.

In terms of more study-specific next steps for research, there are many clear and exciting avenues that have emerged following this thesis work. Firstly, this thesis adds to the existing literature exploring the influence of test methods (and rate of loading) on measures of proximal femur strength. The inconsistencies in findings suggest the need to more comprehensively

characterize potential rate-dependencies, and identify whether loading rate should be standardized between experiments towards having comparable, and ultimately, accurate measures/predictive models of bone strength. Secondly, repeating Study 2 with a larger and more balanced sample, in terms of specimen donor sex, could more precisely assess the relationship between sex and femoral neck bone mineral density, and ultimately femoral bone strength. Thirdly, while limited by monetary and logistical barriers for the thesis, future research into the collagen crosslink content of the sample of specimens collected in Study 3 is already planned, with high performance liquid chromatography (HPLC) and Raman spectroscopy to be used to identify relative concentrations of crosslinks, and carboxy methyl lysine assays planned to assess the concentration of CML ligands. These analyses will allow for further characterization of the collagen network, and provide information related to the relative concentrations of certain enzymatic crosslinks, crosslinking and non-crosslinking AGEs. This line of future research is vital towards understanding the link between the mechanical properties of bone and the state of the collagen network. Related to this point is the need for future work to sufficiently characterize the microscale structure of the cortical bone in order to quantify and account for pre-existing microdamage and micro-cracks. As fracture mechanics are dependant on the interaction of load, toughness, and the size of defects or stress-risers, the most comprehensive characterization efforts would consider all aspects of the fracture mechanics triad. Therefore, future work should include explicit measures to quantify microdamage of cortical bone, which could be achieved through 3D volumetric micro computed tomography. Lastly, due to the limited statistical power resulting from the limited sample size, Study 4 would benefit from repetition or continuation with a larger sample size. Notwithstanding sample size, the findings of study 4 are some of the most intriguing and promising of the thesis, and have generated a host of new hypotheses for follow-up. These findings are some of the first evidence showing a link between human femur whole bone strength and the state of bone collagen, and if nothing else, provide evidence that further research is warranted and could lead to exciting and impactful advancements in this field.

Bibliography

Abdollahi, M., Larijani, B., Rahimi, R., Salari, P., 2005. Role of oxidative stress in osteoporosis. Therapy 2, 787–796. https://doi.org/10.1586/14750708.2.5.787

Ahn, S.H., Lee, S.H., Kim, H., Kim, B.J., Koh, J.M., 2014. Different relationships between body compositions and bone mineral density according to gender and age in Korean populations (KNHANES 2008-2010). J. Clin. Endocrinol. Metab. 99, 3811–3820. https://doi.org/10.1210/jc.2014-1564

Akdeniz, N., Akpolat, V., Kale, A., Erdemoglu, M., Kuyumcuoglu, U., Celik, Y., 2009. Risk factors for postmenopausal osteoporosis: anthropometric measurements, age, age at menopause and the time elapsed after menopause onset. Gynecol. Endocrinol. 25, 125–129. https://doi.org/10.1080/09513590802549817

Akkus, O., Rimnac, C.M., 2001. Fracture resistance of gamma radiation sterilized cortical bone allografts. J. Orthop. Res. 19, 927–934. https://doi.org/10.1016/S0736-0266(01)00004-3

Arakawa, S., Suzuki, R., Kurosaka, D., Ikeda, R., Hayashi, H., Kayama, T., Ohno, R. ichi, Nagai, R., Marumo, K., Saito, M., 2020. Mass spectrometric quantitation of AGEs and enzymatic crosslinks in human cancellous bone. Sci. Rep. 10, 1–12. https://doi.org/10.1038/s41598-020-75923-8

Ardawi, M.S.., Mainmany, A.., Bahksh, T.., Nasrat, H.A.., Milaat, W.., Al-Raddadi, R.., 2005. Bone mineral density of the spine and femur in healthy Saudis. Osteoporos. Int. 16, 43–55. https://doi.org/10.1016/j.bone.2008.12.025

Askarinejad, S., Johnson, J.E., Rahbar, N., Troy, K.L., 2019. Effects of loading rate on the of mechanical behavior of the femur in falling condition. J. Mech. Behav. Biomed. Mater. 96, 269–278. https://doi.org/10.1016/j.jmbbm.2019.04.038

Aspray, T.J., 2015. Fragility fracture : recent developments in risk assessment 17–25. https://doi.org/10.1177/1759720X14564562

ASTM E1820-20a, 2020. Standard Test Method for Measurement of Fracture Toughness. Conshohocken, PA: https://doi.org/10.1520/E1820-20A

Augat, P., Schorlemmer, S., 2006. The role of cortical bone and its microstructure in bone strength. Age Ageing 35, 27–31. https://doi.org/10.1093/ageing/afl081

Bachmann, K.N., Fazeli, P.K., Lawson, E.A., Russell, B.M., Riccio, A.D., Meenaghan, E., Gerweck, A. V., Eddy, K., Holmes, T., Goldstein, M., Weigel, T., Ebrahimi, S., Mickley, D., Gleysteen, S., Bredella, M.A., Klibanski, A., Miller, K.K., 2014. Comparison of hip geometry, strength, and estimated fracture risk in women with anorexia nervosa and overweight/obese women. J. Clin. Endocrinol. Metab. 99, 4664–4673. https://doi.org/10.1210/jc.2014-2104

Bailey, A.J., Lister, D., 1968. Thermally Labile Cross-links in Native Collagen. Nature 220, 280–281. https://doi.org/10.1038/220280a0

Barry, P., Aspray, T., Briers, K., Collins, G., Compston, J., Dockery, F., Ruddick, S., Selby, P., Stephens, D., Thornhill, A., Tobias, J., 2012. Osteoporosis : fragility fracture risk. Natl. Inst. Heal. Clin. Excell. 1–97.

Barth, H.D., Launey, M.E., MacDowell, A.A., Ager, J.W., Ritchie, R.O., 2010. On the effect of X-ray irradiation on the deformation and fracture behavior of human cortical bone. Bone 46, 1475–1485. https://doi.org/10.1016/j.bone.2010.02.025

Barth, H.D., Zimmermann, E.A., Schaible, E., Tang, S.Y., Alliston, T., Ritchie, R.O., 2011. Characterization of the effects of x-ray irradiation on the hierarchical structure and mechanical properties of human cortical bone. Biomaterials 32, 8892–8904. https://doi.org/10.1016/j.biomaterials.2011.08.013

Beck, T.J., Petit, M.A., Wu, G., LeBoff, M.S., Cauley, J.A., Chen, Z., 2009. Does obesity really make the femur stronger? BMD, geometry, and fracture incidence in the women's health initiative-observational study. J. Bone Miner. Res. 24, 1369–1379. https://doi.org/10.1359/jbmr.090307

Bell, K.L., Loveridge, N., Power, J., Garrahan, N., Meggitt, B.F., Reeve, J., 1999. Regional differences in cortical porosity in the fractured femoral neck. Bone 24, 57–64. https://doi.org/10.1016/S8756-3282(98)00143-4

Berg, K.M., Kunins, H. V., Jackson, J.L., Nahvi, S., Chaudhry, A., Harris, K.A., Malik, R.,

Arnsten, J.H., 2008. Association Between Alcohol Consumption and Both Osteoporotic Fracture and Bone Density. Am. J. Med. 121, 406–418. https://doi.org/10.1016/j.amjmed.2007.12.012

Berg, R.A., Prockop, D.J., 1973. The thermal transition of a non-hydroxylated form of collagen. Evidence for a role for hydroxyproline in stabilizing the triple-helix of collagen. Biochem. Biophys. Res. Commun. 52, 115–120. https://doi.org/10.1016/0006-291X(73)90961-3

Bergland, A., Wyller, T.B., 2004. Risk factors for serious fall related injury in elderly women living at home. Inj. Prev. 10, 308–313. https://doi.org/10.1136/ip.2003.004721

Bhan, S., Levine, I., Laing, A.C., 2013. The influence of body mass index and gender on the impact attenuation properties of flooring systems. J. Appl. Biomech. 29, 731–739.

Bhattacharya, B., Maung, A., Schuster, K., Davis, K.A., 2016. The older they are the harder they fall: Injury patterns and outcomes by age after ground level falls. Injury 47, 1955–1959. https://doi.org/10.1016/j.injury.2016.06.019

Billette, J., Janz, T., 2011. Injuries in Canada : Insights from the Canadian Community Health Survey. Stat. Canada Cat. 82, 1–16.

Blaha, J.D., Logue, C.M., 1989. The biomechanics of hip fractures. Tech. Orthop. 4, 7–18. https://doi.org/10.1097/00013611-198907000-00005

Blake, A.J., Morgan, K., Bendall, M.J., 1988. Falls by elderly people at home: prevalence and associated factors. Age Ageing 17, 365–372.

Bolland, M.J., Siu, A.T., Mason, B.H., Horne, A.M., Ames, R.W., Grey, A.B., Gamble, G.D., Reid, I.R., 2011. Evaluation of the FRAX and Garvan fracture risk calculators in older women. J. Bone Miner. Res. 26, 420–427. https://doi.org/10.1002/jbmr.215

Boskey, A.L., Wright, T.M., Blank, R.D., 1999. Collagen and bone strength. J. Bone Miner. Res. 14, 330–335. https://doi.org/10.1359/jbmr.1999.14.3.330

Bouxsein, M.L., 2005. Determinants of skeletal fragility. Best Pract. Res. Clin. Rheumatol. 19, 897–911. https://doi.org/10.1016/j.berh.2005.07.004

Bouxsein, M.L., Coan, B.S., Lee, S.C., 1999. Prediction of the strength of the elderly proximal

femur by bone mineral density and quantitative ultrasound measurements of the heel and tibia. Bone 25, 49–54. https://doi.org/10.1016/S8756-3282(99)00093-9

Bouxsein, M.L., Szulc, P., Munoz, F., Thrall, E., Sornay-Rendu, E., Delmas, P.D., 2007. Contribution of trochanteric soft tissues to fall force estimates, the factor of risk, and prediction of hip fracture risk. J. Bone Miner. Res. 22, 825–831. https://doi.org/10.1359/jbmr.070309

Brennan, M., 1989. Changes in solubility, non-enzymatic glycation, and fluorescence of collagen in tail tendons from diabetic rats. J. Biol. Chem. 264, 20947–20952. https://doi.org/10.1016/s0021-9258(19)30028-6

Buehler, M.J., 2007. Molecular nanomechanics of nascent bone: Fibrillar toughening by mineralization. Nanotechnology 18. https://doi.org/10.1088/0957-4484/18/29/295102

Burge, R., Dawson-hughes, B., Solomon, D.H., Wong, J.B., King, A., Tosteson, A., 2007. Incidence and Economic Burden of Osteoporosis-Related Fractures in the United States, 2005–2025. J. Bone Miner. Res. 22, 465–475. https://doi.org/10.1359/JBMR.061113

Burr, D.B., 2002. The contribution of the organic matrix to bone's material properties. Bone 31, 8–11. https://doi.org/10.1016/S8756-3282(02)00815-3

Burton, B., Gaspar, A., Josey, D., Tupy, J., Grynpas, M.D., Willett, T.L., 2014. Bone embrittlement and collagen modifications due to high-dose gamma-irradiation sterilization. Bone 61, 71–81. https://doi.org/10.1016/j.bone.2014.01.006

Caillet, P., Klemm, S., Ducher, M., Aussem, A., Schott, A.M., 2015. Hip fracture in the elderly: A re-analysis of the EPIDOS study with causal Bayesian networks. PLoS One 10, 1–12. https://doi.org/10.1371/journal.pone.0120125

Campbell, A.J., Borrie, M.J., Spears, G.F., 1989. Risk factors for falls in a community-based prospective study of people 70 years and older. J Gerontol 44, M112-7.

Carter, D.R., Hayes, W.C., 1977. The compressive behavior of bone as a two-phase porous structure. JBJS 59.

Chappard, C., Bousson, V., Bergot, C., Mitton, D., Marchadier, A., Moser, T., Benhamou, C.L.,

Laredo, J.-D., 2010. Prediction of femoral fracture load: cross-sectional study of texture analysis and geometric measurements on plain radiographs versus bone mineral density. Radiology 255, 536–543. https://doi.org/10.1148/radiol.10090232

Cheng, X., Li, J., Lu, Y., Keyak, J., Lang, T., 2007. Proximal femoral density and geometry measurements by quantitative computed tomography: Association with hip fracture. Bone 40, 169–174. https://doi.org/10.1016/j.bone.2006.06.018

Cheng, X.G., Lowet, G., Boonen, S., Nicholson, P.H.F., Brys, P., Nijs, J., Dequeker, J., 1997. Assessment of the strength of proximal femur in vitro: Relationship to femoral bone mineral density and femoral geometry. Bone 20, 213–218. https://doi.org/10.1016/S8756-3282(96)00383-3

Chevalley, T., Bonjour, J.P., Van Rietbergen, B., Rizzoli, R., Ferrari, S., 2012. Fractures in healthy females followed from childhood to early adulthood are associated with later menarcheal age and with impaired bone microstructure at peak bone mass. J. Clin. Endocrinol. Metab. 97, 4174–4181. https://doi.org/10.1210/jc.2012-2561

Choi, W.J., Wakeling, J.M., Robinovitch, S.N., 2015. Kinematic analysis of video-captured falls experienced by older adults in long-term care. J. Biomech. 48, 911–920. https://doi.org/10.1016/j.jbiomech.2015.02.025

Compston, J.E., Bhambhani, M., Laskey, M.A., Murphy, S., Khaw, K.T., 1992. Body composition and bone mass in post-menopausal women. Clin. Endocrinol. (Oxf). 37, 426–431. https://doi.org/10.1111/j.1365-2265.1992.tb02354.x

Courtney, A.C., Wachtel, E.F., Myers, E.R., Hayes, W.C., 1995. Age-related reductions in the strength of the femur tested in a fall-loading configuration. J. Bone Jt. Surg. 77, 387–395. https://doi.org/10.2106/00004623-199503000-00008

Courtney, A.C., Wachtel, E.F., Myers, E.R., Hayes, W.C., 1994. Effects of loading rate on strength of the proximal femur. Calcif. Tissue Int. 55, 53–58. https://doi.org/10.1007/BF00310169

Crabtree, N.J., Kroger, H., Martin, A., Pols, H.A.P., Lorenc, R., Nijs, J., Stepan, J.J., Falch, J.A., Miazgowski, T., Grazio, S., Raptou, P., Adams, J., Collings, A., Khaw, K.T., Rushton, N.,

Lunt, M., Dixon, A.K., Reeve, J., 2002. Improving risk assessment: Hip geometry, bone mineral distribution and bone strength in hip fracture cases and controls. The EPOS study. Osteoporos. Int. 13, 48–54. https://doi.org/10.1007/s198-002-8337-y

CSA Group, 2020. National Standards of Canada: Hip Protectors (CSA Z325:20).

Cummings-Vaughn, L.A., Gammack, J.K., 2011. Falls, Osteoporosis, and Hip Fractures. Med. Clin. North Am. 95, 495–506. https://doi.org/10.1016/j.mcna.2011.03.003

Cummings, S., 2002. Epidemiology and outcomes of osteoporotic fractures. Lancet 359, 1761–1767.

Cummings, S.R., Nevitt, M.C., 1994. Non-skeletal determinants of fractures: the potential importance of the mechanics of falls. Osteoporos. Int. 4, 67–70. https://doi.org/10.1007/BF01623439

Cummins, N.M., Poku, E.K., Towler, M.R., O'Driscoll, O.M., Ralston, S.H., 2011. Clinical risk factors for osteoporosis in Ireland and the UK: A comparison of FRAX and QFractureScores. Calcif. Tissue Int. 89, 172–177. https://doi.org/10.1007/s00223-011-9504-2

Currey, J.D., 2012. The structure and mechanics of bone. J. Mater. Sci. 47, 41–54. https://doi.org/10.1007/s10853-011-5914-9

Currey, J.D., 1988. Strain rate and mineral content in fracture models of bone. J. Orthop. Res. 6, 32–38. https://doi.org/10.1002/jor.1100060105

Dagan, N., Cohen-Stavi, C., Leventer-Roberts, M., Balicer, R.D., 2017. External validation and comparison of three prediction tools for risk of osteoporotic fractures using data from population based electronic health records: Retrospective cohort study. BMJ 356. https://doi.org/10.1136/bmj.i6755

Dall'Ara, Enrico, Luisier, B., Schmidt, R., Kainberger, F., Zysset, P.K., Pahr, D.H., 2013. A nonlinear QCT-based finite element model validation study for the human femur tested in two configurations in vitro. Bone 52, 27–38. https://doi.org/10.1016/j.bone.2012.09.006

Dall'Ara, E., Luisier, B., Schmidt, R., Pretterklieber, M., Kainberger, F., Zysset, P., Pahr, D.,

2013. DXA predictions of human femoral mechanical properties depend on the load configuration. Med. Eng. Phys. 35, 1564–1572. https://doi.org/10.1016/j.medengphy.2013.04.008

Davis, J.C., Robertson, M.C., Ashe, M.C., Liu-Ambrose, T., Khan, K.M., Marra, C.A., 2010. International comparison of cost of falls in older adults living in the community: A systematic review. Osteoporos. Int. 21, 1295–1306. https://doi.org/10.1007/s00198-009-1162-0

Davis, W.A., Hamilton, E.J., Bruce, D.G., Davis, T.M.E., 2019. Development and validation of a simple hip fracture risk prediction tool for type 2 diabetes: The fremantle diabetes study phase I. Diabetes Care 42, 102–109. https://doi.org/10.2337/dc18-1486

de Bakker, P.M., Manske, S.L., Ebacher, V., Oxland, T.R., Cripton, P.A., Guy, P., 2009. During sideways falls proximal femur fractures initiate in the superolateral cortex: Evidence from high-speed video of simulated fractures. J. Biomech. 42, 1917–1925. https://doi.org/10.1016/j.jbiomech.2009.05.001

De Laet, C., Kanis, J.A., Od??n, A., Johanson, H., Johnell, O., Delmas, P., Eisman, J.A., Kroger, H., Fujiwara, S., Garnero, P., McCloskey, E. V., Mellstrom, D., Melton, L.J., Meunier, P.J., Pols, H.A.P., Reeve, J., Silman, A., Tenenhouse, A., 2005. Body mass index as a predictor of fracture risk: A meta-analysis. Osteoporos. Int. 16, 1330–1338. https://doi.org/10.1007/s00198-005-1863-y

De Liefde, I.I., Van Der Klift, M., De Laet, C.E.D.H., Van Daele, P.L.A., Hofman, A., Pols, H.A.P., 2005. Bone mineral density and fracture risk in type-2 diabetes mellitus: The Rotterdam Study. Osteoporos. Int. 16, 1713–1720. https://doi.org/10.1007/s00198-005-1909-1

Dinçel, V.E., Şengelen, M., Sepici, V., Çavuşoğlu, T., Sepici, B., 2008. The association of proximal femur geometry with hip fracture risk. Clin. Anat. 21, 575–580. https://doi.org/10.1002/ca.20680

Dragomir-Daescu, D., Op Den Buijs, J., McEligot, S., Dai, Y., Entwistle, R.C., Salas, C., Melton, L.J., Bennet, K.E., Khosla, S., Amin, S., 2011. Robust QCT/FEA models of

proximal femur stiffness and fracture load during a sideways fall on the hip. Ann. Biomed. Eng. 39, 742–755. https://doi.org/10.1007/s10439-010-0196-y

Dragomir-Daescu, D., Rossman, T.L., Rezaei, A., Carlson, K.D., Kallmes, D.F., Skinner, J.A., Khosla, S., Amin, S., 2018. Factors associated with proximal femur fracture determined in a large cadaveric cohort. Bone 116, 196–202. https://doi.org/10.1016/j.bone.2018.08.005

Dubey, A.K., Balani, K., Basu, B., 2012. 18 - Electrically active biocomposites as smart scaffolds for bone tissue engineering, in: Webster, T.J.B.T.-N. (Ed.), Woodhead Publishing Series in Biomaterials. Woodhead Publishing, pp. 537–570. https://doi.org/https://doi.org/10.1533/9780857096449.4.537

Dufour, A.B., Roberts, B., Broe, K.E., Kiel, D.P., Bouxsein, M.L., Hannan, M.T., 2012. The factor-of-risk biomechanical approach predicts hip fracture in men and women: The Framingham Study. Osteoporos. Int. 23, 513–520. https://doi.org/10.1007/s00198-011-1569-2

E399-20, A., 2020. Standard Test Method for Linear-Elastic Plane-Strain Fracture Toughness of Metallic Materials. West Conshohocken.

Eastell, R., Hannon, R.A., 2008. Biomarkers of bone health and osteoporosis risk. Proc. Nutr. Soc. 67, 157–162. https://doi.org/10.1017/S002966510800699X

Eckstein, F., Lochmüller, E.M., Lill, C.A., Kuhn, V., Schneider, E., Delling, G., Müller, R., 2002. Bone strength at clinically relevant sites displays substantial heterogeneity and is best predicted from site-specific bone densitometry. J. Bone Miner. Res. 17, 162–171. https://doi.org/10.1359/jbmr.2002.17.1.162

Edelstein, S.L., Barrett-connor, E., 1993. Relation between body size and bone mineral density in elderly men and women. Am. J. Epidemiol. 138, 160–169. https://doi.org/10.1093/oxfordjournals.aje.a116842

Elbuken, F., Baykara, M., Ozturk, C., 2012. Standardisation of the neck-shaft angle and measurement of age-, gender- and BMI-related changes in the femoral neck using DXA. Singapore Med. J. 53, 587–590.

Enns-Bray, W.S., Ariza, O., Gilchrist, S., Widmer Soyka, R.P., Vogt, P.J., Palsson, H., Boyd,

S.K., Guy, P., Cripton, P.A., Ferguson, S.J., Helgason, B., 2016. Morphology based anisotropic finite element models of the proximal femur validated with experimental data. Med. Eng. Phys. 38, 1339–1347. https://doi.org/10.1016/j.medengphy.2016.08.010

Enns-Bray, W.S., Bahaloo, H., Fleps, I., Pauchard, Y., Taghizadeh, E., Sigurdsson, S., Aspelund, T., Büchler, P., Harris, T., Gudnason, V., Ferguson, S.J., Pálsson, H., Helgason, B., 2019a. Biofidelic finite element models for accurately classifying hip fracture in a retrospective clinical study of elderly women from the AGES Reykjavik cohort. Bone 120, 25–37. https://doi.org/10.1016/j.bone.2018.09.014

Enns-Bray, W.S., Bahaloo, H., Fleps, I., Pauchard, Y., Taghizadeh, E., Sigurdsson, S., Aspelund, T., Büchler, P., Harris, T., Gudnason, V., Ferguson, S.J., Pálsson, H., Helgason, B., 2019b. Biofidelic finite element models for accurately classifying hip fracture in a retrospective clinical study of elderly women from the AGES Reykjavik cohort. Bone 120, 25–37. https://doi.org/10.1016/j.bone.2018.09.014

Fatayerji, D., Cooper, A.M., Eastell, R., 1999. Total body and regional bone mineral density in men: Effect of age. Osteoporos. Int. 10, 59–65. https://doi.org/10.1007/s001980050195

Faulkner, K.G., Von Stetten, E., Miller, P., 1999. Discordance in patient classification using T-scores. J. Clin. Densitom. 2, 343–350. https://doi.org/10.1385/JCD:2:3:343

Feldman, F., Robinovitch, S.N., 2007. Reducing hip fracture risk during sideways falls: Evidence in young adults of the protective effects of impact to the hands and stepping. J. Biomech. 40, 2612–2618. https://doi.org/10.1016/j.jbiomech.2007.01.019

Fernandes, H., Dechering, K., Van Someren, E., Steeghs, I., Apotheker, M., Leusink, A., Bank, R., Janeczek, K., Van Blitterswijk, C., de Boer, J., 2009. The Role of Collagen Crosslinking in Differentiation of Human Mesenchymal Stem Cells and MC3T3-E1 Cells. Tissue Eng. Part A 15, 3857–3867. https://doi.org/10.1089/ten.tea.2009.0011

Fessel, G., Li, Y., Diederich, V., Guizar-Sicairos, M., Schneider, P., Sell, D.R., Monnier, V.M., Snedeker, J.G., 2014. Advanced glycation end-products reduce collagen molecular sliding to affect collagen fibril damage mechanisms but not stiffness. PLoS One 9. https://doi.org/10.1371/journal.pone.0110948

Fleps, I., Enns-Bray, W.S., Guy, P., Ferguson, S.J., Cripton, P.A., Helgason, B., 2018. On the internal reaction forces, energy absorption, and fracture in the hip during simulated sideways fall impact. PLoS One 13, 1–18. https://doi.org/10.1371/journal.pone.0200952

Fleps, I., Fung, A., Guy, P., Ferguson, S.J., Helgason, B., Cripton, P.A., 2019. Subject-specific ex vivo simulations for hip fracture risk assessment in sideways falls. Bone 125, 36–45. https://doi.org/10.1016/j.bone.2019.05.004

Flory, P.J., Garrett, R.R., 1958. Phase Transitions in Collagen and Gelatin Systems1. J. Am. Chem. Soc. 80, 4836–4845. https://doi.org/10.1021/ja01551a020

Fois, M., Lamure, A., Fauran, M.J., Lacabanne, C., 2001. Study of Human Cortical Bone and Demineralized Human 2527–2533.

Folbert, E.C., Hegeman, J.H., Gierveld, R., van Netten, J.J., Velde, D. van der, Ten Duis, H.J., Slaets, J.P., 2017. Complications during hospitalization and risk factors in elderly patients with hip fracture following integrated orthogeriatric treatment. Arch. Orthop. Trauma Surg. 137, 507–515. https://doi.org/10.1007/s00402-017-2646-6

Földhazy, Z., Arndt, A., Milgrom, C., Finestone, A., Ekenman, I., 2005. Exercise-induced strain and strain rate in the distal radius. J. Bone Jt. Surg. - Ser. B 87, 261–266. https://doi.org/10.1302/0301-620X.87B2.14857

Forsén, L., Meyer, H.E., Midthjell, K., Edna, T.H., 1999. Diabetes mellitus and the incidence of hip fracture: Results from the Nord-Trondelag health survey. Diabetologia 42, 920–925. https://doi.org/10.1007/s001250051248

Fraser, L.A., Langsetmo, L., Berger, C., Ioannidis, G., Goltzman, D., Adachi, J.D., Papaioannou, A., Josse, R., Kovacs, C.S., Olszynski, W.P., Towheed, T., Hanley, D.A., Kaiser, S.M., Prior, J., Jamal, S., Kreiger, N., Brown, J.P., Johansson, H., Oden, A., McCloskey, E., Kanis, J.A., Leslie, W.D., 2011. Fracture prediction and calibration of a Canadian FRAX® tool: A population-based report from CaMos. Osteoporos. Int. 22, 829–837. https://doi.org/10.1007/s00198-010-1465-1

Frost, H., 1960. Presence of microscopic cracks in vivo in bone. Henry Ford Hosp. Med. Bull. 8, 25–35.

Frost, H.M., 1996. Perspectives: A proposed general model of the "Mechanostat" (Suggestions from a new skeletal-biologic paradigm). Anat. Rec. 244, 139–147. https://doi.org/10.1002/(SICI)1097-0185(199602)244:2<139::AID-AR1>3.0.CO;2-X

Gaar, J., Naffa, R., Brimble, M., 2020. Enzymatic and non-enzymatic crosslinks found in collagen and elastin and their chemical synthesis. Org. Chem. Front. 7, 2789–2814. https://doi.org/10.1039/d0qo00624f

Garnero, P., Hausherr, E., Chapuy, M.-C., Marcelli, C., Grandjean, H., Muller, C., Cormier, C., Bréart, G., Meunier, P.J., Delmas, P.D., 1996. Markers of bone resorption predict hip fracture in elderly women: The EPIDOS prospective study. J. Bone Miner. Res. 11, 1531–1538. https://doi.org/10.1002/jbmr.5650111021

Gauthier, R., Follet, H., Langer, M., Meille, S., Chevalier, J., Rongiéras, F., Peyrin, F., Mitton, D., 2017. Strain rate influence on human cortical bone toughness: A comparative study of four paired anatomical sites. J. Mech. Behav. Biomed. Mater. 71, 223–230. https://doi.org/10.1016/j.jmbbm.2017.03.015

Gauthier, R., Langer, M., Follet, H., Olivier, C., Gouttenoire, P.J., Helfen, L., Rongiéras, F., Mitton, D., Peyrin, F., 2019. Influence of loading condition and anatomical location on human cortical bone linear micro-cracks. J. Biomech. 85, 59–66. https://doi.org/10.1016/j.jbiomech.2019.01.008

Gautieri, A., Buehler, M.J., Redaelli, A., 2009. Deformation rate controls elasticity and unfolding pathway of single tropocollagen molecules. J. Mech. Behav. Biomed. Mater. 2, 130–137. https://doi.org/10.1016/j.jmbbm.2008.03.001

Giangregorio, L.M., Leslie, W.D., Lix, L.M., Johansson, H., Oden, A., McCloskey, E., Kanis, J.A., 2012. FRAX underestimates fracture risk in patients with diabetes. J. Bone Miner. Res. 27, 301–308. https://doi.org/10.1002/jbmr.556

Gilchrist, S., Nishiyama, K.K., de Bakker, P., Guy, P., Boyd, S.K., Oxland, T., Cripton, P.A., 2014. Proximal femur elastic behaviour is the same in impact and constant displacement rate fall simulation. J. Biomech. 47, 3744–3749. https://doi.org/10.1016/j.jbiomech.2014.06.040

Gong, J., Tang, M., Guo, B., Shang, J., Tang, Y., Xu, H., 2016. Sex- and age-related differences in femoral neck cross-sectional structural changes in mainland Chinese men and women measured using dual-energy X-ray absorptiometry. Bone 83, 58–64. https://doi.org/10.1016/j.bone.2015.09.017

Granke, M., Makowski, A.J., Uppuganti, S., Does, M.D., Nyman, J.S., 2015. Identifying Novel Clinical Surrogates to Assess Human Bone Fracture Toughness. J. Bone Miner. Res. 30, 1290–1300. https://doi.org/10.1002/jbmr.2452

Greenspan, S.L., Myers, E.R., Kiel, D.P., Parker, R.A., Hayes, W.C., Resnick, N.M., 1998. Fall direction, bone mineral density, and function: Risk factors for hip fracture in frail nursing home elderly. Am. J. Med. 104, 539–545. https://doi.org/10.1016/S0002-9343(98)00115-6

Greenspan, S L, Myers, E.R., Maitland, L. a, Resnick, N.M., Hayes, W.C., 1994. Fall severity and bone mineral density as risk factors for hip fracture in ambulatory elderly. JAMA 271, 128–133. https://doi.org/10.1001/jama.271.2.128

Greenspan, Susan L., Myers, E.R., Maitland, L.A., Kido, T.H., Krasnow, M.B., Hayes, W.C., 1994. Trochanteric bone mineral density is associated with type of hip fracture in the elderly. J. Bone Miner. Res. 9, 1889–1894. https://doi.org/10.1002/jbmr.5650091208

Gregory, J.S., Testi, D., Stewart, A., Undrill, P.E., Reid, D.M., Aspden, R.M., 2004. A method for assessment of the shape of the proximal femur and its relationship to osteoporotic hip fracture. Osteoporos. Int. 15, 5–11. https://doi.org/10.1007/s00198-003-1451-y

Grisso, J.A., Kelsey, J.L., Strom, B.L., Ghiu, G.Y., Maislin, G., O'Brien, L.A., Hoffman, S., Kaplan, F., 1991. Risk Factors for Falls as a Cause of Hip Fracture in Women. N. Engl. J. Med. 324, 1326–1331. https://doi.org/10.1056/NEJM199105093241905

Gryfe, C.I., Amies, A., Ashley, M.J., 1977. A longitudinal study of falls in an elderly population: I. Incidence and morbidity. Age Ageing 6, 201–210. https://doi.org/10.1093/ageing/6.4.201

Guo, X.E., Liang, L.C., Goldstein, S.A., 1998. Micromechanics of Osteonal Cortical Bone Fracture. J. Biomech. Eng. 120, 112–117. https://doi.org/10.1115/1.2834290

Hamada, Y., Fujii, H., Fukagawa, M., 2009. Role of oxidative stress in diabetic bone disorder. Bone 45, S35–S38. https://doi.org/10.1016/j.bone.2009.02.004

Hansen, S., Jensen, J.E.B., Ahrberg, F., Hauge, E.M., Brixen, K., 2011. The combination of structural parameters and areal bone mineral density improves relation to proximal femur strength: An in vitro study with high-resolution peripheral quantitative computed tomography. Calcif. Tissue Int. 89, 335–346. https://doi.org/10.1007/s00223-011-9523-z

Hayes, W.C., Myers, E.R., Morris, J.N., Gerhart, T.N., Yett, H.S., Lipsitz, L. a, 1993. Impact near the hip dominates fracture risk in elderly nursing home residents who fall. Calcif. Tissue Int. 52, 192–198. https://doi.org/10.1007/BF00298717

Hayes, W.C., Piazza, S.J., Zysset, P.K., 1991. Biomechanics of fracture risk prediction of the hip and spine by quantitative computed tomography. Radiol. Clin. North Am. 29, 1–18.

Hazenberg, J.G., Taylor, D., Lee, T.C., 2007. The role of osteocytes and bone microstructure in preventing osteoporotic fractures. Osteoporos. Int. 18, 1–8. https://doi.org/10.1007/s00198-006-0222-y

Heinrich, S., Rapp, K., Rissmann, U., Becker, C., König, H.H., 2010. Cost of falls in old age: A systematic review. Osteoporos. Int. 21, 891–902. https://doi.org/10.1007/s00198-009-1100-1

Hendrickx, G., Boudin, E., Van Hul, W., 2015. A look behind the scenes: the risk and pathogenesis of primary osteoporosis. Nat. Rev. Rheumatol. 11, 462–474. https://doi.org/10.1038/nrrheum.2015.48

Holt, G., Smith, R., Duncan, K., Hutchison, J.D., Reid, D., 2009. Changes in population demographics and the future incidence of hip fracture. Injury 40, 722–726. https://doi.org/10.1016/j.injury.2008.11.004

Hwang, H.F., Lee, H.D., Huang, H.H., Chen, C.Y., Lin, M.R., 2011. Fall mechanisms, bone strength, and hip fractures in elderly men and women in Taiwan. Osteoporos. Int. 22, 2385–2393. https://doi.org/10.1007/s00198-010-1446-4

Ioannidis, G, Papaioannon, A., Hopman, W, M., AkhtarDanesh, N., Anastassiades, T., Pickard, L., 2009. Relation between fractures and mortality: Results from the Canadian Multicentre Osteoporosis Study. CMAJ 181, 265–271.

Ioannidis, George, Papaioannou, A., Hopman, W.M., Akhtar-Danesh, N., Anastassiades, T.,

Pickard, L., Kennedy, C.C., Prior, J.C., Olszynski, W.P., Davison, K.S., Goltzman, D., Thabane, L., Gafni, A., Papadimitropoulos, E.A., Brown, J.P., Josse, R.G., Hanley, D.A., Adachi, J.D., 2009. Relation between fractures and mortality: Results from the Canadian Multicentre Osteoporosis Study. Cmaj 181, 265–271. https://doi.org/10.1503/cmaj.081720

Janghorbani, M., Van Dam, R.M., Willett, W.C., Hu, F.B., 2007. Systematic review of type 1 and type 2 diabetes mellitus and risk of fracture. Am. J. Epidemiol. 166, 495–505. https://doi.org/10.1093/aje/kwm106

Järvinen, T.L.N., Michaëlsson, K., Aspenberg, P., Sievänen, H., 2015. Osteoporosis: The emperor has no clothes. J. Intern. Med. 277, 662–673. https://doi.org/10.1111/joim.12366

Jazinizadeh, F., Mohammadi, H., Quenneville, C.E., 2020. Comparing the fracture limits of the proximal femur under impact and quasi-static conditions in simulation of a sideways fall. J. Mech. Behav. Biomed. Mater. 103, 103593. https://doi.org/10.1016/j.jmbbm.2019.103593

Jean, S., O'Donnell, S., Lagacé, C., Walsh, P., Bancej, C., Brown, J.P., Morin, S., Papaioannou, A., Jaglal, S.B., Leslie, W.D., 2013. Trends in hip fracture rates in Canada: An age-period-cohort analysis. J. Bone Miner. Res. 28, 1283–1289. https://doi.org/10.1002/jbmr.1863

Jiang, H.X., Majumdar, S.R., Dick, D.A., Moreau, M., Raso, J., Otto, D.D., Johnston, D.W.C., 2005. Development and Initial Validation of a Risk Score for Predicting In-Hospital and 1-Year Mortality in Patients With Hip Fractures. J. Bone Miner. Res. 20, 494–500. https://doi.org/10.1359/JBMR.041133

Johannesdottir, F., Thrall, E., Muller, J., Keaveny, T.M., Kopperdahl, D.L., Bouxsein, M.L., 2017. Comparison of non-invasive assessments of strength of the proximal femur. Bone 105, 93–102. https://doi.org/10.1016/j.bone.2017.07.023

Johansen, A., 2012. QFracture is better than FRAX tool in assessing risk of hip fracture. BMJ 345, 4988. https://doi.org/10.1136/bmj.e4988

Johnell, O., Kanis, J.A., 2004. An estimate of the worldwide prevalence, mortality and disability associated with hip fracture. Osteoporos. Int. 15, 897–902. https://doi.org/10.1007/s00198-004-1627-0

Johnell, O., Kanis, J.A., Oden, A., Johansson, H., De Laet, C., Delmas, P., Eisman, J.A.,

Fujiwara, S., Kroger, H., Mellstrom, D., Meunier, P.J., Melton, L.J., O'Neill, T., Pols, H., Reeve, J., Silman, A., Tenenhouse, A., 2005. Predictive value of BMD for hip and other fractures. J. Bone Miner. Res. 20, 1185–1194. https://doi.org/10.1359/JBMR.050304

Jones, H., Priest, J., Hayes, W., Tichenor, C., Nagel, D., 1977. Humeral hypertrophy in response to exercise. J. Bone Jt. Surg. 204–208. https://doi.org/10.1007/978-1-4471-5451-8_104

Kanis, J.A., Harvey, N.C., Johansson, H., Odén, A., Eugene, V., Leslie, W.D., 2018. Europe PMC Funders Group Overview of fracture prediction tools 20, 444–450. https://doi.org/10.1016/j.jocd.2017.06.013.Overview

Kanis, J.A., Johnell, O., Oden, A., Johansson, H., McCloskey, E., 2008a. FRAX and the assessment of fracture probability in men and women from the UK. Osteoporos. Int. 19, 385–397. https://doi.org/10.1007/s00198-007-0543-5

Kanis, J.A., McCloskey, E., Johansson, H., Oden, A., Leslie, W.D., 2012. FRAX® with and without bone mineral density. Calcif. Tissue Int. 90, 1–13. https://doi.org/10.1007/s00223-011-9544-7

Kanis, J.A., McCloskey, E. V., Johansson, H., Strom, O., Borgstrom, F., Oden, A., Compston, J.E., Cooper, A.L., Cooper, C., Francis, R., Marsh, D., Reid, D., Selby, P., Wilkins, M., 2008b. Case finding for the management of osteoporosis with FRAX® - Assessment and intervention thresholds for the UK. Osteoporos. Int. 19, 1395–1408. https://doi.org/10.1007/s00198-008-0712-1

Kannus, P., Leiponen, P., Parkkari, J., Palvanen, M., Järvinen, M., 2006. A sideways fall and hip fracture. Bone 39, 383–384. https://doi.org/10.1016/j.bone.2006.01.148

Kaptoge, S., Dalzell, N., Loveridge, N., Beck, T.J., Khaw, K.T., Reeve, J., 2003. Effects of gender, anthropometric variables, and aging on the evolution of hip strength in men and women aged over 65. Bone 32, 561–570. https://doi.org/10.1016/S8756-3282(03)00055-3

Kazama, J.J., Iwasaki, Y., Fukagawa, M., 2013. Uremic osteoporosis. Kidney Int. Suppl. 3, 446–450. https://doi.org/10.1038/kisup.2013.93

Keaveny, T.M., Hayes, W.C., 1993. Mechanical Properties of Cortical and Trabecular Bone. Bone growth 285–344.

Kida, Y., Saito, M., Shinohara, A., Soshi, S., Marumo, K., 2019. Non-invasive skin autofluorescence, blood and urine assays of the advanced glycation end product (AGE) pentosidine as an indirect indicator of AGE content in human bone. BMC Musculoskelet. Disord. 20, 1–8. https://doi.org/10.1186/s12891-019-3011-4

King, A.I., 2000. Fundamentals of Impact Biomechancis: Part I - Biomechanics of the Head, Neck, and Thorax. Annu. Rev. Biomed. Eng. https://doi.org/10.1016/B978-1-4557-5134-1.00001-9

Knott, L., Whitehead, C.C., Fleming, R.H., Bailey, A.J., 1995. Biochemical changes in the collagenous matrix of osteoporotic avian bone. Biochem. J. 310, 1045–1051. https://doi.org/10.1042/bj3101045

Koester, K.J., Barth, H.D., Ritchie, R.O., 2011. Effect of aging on the transverse toughness of human cortical bone: Evaluation by R-curves. J. Mech. Behav. Biomed. Mater. 4, 1504–1513. https://doi.org/https://doi.org/10.1016/j.jmbbm.2011.05.020

Kolta, S., Paratte, S., Amphoux, T., Persohn, S., Campana, S., Skalli, W., Paternotte, S., Argenson, J.N., Bouler, J.M., Gagey, O., Roux, C., 2012. Bone texture analysis of human femurs using a new device (BMA^{TM}) improves failure load prediction. Osteoporos. Int. 23, 1311–1316. https://doi.org/10.1007/s00198-011-1674-2

Korall, A.M.B., Feldman, F., Scott, V.J., Wasdell, M., Gillan, R., Ross, D., Thompson-Franson, T., Leung, P.M., Lin, L., 2015. Facilitators of and barriers to hip protector acceptance and adherence in long-term care facilities: A systematic review. J. Am. Med. Dir. Assoc. 16, 185–193. https://doi.org/10.1016/j.jamda.2014.12.004

Korhonen, N., Niemi, S., Parkkari, J., Sievänen, H., Palvanen, M., Kannus, P., 2013. Continuous decline in incidence of hip fracture: Nationwide statistics from Finland between 1970 and 2010. Osteoporos. Int. 24, 1599–1603. https://doi.org/10.1007/s00198-012-2190-8

Kröger, H., Tuppurainen, M., Honkanen, R., Alhava, E., Saarikoski, S., 1994. Bone mineral density and risk factors for osteoporosis-A population-based study of 1600 perimenopausal women. Calcif. Tissue Int. 55, 1–7. https://doi.org/10.1007/BF00310160

Kuo, T.R., Chen, C.H., 2017. Bone biomarker for the clinical assessment of osteoporosis: Recent

developments and future perspectives. Biomark. Res. 5, 5–13. https://doi.org/10.1186/S40364-017-0097-4

Lachance, C.C., Jurkowski, M.P., Dymarz, A.C., Robinovitch, S.N., Feldman, F., Laing, A.C., Mackey, D.C., 2017. Compliant flooring to prevent fall-related injuries in older adults: A scoping review of biomechanical efficacy, clinical effectiveness, cost-effectiveness, and workplace safety. PLoS One 12, 1–23. https://doi.org/10.1371/journal.pone.0171652

LaCroix, A.Z., Beck, T.J., Cauley, J.A., Lewis, C.E., Bassford, T., Jackson, R., Wu, G., Chen, Z., 2010. Hip structural geometry and incidence of hip fracture in postmenopausal women: What does it add to conventional bone mineral density? Osteoporos. Int. 21, 919–929. https://doi.org/10.1007/s00198-009-1056-1

Laing, A.C., Feldman, F., Jalili, M., Tsai, C.M. (Jimmy), Robinovitch, S.N., 2011. The effects of pad geometry and material properties on the biomechanical effectiveness of 26 commercially available hip protectors. J. Biomech. 44, 2627–2635. https://doi.org/10.1016/j.jbiomech.2011.08.016

Laing, A.C., Robinovitch, S.N., 2010. Characterizing the effective stiffness of the pelvis during sideways falls on the hip. J. Biomech. 43, 1898–1904.

Laing, A.C., Robinovitch, S.N., 2008. The force attenuation provided by hip protectors depends on impact velocity, pelvic size, and soft tissue stiffness. J. Biomech. Eng. 130, 1–9. https://doi.org/10.1115/1.2979867

Laing, A.C., Tootoonchi, I., Hulme, P.A., Robinovitch, S.N., 2006. Effect of compliant flooring on impact force during falls on the hip. J. Orthop. Res. 24, 1405–1411. https://doi.org/10.1002/jor.20172

Launey, M.E., Buehler, M.J., Ritchie, R.O., 2010a. On the mechanistic origins of toughness in bone. Annu. Rev. Mater. Res. 40, 25–53. https://doi.org/10.1146/annurev-matsci-070909-104427

Launey, M.E., Buehler, M.J., Ritchie, R.O., 2010b. On the mechanistic origins of toughness in bone. Annu. Rev. Mater. Res. 40, 25–53. https://doi.org/10.1146/annurev-matsci-070909-104427

Le Corroller, T., Halgrin, J., Pithioux, M., Guenoun, D., Chabrand, P., Champsaur, P., 2012. Combination of texture analysis and bone mineral density improves the prediction of fracture load in human femurs. Osteoporos. Int. 23, 163–169. https://doi.org/10.1007/s00198-011-1703-1

Leslie, W.D., 2009. Trends in Hip Fracture Rates in Canada. JAMA 302, 883. https://doi.org/10.1001/jama.2009.1231

Leslie, W. D., Giangregorio, L.M., Yogendran, M., Azimaee, M., Morin, S., Metge, C., Caetano, P., Lix, L.M., 2012. A population-based analysis of the post-fracture care gap 1996-2008: The situation is not improving. Osteoporos. Int. 23, 1623–1629. https://doi.org/10.1007/s00198-011-1630-1

Leslie, William D., Rubin, M.R., Schwartz, A. V., Kanis, J.A., 2012. Type 2 diabetes and bone. J. Bone Miner. Res. 27, 2231–2237. https://doi.org/10.1002/jbmr.1759

Levine, I.C., Bhan, S., Laing, A.C., 2013. The effects of body mass index and sex on impact force and effective pelvic stiffness during simulated lateral falls. Clin. Biomech. 28, 1026–1033.

Levine, I.C., Pretty, S.P., Nouri, P.K., Mourtzakis, M., Laing, A.C., 2018. Pelvis and femur geometry: Relationships with impact characteristics during sideways falls on the hip. J. Biomech. 80, 72–78. https://doi.org/10.1016/j.jbiomech.2018.08.029

Li, C., Chen, L., Feng, J., Wu, D., Wang, Z., Liu, J., Xu, W., 2019. Prediction of length of stay on the intensive care unit based on least absolute shrinkage and selection operator. IEEE Access 7, 110710–110721. https://doi.org/10.1109/ACCESS.2019.2934166

Lochmüller, E.-M., Müller, R., Kuhn, V., Lill, C.A., Eckstein, F., 2003. Can Novel Clinical Densitometric Techniques Replace or Improve DXA in Predicting Bone Strength in Osteoporosis at the Hip and Other Skeletal Sites? J. Bone Miner. Res. 18, 906–912. https://doi.org/10.1359/jbmr.2003.18.5.906

Lodish, H., Berk, A., Zipursky, S., 2000. Collagen: The fibrous Proteins of the Matrix, in: Molecular Cell Biology. W.H. Freeman, New York, p. Section 22.3.

Lorenzo, A.C., Caffarena, E.R., 2005. Elastic properties, Young's modulus determination and

structural stability of the tropocollagen molecule: A computational study by steered molecular dynamics. J. Biomech. 38, 1527–1533. https://doi.org/10.1016/j.jbiomech.2004.07.011

Lotz, J.C., Cheal, E.J., Hayes, W.C., 1995. Stress distributions within the proximal femur during gait and falls: Implications for osteoporotic fracture. Osteoporos. Int. 5, 252–261. https://doi.org/10.1007/BF01774015

Lotz, J.C., Hayes, W.C., 1990. The use of quantitative computed tomography to estimate risk of fracture of the hip from falls. J. Bone Joint Surg. Am. 72, 689–700.

Loughlin, J.L.O., Robitaille, Y., Boivin, J., Suissa, S., 1993. Incidence of and Risk Factors for Falls and Injurious Falls among the Community-dwelling Elderly. Am. J. Epidemiol. 137, 342–354.

Luo, Y., 2020. Age-related periosteal expansion at femoral neck among elderly women may maintain bending stiffness, but not femoral strength. Osteoporos. Int. 31, 371–377. https://doi.org/10.1007/s00198-019-05165-6

Luo, Y., 2017. Image-based multilevel biomechanical modeling for fall-induced hip fracture, Image-Based Multilevel Biomechanical Modeling for Fall-Induced Hip Fracture. https://doi.org/10.1007/978-3-319-51671-4

Luo, Y., Wu, X., 2020. Bone Quality is Dependent on the Quantity and Quality of Organic–Inorganic Phases. J. Med. Biol. Eng. 40, 273–281. https://doi.org/10.1007/s40846-020-00506-x

Ma, Z., Qiang, Z., Zhao, H., Piao, H., Ren, L., 2020. Mechanical properties of cortical bones related to temperature and orientation of Haversian canals. Mater. Res. Express 7. https://doi.org/10.1088/2053-1591/ab6899

Maeda, Y., Sugano, N., Saito, M., Yonenobu, K., 2011. Comparison of femoral morphology and bone mineral density between femoral neck fractures and trochanteric fractures. Clin. Orthop. Relat. Res. 469, 884–889. https://doi.org/10.1007/s11999-010-1529-8

Magaziner, J., Simonsick, E.M., Kashner, T.M., Hebel, J.R., Kenzora, J.E., 1989. Survival experience of aged hip fracture patients. Am. J. Public Health 79, 274–278.

https://doi.org/10.2105/AJPH.79.3.274

Majumder, S., Roychowdhury, A., Pal, S., 2013. Hip fracture and anthropometric variations: Dominance among trochanteric soft tissue thickness, body height and body weight during sideways fall. Clin. Biomech. 28, 1034–1040. https://doi.org/10.1016/j.clinbiomech.2013.09.008

Majumder, S., Roychowdhury, A., Pal, S., 2007. Simulation of hip fracture in sideways fall using a 3D finite element model of pelvis-femur-soft tissue complex with simplified representation of whole body. Med. Eng. Phys. 29, 1167–1178.

Manske, S.L., Liu-Ambrose, T., Cooper, D.M.L., Kontulainen, S., Guy, P., Forster, B.B., McKay, H.A., 2009. Cortical and trabecular bone in the femoral neck both contribute to proximal femur failure load prediction. Osteoporos. Int. 20, 445–453. https://doi.org/10.1007/s00198-008-0675-2

Martel, D.R., Levine, I.C., Pretty, S.P., Laing, A.C., 2018. The influence of muscle activation on impact dynamics during lateral falls on the hip. J. Biomech. 66, 111–118. https://doi.org/10.1016/j.jbiomech.2017.11.002

Martel, D.R., Lysy, M., Laing, A.C., 2020. Predicting population level hip fracture risk: a novel hierarchical model incorporating probabilistic approaches and factor of risk principles. Comput. Methods Biomech. Biomed. Engin. 23, 1201–1214. https://doi.org/10.1080/10255842.2020.1793331

Massé, P.G., Rimnac, C.M., Yamauchi, M., Coburn, S.P., Rucker, R.B., Howell, D.S., Boskey, A.L., 1996. Pyridoxine deficiency affects biomechanical properties of chick tibial bone. Bone 18, 567–574. https://doi.org/https://doi.org/10.1016/8756-3282(96)00072-5

McCarthy, A.D., Etcheverry, S.B., Bruzzone, L., Lettieri, G., Barrio, D.A., Cortizo, A.M., 2001. Non-enzymatic glycosylation of a type 1 collagen matrix: Effects on osteoblastic development and oxidative stress. BMC Cell Biol. 2. https://doi.org/10.1186/1471-2121-2-16

McElhaney, J.H., 1966. Dynamic response of bone and muscle tissue. J. Appl. Physiol. 21, 1231–1236. https://doi.org/10.1152/jappl.1966.21.4.1231

McNerny, E.M.B., Nickolas, T.L., 2017. Bone Quality in Chronic Kidney Disease: Definitions and Diagnostics. Curr. Osteoporos. Rep. 15, 207–213. https://doi.org/10.1007/s11914-017-0366-z

Miles, C.A., Avery, N.C., 2011. Thermal stabilization of collagen in skin and decalcified bone. Phys. Biol. 8. https://doi.org/10.1088/1478-3975/8/2/026002

Miles, C.A., Bailey, A.J., 2001. Thermally labile domains in the collagen molecule. Micron 32, 325–332. https://doi.org/10.1016/S0968-4328(00)00034-2

Miller, P.D., 2014. Bone disease in CKD: A focus on osteoporosis diagnosis and management. Am. J. Kidney Dis. 64, 290–304. https://doi.org/10.1053/j.ajkd.2013.12.018

Modaresi, A., Nafar, M., Sahraei, Z., 2015. Oxidative stress in chronic kidney disease. Iran. J. Kidney Dis. 9, 165–79. https://doi.org/10.1186/s41100-018-0195-2

Monnier, V.M., Glomb, M., Elgawish, A., Sell, D.R., 1996. The mechanism of collagen cross-linking in diabetes: A puzzle nearing resolution. Diabetes 45. https://doi.org/10.2337/diab.45.3.s67

Moore, M.A., Chen, W.-M., Phillips, R.E., Bohachevsky, I.K., McIlroy, B.K., 1996. Shrinkage temperature versus protein extraction as a measure of stabilization of photooxidized tissue. J. Biomed. Mater. Res. 32, 209–214. https://doi.org/10.1002/(SICI)1097-4636(199610)32:2<209::AID-JBM9>3.0.CO;2-X

Mourtada, F.A., Beck, T.J., Hauser, D.L., Ruff, C.B., Bao, G., 1996. Curved beam model of the proximal femur for estimating stress using dual- energy x-ray absorptiometry derived structural geometry. J. Orthop. Res. 14, 483–492. https://doi.org/10.1002/jor.1100140319

Museyko, O., Bousson, V., Adams, J., Laredo, J.D., Engelke, K., 2016. QCT of the proximal femur—which parameters should be measured to discriminate hip fracture? Osteoporos. Int. 27, 1137–1147. https://doi.org/10.1007/s00198-015-3324-6

Nalla, R.K., Kinney, J.H., Ritchie, R.O., 2003. Mechanistic fracture criteria for the failure of human cortical bone. Nat. Mater. 2, 164–168. https://doi.org/10.1038/nmat832

Nankaku, M., Kanzaki, H., Tsuboyama, T., Nakamura, T., 2005. Evaluation of hip fracture risk

in relation to fall direction. Osteoporos. Int. 16, 1315–1320. https://doi.org/10.1007/s00198-005-1843-2

Nikitovic, M., Wodchis, W.P., Krahn, M.D., Cadarette, S.M., 2013. Direct health-care costs attributed to hip fractures among seniors: A matched cohort study. Osteoporos. Int. 24, 659–669. https://doi.org/10.1007/s00198-012-2034-6

Nose, K., 2000. Role of reactive oxygen species in the regulation of physiological functions. Biol. Pharm. Bull. 23, 897–903. https://doi.org/10.1248/bpb.23.897

Nyman, J.S., Roy, A., Tyler, J.H., Acuna, R.L., Gayle, H.J., Wang, X., 2007. Age-Related Factors Affecting the Postyield Energy Dissipation of Human Cortical Bone 646–655. https://doi.org/10.1002/jor

Oxlund, H., Barckman, M., Ørtoft, G., Andreassen, T.T., 1995. Reduced concentrations of collagen cross-links are associated with reduced strength of bone. Bone 17, 365–371. https://doi.org/10.1016/8756-3282(95)00328-B

Oxlund, H., Sekilde, L., Ørtoft, G., 1996. Reduced concentration of collagen reducible cross links in human trabecular bone with respect to age and osteoporosis. Bone 19, 479–484. https://doi.org/https://doi.org/10.1016/S8756-3282(96)00283-9

Parker, M.J., Gurusamy, K., 2005. Modern methods of treating hip fractures. Disabil. Rehabil. 27, 1045–1051. https://doi.org/10.1080/09638280500056626

Partanen, J., Jämsä, T., Jalovaara, P., 2001. Influence of the upper femur and pelvic geometry on the risk and type of hip fractures. J. Bone Miner. Res. 16, 1540–1546. https://doi.org/10.1359/jbmr.2001.16.8.1540

Pinilla, T.P., Boardman, K.C., Bouxsein, M.L., Myers, E.R., Hayes, W.C., 1996. Impact direction from a fall influences the failure load of the proximal femur as much as age-related bone loss. Calcif. Tissue Int. 58, 231–235. https://doi.org/10.1007/BF02508641

Poundarik, A.A., Wu, P.C., Evis, Z., Sroga, G.E., Ural, A., Rubin, M., Vashishth, D., 2015. A direct role of collagen glycation in bone fracture. J. Mech. Behav. Biomed. Mater. 50, 82–92. https://doi.org/10.1016/j.jmbbm.2015.08.012

Pretty, S.P., 2018. Participant-Specific Modelling of the Proximal Femur during Lateral Falls : A Mechanistic Evaluation of Risk Factors.

Pretty, S.P., Martel, D.R., Laing, A.C., 2017. The Influence of Body Mass Index, Sex, & Muscle Activation on Pressure Distribution During Lateral Falls on the Hip. Ann. Biomed. Eng. 45, 2775–2783. https://doi.org/10.1007/s10439-017-1928-z

Pruitt, L.A., Chakravartula, A.M., 2011. Mechanics of Biomaterials - Fundamental Principles for Implant Design. Cambrudge University Press.

Ravarotto, V., Simioni, F., Pagnin, E., Davis, P.A., Calò, L.A., 2018. Oxidative stress – chronic kidney disease – cardiovascular disease: A vicious circle. Life Sci. 210, 125–131. https://doi.org/10.1016/j.lfs.2018.08.067

Rice, J.R., 1968. A Path Independent Integral and the Approximate Analysis of Strain Concentration by Notches and Cracks. J. Appl. Mech. 35, 379–386. https://doi.org/10.1115/1.3601206

Ritchie, R.O., Knott, J.F., Rice, J.R., 1973. On the relationship between critical tensile stress and fracture toughness in mild steel. J. Mech. Phys. Solids 21, 395–410. https://doi.org/https://doi.org/10.1016/0022-5096(73)90008-2

Rivadeneira, F., Zillikens, M.C., De Laet, C.E.D.H., Hofman, A., Uitterlinden, A.G., Beck, T.J., Pols, H.A.P., 2007. Femoral neck BMD is a strong predictor of hip fracture susceptibility in elderly men and women because it detects cortical bone instability: The Rotterdam Study. J. Bone Miner. Res. 22, 1781–1790. https://doi.org/10.1359/jbmr.070712

Roberts, B.J., Thrall, E., Muller, J.A., Bouxsein, M.L., 2010. Comparison of hip fracture risk prediction by femoral aBMD to experimentally measured factor of risk. Bone 46, 742–746. https://doi.org/10.1016/j.bone.2009.10.020

Robinovitch, S.N., Feldman, F., Yang, Y., Schonnop, R., Leung, P.M., Sarraf, T., Sims-Gould, J., Loughi, M., 2013. Video capture of the circumstances of falls in elderly people residing in long-term care: An observational study. Lancet 381, 47–54. https://doi.org/10.1016/S0140-6736(12)61263-X

Robinovitch, S.N., Hayes, W.C., McMahon, T. a, 1997. Predicting the impact response of a

nonlinear single-degree-of-freedom shock-absorbing system from the measured step response. J. Biomech. Eng. 119, 221–227. https://doi.org/10.1115/1.2796083

Robinovitch, S.N., Hayes, W.C., McMahon, T. a, 1991. Prediction of femoral impact forces in falls on the hip. J. Biomech. Eng. 113, 366–374. https://doi.org/10.1115/1.2895414

Robinovitch, S.N., McMahon, T.A., Hayes, W.C., 1995. Force attenuation in trochanteric soft tissues during impact from a fall. J. Orthop. Res. 13, 956–962.

Rubenstein, L.Z., 2006. Falls in older people: Epidemiology, risk factors and strategies for prevention. Age Ageing 35, 37–41. https://doi.org/10.1093/ageing/afl084

Saito, M., Fujii, K., Mori, Y., Marumo, K., 2006. Role of collagen enzymatic and glycation induced cross-links as a determinant of bone quality in spontaneously diabetic WBN/Kob rats. Osteoporos. Int. 17, 1514–1523. https://doi.org/10.1007/s00198-006-0155-5

Saito, M., Marumo, K., 2015. Effects of Collagen Crosslinking on Bone Material Properties in Health and Disease. Calcif. Tissue Int. 97, 242–261. https://doi.org/10.1007/s00223-015-9985-5

Saito, M., Marumo, K., 2010. Collagen cross-links as a determinant of bone quality: A possible explanation for bone fragility in aging, osteoporosis, and diabetes mellitus. Osteoporos. Int. 21, 195–214. https://doi.org/10.1007/s00198-009-1066-z

Saito, M., Marumo, K., Kida, Y., Ushiku, C., Kato, S., Takao-Kawabata, R., Kuroda, T., 2011. Changes in the contents of enzymatic immature, mature, and non-enzymatic senescent cross-links of collagen after once-weekly treatment with human parathyroid hormone (1-34) for 18 months contribute to improvement of bone strength in ovariectomized monkeys. Osteoporos. Int. 22, 2373–2383. https://doi.org/10.1007/s00198-010-1454-4

Santos, L., Elliott-Sale, K.J., Sale, C., 2017. Exercise and bone health across the lifespan. Biogerontology 18, 931–946. https://doi.org/10.1007/s10522-017-9732-6

Sarvi, M.N., Luo, Y., 2019. Improving the prediction of sideways fall-induced impact force for women by developing a female-specific equation. J. Biomech. 88, 64–71. https://doi.org/10.1016/j.jbiomech.2019.03.019

Schaffler, M.B., Choi, K., Milgrom, C., 1995. Aging and matrix microdamage accumulation in human compact bone. Bone 17, 521–525. https://doi.org/10.1016/8756-3282(95)00370-3

Schuit, S.C.E., Van Der Klift, M., Weel, A.E.A.M., De Laet, C.E.D.H., Burger, H., Seeman, E., Hofman, A., Uitterlinden, A.G., Van Leeuwen, J.P.T.M., Pols, H.A.P., 2004. Fracture incidence and association with bone mineral density in elderly men and women: The Rotterdam Study. Bone 34, 195–202. https://doi.org/10.1016/j.bone.2003.10.001

Shoulders, M.D., Raines, R.T., 2009. Collagen Structure and Stability. Annu. Rev. Biochem. 78, 929–958. https://doi.org/10.1146/annurev.biochem.77.032207.120833

Silva, M.J., Brodt, M.D., Lynch, M.A., McKenzie, J.A., Tanouye, K.M., Nyman, J.S., Wang, X., 2009. Type 1 diabetes in young rats leads to progressive trabecular bone loss, cessation of cortical bone growth, and diminished whole bone strength and fatigue life. J. Bone Miner. Res. 24, 1618–1627. https://doi.org/10.1359/jbmr.090316

Siris, E.S., Chen, Y.T., Abbott, T.A., Barrett-Connor, E., Miller, P.D., Wehren, L.E., Berger, M.L., 2004. Bone mineral density thresholds for pharmacological intervention to prevent fractures. Arch. Intern. Med. 164, 1108–1112. https://doi.org/10.1001/archinte.164.10.1108

Spaniolas, K., Cheng, J.D., Gestring, M.L., Sangosanya, A., Stassen, N.A., Bankey, P.E., 2010. Ground level falls are associated with significant mortality in elderly patients. J. Trauma - Inj. Infect. Crit. Care 69, 821–824. https://doi.org/10.1097/TA.0b013e3181efc6c6

Stevens, J.A., Mack, K.A., Paulozzi, L.J., Ballesteros, M.F., 2008. Self-Reported Falls and Fall-Related Injuries Among Persons Aged ≥ 65 Years-United States, 2006. J. Safety Res. 39, 345–349. https://doi.org/10.1016/j.jsr.2008.05.002

Stevens, J.A., Sogolow, E.D., 2005. Gender differences for non-fatal unintentional fall related injuries among older adults. Inj. Prev. 11, 115–119. https://doi.org/10.1136/ip.2004.005835

Stinchcombe, A., Kuran, N., Powell, S., 2014. Seniors' falls in Canada: Second report: Key highlights, Chronic Diseases and Injuries in Canada.

Stock, S.R., 2015. The Mineral–Collagen Interface in Bone. Calcif. Tissue Int. 97, 262–280. https://doi.org/10.1007/s00223-015-9984-6

Stone, K.L., Seeley, D.G., Lui, L., Cauley, J.A., Ensrud, K., Browner, W.S., Nevitt, M.C., Cummings, S.R., 2003. BMD at Multiple Sites and Risk of Fracture of Multiple Types : Long-Term. J Bone Min. Res 18.

Sun, W.Q., Leung, P., 2008. Calorimetric study of extracellular tissue matrix degradation and instability after gamma irradiation. Acta Biomater. 4, 817–826. https://doi.org/10.1016/j.actbio.2008.02.006

Szulc, P., Duboeuf, F., Schott, A.M., Dargent-Molina, P., Meunier, P.J., Delmas, P.D., 2006. Structural determinants of hip fracture in elderly women: Re-analysis of the data from the EPIDOS study. Osteoporos. Int. 17, 231–236. https://doi.org/10.1007/s00198-005-1980-7

Tal, S., Gurevich, A., Sagiv, S., Guller, V., 2015. Differential impact of some risk factors on trochanteric and cervical hip fractures. Geriatr. Gerontol. Int. 15, 443–448. https://doi.org/10.1111/ggi.12294

Tibshirani, R., 2011. Regression shrinkage and selection via the lasso: A retrospective. J. R. Stat. Soc. Ser. B Stat. Methodol. 73, 273–282. https://doi.org/10.1111/j.1467-9868.2011.00771.x

Tibshirani, R.J., 1994. Regression shrinkage and slection via the lasso.

Tomasek, J.J., Meyers, S.W., Basinger, J.B., Green, D.T., Shew, R.L., 1994. Diabetic and age-related enhancement of collagen-linked fluorescence in cortical bones of rats. Life Sci. 55, 855–861. https://doi.org/10.1016/0024-3205(94)90041-8

Turecek, C., Fratzl-Zelman, N., Rumpler, M., Buchinger, B., Spitzer, S., Zoehrer, R., Durchschlag, E., Klaushofer, K., Paschalis, E.P., Varga, F., 2008. Collagen cross-linking influences osteoblastic differentiation. Calcif. Tissue Int. 82, 392–400. https://doi.org/10.1007/s00223-008-9136-3

Unal, M., 2021. Raman spectroscopic determination of bone matrix quantity and quality augments prediction of human cortical bone mechanical properties. J. Biomech. 119, 110342. https://doi.org/10.1016/j.jbiomech.2021.110342

Unal, M., Jung, H., Akkus, O., 2016. Novel Raman Spectroscopic Biomarkers Indicate That Postyield Damage Denatures Bone's Collagen. J. Bone Miner. Res. 31, 1015–1025. https://doi.org/10.1002/jbmr.2768

Uppuganti, S., Granke, M., Makowski, A.J., Does, M.D., Nyman, J.S., 2016. Age-related changes in the fracture resistance of male Fischer F344 rat bone. Bone 83, 220–232. https://doi.org/10.1016/j.bone.2015.11.009

van den Kroonenberg, A.J., Hayes, W.C., McMahon, T.A., 1995. Dynamic models for sideways falls from standing height. J. Biomech. Eng. 117, 309–318. https://doi.org/10.1115/1.2794186

Vashishth, D., Behiri, J.C., Bonfield, W., 1997. Crack growth resistance in cortical bone: Concept of microcrack toughening. J. Biomech. 30, 763–769. https://doi.org/10.1016/S0021-9290(97)00029-8

Vashishth, D., Gibson, G.J., Khoury, J.I., Schaffler, M.B., Kimura, J., Fyhrie, D.P., 2001. Influence of nonenzymatic glycation on biomechanical properties of cortical bone. Bone 28, 195–201. https://doi.org/10.1016/S8756-3282(00)00434-8

Vestergaard, P., 2007. Discrepancies in bone mineral density and fracture risk in patients with type 1 and type 2 diabetes - A meta-analysis. Osteoporos. Int. 18, 427–444. https://doi.org/10.1007/s00198-006-0253-4

Viguet-carrin, P., Garnero, P., Delmas, P., 2006. The role of collagen in bone strength 319–336. https://doi.org/10.1007/s00198-005-2035-9

Wang, X., Shen, X., Li, X., Mauli Agrawal, C., 2002. Age-related changes in the collagen network and toughness of bone. Bone 31, 1–7. https://doi.org/10.1016/S8756-3282(01)00697-4

Weiner, S., Wagner, H.D., 1998. The material bone: Structure-mechanical function relations. Annu. Rev. Mater. Sci. 28, 271–298. https://doi.org/10.1146/annurev.matsci.28.1.271

Wiktorowicz, M.E., Goeree, R., Papaioannou, a, Adachi, J.D., Papadimitropoulos, E., 2001. Economic implications of hip fracture: health service use, institutional care and cost in Canada. Osteoporos. Int. 12, 271–278. https://doi.org/10.1007/s001980170116

Willett, T.L., Burton, B., Woodside, M., Wang, Z., Gaspar, A., Attia, T., 2015. γ-Irradiation sterilized bone strengthened and toughened by ribose pre-treatment. J. Mech. Behav. Biomed. Mater. 44, 147–155. https://doi.org/10.1016/j.jmbbm.2015.01.003

Willett, Thomas L, Dapaah, D.Y., Uppuganti, S., Granke, M., 2019. Bone collagen network integrity and transverse fracture toughness of human cortical bone 120, 187–193. https://doi.org/10.1016/j.bone.2018.10.024

Willett, Thomas L., Dapaah, D.Y., Uppuganti, S., Granke, M., Nyman, J.S., 2019. Bone collagen network integrity and transverse fracture toughness of human cortical bone. Bone 120, 187–193. https://doi.org/10.1016/j.bone.2018.10.024

Willett, T.L., Labow, R.S., Lee, J.M., 2008. Mechanical overload decreases the thermal stability of collagen in an in vitro tensile overload tendon model. J. Orthop. Res. 26, 1605–1610. https://doi.org/10.1002/jor.20672

Willett, T.L., Sutty, S., Gaspar, A., Avery, N., Grynpas, M., 2013. In vitro non-enzymatic ribation reduces post-yield strain accommodation in cortical bone. Bone 52, 611–622. https://doi.org/10.1016/j.bone.2012.11.014

Wolff, J., 1892. Das Gesetz der Transfomation der Knochen (The Law of Bone Transformation). Hirschwald, Berlin.

Wolinsky, F.D., Bentler, S.E., Liu, L., Obrizan, M., Cook, E.A., Wright, K.B., Geweke, J.F., Chrischilles, E.A., Pavlik, C.E., Ohsfeldt, R.L., Jones, M.P., Richardson, K.K., Rosenthal, G.E., Wallace, R.B., 2009. Recent hospitalization and the risk of hip fracture among older Americans. Journals Gerontol. - Ser. A Biol. Sci. Med. Sci. 64, 249–255. https://doi.org/10.1093/gerona/gln027

Woo, S.L., Kuei, S.C., Amiel, D., Gomez, M.A., Hayes, W.C., White, F.C., Akeson, W.H., 1981. The effect of prolonged physical training on the properties of long bone: a study of Wolff's Law. JBJS 63.

Woodside, C.M., 2015. Fracture Resistance Behaviour of γ-Irradiation Sterilized Cortical Bone Protected with a Ribose Pre-Treatment. Mater. Sci. Eng. MASc, 124.

Woodside, M., Willett, T.L., 2016. Elastic–plastic fracture toughness and rising JR-curve behavior of cortical bone is partially protected from irradiation–sterilization-induced degradation by ribose protectant. J. Mech. Behav. Biomed. Mater. 64, 53–64. https://doi.org/10.1016/j.jmbbm.2016.07.001

Yamashita, J., Li, X., Furman, B.R., Rawls, H.R., Wang, X., Agrawal, C.M., 2001. Collagen and Bone Viscoelasticity : A Dynamic Mechanical Analysis 31–36. https://doi.org/10.1002/jbm.10086

Yang, L., Peel, N., Clowes, J.A., McCloskey, E. V., Eastell, R., 2009. Use of DXA-based structural engineering models of the proximal femur to discriminate hip fracture. J. Bone Miner. Res. 24, 33–42. https://doi.org/10.1359/jbmr.080906

Yeung, Y., Chiu, K.Y., Yau, W.P., Tang, W.M., Cheung, W.Y., Ng, T.P., 2006. Assessment of the Proximal Femoral Morphology Using Plain Radiograph-Can it Predict the Bone Quality? J. Arthroplasty 21, 508–513. https://doi.org/10.1016/j.arth.2005.04.037

Zimmermann, E.A., Gludovatz, B., Schaible, E., Busse, B., Ritchie, R.O., 2014. Fracture resistance of human cortical bone across multiple length-scales at physiological strain rates. Biomaterials 35, 5472–5481. https://doi.org/10.1016/j.biomaterials.2014.03.066

Zioupos, P., Currey, J.D., 1998. Changes in the stiffness, strength, and toughness of human cortical bone with age. Bone 22, 57–66. https://doi.org/10.1016/S8756-3282(97)00228-7

Zioupos, P., Currey, J.D., Hamer, A.J., 1999. The role of collagen in the declining mechanical properties of aging human cortical bone. J. Biomed. Mater. Res. 45, 108–116. https://doi.org/10.1002/(SICI)1097-4636(199905)45:2<108::AID-JBM5>3.0.CO;2-A

Zioupos, P., Kirchner, H.O.K., Peterlik, H., 2020. Ageing bone fractures: The case of a ductile to brittle transition that shifts with age. Bone 131, 115176. https://doi.org/10.1016/j.bone.2019.115176

Zysset, P.K., Edward Guo, X., Edward Hoffler, C., Moore, K.E., Goldstein, S.A., 1999. Elastic modulus and hardness of cortical and trabecular bone lamellae measured by nanoindentation in the human femur. J. Biomech. 32, 1005–1012. https://doi.org/10.1016/S0021-9290(99)00111-6

Appendices

Appendix A

Limitations and concerns associated with the design of the HIS pelvis/spring system

While the design of the HIS was based on the current understanding of hip impact biomechanics and designed to align with CSA standards for hip protector testing (the HIS is an alternative version of test rig design A) (CSA Group, 2020), the high-energy nature of the experiments resulted in unexpected behaviour of the mechanical system, differences that weren't clearly identified until the data processing phase. First of these was the unexpected bending or deflection of the impact plate, rending the impact plate to have an orientation that was no longer parallel with the surface of the force plate or floor. This occurred in the phase of the impact between initial contact and peak force (or earlier in the case of fractures), likely caused by the point of force application being different than the effective center of the impact plate and overall load carriage. It should be noted that both the experimental design and the mechanical design of the test system attempted to take this into account in order to mitigate this effect. Firstly, part of the experimental design dealt with attempting to align the greatest lateral protuberance of the greater trochanter of the specimens (which would be the highest vertical point of the specimens and therefore the primary point of force application) with the center of the impact plate. Beyond visual inspection, a plumb line was used to align these points without prematurely loading the specimen, and this was generally confirmed during the static preload. From a mechanical design standpoint, guide rod/support columns, which were partly used to connect the impact plate to the load carriage (with the springs confined between these boundaries) were also designed to guide the vertical translation of the entire spring/impact system and prevent horizontal deformation or deflection. However, likely due to the high energy nature of the impacts, these guide bars did not adequately prevent this deflection, likely due to deformation at the guide bar/impact plate interface. More specifically, the guide bars were attached to the impact plate via bolts, and as observed part way through experimentation, one of these bolts broke, and there was obvious necking in the remaining bolt, which indicated large tensile forces. These tensile forces were likely caused by bending of the plate (as can be seen in some of the high-speed videos). A 3D representation of the mechanical system, as well as the hypothesized method of failure can be seen in Figure A-1. When combined, this bending in the impact plate likely affected the impact force vector/direction of loading, which

could have been a source of the variance seen in the measured values. An analysis of the forces in the X and Y axes at the moment of Fx revealed a mean (SD) X axis shear force of -1.10 (1.78) % of Fx, and a mean (SD) Y axis shear force of -1.33 (4.23)% of Fx. These values reveal a slight rightward and backward bias during the impact (from a frontal view frame of reference of the HIS drop tower). However, despite the potential variance introduced by these sources, the findings were still clear, likely due to the robust effects of the considered factors on bone strength. Improvements to the mechanical design of the test system and more rigorous experimental methods would likely lead to improved results through reduced introduced error or variance. This, in general, is a limitation of using a HIS type experimental paradigm compared to the traditional MTS paradigm, which has relatively fewer degrees of freedom, and more controlled boundary conditions. Despite this, it is possible that the increased biofidelic loading and more physiologically accurate measures of bone strength outweigh the error introduced through a less constrained mechanical system.

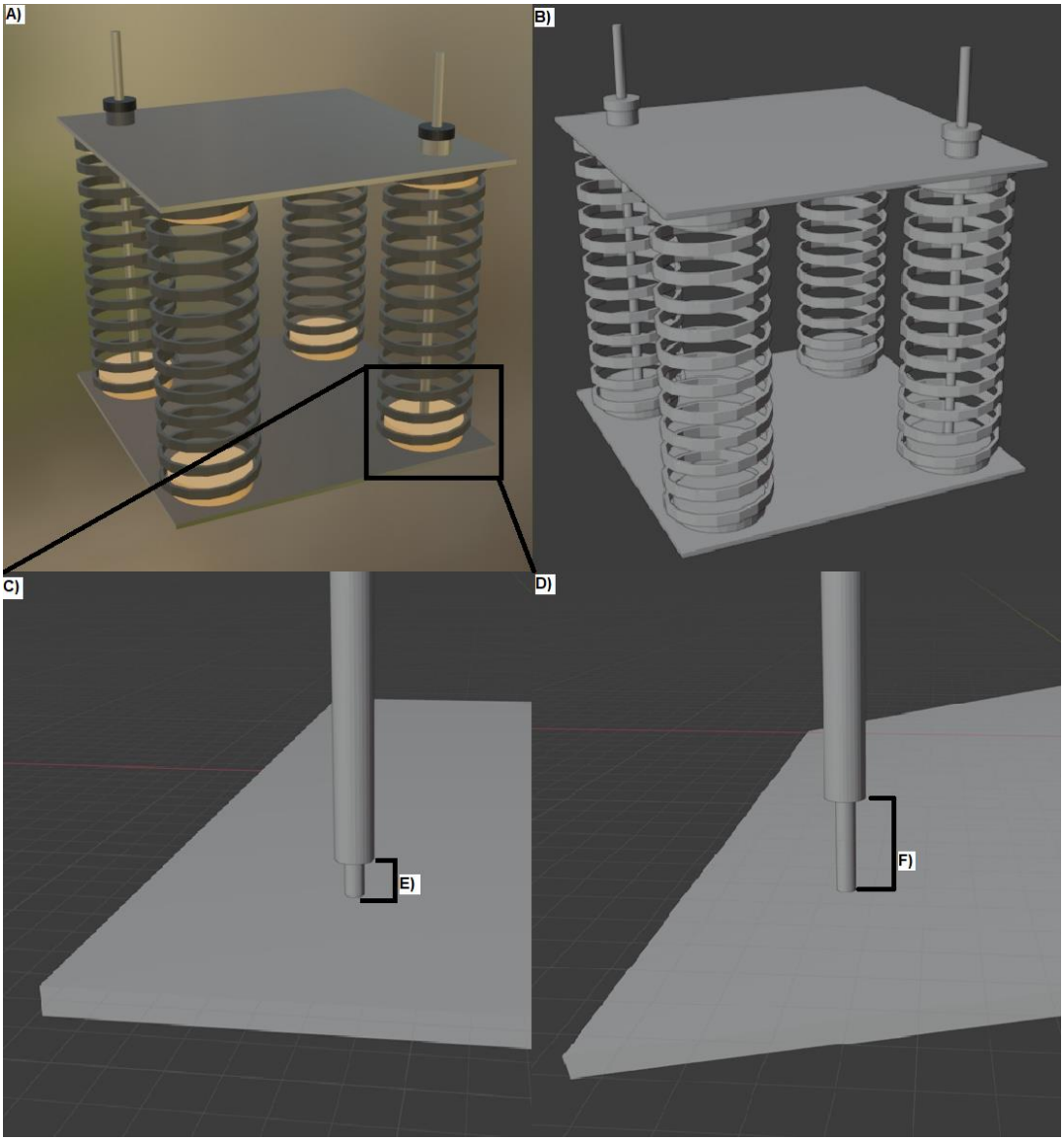

Figure A-1: A composite image of a 3D render of the spring system (A) with material, B) with no material). Panel C) represents the guide rod/impact plate interface with the connecting screw presented; note that the gap shown (E) is only to help visualize, whereas in reality, there is contact between bottom of the rod and the top of the impact plate (with no screw exposed). Panel D) represents the suspected plastic lengthening of the screw (F) that occurs due to multiplanar deflection of the impact plate. It is hypothesized that, due to the rotation of the impact plate relative to the guide rod, a mechanical hinge between guide rod and impact late on one side acts as a lever, resulting in tension on the screw that resulted in the stretching of the screw. The lengthening shown (F) is exaggerated and does not demonstrate the mechanical hinge.

Appendix B

Supplemental investigation to evaluate the biofidelity of HIS and MTS loading (for simulated lateral hip impacts) via comparisons with lateral pelvis release experiments of live volunteers.

Purpose: The goal of this supplemental analysis was to quantify the biofidelity of the HIS experimental paradigm, specifically in relation to fall-related lateral hip impacts. An additional goal of this analysis was to contrast the biofidelity of both experimental paradigms used in this thesis (HIS and MTS) when compared to lateral hip impact data from live volunteers (collected as part of Martel et al., 2018). In order to do this, a more specific definition of biofidelity was proposed, which allowed for the evaluation of biofidelity (in this context) on a spectrum. Overall, the hypothesis throughout the thesis was that HIS experiments were more biofidelic than MTS experiments, and this supplemental analysis provides a more direct method to test this hypothesis, albeit on a limited scale.

Biofidelity: While "biofidelity" is not a recognized word according to English-language dictionary Meriam-Webster, it is, however, a term that has been used in scientific contexts to explain a state of being similar/true/accurate to a biological organism/system/function, with the word "biodfidelic" being an adjective with the same meaning. A combination of the words "bio" (short for biologic/biological) and "fidelity" (meaning "the degree to which something matches or copies something else," as defined by the Merriam-Webster dictionary), the word "biofidelity" and its adjective "biofidelic" are used throughout this thesis to either describe presence, or lack of, a close similarity to the true biological, or more precisely biomechanical function or response to an input stimulus. This word is used in this thesis almost exclusively in the context of discussing the input stimulus of two experimental paradigms (the HIS and MTS bone strength experiments conducted in study 1 of thesis [Chapter 3]) and mechanical response of the cadaveric femur specimen when subjected to simulated lateral impacts via either experimental paradigm. Therefore, a more specific or accurate definition of "biofidelity" in the context of this thesis would be: "the degree to which the simulated lateral impacts produces loading of a cadaveric proximal femur specimen that matches that measured from human volunteers during a fall-related lateral hip impact ".

Methods: Towards quantifying the biofidelity of both the HIS and MTS experimental paradigms, and more specifically, the simulated lateral impact loading scenarios produced by either paradigm, the load displacement curves of the femur specimens included in study 1 were compared to the

load displacement curves of six lateral pelvis release experiments (1 m/s impacts) from live human volunteers (1 male, 1 female, 3 impacts each) that were collected as part of Martel et al., 2018. In general, HIS and MTS experiment curves that more closely match the curves from the lateral pelvis release impacts were deemed more biofidelic. In order to quantify this, the time to peak force (T_p) of each of the HIS and MTS experiments were compared to the mean values of the lateral pelvis release impacts. Additionally, as biofidelity is defined as a spectrum in this investigation, the relative difference in time to peak force (ΔT_p) of the HIS and MTS curves compared to the mean values of the lateral pelvis release impacts were also extracted, allowing for the comparison of biofidelity between the HIS and MTS experiments. Paired-samples t-test was conducted to compare ΔT_p of both paradigms, in order to determine a given paradigm was significantly lower than the other, which would by the definition proposed in this investigation, mean that the paradigm is more biofidelic than the other. Finally, as the proposed comparison between HIS, MTS, and pelvis release experiments is inherently flawed, due to the large discrepancies in impact velocities and displacement rates (4 m/s for HIS, 1 m/s for pelvis release, and 0.06 m/s for MTS). Therefore, in an attempt to more appropriately compare the HIS and MTS experiments to the pelvis release experiments (the standard which was used to assess biofidelity), each of the HIS and MTS experiment curves were characterized as an exponential function. The exponent was then normalized to the trial specific velocity or displacement rate, and new curves were generated using trial specific exponential fit functions, using the normalized exponents to generate a theoretical 1 m/s velocity curve (up to the mean time to peak force of the pelvis release experiments). Paradigm specific mean curves were also computed for these fitted curves, and RMSE was computed (comparing paradigm specific mean curves to the mean curve of the pelvis release experiments). The paradigm specific mean fitted curve with the lowest RMSE would be deemed more biofidelic, as well as help quantify the degree of biofidelity if assessed on a spectrum.

Results: Force time curves for the experiments can be seen in Figure B-1. Mean T_p and ΔT_p for the HIS experiments were 0.007 and -0.017 s, respectively, compared to the mean T_p and ΔT_p of the MTS experiments (0.507 and 0.483 s, respectively). Based on T_p, HIS experiments were more biofidelic in terms of Tp. Paired-samples T-tests comparing HIS and MTS ΔT_p revealed that HIS ΔT_p was significantly lower than MTS ΔT_p (95% CI [-0.504: -0.428 s], t(df = 5) = -31.102, $p <$ 0.0001). Paradigm specific mean normalized fit curves were generated (Figure B-2), and RMSE was computed, revealing that the mean normalized HIS curve has a lower RMSE (63.978)

compared to the mean normalized MTS curves (194.260). Visual inspection of the mean and +/-1 SD corridor curves (Figure B-2), the mean normalized HIS curve more closely aligns the mean pelvis release curve.

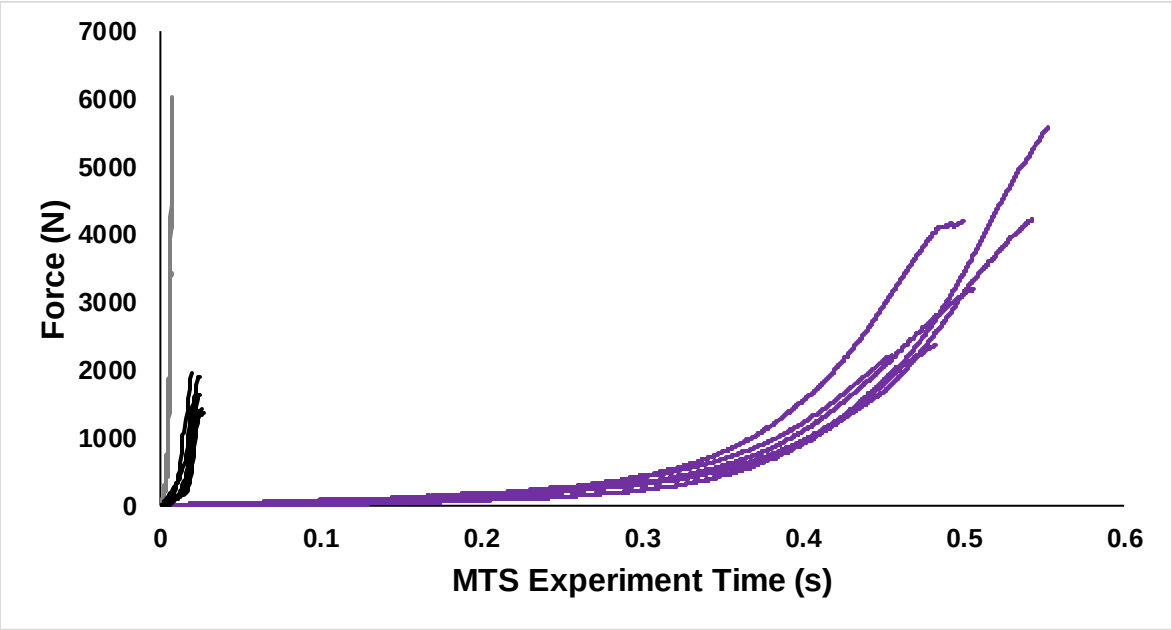

Figure B-1: Force over time of the HIS (dark gray lines), MTS (purple lines) and Pelvis Release experiments (black).

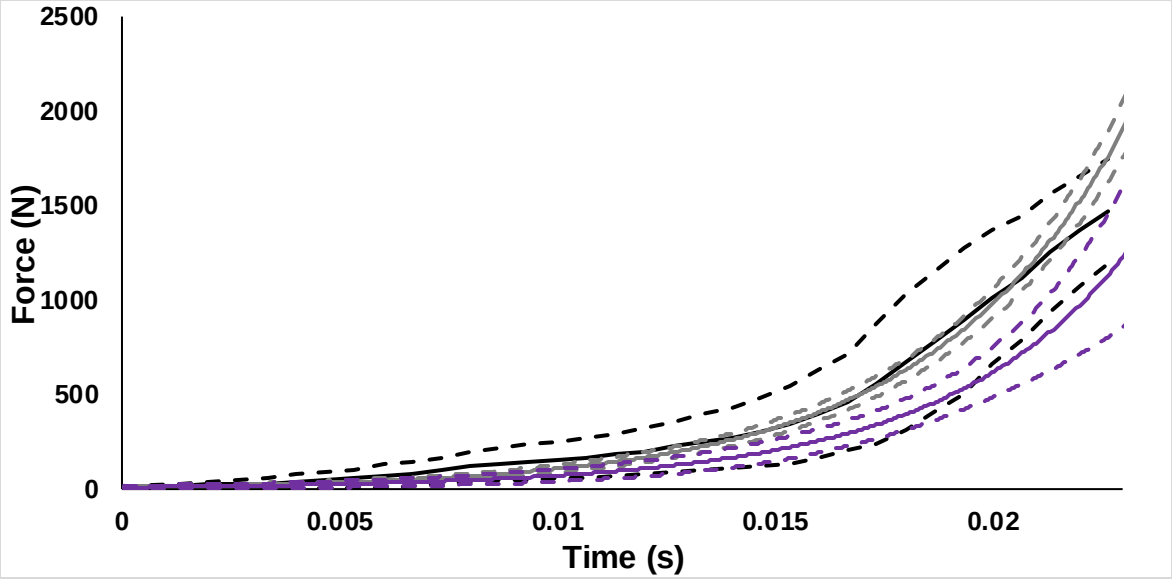

Figure B-2: Pelvis release (black line, solid = mean, dashed = 1 SD), HIS normalized (dark gray, solid = mean, dashed = 1 SD), and MTS normalized (purple, solid = mean, dashed = 1 SD).

Discussion: Based on all considered metrics and the proposed definition of biofidelity, the HIS experiments are more biofidelic than the MTS experiments. Not only do the timing-related characteristics of the HIS experiments more closely match those of the pelvis release experiments, the shape and magnitude of the velocity normalized mean curves of the HIS experiments closely match those of the pelvis release experiments. In this sense, when normalizing for velocity, the impact dynamics of HIS experiments more closely match the impact dynamics of simulated lateral hip impacts of live volunteers (compared to the MTS experiments), and thus, more closely satisfies the proposed definition of biofidelity. While there are many limitations associated with this supplemental analysis (with the primary limitation being a small sample size), the results are promising, and based on the hypothesis tested by this analysis, suggest that the HIS experimental paradigm is a more biofidelic method for simulating fall-related lateral hip impacts and fractures compared to the traditionally used MTS approach.

Appendix C

Reasoning for the Failed Trial Contingency

The reasoning for this contingency protocol is to prevent introducing additional variance in the dataset. While specimens which do not fracture in the first trial and have no noticeable changes upon inspection of the X-ray are still accumulating microdamage (Hazenberg et al., 2007; Schaffler et al., 1995), the methods that will be used to characterize the specimens prior to the impact trials do not offer sufficient resolution to characterize or quantify the degree of microdamage present. In fact, prior to testing it is not possible for us accurately quantify the level of microdamage present in specimens, which is a level of variance that cannot currently be accounted for. Hence, while microdamage will be introduced in impacts wherein fracture does not occur, it is possible that the microdamage that occurs is still within the range of microdamage present within specimens of this sample. However, a second failed impact trial may introduce more microdamage to a specimen already in a state of heightened microdamage and will therefore be excluded. The rate or magnitude of microdamage accumulation from subsequent impacts has not yet been investigated, and further research of this phenomena is warranted.

Appendix D

LASSO-GLM Process and Rationale

LASSO regression equations predicted F_x from all possible combinations of the 4 variables (*age*, *sex*, *r*, and *BMD*), given a range of 101 lambda values (the regularization parameter) ranging from 10^3 to 10^-2, decreasing the exponent by 0.05 increments. An additional model parameter was provided in the form of a constraint that limited the number of predictors *p* in the considered models to be less than the number of predictors included in the largest model generated from the stepwise regression process. Beyond limiting the number of final predictors, the purpose of this additional constraint was to reduce the problem space for possible regression models generated.

Towards identifying the optimal lambda value used to identify the resulting LASSO-GLM model, a 10-fold cross-validation was conducted for the full range of generated LASSO models on the same range of lambda values (Johannesdottir et al., 2017; Li et al., 2019). With 10 folds, the model data sample (N = 20) was divided into 10 equally sized sets (termed folds); the process then used 9 folds to generate a model and tests it against the remaining fold. This process is then repeated such that each fold is used exactly once as the test fold. From this cross-validation, the mean squared error (MSE) was computed for the 10 folds of each generated model, which allows for the identification of the lambda value that results in the model with the lowest average error (referred to as λ_{min}). Due to the resulting bootstrapping, repeated cross-validation evaluations can result in varying λ_{min} values, even when the lambda range evaluated is held constant. To combat this, the cross-validation was repeated 10 times, and the mean λ_{min} value was selected and used to generate the final LASSO-GLM model.

Appendix E

Survey of Previous Femoral Bone Strength Studies

Table E-1: List of previously conducted experiments wherein proximal femur bone strength was related to bone mineral density. Adapted from Table 1 of Dall'Ara et al. 2013a, with the addition of Gilchrist 2014.

Reference	Loading Rate (mm/s)	Sample Size	Best Predictor	Best R^2
Bouxsein et al., 1999	100	25	Trochanteric BMD	0.92
Cheng et al., 1997	14	70	Trochanteric BMD	0.88
Courtney et al., 1994	100	20	Femoral Neck BMD	0.72
Courtney et al., 1995	2	17	Femoral Neck BMD	0.92
Dall'Ara et al., 2013a	0.082	36	Femoral Neck BMD	0.80
Dragomir-Daescu et al., 2011	100	18	Total Hip BMD	0.79
Gilchrist et al., 2014	0.5	20	Total Hip BMD	0.94
Hansen et al., 2011	0.033	31	Trochanteric BMD	0.78
Kolta et al., 2012	2	12	Trochanteric BMD	0.78
Le Corroller et al., 2012	0.167	21	Femoral Neck BMD*	0.77
Manske et al., 2009	100	35	Femoral Neck BMD	0.64
Pinilla et al., 1996	100	11	Total Hip BMD	0.68
Roberts et al., 2010	100	73	Femoral Neck BMD	0.70
Mean (Median) Sample size	-	29.9 (21)	-	-

Appendix F

Displacement Rate Rationale for Study 3 (SENB protocol)

This displacement rate differs from the rate used during pilot work conducted, where it was found that the 40 mm/s displacement rate use resulted in a time to peak force ~3-4 times larger than those extracted from the HIS impact experiments. By scaling down the 40 mm/s displacement rate by 3-4 times (resulting in a new displacement rate of 10-13 mm/s), we should achieve a time to peak force in the MMTS experiments that mimic those observed in the HIS experiments. This is done in an attempt to match the dynamics of impact loading. While the higher 40 mm/s displacement rate was used in the pilot study to attempt to elicit the loading rate observed in the HIS impact experiments, the loads experienced during these two different experiments differ by orders of magnitude. Upon further consideration, mimicking time to peak force is more feasible and should properly mimic the impact dynamics in this MMTS test paradigm. Further support for the choice of 13 mm/s as the new target displacement rate comes from a previous fracture toughness experiment conducted by Gauthier and colleagues in 2017, wherein they investigated differences in fracture toughness of femoral neck and diaphysis cortical bone (as well as the diaphysis of the radius and tibia). In Gauthier's study, a displacement rate of 10 mm/s was used, with their justification stemming from a study by Foldhazy and colleagues in 2005, in which the strain at the distal radius was measured during standing falls onto outstretched hands (Földhazy et al., 2005). A median strain rate of 45954 microstrain/s was reported by Foldhazy et al. 2005, which in tum Gauthier et al. 2017 used to set their fall/impact loading displacement rate to 10 mm/s (Gauthier et al., 2017). From the pilot work previously described in Chapter 3.1.1, strain and strain rate were measured at the inferior femoral neck during simulated lateral hip impacts (and ultimately hip fracture), wherein median and mean strain rates measured were 11 to 35% higher than those reported by Foldhazy et al. 2005. As the pilot work included multiple different impact velocities, including extremely low velocity impacts (< 1 m/s), the range of strain values measures may not properly represent fall-related hip impacts/fractures. Therefore, data from trials with impact velocities below 1 m/s where excluded, resulting in median and mean strain rates of 57088 and 58055 microstrain/s (representing median and mean impact velocities of 3.17 and 2.95 m/s), which correspond to strain rates 24.2 and 26.3 % higher than those reported by Foldhazy et al. 2005. If the logic used by Gauthier et al. 2017 to determine displacement rate is used, it follows that a displacement rate that is 24-26% higher than 10 mm/s should more accurately match the loading

dynamics seen in lateral hip impacts. Consequently, this results in a targeted displacement rate of 12.4 to 12.6 mm/s, which aligns with the targeted 10-13 mm/s displacement rate suggested by matching time to peak force. However, an argument can be made to maintain the 10 mm/s used by Gauthier and colleagues, including one that goes beyond simple experimental method history.

The main argument for maintaining the 10 mm/s displacement rate, targeting the low end of the displacement rates expected to mimic the loading dynamics of HIS impact tests (10 mm/s instead of 13 mm/s), is due to the fact that high-frequency oscillations were observed in the load displacement data, superimposed above the expected signal of interest, of the pilot study experiments (using the 40 mm/s displacement rate), which is suspected to be driven entirely by the high-displacement of the system itself. By using a lower displacement rate, the magnitude of these high-frequency oscillations should be minimized. ASTM E1820-20, which was originally developed for testing of metals, does have a sub-section for high-rate fracture toughness testing, wherein it describes the possibility of observing these high-frequency oscillations. The standards document does provide options, primarily test system modifications, to mitigate or account for these oscillations; if these oscillations are still present in further pilot testing under the 10 mm/s displacement rate, the suggested modifications described in ASTM E1820-20 will be considered. Lastly, it should be noted to high-rate fracture toughness testing of bone tissue is rare, and in the few cases in the literature had derived their loading or displacement rate by attempting to match the strain rate experienced during an impact (refs) or (blank, if other refs found). The reason for not using the same displacement rate described by these studies is derived from the strain rate of a jump landing impact, as measured at the tibia, and (blank, if other refs found). While it is possible that this strain rate is similar to that experienced at the femoral neck during a lateral hip impact, it was decided to derive a displacement rate from the data acquired through the pilot work.

Appendix G

Study 3 Pilot Study

Building from the pilot work previously discussed in Chapter 3.2.6 and 4.2.6, fracture toughness testing was conducted as part of the collaborative project funded by the University of Waterloo Network for Aging Research investigating the influence of bone collagen on femoral neck fracture force and femoral bone beam fracture toughness. To do so, the unused matched pair of the femurs used in the previous pilot work were used for this study, in addition to the remaining distal portions of the femurs used in the previous pilot work. From the unused matched pair femurs, one SENB (30 mm length x 4 mm width x 2 mm) was cut from the inferior femoral neck, and two SENB (40 mm length x 4 mm width x 2 mm) were cut from the diaphysis (one more proximal, one more distal). While femoral neck, nor proximal femur, SENB could be extracted from the femur that was tested in the previous pilot work (Chapter 3.2.6), one distal diaphysis SENB was extracted from the distal portion of the femur that resulted following specimen bisection. This resulted in 4 unique SENB specimens from each femur pair; Three from one femur, and 1 from the femur used in the previous pilot work. Specifics about SENB preparation, extraction, and notch creation are outlined in Chapter 5.2.2.1, as the same standard methods were used.

For this experiment, the influence of loading rate (through constant displacement) and location (femoral neck versus diaphysis) on fracture toughness, the resistance to crack growth. However, due to the small sample size, a full-factorial study design could not be completed. Instead, high displacement rate (40 mm/s) test were conducted on both the femoral neck and proximal diaphysis SENB specimens, whereas low displacement rate (0.083 mm/s) test were conducted on the distal diaphysis SENB samples. This was done due to the primary interest of measuring fracture toughness of a clinically relevant site (inferior femoral neck) under physiologic loading (high displacement rate to mimic high loading rate), while allowing us to compare those results to low displacement rate fracture toughness test results of the distal diaphysis, as it is the current methods for cortical bone fracture toughness testing (Willet et al. 2019). The purpose of these measures and comparisons was ultimately to relate fracture toughness back to femoral bone strength/fracture force of simulated lateral hip impacts, which is discussed in further detail in Chapter 6.

Fracture toughness tests were conducted in accordance with ASTM E1820-20 procedures for both low and high rate fracture toughness tests of SENB specimens, with modifications to accommodate testing of cortical bone, ultimately following previously established methods (Willett et al., 2019; Willett et al., 2015; Woodside and Willett, 2016). A micro material testing system (MMTS) (μTS, Psylotech Inc, Evanston, IL, USA) was used to conduct three-point bending while measuring load and displacement. Experiments were performed under a high-powered microscope with a mounted high-speed video camera, which collected video of the experiment; this was later used to extract crack length. Analysis of the load displacement data of the high displacement rate tests revealed high frequency oscillations in the signal (a possibility outlined in ASTM E1820-20), which resulted in some trials violating the data smoothness criteria outlined in ASTM E1820-20. To remedy this, a low-pass filter (2nd order Butterworth filter, dual-pass) with a 750 Hz cutoff was used to mitigate the high frequency oscillations, which resulted in all trials satisfying the data smoothness criteria (Figure G-1).

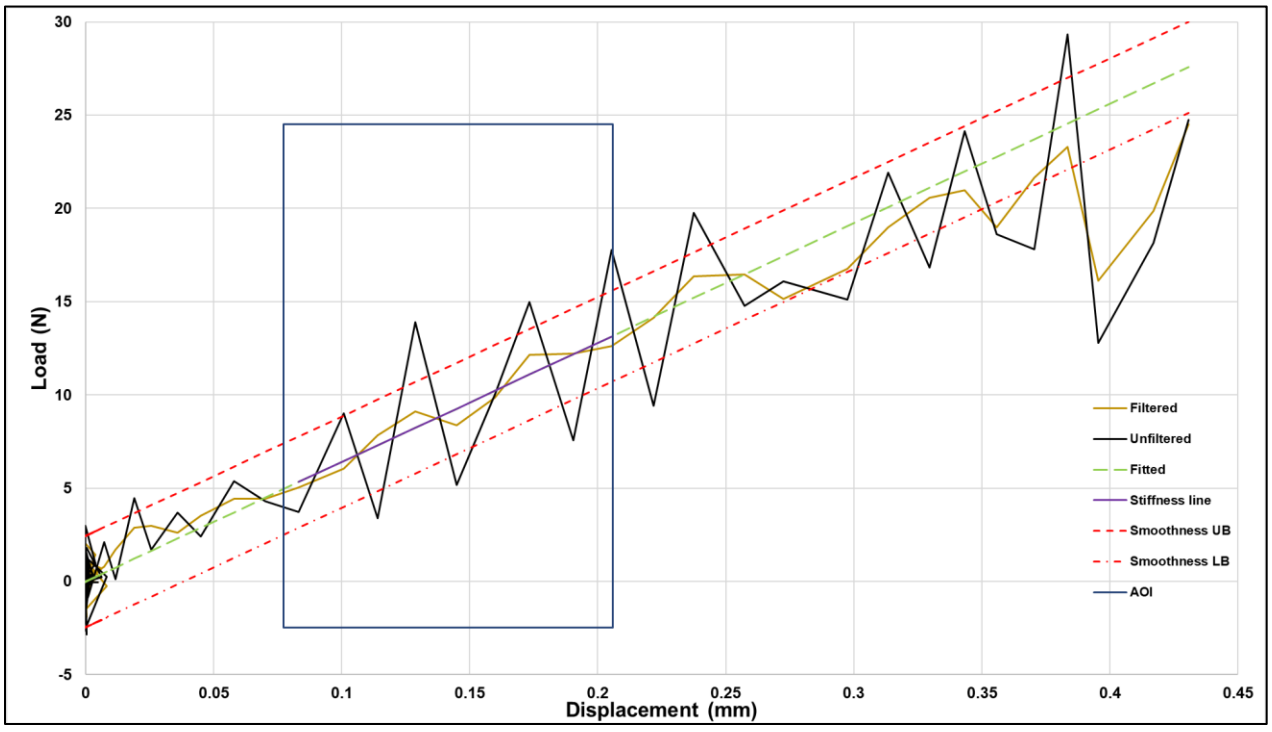

Figure G-1: Load displacement for a high displacement rate three-point bending test of a cortical bone SENB specimen. Dashed lines represent the data smoothness criteria (red) and linear model fitted data (green) as outlined in ASTM E1820-20.

Two separate fracture toughness values were computed: critical elastic-plastic fracture toughness (J_{IC}), and critical elastic fracture toughness (K_{IC}). J_{IC} was computed for both high and low displacement rate tests, whereas K_{IC} was only computed for the high-rate tests. While the specifics of fracture toughness calculations can be found in section 5.2.2.3, mean(SD) J_{IC} measured during high rate tests was 0.26 (0.14) N/mm for the femoral neck specimens, 0.30 (0.10) N/mm for the proximal diaphysis, whereas J_{IC} for the distal diaphysis during slow rate tests was 2.8 (2.6) N/mm. While the variance was large, these results suggest that fracture toughness may be lower when under high-rate loading, as even the lowest measured J_{IC} value during the slow rate test (0.66 N/mm) was higher than the highest value measured during high-rate tests (0.48 N/mm). As for elastic fracture toughness, K_{IC} was slightly lower on average in the femoral neck, with a mean(SD) value of 159.8 (17.1) MPa$\sqrt{\text{mm}}$, compared to the proximal diaphysis with a mean(SD) of 169.7 (23.8) MPa$\sqrt{\text{mm}}$. In general, these results suggest that, while fracture toughness may not differ between locations, the rate at which specimens are loaded seems to have an effect on fracture toughness. These findings may have important implications when relating fracture toughness back to bone strength/fracture force, especially if inferences on fracture risk are made from low-rate fracture toughness tests, which warrants further investigation.

Appendix H

Computing KJ equivalent using measured Young's modulus

Purpose: Due to the high-rate nature of the experiments, less plastic deformation was anticipated when compared to similar experiments under quasi-static loading conditions. This brings into question the appropriateness of using metric of elastic plastic toughness, *J*. While the implementation of J_q and J_{Max} attempt to address this, an alternative exists wherein the plane strain fracture toughness, *K*, equivalent of *J* fracture toughness can be computed. In this analysis, this value, the K_J equivalent, was computed and utilized in the regression analyses relating to collagen connectivity and quality, as done in Study 3, Chapter 5.

Methods: The general equation to compute the K_J equivalent is presented in ASTM E1820 (referred to therein K_{JIC}) as:

$$K_J = \sqrt{E'JIC}, \text{where}$$
$$E' = \frac{E}{1-\nu^2}$$

These equations can then be simplified to

$$K_J = \sqrt{\left(\frac{E}{1-\nu^2}\right)J}$$

where J_d is the value of the J-integral fracture toughness at just before ultimate failure. Therefore, as per the notation used throughout this thesis, *J* becomes J_{Max}, and the equation becomes

$$K_{J_{Max}} = \sqrt{\left(\frac{E}{1-\nu^2}\right)J_{Max}}$$

While J_{Max} has already been computed as part of Study 3 (Chapter 5), both *E* and *v* need to be defined. As the experimental setup did not allow for the quantification of Poisson's ratio, a value of 0.3 was used for cortical bone, as established by Koester et al., 2011 and Zimmermann et al., 2014 and has been used in similar investigations (Burton et al., 2014; Gauthier et al., 2017; Willett et al., 2015). As for Young's modulus, the load deflection data paired with the SENB beam measurements allow us to compute E, as defined by Woodside in the 2015 MASc thesis, where

$$E_{meas} = \frac{MS^3}{4BW^3}$$

Analysis: These equations were used to compute E_{meas} followed by K_{JMax} (Table H-1). These values were then used in the same regression analyses conducted in Study 3 (Chapter 5). Briefly, the relationship between K_{JMax} and the independent variables *Age*, *Max slope*, and T_d were investigated in a backwards stepwise manner (Table H-2).

Table H-1: Mean and SD values for SENB beam dimensions, E_{meas}, and K_{JMax}; K_{Max} is presented with the units as K_{JMax} to compare

	B (mm)	W (mm)	M (kN/m)	E_{meas} (GPa)	K_{JMax} (MPa√m)	K_{Max} (MPa√m)
Mean	2.06	3.99	79.6	3.89	4.00	3.61
Sd	0.06	0.05	2.76	1.30	1.28	0.99

Table H-2: Linear models predicting fracture toughness K_J using E_{meas} from *Age*, *Max Slope*, and T_d; Best overall K_{Max} and J_{Max} models are presented for comparison.

Fracture Property	Linear Model			Adj-R^2 (p)
K_{JMax}	*Age*	***Max Slope***	*Td*	0.315
	(β = 0.06,	***(β = 0.60,***	*(β = -0.14,*	(*p* = 0.008)
	p =0.725)	***p = 0.002)***	*p = 0.402)*	
		Max Slope	*Td*	0.340
		(β = 0.59,	*(β = -0.16,*	(*p* = 0.003)
		p = 0.001)	*p = 0.339)*	
		Max Slope		0.341
		(β = 0.61,		(*p* = 0.001)
		p = 0.001)		
K_{Max}		***Max Slope***		0.299
		(β = 0.57,		(*p* = 0.002)
		p = 0.002)		
J_{Max}		***Max Slope***		0.163
		(β = 0.44,		(*p* = 0.021)
		p = 0.021)		

Discussion: Unlike K_{Max} and even J_{Max}, K_{JMax} directly considers the Young's modulus of each specimen. This direct consideration of the material properties of the specimens in question may provide a more specimen-accurate metric of fracture toughness. However, it should be noted that

this purpose is not outlined in ASTM E1820. Rather, the standard defines K_J as simply as the equivalent of K for J_{IC}. Nevertheless, it is interesting that accounting for specimen elastic modulus resulted in an improvement in the model predicting fracture toughness from Max Slope, where an additional 4.2% was explained when compared to K_{Max}, and 17.8% when compared to J_{Max}. However, this is a modest improvement when compared to $\underline{K_{Max}}$, and the use of K_{JMax} does not necessarily provide a clearer explanation as to the relationship between fracture toughness and collagen network connectivity. Therefore, the appropriateness of using K_{JMax} is still debatable, though the improvement in model strength may suggest that it is indeed more appropriate than J_{Max} and potentially K_{Max}.

Limitation: Previous work by Woodside in 2015 (MASc thesis) defines this relationship, and states that the modulus must be corrected by the compliance of the test system (*ks*). Unfortunately, this value is currently unknown for the mechanical testing system used in this study. Due to the nature of the work, the stiffness of the testing system should be orders of magnitude larger than that of the samples tested. To get an idea of the relative effect of this correction, the stiffness of the system used in the Woodside 2015 thesis (similar in design and function to that used in the current thesis) was used, where *ks* = 1.26 kN/mm. The ratio between the corrected Young's modulus (E_{true}) and E_{meas} is as follows:

$$\frac{E_{true}}{E_{meas}} = \frac{1}{1 - \frac{M}{ks}}$$

where M is the elastic modulus (of stiffness) of the tested specimen. It should be noted that the above equation is different than that presented in the Woodside 2015 thesis, as it is believed that there was a typo inverting the position of *M* and *ks*. Using this to compute E_{true} allowed for new K_{JMax} values (Table H-3), which were then used in the same regression analyses (Table H-4).

Table H-3: Mean and SD values for SENB beam dimensions, E_{meas}, E_{true*} and K_{JMax}; K_{Max} is presented with the units as K_{JMax} to compare

	B (mm)	W (mm)	M (kN/m)	E_{meas} (GPa)	E_{true*} (GPa)	K_{Max} (MPa√m)	K_{JMax} (MPa√m)
Mean	2.06	3.99	79.6	3.89	4.18	3.61	4.15
Sd	0.06	0.05	2.76	1.30	1.47	0.99	1.36

Table H-4: Linear models predicting fracture toughness K_{JMax} using E_{true*} from *Age*, *Max Slope*, and T_d. Best overall K_{Max} model presented for comparison.

Fracture Property	Linear Model			Adj-R^2 (p)
K_J	*Age*	***Max Slope***	*Td*	0.311
	(β = 0.07,	***(β = 0.60,***	*(β = -0.14,*	(*p* = 0.009)
	p =0.739)	***p = 0.002)***	*p = 0.416)*	
		Max Slope	*Td*	0.337
		(β = 0.59,	*(β = -0.15,*	(*p* = 0.003)
		p = 0.001)	*p = 0.354)*	
		Max Slope		0.339
		(β = 0.60,		(*p* = 0.001)
		p = 0.001)		
K_{Max}		***Max Slope***		0.299
		(β = 0.57,		(*p* = 0.002)
		p = 0.002)		